Immunotoxicology of high aspect ratio nanomaterials

by

James Dean Ede

A thesis submitted in partial fulfillment of the requirements for the degree of

Doctor of Philosophy

In

Physiology, Cell and Developmental Biology

Department of Biological Sciences
University of Alberta

ABSTRACT

Immune models have been highlighted in nanotoxicology for their applicability in understanding the effects of both accidental exposure (e.g. environmental exposure) and therapeutic exposure (e.g. targeted drug delivery) to nanomaterials (NMs). The experiments presented here examine the immunotoxicology of three high aspect ratio nanomaterials (HARNs), rosette nanotubes (RNTs), carbon nanotubes (CNTs) and cellulose nanocrystals (CNCs), using *in vitro* teleost and mammalian models. The data presented in this thesis adds to reports that HARNs are not necessarily associated with high levels of cytotoxicity and declines in viability in mammalian models occur at concentrations of HARNs that are above those anticipated for either environmental or therapeutic applications. I observe differential cytotoxicity for all three HARNs examined and the toxicity of each material is altered with differential surface functionalization. In addition, several HARNs interfered with receptor-mediated immune effector responses *in vitro* at sub-lethal levels of exposure and these effects differed between the type of HARNs and their functionalization. Sub-lethal exposure to RNTs enhanced, while sub-lethal CNT exposure reduced, IgE-FcεRI-mediated degranulation. I propose a mechanism for the observed immunomodulation of receptor-mediated effector function following HARN exposure, suggesting that the presence of NMs interferes with receptor engagement of their respective ligand.

The work presented here is also one of the first to examine the effect of NM exposure on fish lymphoid cells. Exposure of fish lymphocytes to HARNs resulted in significant declines in viability at concentrations that were an order of magnitude lower than mammalian leukocytes. In addition, immunomodulation of teleost receptor-mediated effector responses was observed following HARN exposure. RNT and CNT exposure significantly reduced *Ictalurus punctatus* Leukocyte Immune Type Receptor (IpLITR)-mediated phagocytosis at sub-lethal levels of exposure and was functionalization dependent. The availability of several *in vitro* leukocyte cell lines and the use of IpLITR as a model to examine the sub-lethal effect of NM exposure on immune cell effector function make channel catfish an ideal model for future aquatic nanotoxicity testing.

ACKNOWLEDGEMENTS

First and foremost I would like to recognize my supervisors, Dr. Greg Goss and Dr. James Stafford. I would like to thank you for supporting my research and for your mentorship as well as providing me with many incredible opportunities throughout the course of my Ph.D. Thank you for your patience and encouragement. Your advice, on both my research and my career, has been priceless.

I would also like to express my gratitude and thanks to the many people that contributed to my research, it wouldn't have been possible without their support. Thank you to committee member Dr. Hicham Fenniri for all your help with material characterization, advice, support, comments and suggestions. I would also like to thank several collaborators that provided the materials for these studies and did extensive characterization including Dr. Rachel Beingessner, Dr. Benoit Simard, Dr. Yadienka Martinez-Rubi, Dr. John Luong and Dr. John Veinot. Thanks to Dr. Benjamin Montgomery and Herman Cortes for all the help with cell culturing, cell transfections and assay development. I would also like to thank Geraldine Barron and Dr. Xuejun Sun for your help with confocal microscopy experiments.

I am also grateful to the many members of the Goss Lab group, past and present, that have contributed to my time at the University of Alberta. You have all been great collaborators and sources of friendship. I am especially indebted to Dr. Tyson MacCormack, Dr. Kimberly Ong, Dr. David

Boyle, Dr. Aga Dymowska, Van Ortega and Lindsey Felix for your help, support and friendship throughout the years.

A special thanks to my friends and family. Words cannot express how grateful I am for your love and support. To my parents, thank you for your unconditional support and for all the sacrifices you've made on my behalf. You're both a source of inspiration and this wouldn't have been possible without you. To my brothers and sisters-in-law, thank you for your encouragement and endless supply of laughs. Finally, I would like to express my gratitude to Anthony Auger for your constant encouragement, love and support. Your faith in me never faltered. I love you very much.

TABLE OF CONTENTS

LIST OF TABLES

LIST OF FIGURES

LIST OF ABBREVIATIONS

AF-CNTs	Acid functionalized CNTs
AFM	Atomic force microscopy
ANOVA	Analysis of variance
ASB	Antibody staining buffer
APS	Ammonium persulfate
B-cells	B lymphocytes
BET	Brunauer-Emmett-Teller
BSA	Bovine serum albumin
CNC	Cellulose nanocrystal
CNT	Carbon nanotube
CNT-30	Carboxylic acid functionalized CNTs oxidized at 30 °C
CNT-40	Carboxylic acid functionalized CNTs oxidized at 40 °C
CNT-50	Carboxylic acid functionalized CNTs oxidized at 50 °C
Co	Cobalt
CTL	Cytotoxic T lymphocyte
CVD	Chemical vapor deposition
DCF	Dichlorofluorescein
ddH_2O	Double distilled water
DLS	Dynamic light scattering
DDLS	Depolarized dynamic light scattering
DNP-HSA	Dinitrophenyl-human serum albumin
ELISA	Enzyme-linked immunosorbent assay
ERK	Extracellular signal-related kinases
FBS	Fetal bovine serum
FITC	Fluorescein isothiocyanate
FcεRI	High affinity receptors for IgE
FS	Forward scatter
GADS	GRB2-related adaptor protein
G□C	Guanine-cytosine
HA	Hemagglutinin
HARN	High aspect ratio nanomaterial
HD	Hydrodynamic diameter
HEK	Human embryonic kidney
ICP-AES	Inductively coupled plasma atomic emission spectrosco
Ig	Immunoglobulin
IgE	Immunoglobulin E
IgG	Immunoglobulin G
IgSF	Immunoglobulin superfamily
IL	Interleukin
IpLITRs	*Ictalurus punctatus* leukocyte immune-type receptor
ITP	Induction thermal plasma
K-RNT	Lysine functionalized rosette nanotubes
LAT	Linker for activation of T cells

mAb	Monoclonal antibody
MAPK	Mitogen activated protein kinase
MCC	Microcrystalline cellulose
MEM	Minimum essential media
MHC	Major Histocompatibility Complex
MTS	3-(4,5-dimethylthiazol-2-yl)-5-(3-carboxymethoxyphenyl)-2-(4-sulfophenyl)-2H-tetrazolium
Ni	Nickel
NM	Nanomaterial
NP	Nanoparticle
NT	Nanotechnology
P-CNTs	Pristine carbon nanotubes
pAb	Polyclonal antibody
PBS	Phosphate buffered saline
PFA	Paraformaldehyde
PI	Propidium iodide
PKC	Protein kinase C
PLCγ	Phospholipase $C\gamma_1$
RBL	Rat basophilic leukemia
RFU	Relative fluorescent units
RNT	Rosette nanotube
ROS	Reactive oxygen species
SD	Standard deviation
SE	Standard error of the mean
SEM	Scanning electron microscopy
SLP76	SH2-domain-containing leukocyte protein of 76 kDa
SS	Side scatter
TB	Twin based
TB-RGDSK	Arg-Gly-Asp-Ser-Lys functionalized G□C motifs
TB-TBL	butylamine functionalized G□C motifs
TBL-RNTS	butylamine functionalized rosette nanotubes
RGDSK-RNTs	RGDSK peptide functionalized rosette nanotubes
TEM	Transmission electron microscopy
T_H cells	T helper cells
T_C cells	T cytotoxic cells
T-cells	T lymphocytes
U-CNTS	Unfunctionalized CNTs
ζ	Zeta
ZP	Zeta potential

CHAPTER 1

Introduction

1.1 INTRODUCTION

Viewed by many as the next industrial revolution, the field of nanotechnology has experienced exponential growth over the last decade (Schultz, 2007). The rapid rise of nanomaterial (NM) development and production has been stimulated by the unique electronic, physical and chemical properties of these materials at the nanoscale. In addition, the increased reactivity of NMs due to their high surface area to volume ratio is being exploited in several applications and has contributed to the fields accelerating development. With many novel properties to be exploited, investment in NM research has seen tremendous growth. For example, between 1997 and 2005 the United States government funding for nanotechnology research increased from 116 million to over 1.7 billion (Schultz, 2007). Concomitant with this research has been the rapid expansion of nanotechnologies into the marketplace (De Volder et al., 2013). The advent of cost-effective, large-scale production of NMs means these materials are now being incorporated into products with commercial, industrial, medical and environmental applications (De Volder et al., 2013; Vardharajula et al., 2012).

Despite its rapid recent development, the field of nanotechnology has a long history. Credited as the start of modern nanotechnology, physicist Doctor Richard Feynman gave a landmark speech in 1959 entitled 'There is plenty of room at the bottom' where he outlined some of the significant advances that nanotechnology could provide. Although he didn't coin the

term ‘nanotechnology’, Feynman recognized the opportunity at the nanoscale for the storage of vast amounts of information (Feynman, 1960). In 1974 the term ‘nanotechnology’ was first introduced by Doctor Norio Taniguchi and was popularized in 1986 by Doctor Eric Drexler’s book ‘Engines of Creation: The Coming Era of Nanotechnology’ (Shew, 2008). Several discoveries of novel NMs spurred the development of nanotechnology including the buckyball in 1985, quantum dots in 1988 and carbon nanotubes (CNTs) in 1991 (Schultz, 2007). However, the use of NMs can be traced back much further in history. Artifacts dating back as early as the fifth century BCE indicate the Chinese and Egyptians were using gold NPs to colour glass and ceramic (Daniel and Astruc, 2004).

Currently there is debate over what the field of nanotechnology encompasses and contributing to this ambiguity, no formal definition of a NM exists (Shew, 2008). Even today, discussion continues on what size range and physico-chemical properties define a NM. The current working definition of a NP used by Health Canada is a material that ranges between 1 – 100 nm in at least one dimension, and/or has an internal or surface structure within 1 – 100 nm, and/or exhibits one or more nanoscale property or phenomenon (Health Canada 2011). Using this definition, NMs currently exist in atmospheric, terrestrial and aquatic environments, produced through natural processes such as volcanism or produced as unintended by-products, for example, in combustion of diesel fuels (Schultz, 2007). However, it is the intentional production and use of NMs that is fundamental to what we

currently call nanotechnology. These manufactured NMs are commonly known as engineered NMs and it is the exponential increase in their large-scale production and use that has been highlighted as a cause for concern (Maynard, 2006; Maynard et al., 2006). This thesis will focus solely on these engineered NMs and herein the term 'nanomaterial' will refer to only intentionally produced NMs.

Rapid development of large-scale production of NMs means these materials are being produced and potentially released to the environment. The ability to predict the magnitude of NMs that will reach the environment has been identified as a major hurdle in the risk assessment of NMs (Hendren et al., 2011). This is due, in part, to a lack of data on the current production levels. Current regulations do not require the reporting of NM production unless the NMs have unique structural forms or molecular arrangements compared to their bulk counterparts (CEPA 2007). While voluntary inventories such as the 'Project on Emerging Nanotechnologies' do exist, a lack of reliable data makes NM production estimates remarkably difficult. Most attempts to quantify production levels of NMs explicitly state the uncertainty in their estimations due to poor data quality; best estimates of some NMs based on largely extrapolated data suggest upper limits of production in the United States of 38,000 tons per year of nano-titanium dioxide, 20 tons per year of nano-silver, 700 tons per year of nano-cerium oxide, 1,101 tons per year of carbon nanotubes and 80 tons per year of fullerenes (Hendren et al., 2011).

1.2 NANOTOXICOLOGY

The exponential increase in nanotechnology research and concomitant increase in NM production led to reports questioning the safety and associated risks of NP use (Nel et al., 2006; Oberdörster et al., 2005). These concerns led to studies that began examining the biological effects of NMs and would form what is now the field of Nanotoxicology. As nanotechnology research and production continues its exponential increase, thorough and extensive research on NMs and their biological interactions is required to ensure proper regulation and safe development of these materials. However, NMs display several unique physico-chemical properties that have presented challenges to toxicologists as classical protocols for toxicants such as metals, solvents and pesticides are not always appropriate (Ong et al., 2014). As a result of these challenges, nanotoxicology research has lagged behind research in nanotechnology and nanomaterials.

1.2.1 Challenges in nanotoxicity testing

As an emerging discipline, there were many early issues in nanotoxicity testing. Batch to batch inconsistency in NM production, unreliable characterization data from manufacturers and the use of toxic solvents to disperse NMs resulted in reports that often contradicted one another and ultimately slowed research progress (Henry et al., 2011; Klaine et al., 2008; Park and Grassian, 2010). At the heart of these issues was a lack of technology to reliably characterize the materials being tested and

scientists could only report the chemical composition, purity and exposure concentration of NMs. Such information was sufficient in the toxicological evaluation of classical toxicants such as metals; however, reports began emerging that physico-chemical characteristics of NMs such as shape, size, surface functionalization and agglomeration changed the behavior of NMs and ultimately affected the toxicity of these materials (see section 1.2.2 below) (Fubini et al., 2010). Several prominent publications began emphasizing a more complete characterization of NMs physico-chemical characteristics in order to progress our understanding of nanomaterial toxicity including characterization in more complex biological media and physiological fluids (Burleson et al., 2012; Holsapple et al., 2005; Oberdörster et al., 2005).

Unfortunately, the characterization of these materials is still a major limiting factor in the field of nanotoxicology. Often, complete characterization of materials is not possible with available techniques, especially in a complex medium such as cell culture media containing serum. For example, dynamic light scattering (DLS) is a technique employed to calculate NM size (hydrodynamic radius) by measuring the translational diffusion coefficient of NMs in solution. However, there are several limitations of DLS that often prevent NM characterization in the complex mixture of proteins, vitamins, lipids and salts that constitute serum supplemented cell culture media. DLS calculations of hydrodynamic radius have an inherent bias towards the largest particles present, limiting its

applications for size analysis of polydisperse systems (Anderson et al., 2013). Balog et al., (2015) found that the biomolecules present in serum supplemented cell culture media introduced significant light scattering that completely prevented the accurate characterization of suspended gold NMs hydrodynamic radius. DLS also requires well dispersed suspensions and NMs that agglomerate in solution are not accurately characterized with this technique (Rai et al., 2007). NM architecture also influences the accuracy of DLS measurements. Non-spherical NMs undergo slow translational diffusion perpendicular to their axis and fast translational diffusion parallel to their axis. This means the reported hydrodynamic diameter for high aspect ratio nanomaterials is not equal to either their diameter or their length (Boluk and Danumah, 2014). Several other techniques have also been used in an attempt to characterize NM suspensions including transmission electron microscopy (TEM), scanning electron microscopy (SEM) and atomic force microscopy (AFM); however, microscopy techniques typically measure NM size under dry states not necessarily representative of size in suspension and often introduce artifacts during sample preparation (Pal et al., 2014). What this highlights is that even with a variety of available techniques, characterization of basic physico-chemical parameters of NMs in complex mediums is still a major limiting factor in nanotoxicological assessment. Another limiting factor in NM characterization, the techniques to characterize materials at the nanoscale often require expensive equipment that requires extensive training and expertise. Access to these facilities is

often a major hurdle in nanotoxicological evaluations and has fostered collaboration between nantoxicologists, chemists, engineers and physicists.

Critical in any toxicological evaluation is the correct assessment of the dose-response relationship. However, even the metrics for dosage have posed a challenge in nanotoxicology. Traditionally in toxicology dose was defined gravimetrically; the majority of nanotoxicity studies to date have followed this approach, basing exposure on the mass of the NMs (Dhawan and Sharma, 2010; Rivera-Gil et al., 2013). However, several studies have suggested surface area to be a better predictor of toxicity of NMs and suggest it may be a more appropriate dose metric. The large increase in surface area associated with decreasing particle size to the nanoscale range has a concomitant increase in surface reactivity and as such, many studies have considered surface area as their dosing metric (Dhawan and Sharma, 2010; Oberdörster et al., 2007). Alternatively, others have suggested particle number is the most appropriate dosing metric. For example, Wittmaack (2007) concluded that particle number is the most appropriate dosing metric for predicting NP toxicity after comparing four different dosing metrics including number of particles, joint length, Brunauer-Emmett-Teller (BET) measured surface area and calculated surface area.

Aside from choosing the actual dose metric, there are other factors to consider in the dosimetry of *in vitro* nanotoxicity studies. Three levels of NM exposure have now been defined: administered dose, delivered dose and cellular dose based on the kinetics of NMs in solution (Teeguarden et al.,

2007). Administered dose is most commonly reported and represents the media concentration of NMs. However, depending on their physico-chemical properties, NMs can interact with each other or media components causing agglomeration or dispersion and ultimately affecting how NMs behave in solution. This has the consequence of changing the effective dose cells are exposed to and has important implications for nanotoxicological assessment; in some cases, administered and cellular dose differ by several orders of magnitude (Teeguarden et al., 2007).

Nanotoxicologists must also determine if many of the classical toxicity testing protocols are appropriate for nanotoxicity testing. With many factors of NMs contributing to changing toxicity, toxicity endpoints such as LC50 may not be possible or informative given the vast number of different materials being produced. In addition, many assays classically used in toxicological evaluations rely on multi-step biochemical reactions involving proteins and/or reagents. These reactions commonly cause a change in absorbance, fluorescence or luminescence that can be quantified to provide information on cellular or biochemical endpoints. However, the unique physico-chemical properties of NMs have been demonstrated to interfere with many of these assays classically used to gauge toxicity. Such NM properties include high absorption capacity, optical properties, catalytic activity, and magnetic properties (Kroll et al., 2009). We have published data showing inconsistencies with many biochemical assays including protein quantification assays, cell proliferation assays and cell viability

assays (Ong et al., 2014).

Due to the many different types of NMs and their varied formulations, the mechanism of interference in toxicological assays appear equally diverse. For example, carbon nanotubes (CNTs) have been documented to interact with a variety of indicator dies used in cytotoxicity evaluations. CNTs bind formazan crystals and stabilize their chemical structure (Wörle-Knirsch et al., 2006). Their unique high aspect ratio architecture makes this effect unique to CNTs. NMs unique properties have also been shown to prevent receptor-ligand binding, a mechanism utilized in several nanotoxicological assays. For example, NMs absorptive properties have been documented to interfere with antibody binding in apoptosis assays and enzyme linked immunosorbent assay (ELISA) (Monteiro-Riviere et al., 2009; Ravi Shukla et al., 2005). Enzyme catalyzed reactions are often a feature of toxicological assays and NMs have been documents to bind enzymes and inhibit their activity (Maccormack et al., 2012). Other NMs optical properties have been shown to interfere with the fluorescence emission of reagents such as dichlorofluorescein (DCF) (Aam and Fonnum, 2007) or affect absorbance, such as titanate nanoparticles (Davis et al., 2007).

Due to the unique nature of NMs, many assays used to assess toxicity need to be re-evaluated. These findings demonstrate that a large consideration in toxicity testing of NMs is assay validation. This is especially concerning given that approximately 95% of papers from 2010 surveyed did not run appropriate controls to account for this assay interference and may

contribute to the conflicting reports on NM toxicity (Ong et al., 2014).

1.2.2 Physico-chemical characteristics affecting nanomaterial toxicity

Due to the number of unique NMs that are being produced, toxicological evaluation of NMs has moved away from assessments of individual formulations of NMs and towards understanding the physico-chemical parameters of materials that are key determinants of toxicity. The evaluation of NM toxicity includes consideration of viability endpoints as well as a variety of functional endpoints including DNA synthesis and damage, altered gene expression, immunogenicity and oxidative stress (Love et al., 2012). The discussion below focuses on physico-parameters identified as important determinants of high aspect ratio nanomaterial (HARN) toxicity.

1.2.2.1 Dimensions

The overall length of HARNs has been shown to affect their toxicity. Poland et al. (2008) documented that the asbestos like-toxicity observed in mice after CNT exposure was length-dependent. Exposure to long CNTs (bundles >15 μm) produced granuloma formation and inflammation while short CNTs (bundles < 5 μm) did not. Murphy et al. (2012) found the cytotoxic and pro-inflammatory response in human macrophages (THP-1) following CNT exposure was also length dependent, with significantly elevated release of cytokines IL-1β, TNF-α, IL-6 and IL-8 following exposure to long (bundles >15 μm) CNTs only. The authors suggest that the toxicity

they observe was a consequence of frustrated phagocytosis, the impaired uptake of long CNTs by cells (Murphy et al., 2012). A similar finding showed frustrated phagocytosis of long CNTs that caused the released of TNF-α and reactive oxygen species (ROS) from monocytic cells (Brown et al., 2007) and several other studies have reported similar length-dependent toxicity of CNTs (Sato et al., 2005; Yamashita et al., 2010). Interestingly, Liu et al. (2012) demonstrated that long CNTs (>3-14 μm) were more cytotoxic compared to short CNTs (<1.5 μm); however, both long and short CNTs induced release of pro-inflammatory mediators and ROS production in RAW-264.7 cells.

1.2.2.2 Charge

Surface charge is another physico-chemical parameter affecting NM toxicity (Liu et al., 2012). Surface charge affects the agglomeration of NMs in solution, and the state of agglomeration is another parameter linked to NM toxicity (see section 1.2.2.3). In general, the introduction of surface charge to NMs causes electrostatic repulsion so they resist agglomeration and stay suspended in solution (Rivera-Gil et al., 2013).

NM surface charge has also been shown to affect the interaction of these materials with biological membranes, lead to differential uptake of NMs in cells and has important implications for material toxicity (Arvizo et al., 2010). The negatively charged cell membrane surface (Verma and Stellacci, 2010) has been hypothesized to attract and adsorb positively charged NMs

while minimizing interactions with negatively and neutrally charged NMs (Park et al., 2011). This notion has been supported by several studies. For example, Arvizo et al. (2010) examined the effect of positive, negative, neutral and zwitterionic gold NM exposure to several cell lines and found that positively charged NMs interacted with and destabilized the plasma membrane, caused depolarization, reduced viability and induced apoptosis; no effects were observed for negative, neutral or zwitterionic gold NMs. Several studies have also demonstrated that coating NMs with a neutral ligand such as poly(ethylene glycol) dramatically reduces the cellular uptake and toxicity of NMs (Chang et al., 2005; Xie et al., 2007). However, many reports have demonstrated the internalization and toxicity of both negatively and neutrally charged NMs (Verma and Stellacci, 2010; Zhang and Monteiro-Riviere, 2009) and suggests that although negative charges may not prevent NM internalization, charge does influence the rate and/or mechanism of uptake (Cho et al., 2009; Park et al., 2011). For example, Cho et al., (2009) found internalization of neutrally, negatively and positively charged NMs; however, NMs with a neutral and negative surface charge had significantly reduced adsorption on the cellular membrane and consequently lower levels of internalization compared to NMs with a positive surface charge. In agreement, other studies have found that differential NM surface charge impacts the mechanism of internalization and consequentially affects the rate of uptake and toxicity of NMs (Harush-Frenkel et al., 2008; Kim et al., 2013).

Additional complexity arises in relating charge to cellular uptake and toxicity due to the modification of material charge characteristics in solution, including interactions with various biomolecules and with properties of the media such as pH (Bian et al., 2011; Park et al., 2011). For example, Mahmoud et al. (2010) found limited cellular uptake of negatively charged FITC functionalized cellulose nanocrystals (CNCs) in HEK-293T cells; however, manipulation of media pH from 8.0 to 5.0 caused a corresponding change in FITC-CNC ζ-potential, increasing from -48.7 mV to -3.9 mV. The more positive CNC surface charge in pH 5.0 was associated with significantly elevated CNC internalization (Mahmoud et al., 2010).

In addition to the overall surface charge of NMs, alterations in NM surface charge density has been shown to impact the cellular association and toxicity of NMs. In modeled simulations of gold NMs, materials with a high cationic surface charge density caused significantly increased penetration and disruption of cellular membranes compared to low charge density cationic gold NMs (Lin et al., 2010). The disruption of lysosomal membranes by carbon NMs has been proposed as a major mechanism of CNT toxicity (Tahara et al., 2012).

1.2.2.3 Agglomeration

The degree and type of agglomeration of NMs have been shown to impact toxicity and is influenced by a number of factors including NM size, NM charge, NM surface functionalization, and several characteristics of the

suspending media (Fubini et al., 2010). In general, materials that are well dispersed and suspended in solution have shown reduced toxicity compared to materials that form large agglomerates. For example, well dispersed CNTs had significantly reduced cytotoxic effects in human MSTO-211H cells compared to the same material in its agglomerated state (Wick et al., 2007). Agglomeration and subsequent sedimentation of NMs on the cell surface effectively concentrates these materials, resulting in increased toxicity (Laurent et al., 2012). In addition, the type of agglomeration in HARNs is an important determinant of their toxicity. Palomaki et al. (2011) found that CNTs that formed long, parallel, bundled agglomerates in solution induced the secretion of pro-inflammatory cytokines from human primary macrophages while CNTs that formed tangled, spherical agglomerates did not. The authors suggest that CNTs pro-inflammatory effects result from the activation of the NLRP3 inflammasome through CNT-induced reactive oxygen species (ROS) formation in macrophages (Palomäki et al., 2011).

1.2.2.4 Surface functionalization

There are several strategies for the covalent and non-covalent functionalization of NMs to a variety of molecules. The multitude of potential functionalizations has resulted in an equal number of unique NMs each with unique physico-chemical properties. Important in the toxicological evaluation of NMs is examining how surface functionalization alters the physico-chemical parameters of that material and the potential impact on

toxicity. For example, CNTs are frequently oxidized to yield carboxylic acid groups on their ends or sidewalls (Price et al., 2009). The introduction of carboxy-functionalization alters several of the physico-chemical parameters described above, including dispersibility and aggregation, surface charge and architecture all with potential impacts on toxicity (Price et al., 2009). Difficulty in assessing the toxicity of NMs arises from the manipulation of several physico-chemical parameters simultaneously with new functionalizations and represents an on-going difficulty in nanotoxicity assessment.

1.2.2.5 Interactions with biomolecules

In biological matrices, NMs have been shown to interact with a wide variety of biomolecules including vitamins, polysaccharides, amino acids, nucleic acids, lipids and proteins (Nel et al., 2009). These interactions change the surface chemistry of NMs and can ultimately change their toxicity in different mediums (Shemetov et al., 2012). The affiliation of various biomolecules with NMs has been proposed as a mechanism of NM cytotoxicity. For example, Casey et al. (2008) found that CNTs deplete cell culture medium of essential nutrients vital to cells. Another study by Guo et al. (2008) found that suspension of CNTs in cell culture medium significantly altered the micronutrient content by adsorbing amino acids and vitamins at doses as low as 0.01 mg L^{-1}. This altered medium resulted in reduced HepG2 cell viability.

Of the various biomolecules shown to associate with NMs, proteins in particular form complex associations with NMs upon their introduction into biological media with important consequences for toxicity. Adsorbed proteins are organized into a dynamic protein corona that is continuously exchanging with proteins in the environment (Lundqvist et al., 2008). These exchanges have led to the designation of a soft protein corona characterized by frequent and rapid exchange of protein constituents and a hard protein corona, comprised of proteins with a high affinity for the NM surface (Cedervall et al., 2007; Lundqvist et al., 2008). A wide variety of proteins from several classes have been shown to associate with NMs and include immunoglobulins, lipoproteins, complement proteins, acute-phase proteins and coagulation factors (Lundqvist et al., 2008). CNTs in particular have shown an affinity for albumin, immunoglobulins, complement and fibrinogen; however, the formation of protein coronas is NM specific and varies based on NM hydrophobicity, size, radius of curvature, charge and steric or electrostatic effects of surface functionalizations (Linse et al., 2007; Lundqvist et al., 2008; Nel et al., 2009; Owens and Peppas, 2006). Protein coronas are important determinates of NM toxicity, impacting how NMs behave in biological matrices. The formation of a protein corona alters the surface properties of NMs, changing several physico-chemical parameters including the charge and aggregation of NMs in solution with implications for toxicity (Nel et al., 2009). The adsorption of proteins on NMs can also affect their transportation, cellular uptake and activity. For example,

apolipoprotein complexes, important in transporting lipids and cholesterol, are bound by multiple receptors for cellular internalization. Apoliproteins have also been shown to adsorb to CNTs and could therefor significantly affect the intracellular uptake and fate of CNTs (Lundqvist et al., 2008). The adsorption of immunoglobulins and complement leads to NM opsonization and could cause recognition by the immune system and promote receptor mediate phagocytosis (Nel et al., 2009). In addition, the formation of a protein corona has been shown to induce conformational changes in constituent proteins; these changes could cause the exposure of new epitopes or alter the function of bound catalytic proteins with potential impacts on NM toxicity (Maccormack et al., 2012; Stueker et al., 2014).

1.2.2.6 Other parameters

Several other parameters not discussed here have been implicated in the toxicity of NMs. For example, core composition and rate of core dissolution has important consequences on the toxicity of metal oxide NMs (Ortega et al., 2013; Shaw and Handy, 2011) and the level of hydrophobicity of NMs has been implicated as a determinate of toxicity by affecting interactions with cellular membranes (Nel et al., 2009). The above characteristics are do not represent a comprehensive summary of the determinates of NM toxicity, rather they focus on some of the highlighted physico-chemical properties of HARNs that contribute to their toxicity. Linking physico-chemical parameters to toxicity has proven to be challenging

for nanotoxicologists given that many of these parameters are interdependent and depend on exposure conditions.

1.2.3 Models in Nanotoxicology

Thorough NM testing requires inquiry across all levels of biological organization, ranging from biochemical alterations to cellular effects to whole animal responses and ultimately consequences on ecosystems (**Figure 1-1**) (Dhawan and Sharma, 2010). Testing at each level of inquiry has its associated strengths and drawbacks, but each is necessary to form a holistic picture of nanotoxicity. Highlighted in the literature is the need to include more biochemical, cellular and physiological effects of NMs and examine the mechanisms by which NPs cause their effects (Nel et al., 2013). The focus of this thesis will be at the lower end of the continuum, at the molecular and cellular level of biological organization utilizing *in vitro* models. This level of inquiry has several advantages. Time scale is an important consideration, and working at the cellular level allows inquiry from seconds to hours. As one progresses up the continuum, processes at the community and ecosystem level can occur over years and even decades adding huge complexity to scientific inquiry and demanding considerable resources to complete such studies. In addition, working at the molecular and cellular level means specific biomarkers can be used to assess cause-and-effect relationships under simplified and controlled experimental conditions. This allows examination of the mechanisms behind the modes of action of NMs, an

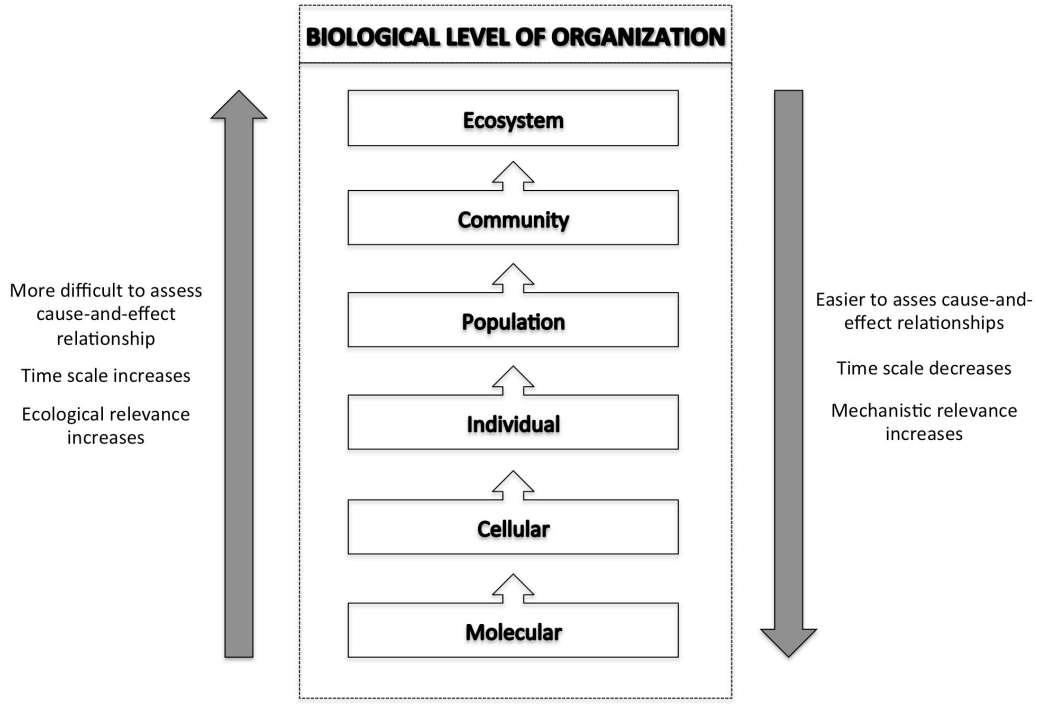

Figure 1-1. Levels of inquiry for nanotoxicity assessment. The focus of this thesis is examining nanotoxicity at the molecular and cellular level of biological organization to contribute to a holistic picture of nanotoxicity.

important factor in nanotoxicological evaluation. The use of *in vitro* models with their relative ease to perform, control and interpret means a large amount of data can be generated. This is in addition to the more obvious advantages of *in vitro* testing including the relatively lower cost compared to *in vivo* studies, the ethical obligation to reduce animal testing and the high through-put efficiency of *in vitro* studies. These benefits mean *in vitro* studies will be essential in contributing to nanotoxicity assessment given the vast number of unique NMs being produced every year. There are, of course, a number of disadvantages in studying the molecular and cellular levels of biological organization and in using *in vitro* systems. One major drawback to i*n vitro* experimentation is that these represent highly simplified systems, and it can be a challenge to extrapolate the results to higher levels of biological complexity. A complete picture of nanotoxicity will only be gained by studying all levels of biological organization and utilizing *in vitro* and *in vivo* systems.

Given the vast amount of NMs being produced a predictive toxicological approach to NM testing has been proposed, using high through-put *in vitro* screening to correlate physico-chemical properties of NMs with toxicological responses (Nel et al., 2013). However, correlating physicochemical properties and toxicological responses is not straightforward and has proven to be a challenge to nanotoxicologists. Basic physicochemical properties such as colloidal stability, size, shape, charge, and absorptive capacity can change based on the environment NMs are placed in,

and, as highlighted above, can be difficult to characterize in complex matrices. In addition, many of these properties are strongly interconnected and it can be a challenge to isolate and vary an individual physico-chemical property while controlling others (Rivera-Gil et al., 2013). Others have argued for the introduction of more complex scenarios, incorporating complex abiotic factors to NM testing to more accurately reflect NM exposure conditions (Kammer et al., 2012; Klaine et al., 2008). What these highlight is the careful choice of experimental design. Due to the unique characteristics of NMs, they are being developed for a myriad of applications. These applications need to be considered during NP development and toxicity testing. Biomedical NPs may be designed for biocompatibility and intracellular localization while those NPs for use in personal care products might be engineered for minimal interactions (Cormode et al., 2009; Cross et al., 2007). Predicting the fate of NMs and how they might interact with biological matrices will help toxicologists in choosing the types of tests to investigate NM toxicity.

1.3 IMMUNOTOXICOLOGY

The evaluation of the immunomodulatory potential of NMs is one level of inquiry required for a nanotoxicity assessment. NM interactions with components of the immune system is an important consideration given that initial recognition of NMs by the immune system is an essential determinate for the fate, distribution and biocompatibility of these materials

in the body (Hussain et al., 2012). In addition, declines in immune cell viability or functional impairments in immunity incited by these NMs will contribute to the compatibility of these materials and could lead to a state of immunosuppression or immunostimulation (**Figure 1-2**) within the organism. Nano-immunotoxicity is defined as any adverse effect on the immune system or its function that results from exposure to NMs (Hussain et al., 2012). Potential adverse effects on the immune system from exposure are broadly classified into five categories: immunosuppression, immunogenicity, hypersensitivity, autoimmunity and adverse immunostimulation (Hussain et al., 2012). Such immune dysfunction could contribute to susceptibility to disease, autoimmunity or allergy with consequences on whole animal viability. Given that many NMs are being developed for deliberate introduction into the body for medical applications, nano-immunotoxicity is a particularly important endpoint to consider.

The immune system is a system of interacting tissues, effector cells and molecules that protect an organism against foreign pathogens. We commonly divide this complex network into the innate and adaptive divisions; however, these responses are really integrated and work in concert. The overview presented here is not meant to be exhaustive, but provide a basic framework of the immune response.

1.3.1 Innate and adaptive immunity

Innate immunity is commonly referred to as the first line of defense against infection as its components are present before the onset of infection and are capable of immediately responding to pathogens. Innate immunity consists of both humoral components, which includes macromolecules such as antibodies and complement proteins in extracellular fluids, and cellular components, which includes the various cells of immunity including both myeloid and lymphoid cells. Myeloid cells arise from a common progenitor and include granulocytes such as basophils, eosinophils and neutrophils, as well as macrophages. Lymphoid cells include T lymphocytes (T-cells), B lymphocytes (B-cells) and natural killer cells. Innate immunity constitutes a series of mechanisms that are not specific to any particular pathogen; rather, the cellular and molecular components of innate immunity recognize or defend against broad classes of molecules found on common pathogens (Goldsby, Immunology 5th edition). These non-specific defenses form the four types of defensive barriers: anatomic, physiologic, phagocytic and inflammatory (Hussain et al., 2012). Anatomic barriers include the skin and mucous membranes that prevent the entry of pathogens into an organism (Hussain et al., 2012). Physiologic barriers include organismal temperature and pH that prevent the growth of many microorganisms (Hussain et al., 2012).

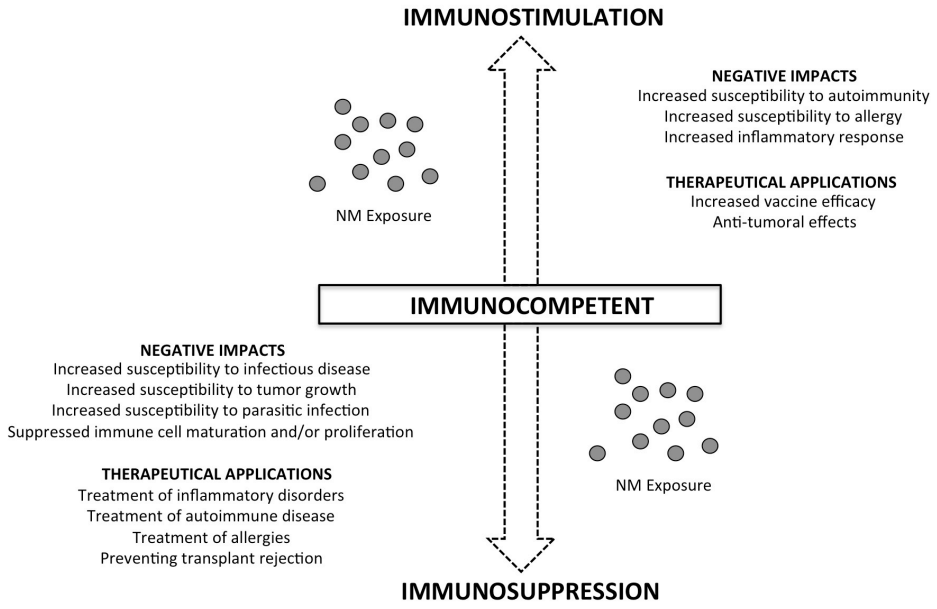

Figure 1-2. Nanomaterial exposure can lead to states of immunostimulation or immunosuppression. Immunostimulation refers to adverse, inappropriate or uncontrolled activation of a component of the immune system and can result in increased susceptibility to autoimmunity, allergy or inflammation. Immunosuppression refers to decreased immune function resulting from impairment in a component of the immune system. Potential consequences of immunosuppression include increased susceptibility to infectious disease, tumor growth and parasitic infection as well as suppressed immune cell maturation and/or proliferation.

Another significant contributor to innate immunity is the phagocytic barrier, made up of cells that ingest extracellular material, including pathogenic microorganisms, through phagocytosis and is conducted mostly by specialized cells such as blood monocytes, neutrophils, and tissue macrophages (Rabinovitch, 1995). Lastly, inflammation constitutes the fourth non-specific defense utilized in innate immunity and refers to a complex sequence of events that serves to stimulate the immune response (Dwivedi et al., 2011; Hussain et al., 2012). Mediators derived from invading microorganisms, released from damaged cells or released by immune cells initiate inflammation. A major mediator of inflammation is histamine, a chemical released by a variety of cells (Naal et al., 2004).

Adaptive immunity is mediated by cellular and molecular components that require exposure to an antigen before they are capable of responding (Fadeel, 2012). Adaptive immunity responds to antigens with a high degree of specificity, although this response can take several days to mount after antigen exposure. Subsequent exposure to the antigen results in a quicker and stronger adaptive immune response, a characteristic referred to as memory. Fundamental to adaptive immunity is cooperation between two large groups of cells referred to as antigen-presenting cells and lymphocytes (Jovanović and Palić, 2012). Antigen-presenting cells, which include macrophages, dendritic cells and B lymphocytes, internalize antigens and subsequently display a part of that antigen on the extracellular surface of their membrane bound to class II major histocompatibility complex (MHC)

for presentation to lymphocytes. Antigen-presenting cells also release co-stimulatory signals that lymphocytes require for activation (Goldsby, Immunology 5th edition).

Lymphocytes display antigen-binding cell surface receptors and are responsible for the specificity of the adaptive immunity. There are two major populations of lymphocytes: B lymphocytes (B cells) and T lymphocytes (T cells). B-cells display membrane bound antibodies that when bound by an antigen and appropriately stimulated, differentiate into memory B-cells and plasma cells. Plasma cells produce and secrete antibody, the major effector molecule of humoral immunity, while memory B cells are activated on subsequent exposures to the antigen, contributing to the memory of adaptive immune responses (Goldsby, Immunology 5th edition). T cells express a T-cell receptor on their membrane that recognize antigens bound to MHC molecules and consists of two major subpopulations: T helper (T_H) and T cytotoxic (T_C) cells. Class I MHC is present on all nucleated cells in the body while antigen-presenting cells express Class II MHC. T_H cells are activated when they recognize a foreign antigen bound in a Class II MHC complex and results in the secretion of cytokines responsible for activating various cells participating in the immune response including B cells, T_C cells and macrophages. T_H cells are important in determining the course of an immune response. A T_H1 response results in the release of cytokines that supports inflammation and T-cell activation; alternatively, a T_H2 response results in the release of cytokines that support B-cell activation. In the development of

a T_H 1 response, T_C cells proliferate and differentiate into cytotoxic T lymphocytes (CTL) when they recognize a foreign antigen bound in a Class I MHC complex and are simultaneously activated by T_H cells. CTLs exhibit cytotoxic activity and are major effectors of cell-mediated immunity (Goldsby, Immunology 5th Edition).

Investigations into the immunotoxicity of NMs includes cell lines that span the cell types involved in both innate and adaptive immunity. Interactions with each cell type is informative and has important implications for how NMs may ultimately affect immunity. The effects of select NMs on macrophages (eg. Klaper et al., 2010; Lucarelli et al., 2004), mast cells (eg. Wingard et al., 2011), neutrophils (eg. Ortega et al., 2013), eosinophils, natural killer cells (eg. Gustafsson et al., 2011), T lymphocytes and B lymphocytes (eg. Ogunwale et al., 2009) have been investigated. However, as discussed above, the immunotoxicology of NMs is complex, and reports of both immunostimulation and immunosuppression have been reported and an assessment of all NMs is far from complete (Hussain et al., 2012). Highlighted specifically, few investigations have examined the effects of NMs on the tissues, cells and molecules involved in adaptive immunity (Hussain et al., 2012; Jovanović and Palić, 2012).

1.3.2 *In vitro* immune models of nanotoxicology

As the field of nano-immunotoxicology has expanded, researchers have utilized several *in vivo*, *ex vivo* and *in vitro* model systems. A thorough

investigation into the immunotoxicity of NMs must span all these domains, as each has its associated strength and drawbacks as discussed above. Discussing all the models utilized is beyond the scope of this discussion; rather, we will highlight the model systems used during the course of my thesis.

1.3.2.1 Mammalian Models

1.3.2.1.1 Rat basophilic leukemia (RBL)-2H3 cell line

I utilize the rat basophilic leukemia (RBL)-2H3 cell line to investigate the effect of NM exposure on granulocyte viability and function. Granulocytes, and mast cells in particular, are crucially located at the host's interfaces with the environment such as the lungs, skin and mucosal surfaces (Gibbs et al., 1997). When stimulated, granulocytes release the contents of granules contained in their cytoplasm. These granular mediators are important in the allergic response and include histamine, serotonin and β-hexosaminidase (Naal et al., 2004). Granulocytes also play an important role in inflammation, recruiting immune cells through the release a variety of cytokines and chemoattractants (Passante et al., 2009). Granulocytes are a fundamental component of innate immunity; however they are also involved in several pathological conditions such as asthma, allergy and anaphylaxis (Abraham and John, 2010). Together, this makes granulocytes an important model to investigate the effects of NM exposure.

RBL-2H3 cells have been utilized as a model granulocyte in studies of allergy and inflammation. In particular, they have been employed in immunological research to study the regulated degranulation of mast cells through FcεRI, a high affinity receptor for IgE. These studies have contributed significant molecular and biochemical characterization of IgE-FcεRI mediated degranulation, including the underlying signal transduction events (Abraham and John, 2010). This knowledge makes RBL-2H3 a powerful model to examine the capacity of toxicants and new drugs to alter mast cell activation (Granberg et al., 2001). We utilized IgE-FcεRI mediated degranulation in RBL-2H3 cells to study the effect of NM exposure on the ability of granulocytes to elicit appropriate receptor-mediated effector functions.

1.3.2.1.2 IgE-FcεRI mediated degranulation

RBL-2H3 cells express FcεRI, a high affinity receptor for IgE, on their surface. FcεRI binds IgE in a process termed sensitization. Aggregation of IgE-FcεRI complexes through antigen binding generates a complex cascade of intracellular events that leads to degranulation (**Figure 1-3**). FcεRI aggregation results in the phosphorylation of adaptor molecule, linker for activation of T cells (LAT). Phosphorylation of LAT results in formation of a macromolecular signaling complex formed from the direct or indirect binding of several factors including signaling enzyme phospholipase Cγ_1v

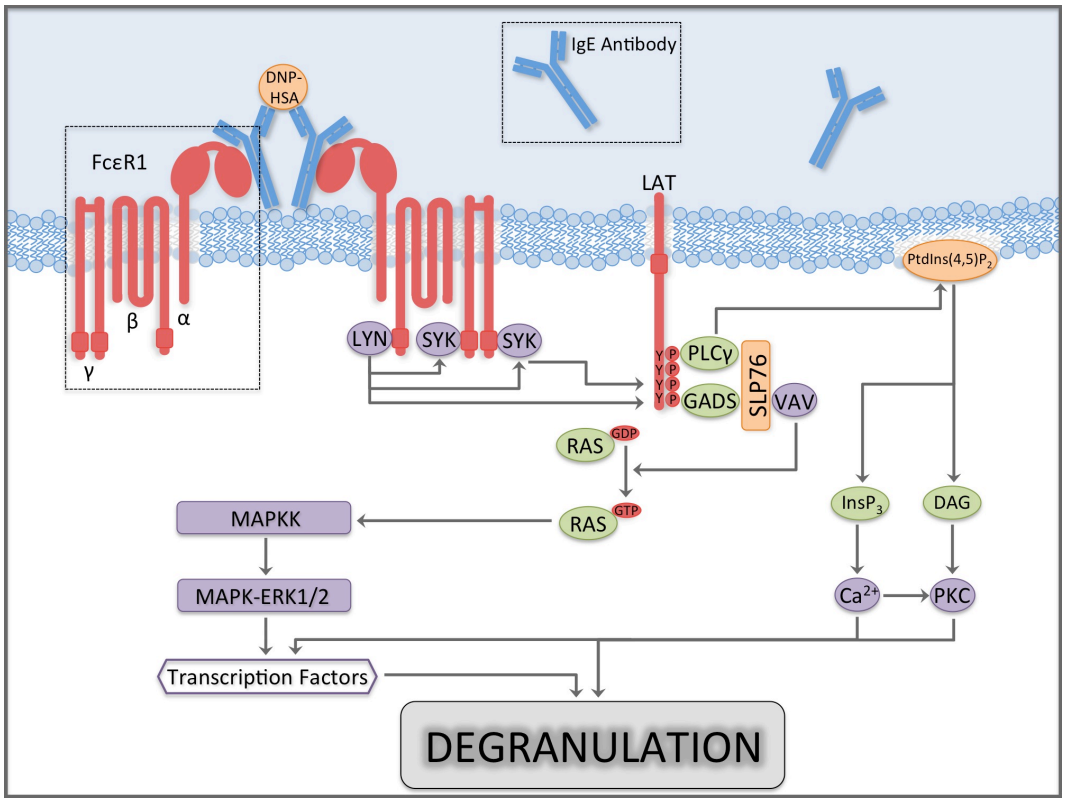

Figure 1-3. Summary of IgE-FcεRI mediated degranulatory signaling cascade in RBL-2H3 cells. Aggregation of IgE-FcεRI complexes following antigen binding result in phosphorylation of linker for activation of T-cells (LAT). LAT phosphorylation results in recruitment of several factors that form a macromolecular signaling complex and results in activation of protein kinase C (PKC), calcium mobilization and activation of mitogen activated protein kinase (MAPK) that trigger degranulation. Adapted from Gilfillan and Tkaczyk (2006) and Metcalfe (2008).

(PLCγ), cytosolic adaptor proteins GRB2-related adaptor protein (GADS) and SH2-domain-containing leukocyte protein of 76 kDa (SLP76), and guanine nucleotide exchange factor VAV (Gilfillan and Tkaczyk, 2006). Assembly of this signaling complex results in activation of protein kinase C (PKC), calcium mobilization, and activation of mitogen activated protein kinase (MAPK) pathway triggering degranulation and leading to cytokine production (**Figure 1-3**)(Gilfillan and Tkaczyk, 2006).

Degranulation releases a variety of chemical mediators including histamine, serotonin and β–hexosaminidase (Huang et al., 2009). We use the β–hexosaminidase release assay to assess degranulation in RBL-2H3 cells following or concurrent with NM exposure. In this assay, β-hexosaminidase activity is quantified using a fluorometric enzyme substrate (methylumbelliferyl-N-acetyl-β-D-glucosaminide) which when cleaved by β-hexosaminidase produces the fluorescent product methylumbelliferone (Naal et al., 2004).

1.3.2.2 Teleost Models

1.3.2.2.1 Channel catfish (Ictalurus punctatus) cell lines

I utilized channel catfish, *Ictalurus punctatus,* to investigate the effect of NM exposure on fish lymphocyte viability and function. To date, only a few studies have examined the effect of NM exposure on fish leukocytes (Jovanović et al., 2011b; Klaper et al., 2010; Ortega et al., 2013) and the effects of NM exposure on fish lymphocytes (i.e. B-cells and T-cells) has been

highlighted as requiring investigation (Jovanović and Palić, 2012). Channel catfish have been utilized as an important model for studying fish immunology and have several distinct, characterized, leukocyte cell lines including myeloid cells (macrophages/monocytes) and lymphoid cells (B-cells, cytotoxic T-cells, noncytotoxic T-cells and NK-like cells)(Stafford et al., 2006; Majji et al., 2009; Miller et al., 1994). In this thesis, we specifically focus on examining the effect of NM exposure to lymphoid fish cells, including two B-cell-like cell lines, 3B11 and 1G8, and one T-cell-like line, 28S.3.

1.3.2.2.2 IpLITR-mediated phagocytosis

As an important immunological model, several studies have identified and characterized the structure and function of catfish surface receptors that belong to the immunoglobulin superfamily (IgSF) (Bengtén et al., 2006; Montgomery et al., 2011) including channel catfish leukocyte immune-type receptors (IpLITRs) (Cortes et al., 2014; 2012; Montgomery et al., 2012). IpLITRs are expressed on myeloid and lymphoid subsets with both stimulatory and inhibitory forms that work in concert to coordinate and regulate fish immune cell effector responses, including degranulation and phagocytosis (Cortes et al., 2014; 2012). We utilize IpLITRs to examine the ability of this fish immune receptor to elicit appropriate effector responses following NM exposure. For these assays, the uptake of fluorescently labeled

beads is used to quantify IpLITR-mediated phagocytosis using flow cytometry.

1.4 MATERIALS

1.4.1 High aspect ratio nanomaterials

HARNs are broadly defined as NMs with an architecture where one dimension greatly exceeds the others; the HARNs studied in this thesis all had an aspect ratio (length:diameter) exceeding 20:1 and includes rosette nanotubes (RNTs), carbon nanotubes (CNTs) and cellulose nanocrystals (CNCs). In the toxicological evaluation of NMs, HARNs have been highlighted for their potential toxicity owing to aspect ratios similar to fibers with documented toxicity such as asbestos (Lanone et al., 2013). The goal of this work was to examine the toxicity of several HARNs, manipulating key physicochemical parameters through differential functionalizations to examine the impact on toxicity.

1.4.1.1 Rosette nanotubes

Rosette nanotubes (RNTs) self-assemble in a hierarchical and entropically driven process from their precursor unit, a guanine□cytosine (G□C) motif (Fenniri et al., 2002b; Moralez et al., 2005). In solution, G□C motifs form hexameric rosettes, maintained by 18 hydrogen bonds. These rosettes subsequently stack upon one another to form a stable tubular

nanostructure (**Figure 1-4**). The ability to covalently functionalize the G□C motif with a variety of ligands means RNTs physico-chemical characteristics can be tailored for a variety of applications. In addition, RNTs are metal-free, hydrophilic and can be dispersed in polar media, offering advantages over several other engineered NMs. Potential biomedical applications include the targeted delivery of hydrophobic drugs (Song et al., 2011), enhancing endothelial cell adherence on vascular stents (Fine et al., 2009) and as an improved hydrogel nanocomposite for orthopedic implants (Zhang et al., 2009). I utilized this tunability to examine if differential surface functionalization of RNTs impacts their toxicity *in vitro*. Lysine functionalized RNTs (K-RNTs) are a single-base RNTs and contrast with butylamine functionalized RNTs (TBL-RNTs) which are twin-base rosette nanotubes. This results in TBL-RNTs having *ca.* half the functionalization density compared to K-RNTs and a lower overall positive charge. By employing these two differentially functionalized RNTs, I examine the impact of charge and functionalization density on the toxicity of HARNs. I hypothesize that a decreased density and lower positive surface charge will reduce the biological interactions of HARNs and ultimately reduce their toxicity *in vitro*.

1.4.1.2 Carbon nanotubes

The structure of CNTs resembles a seamless cylinder comprised of a rolled sheet of graphene (**Figure 1-4**). CNTs can exist as a single cylinder, termed single-walled CNTs, or as several concentric layers of CNTs stacked

one inside the other, termed multi-walled CNTs (Johnston et al., 2010). CNTs are produced from a variety of methods including arc discharge, chemical vapour deposition, laser ablation and induction thermal plasma (Johnston et al., 2010; Kim et al., 2007). These production methods give rise to pristine CNTs with all carbons bound in a hexagonal lattice. The surface of pristine CNTs can be covalently and non-covalently functionalized with a variety of ligands. This has led to a range of commercial applications of CNTs including energy storage, composite materials and electronics (De Volder et al., 2013). Proposed biomedical applications of CNTs include novel cancer therapies, new cellular imaging techniques and vaccine delivery (Fadel and Fahmy, 2014). I examine the toxicity of unfunctionalized CNTs (U-CNTs) as a pristine material produced directly from the induction thermal plasma process. I also examine the toxicity of CNTs that were purified and differentially carboxy-functionalized (AF-CNTs) through oxidation at 30, 40 or 50 °C (termed CNT-30, CNT-40 and CNT-50, respectively). The increasing oxidation temperature had the effect of decreasing the overall length of CNTs, increasing carboxy-functionalization and increasing their solubility, allowing us to examine the effect of manipulating these physicochemical parameters on the toxicity of HARNs *in vitro*. I hypothesize that the increased carboxy surface functionalization, increased solubility and decreased length will increase the biological interactions of HARNs and ultimately increase their toxicity *in vitro*.

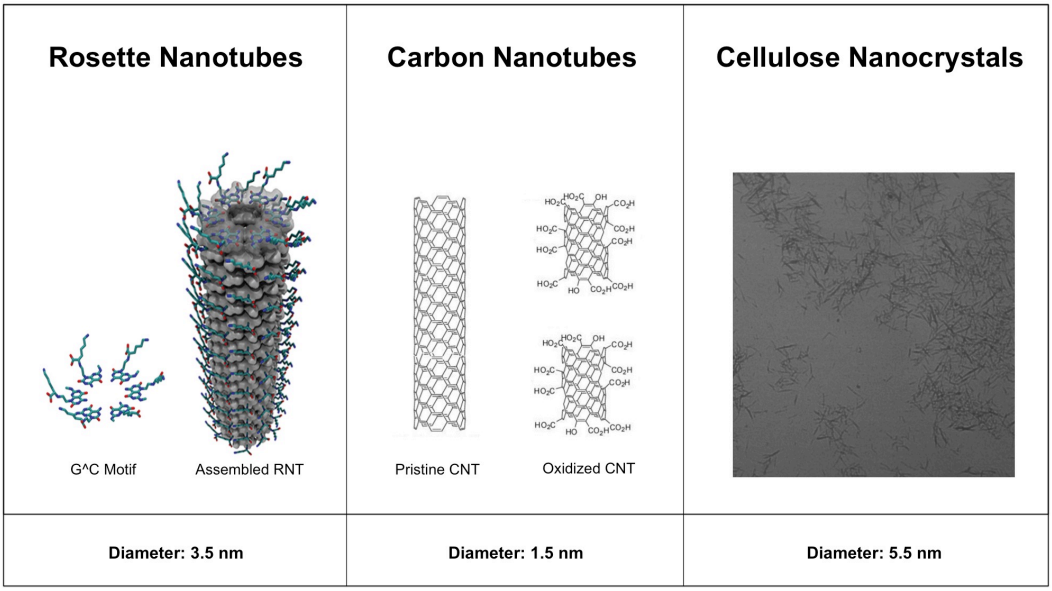

Figure 1-4. High aspect ratio nanomaterials (HARNs) length exceeds their width. The HARNs studied in this thesis included rosette nanotubes (RNTs), carbon nanotubes (CNTs) and cellulose nanocrystals (CNCs). RNTs have a diameter of ~3.5 nm and are a self-assembling tube comprised of its precursor unit, the G^C motif. Pristine CNTs have a diameter of ~1.5 nm and are seamless cylinders of rolled graphine sheets; pristine CNT oxidation introduces structural defects and carboxylic acid (carboxy) functionalization. CNCs are isolated crystalline cellulose from cellulose fibers and have a diameter of ~5.5nm.

1.4.1.3 Cellulose nanocrystals

Cellulose, a major structural component in plants, is one of the most abundant polymers on earth and is comprised of repeating glucose molecules. Cellulose fibers contain both crystalline and amorphous cellulose and acid hydrolysis isolates crystalline cellulose, yielding CNCs (**Figure 1-4**). CNCs can be functionalized with a variety of moieties and has led to several commercial and biomedical applications including incorporation into paper and plastic products (Shatkin et al., 2014), cellular imaging (Dong and Roman, 2007), drug delivery (Akhlaghi et al., 2013) and tissue engineering (Schumann et al., 2009). I examine the toxicity of carboxy-functionalized CNCs produced using the ammonium persulfate method. CNCs utilized in our studies have the same surface functionalization as CNTs, allowing us to examine the effect of HARN core composition on toxicity. I hypothesize that core composition is an important determinate of HARN toxicity and CNCs will have a lower toxicity compared to CNTs.

1.4 THESIS GOALS

The overall goals of my thesis were to (1) develop and optimize a suite of techniques to assess the immunotoxicity of HARNs, (2) to determine the toxicity of carbon nanotube (CNT), helical rosette nanotube (RNT) and nanocrystalline cellulose (NCC) exposure on several immune cell lines and

elucidate the mechanism of any observed toxicity, (3) to determine if exposure to these HARNs can affect the ability of immune cells to elicit effector responses and elucidate the mechanisms of interference and (4) to examine if differential functionalization of HARNs impacts their immunotoxicity *in vitro*.

CHAPTER 2

Functionalization changes the effects of rosette nanotubes on channel catfish (*Ictalurus punctatus*) lymphocyte viability and function

2.1 INTRODUCTION

The development of nanomaterials (NMs) of varying compositions, sizes and surface functionalizations, to suit diverse applications in consumer products, technologies and therapies, has resulted in their widespread use and production (De Volder et al., 2013). Associated with the rapid expansion of nanotechnology is the inevitable release of NMs into the environment; indeed, recent data suggests manufactured NMs are already beginning to accumulate in the environment (Maccormack and Goss, 2008; Scown et al., 2010; Sun et al., 2014). Aquatic environments in particular are receptacles for NMs due to their diverse array of input sources including atmospheric deposition, surface run-off, groundwater leaching and especially industrial and consumer discharges of NMs via wastewater (Gottschalk and Nowack, 2011; Westerhoff and Nowack, 2013). This has led to concerns on the impacts of NMs on the health of aquatic organisms, including fish. For example, carbon nanotubes (CNTs) have been reported to affect fish viability (Cheng and Cheng, 2012; Smith et al., 2007). In addition, significant gaps have been identified in the literature including the potential effects of NMs on fish immunity (Jovanović and Palić, 2012).

Changes in fish immune function can have important effects on an organism's ability to fight against bacterial, viral, fungal and parasitic infections, with potential individual and ecological level consequences. Immune cells occupy sentinel locations within tissues and at interfaces between the body and environment, making them an important early

indicator and likely sensitive target of NM exposure. To date, few studies have examined the effect of NMs on fish myeloid cells (*i.e.,* macrophages and granulocytes) that are involved in innate immunity (Jovanović et al., 2011b; Klaper et al., 2010; Ortega et al., 2013). Reports to date on myeloid cells have documented a myriad of responses to NM exposure, with immunoactivation (Jovanović et al., 2011b; Klaper et al., 2010) and immunosuppression (Jovanović et al., 2011a) described. However, no studies on NM exposure to fish lymphoid cells (*i.e.,* B-cells and T-cells) have been published, highlighting the need for investigation (Jovanović and Palić, 2012).

Channel catfish, *Ictalurus punctatus*, have been utilized as an important model for studying fish immunology. Currently, they are the only fish species with distinct, characterized, clonal leukocyte cell lines including myeloid (macrophages/monocytes) and lymphoid cells (B-cells, cytotoxic T-cells, noncytotoxic T-cells and NK-like cells) (Bengtén et al., 2006; Miller et al., 1994). The availability of these *in vitro* cell cultures allows us to address the effects of NM exposure on lymphoid fish cells such as B- and T-cells. In addition, their use as an immunological model has yielded information on the structure and function of catfish surface receptors that belong to the immunoglobulin superfamily (IgSF) (Bengtén et al., 2006). One member of this family, channel catfish leukocyte immune-type receptors (IpLITRs), are expressed on myeloid and lymphoid subsets (Stafford et al., 2006; 2007). IpLITRs have stimulatory and inhibitory forms that together play a role in regulating fish immune cell effector responses including phagocytosis and

degranulation (Cortes et al., 2014; 2012). The extensive biochemical and molecular characterization of IpLITRs make catfish a powerful model to examine the ability of fish immune receptors to elicit appropriate effector responses when exposed to NMs.

In this study, we examined the effects of rosette nanotubes (RNTs) on channel catfish immune cell viability and function. RNTs are a self-assembled nanomaterial formed through a hierarchical, entropically driven process described previously in detail (Fenniri et al., 2002b; 2001). While RNTs hold tremendous potential in a variety of biomedical applications (Chun et al., 2005; Suri et al., 2007; Zhang et al., 2009; 2008) we utilized them as a model NM to study the effect of surface functionalization on NM immunotoxicity. RNTs can be synthesized with a diverse range of functional groups on their outer surface through covalent attachment to their building block, the guanine-cytosine (G□C) motif (Alsbaiee et al., 2011; Beingessner et al., 2008; 2011; Chhabra et al., 2009; Tikhomirov et al., 2008). Utilizing RNTs, we studied the effect of NM exposure on fish lymphoid cell viability, focusing on (1) the relationship between RNT surface functionalization and their potential immunomodulation, (2) the relationship between different subsets of lymphoid cells and their response to NM exposure and (3) the relationship between RNT surface functionalization and their effect on IpLITR-induced phagocytosis. We hypothesize that by differentially functionalizing RNTs, we will impact how this material interacts with lymphoid cells and ultimately change the effect of RNT exposure on fish lymphoid cell function and

viability. Specifically, our hypothesis is that a decreased functionalization density and lower positive surface charge will reduce the biological interactions of RNTs and ultimately reduce their toxicity *in vitro*.

2.2 MATERIALS AND METHODS

2.2.1 Synthesis and physico-chemical characterization of RNTs

Lysine functionalized G□C motifs, butylamine functionalized G□C motifs (TB-TBL) and Arg-Gly-Asp-Ser-Lys (RGDSK) peptide functionalized G□C motifs (TB-RGDSK) were synthesized and characterized as previously reported (Fenniri et al., 2002b; 2001; Sun et al., 2012). Introduction of these motifs into nanopure water caused the self-assembly of these materials into stock solutions of lysine functionalized rosette nanotubes (K-RNTs; 1 g L^{-1}), butylamine functionalized rosette nanotubes (TBL-RNTs; 0.5 g L^{-1}) and RGDSK peptide functionalized rosette nanotubes (RGDSK-RNTs; 0.5 g L^{-1}). To prepare a stock solution of co-assembled $RGDSK^{1}/TBL^{9}$-RNTs (1:9 molar ratio), the TB-TBL solution in nanopure water was sonicated for 30 s and transferred to a vial containing TB-RGDSK. This suspension was sonicated for 5 min, vortexed for 5 s and subsequently heated with a heat gun for 1 min. This was repeated twice, or until no further dissolution occurred. The suspension was allowed to stand at room temperature for 2 days to allow for the self-assembly of $RGDSK^{1}/TBL^{9}$-RNTs and sedimentation of any un-dissolved TB-RGDSK. Supernatant containing this stock solution of

RGDSK[1]/TBL[9]-RNTs was transferred to a glass vial. Aliquots from the stock solutions of K-RNT, TBL-RNT and RGDSK[1]/TBL[9]-RNTs were diluted in nanopure water and used for subsequent studies.

The hydrodynamic diameters and zeta (ζ) potentials of K-RNTs, TBL-RNTs and RGDSK[1]/TBL[9]-RNTs suspensions were measured using dynamic light scattering (Zetasizer Nano ZS, 633 ηm, Malvern Instrument) at experimental concentrations of 1, 2 and 5 mg L^{-1} in nanopure water. Hydrodynamic radii were obtained in 173° backscattering mode and are reported as the peak value of >99% intensity. Concentrations of RNTs below 1 mg L^{-1} were below accurate limits of detection and are not reported.

To examine the intrinsic optical properties of RNTs, the absorbance spectrum for 100 mg L^{-1} suspensions of K-RNTs, TBL-RNTs and RGDSK[1]/TBL[9]-RNTs in nanopure water were measured. An absorbance spectrum from 300-1100 nm (8452A Diode Array Spectrophotometer, Hewlett Packard) was plotted for K-RNTs and RGDSK[1]/TBL[9]-RNTs and is shown in **Supplemental Figure S2-1**. For extensive characterization details of RNTs under a variety of physiological conditions and with various side-group functionalizations see Fenniri *et al.,* (2001, 2002) and Moralez *et al.,* (2005).

2.2.2 Cell culture

Channel catfish 3B11, 1G8 and 28S.3 cells were grown at 27 °C and 5% CO_2 in 25 cm^2 filtered cell culture flasks (Corning) and passed when 80%

confluence was reached (~3-5 days). Cells were cultured in AL media (50:50, AIM V medium:L-15 medium; Gibco) containing 3% catfish serum, 0.5 g sodium bicarbonate (Sigma), 0.05M 2-mercaptoethanol, 100 units mL^{-1} penicillin (Gibco) and 100 μg mL^{-1} streptomycin (Gibco). Culture media (AL3) was filter sterilized prior to use using a 0.22 μm filter (Corning).

RBL-2H3 cells were grown at 37 °C and 5% CO_2 in 100 mm tissue culture dish (Corning) and passaged when 80% confluence was reached (~3-4 days). Cells were cultured in minimum essential media (MEM/EBSS; Hyclone) with 2 mM L-glutamine (Gibco), 100 units mL^{-1} penicillin (Gibco), 100 μg mL^{-1} streptomycin (Gibco) and 10% heat inactivated fetal bovine serum (FBS, Hyclone) supplemented with G418 selection reagent. Prior to use, culture media (MEM/EBSS/FBS) was filter sterilized using 0.22 μm filter (Corning).

2.2.3 Assessment of channel catfish lymphocyte viability after RNT exposure using the MTS assay

The effect of RNT exposure on cell viability was determined using the MTS assay (Cell Titer 96 Aqueous Non-Radioactive Cell Proliferation Assay; Promega). MTS [3-(4,5-dimethylthiazol-2-yl)-5-(3-carboxymethoxyphenyl)-2-(4-sulfophenyl)-2H-tetrazolium] is a tetrazolium salt that undergoes a color change when bioreduced by viable cells in culture and can be used to gauge relative cell viability by measuring the change in absorbance at 490 nm. 3B11, 1G8 and 28S.3 cells were seeded in round-bottom, 96 well plates

(Becton Dickinson) at a density of 20,000 cells per well in 180 µL AL3. Cells were dosed with 0.125, 0.25, 0.5, 1.0, 2.0 or 5.0 mg L^{-1} RNT (K-, TBL- or $RGDSK^{1}/TBL^{9}$-) for 24 h (27 °C, 5% CO_2). Control cells received 20 µL nanopure water (vehicle control). Following 24 h exposure, cells were treated with prepared kit reagents and incubated for 3 h (27 °C, 5% CO_2). Cells were transferred to a flat-bottom, 96 well plate (Becton Dickinson) and absorbance (Abs) was measured at 490 nm using a microplate reader (Wallac 1420, Perkin Elmer). The absorbance of cells containing only AL3 media was used as background control. Previous studies have shown that RNTs can interfere with the accuracy of colorimetric assays, including the MTS assay (Ong et al., 2014). Wells containing 0.125, 0.25, 0.5, 1.0, 2.0 or 5.0 mg L^{-1} RNT (K-, TBL- or $RGDSK^{1}/TBL^{9}$-) in AL3 media without cells were used as a further control to account for possible background absorption caused by RNTs alone. Viability was calculated based on the following formula:

Viability (% Control) = (Abs of RNT treated cells – Abs of RNT control) / (Abs of control treatment – Abs of background control)

2.2.4 Assessment of channel catfish lymphocyte viability using flow cytometric analysis

For comparison and accuracy viability was also measured using flow cytometry. 3B11, 1G8 or 28S.3 cells were seeded in a round-bottom, 96 well plate (Becton Dickinson) at a density of 20,000 cells per well in 180 µL AL3. Cells were dosed with 0.125, 0.25, 0.5, 1.0, 2.0 or 5.0 mg L^{-1} RNT (K-, TBL- or

RGDSK[1]/TBL[9]-) for 24 h (27 °C, 5% CO_2). Control cells received 20 µL nanopure water (vehicle control). Following 24 h exposure, cells were stained with propidium iodide (PI, 100 µg mL^{-1}) and analyzed by flow cytometry (Quanta SC, Beckman Coulter). Whole cell populations for each treatment with 3B11, 1G8 or 28S.3 cells were gated using side scatter (SS) and forward scatter (FS). We measured PI fluorescence to separate viable from non-viable cells by measuring increased FL2 fluorescence. PI penetrates the membranes of necrotic and late apoptotic cells and intercalates with nucleic acids, enhancing its fluorescence by a factor of 30 (Brana et al., 2002). All gates were established with control treated cells. The percentage of viable cells in culture was calculated from the number of cells within the whole population gate that concurrently exhibited low levels of PI fluorescence.

2.2.5 Transfection of RBL-2H3 cells with IpLITR/IpFcRγ-L chimeric receptor

For phagocytosis studies, we utilized a chimeric receptor constructed from fusing the extracellular domain of channel catfish (*Ictalurus punctatus*) leukocyte immune-type receptor (IpLITRs) with the transmembrane region and cytoplasmic tail of its adaptor protein, IpFcRγ-L. This fusion construct was cloned into the pDISPLAY vector (Invitrogen) to generate an N-terminal HA epitope tagged IpLITR/IpFcRγ-L chimera as described previously (Cortes et al., 2012; Mewes et al., 2009).

To express the IpLITR/IpFcRγ-L chimera in RBL-2H3 cells, transfections, selection and cell sorting was completed as described previously (Cortes et al., 2012; Mewes et al., 2009). Briefly, RBL-2H3 cells were seeded in a 24-well plate (Costar) at a density of 1.25 x 10^5 cells per well and left overnight at 37 °C and 5% CO_2. The media was replaced with OptiMEM (Hyclone) and Xfect transfection reagent (Clontech) was used to transfect 1 μg of pDISPLAY IpLITR/IpFcRγ-L plasmid according to the manufacturers instructions for 4 h at 37 °C and 5% CO_2. Fresh culture media (MEM/EBSS/FBS) was added and cells were further incubated overnight (37 °C and 5% CO_2). The transfection solution was aspirated and cells were incubated in MEM/EBSS/FBS supplemented with the selection reagent G418 disulfate salt (Sigma-Aldrich) for 4 days (37 °C and 5% CO_2). RBL-2H3 cells were washed and the remaining viable cells underwent further selection in G418 supplemented media for 8-12 days until confluence was reached. To test for the surface expression of IpLITR/IpFcRγ-L by flow cytometry, anti-hemagglutinin (HA) monoclonal antibody (mAb; Cedarlane Laboratories Ltd.) and a PE-conjugated goat anti-mouse immunoglobulin (Ig) G polyclonal antibody (pAb; Beckman Coulter) were used. With confirmed surface expression of IpLITR/IpFcRγ-L in RBL-2H3, cells were stained with anti-HA mAb and PE-conjugated secondary pAb and using flow cytometry, sorted into HA-positive and HA-negative populations (FACSAria, Becton Dickinson). HA-positive cells were cultured in MEM/EBSS/FBS supplemented with G418

selection reagent and tested weekly for IpLITR/IpFcRγ-L surface expression by flow cytometry (Quanta SC, Beckman Coulter).

2.2.6 Assessment of IpLITR/IpFcRγ-L mediated phagocytosis after RNT exposure

The effects of RNT exposures on IpLITR/IpFcRγ-L induced phagocytosis were investigated using methods originally described by Garcia et al., (2007) and Cortes et al., (2012). Briefly, 1.25 x 10^8 fluorescent beads (Fluoresbrite Carboxy YG 4.5 micron microspheres; Polysciences) were incubated with 200 µg of protein A (from *Staphylococcus aureus*; Sigma-Aldrich) in borate buffer at room temperature (RT) overnight in a rotating mixer. Protein A adsorbed beads were centrifuged and re-suspended in 10 mg mL^{-1} bovine serum albumin (BSA) in borate buffer after 30 min incubations at RT in a rotating mixer. Beads were re-suspended in 10 mg mL^{-1} BSA in 1x phosphate buffered saline (PBS). To opsonize, 20 µg mL^{-1} of either anti-HA mAb or mouse IgG3 isotype antibody (Beckman Coulter) were added to beads adsorbed with protein A and incubated at 4 °C for 3 h in a rotating mixer. Opsonized beads were washed with 10 mg mL^{-1} BSA in 1x PBS before being used in the phagocytosis assay.

RBL-2H3 cells expressing IpLITR/IpFcRγ-L were harvested and re-suspended in 100 µL of MEM/EBSS at a density of 1 x 10^5 cells. Cells were exposed to 1, 5, 10, 15, 20, 25 mg L^{-1} RNT (K-, TBL- or $RGDSK^1$/TBL^9-) for 2 h at 37 °C, 5% CO_2. Controls, described below, received 10 µL nanopure water

(vehicle) and were incubated as described above. After exposure, each RNT treatment was split into two groups to undergo one of two separate protocols: viability and phagocytosis. For viability, cells were stained with PI (100 μg mL^{-1}) and analyzed by flow cytometry (Quanta SC, Beckman Coulter). Whole cell populations were gated using SS and FS and subsequently, PI fluorescence using FL2 was used to separate viable from non-viable cells. For the phagocytosis protocol, RBL-2H3 cells exposed to RNTs for 2 h were incubated with 4 μL of prepared anti-HA mAb opsonized beads (1 x 10^8 beads mL^{-1}) for 1 h at 37 °C, 5% CO_2. Cells were centrifuged at 5000 *g* for 1 min, supernatant was aspirated and the cell pellet was resuspended in 100 μL 1x PBS containing 0.05% trypsin, 1mM EDTA for 15 min on ice. Treatment with 0.05% trypsin detached non-internalized beads bound to the cell membrane. Cells subsequently received 250 μL 1x PBS containing 0.5% BSA, 2 mM EDTA and were centrifuged 5000*g* for 1 min. Supernatant was aspirated and cells were suspended in 300 μL 1% paraformaldehyde (PFA) in 1x PBS. Samples were then analyzed by flow cytometry (Quanta SC, Beckman Coulter) for fluorescence using FL-1. A shift in FL-1 fluorescence indicates the internalization of one or more fluorescent beads and is used to gauge phagocytosis.

Anti-HA mAb beads, 37 °C served as the control group to which RNT exposed treatments were compared and represent a maximal phagocytic response through IpLITR/IpFcRγ-L receptor engagement. Our negative controls served to verify our experimental protocol. Incubation at 4 °C (anti-

HA mAb beads) ensured the phagocytic response we observed was due to active cell processes requiring ATP hydrolysis and not non-specific mechanisms. Our isotype control (IgG3 Ab beads, 37 °C) was run to verify internalization was proceeding through the transfected teleost IpLITR/IpFcRγ-L chimeric receptor. Treatment with the pharmacological inhibitor PP2, a Src kinase family inhibitor, also verified the route of bead internalization. Src kinases are downstream signaling intermediates of the IpLITR/IpFcRγ-L receptor (Cortes et al., 2012). For control treatments, cells were incubated with 4 µL of prepared anti-HA mAb opsonized beads for 1 h at either 4 °C or 37 °C, except for the IgG3 isotype control, which was incubated with 4 µL of prepared IgG3 isotype Ab opsonized beads for 1 h at 37 °C. PP2 controls were pretreated with 10 µM of PP2 (EMD Biosciences) for 30 min prior to the addition of prepared anti-HA mAb opsonized beads for 1 h at 37 °C.

2.2.7 Statistical analysis

To evaluate the effect of RNT exposure on 3B11, 1G8, 28S.3 and RBL-2H3 cell viability, two-way Analysis of Variance (ANOVA) followed by post-hoc Tukey's test was performed. To compare the toxicity profiles between channel catfish cell lines (3B11, 1G8 and 28S.3), RNT functionalization and RNT concentration, a three-way ANOVA followed by post-hoc Holm-Sidak test was performed. To assess the effect of RNT exposure on phagocytosis, one-way ANOVA followed by post-hoc Tukey's test was performed.

GraphPad 6.0 statistical software was used to perform all statistical analyses with the exception of the three-way ANOVA completed with Sigmaplot 12.0. Data is presented as (mean±SE). Statistical significance was set at $p<0.05$.

2.3 RESULTS

2.3.1 Characterization of RNTs

RNTs with three distinct surface functionalizations were formed from their precursor G□C motifs in nanopure water and characterized. Lysine (K)-functionalized G□C motifs **(Figure 2-1A)** introduced into nanopure water self-assembled into K-functionalized rosette nanotubes (K-RNTs) with an average outer diameter of *ca.* 3.5 nm **(Figure 2-1B,C)**. Representative scanning electron microscope (SEM), transmission electron microscope (TEM) and atomic force microscope (AFM) micrographs of K-RNTs are shown in **Figure 2-1F-H** and highlight the architecture of these nanotubes. The average hydrodynamic diameters of K-RNTs at concentrations of 1, 2 and 5 mg L^{-1} were 266±79, 245±73 and 300±63 nm, respectively **(Table 2-1)**. K-RNTs displayed an overall net positive charge; measured ζ-potential of K-RNTs in solution ranged from 67±4 mV to 74±6 mV **(Table 2-1)**.

Butylamine (TBL) and Arg-Gly-Asp-Ser-Lys (RGDSK)-peptide functionalized rosette nanotubes (TBL-RNTs and RGDSK-RNTs, respectively) are formed from the assembly of their precursor G□C motifs (TB-TBL, TB-RGDSK). TBL- and RGDSK-RNTs are twin-based (TB) rosette nanotubes,

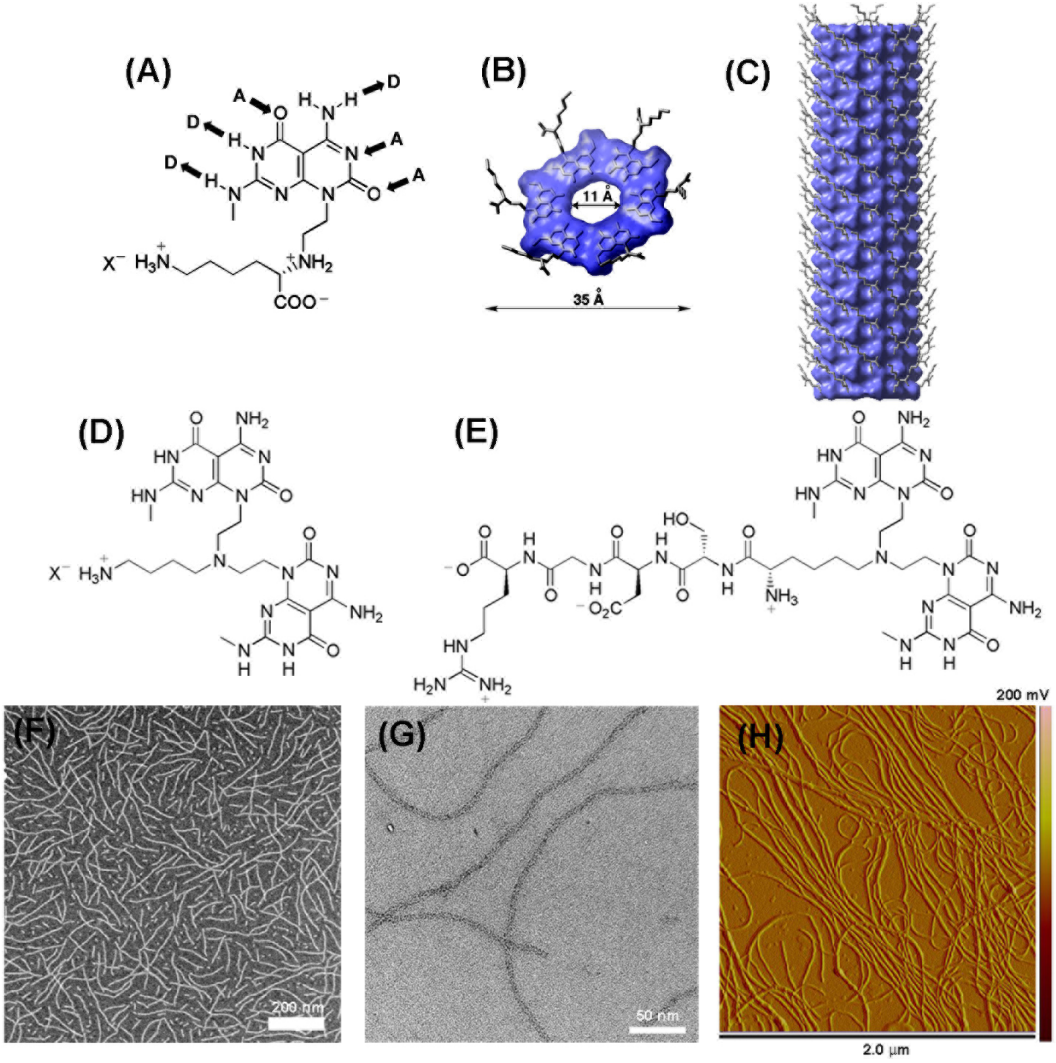

Figure 2-1. (A) Lysine-functionalized G□C motif featuring the donor (D) and acceptor (A) hydrogen bonding arrays of guanine and cytosine self-assembles into (B) hexameric rosettes, which futher stack to form (C) K-RNTs having a tubular architecture. Structures of the twin-G□C motifs functionalized with (D) butylamine (termed TB-TBL) and (E) the peptide Arg-Gly-Asp-Ser-Lys (termed TB-RGDSK) which were co-assembled to form the RGDSK[1]/TBL[9]-RNTs. (F-H) SEM, TEM and AFM images of K-RNTs which have an outer diameter of *ca.* 3.5 nm. Scale bar is in nm.

with precursor units consisting of two G□C motifs covalently attached to a single molecule (here, TBL- or RGDSK-) **(Figure 2-1D, E).** At concentrations of 1, 2 and 5 mg L^{-1}, TBL-RNTs hydrodynamic diameter ranged from 281±60 to 358±59 nm. TBL-RNTs displayed an overall positive charge, with ζ-potentials ranging from 50±8 to 55±4 mV **(Table 2-1)**. Co-assembly of TB-RGDSK **(Figure 2-1E)** and TB-TBL **(Figure 2-1D)** in a 1:9 molar ratio resulted in the formation of a RNT termed $RGDSK^{1}/TBL^{9}$-RNT. This co-assembly created a RNT expressing the RGDSK-peptide that maintains a solubility and surface charge profile similar to TBL-RNTs. At concentrations of 1, 2 and 5 mg L^{-1}, $RGDSK^{1}/TBL^{9}$-RNTs have hydrodynamic diameters of 316±90, 332±84 and 384±84 nm, respectively. Measured ζ-potentials of $RGDSK^{1}/TBL^{9}$-RNTs were positive and ranged from 42±3 to 54±2 mV **(Table 2-1)**.

To test for possible interference with spectroscopic assays, an optical characterization of RNTs was completed and is shown in **Supplemental Figure S2-1**. At 490 nm, K- and $RGDSK^{1}/TBL^{9}$-RNTs have absorbance readings of 0.124 and 0.272 a.u., respectively. All data presented have been corrected for the intrinsic absorbance of RNTs.

Unfortunately, RNTs could not be characterized in complex cell culture media using currently available techniques such as DLS. We have provided information summarizing characterization details from several publications (**Supplemental Table S2-1**). In addition, we recognize that NM

Table 2-1. Physico-chemical characterization of K-, TBL- and RGDSK[1]/TBL[9]-RNTs showing hydrodynamic diameter (nm) and zeta potential (mV) diluted to 1, 2 and 5 mg L^{-1} reported as mean ± SEM (n=3).

Material	Measurement	Concentration		
		1 mg L^{-1}	2 mg L^{-1}	5 mg L^{-1}
K-RNT	HD (nm)	266±79	245±73	300±63
	ZP (mV)	67±4	74±6	72±4
TBL-RNT	HD (nm)	281±60	323±55	358±59
	ZP (mV)	54±8	50±8	55±4
RGDSK[1]/	HD (nm)	316±90	332±84	384±84
TBL[9]-RNTs	ZP (mV)	42±3	47±3	54±2

Abbreviations: (HD) hydrodynamic diameter, (ZP) zeta potential

dosing metrics are complex with several candidates identified. To aid in cross study comparisons, we provide conversions between mass per volume, particles per volume and surface area per volume in **Supplemental Table S2-2**.

2.3.2 Effects of RNTs on channel catfish lymphocyte viability

2.3.2.1 Response of 3B11 cell line to RNT exposure

Exposures to RNTs had significant effects on the viability of channel catfish immune cells after 24 h of exposure and these effects were both dose- and functionalization-dependent. Representative flow cytometric plots for 3B11 cells exposed to 5 mg L^{-1} K-RNT demonstrated a significant reduction in cell viability, indicated through a decreasing proportion of gated cells **(Figure 2-2C)** and a concomitant increase in PI fluorescence **(Figure 2-2D)** when compared to cells exposed to vehicle alone **(Figure 2-2A, B)**. Combined flow cytometric results for 3B11 cells exposed to varying concentrations of RNTs revealed a dose-dependent decrease in cell viability, with significant reductions noted at 1, 2 and 5 mg L^{-1} after 24 h exposure **(Figure 2-2E)**.

In addition to dose, cell viability was dependent on functionalization. When 3B11 cells were exposed to 1 mg L^{-1} TBL-functionalized RNTs, cell viability decreased to 72.2±5 %. However, the K- and $RGDSK^{1}$/TBL^{9}-functionalizations had a greater impact on viability, decreasing to 50.7±6 and 47±8 % respectively, values significantly lower than the TBL-functionalized

RNTs. The response of 3B11 cells exposed to 2 mg L^{-1} RNTs was similarly functionalization dependent. TBL-functionalized RNTs had the smallest impact on viability, declining to 65.6±6 %. This was a significantly different response compared to K- and $RGDSK^{1}/TBL^{9}$-functionalized RNTs (K-RNT: 28.9±6 % viable cells; $RGDSK^{1}/TBL^{9}$-RNT: 45.4±6 % viable cells) at 2 mg L^{-1}. 3B11 cells exposed to 5 mg L^{-1} K-RNT had the greatest decrease in viability (9.5±3 % were viable) and was significantly different compared to $RGDSK^{1}/TBL^{9}$- (45.0±4 %) and TBL- (34.7±9 %) RNTs. To verify our flow cytometric results, the MTS assay was performed. Parallel declines in viability as measured by the MTS assay were observed at exposures of 1, 2 and 5 mg L^{-1} RNTs. Again, the changes in viability were functionalization-dependent, in agreement with our flow cytometric results **(Figure 2-2F)**. In general, 3B11 cells exposed to 2 or 5 mg L^{-1} K-RNTs had a significantly greater decline in viability compared to $RGDSK^{1}/TBL^{9}$- or TBL-functionalized RNTs. Exposure to TBL-RNT at 1 or 2 mg L^{-1} has the smallest impact on 3B11 viability after 24 h exposure compared to K- or $RGDSK^{1}/TBL^{9}$-functionalizations.

2.3.2.2 Response of 1G8 cell line to RNT exposure

Similar to 3B11 cells, 1G8 cell viability was significantly reduced after 1, 2 or 5 mg L^{-1} RNT exposure for 24 h and was influenced by RNT-functionalization **(Figure 2-3A)**. K-RNTs caused the greatest declines in viability at the higher doses of 2 and 5 mg L^{-1}, declining to 34.1±7 and

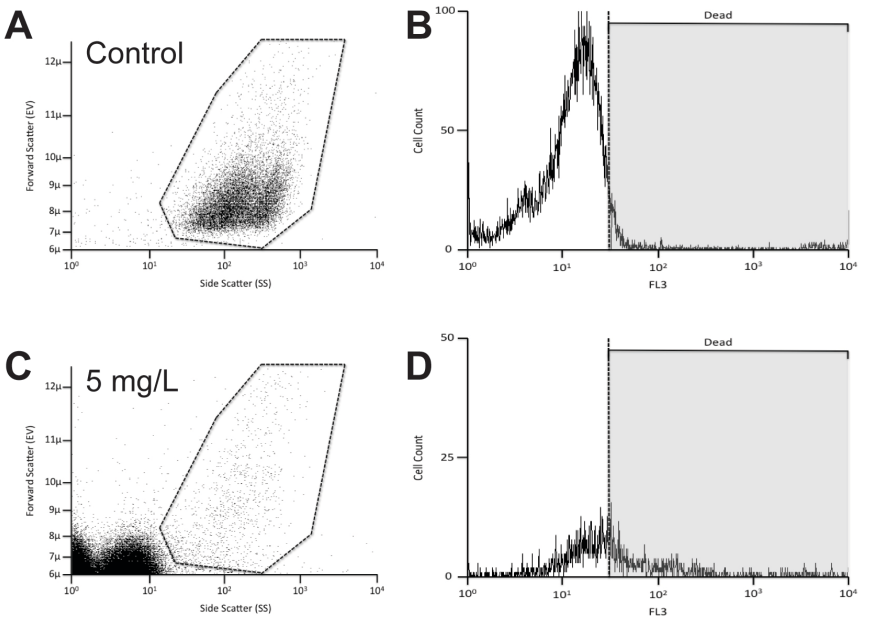
A
Control
Forward Scatter (EV)
Side Scatter (SS)
B
Dead
Cell Count
FL3
C
5 mg/L
Forward Scatter (EV)
Side Scatter (SS)
D
Dead
Cell Count
FL3

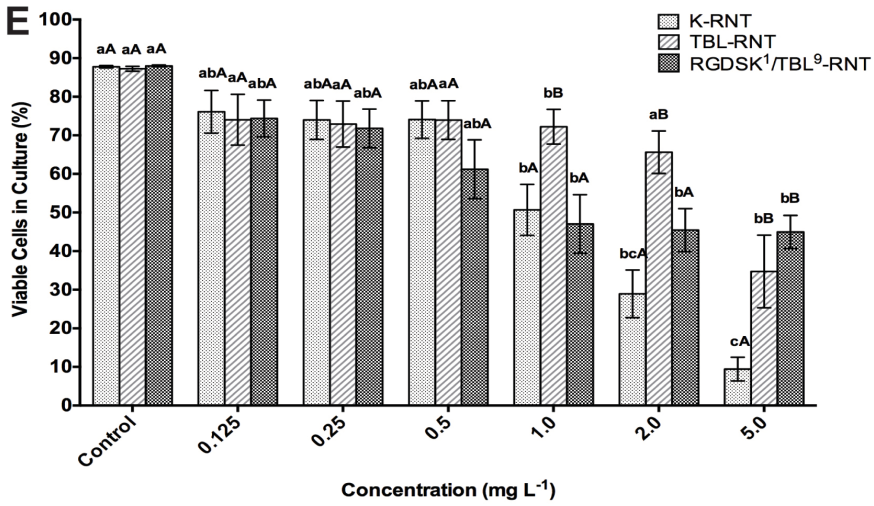
E
K-RNT
TBL-RNT
RGDSK[1]/TBL[9]-RNT
Viable Cells in Culture (%)
Control
0.125
0.25
0.5
1.0
2.0
5.0
Concentration (mg L-1)

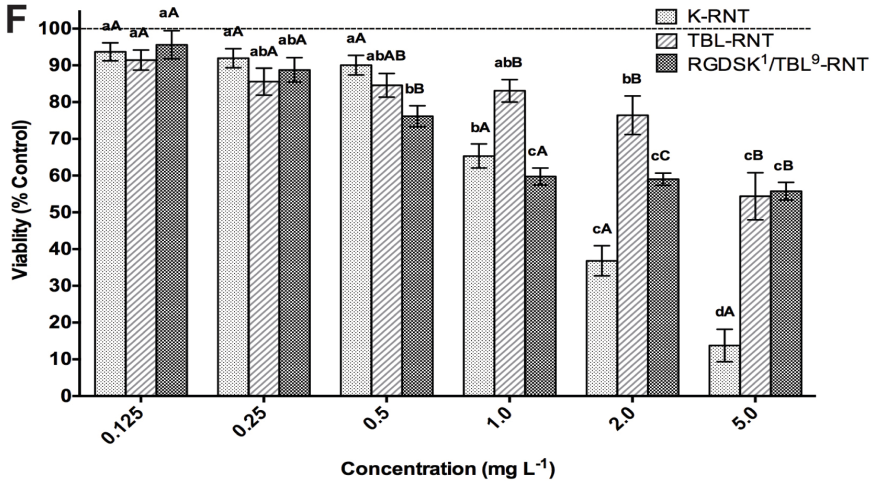
F
K-RNT
TBL-RNT
RGDSK[1]/TBL[9]-RNT
Viablity (% Control)
0.125
0.25
0.5
1.0
2.0
5.0
Concentration (mg L-1)

Figure 2-2. RNT exposure has a significant effect on channel catfish B-cell-like 3B11 viability and depends upon RNT functionalization. $2.0x10^4$ 3B11 cells were incubated with 0.125, 0.25, 0.5, 1.0, 2.0 or 5.0 mg L^{-1} RNT (K-, TBL- or $RGDSK^1/TBL^9$-) for 24 h. Cells were subsequently analyzed by flow cytometry (A-E) or the MTS assay (F). Representative flow cytometric plots of 3B11 cells exposed to 5 mg L^{-1} K-RNT demonstrate the concomitant decrease in the proportion of gated cells (A) and increase in PI fluorescence (B) when compared to control treatments (C, D). Summarized flow cytometric viability data (E) and MTS viability data (F) demonstrate a dose- and functionalization-dependent response to RNT exposure. Data were analyzed by two-way ANOVA with a Tukey's *post hoc* test. Lowercase letters (a,b,c,d) denote significant differences between concentrations tested for each RNT-functionalization. Uppercase letters (A,B,C) denote significant differences between K-, TBL- or $RGDSK^1/TBL^9$-functionalizations for each concentration tested ($p<0.05$). Means±SE are shown, n=5.

8.3±2 % viability respectively, after 24 h exposure. This response differed significantly in cells exposed to either $RGDSK^{1}/TBL^{9}$- or TBL-functionalized RNTs. TBL-RNTs affected 1G8 viability the least of all RNT-functionalizations tested, with significant declines at the highest tested dose of 5 mg L^{-1} (43.7±5 %). Further, the introduction of RGDSK- into TBL-functionalized RNTs ($RGDSK^{1}/TBL^{9}$-RNT) significantly altered the toxicity when compared to TBL-only functionalized RNTs. At 1 or 2 mg L^{-1}, 1G8 viability was 81.2±1 and 76.5±2 %, respectively, for TBL-RNT exposures. Viability after exposure to 1 or 2 mg L^{-1} $RGDSK^{1}/TBL^{9}$-RNT decreased to 49.3±10 and 46.9±4 %, respectively and was significantly reduced compared to TBL-RNTs. A similar trend was observed when viability was assessed with the MTS assay **(Figure 2-3B)**. Significant declines in viability occurred after 24 h exposure to 1, 2 and 5 mg L^{-1} RNTs and were functionalization dependent. K-RNTs had the greatest effect on viability while TBL-RNTs had the least effect at higher doses (2 and 5 mg L^{-1} RNT). Introduction of the RGDSK- ligand ($RGDSK^{1}/TBL^{9}$-RNT) significantly decreased 1G8 viability compared to TBL-RNTs at exposures of 1 and 2 mg L^{-1}.

2.3.2.3 Response of 28S.3 cell line to RNT exposure

Lastly, the effect of RNT exposure on 28S.3 cell viability was examined. Summarized flow cytometric and MTS data indicated that declines in 28S.3 viability after RNT exposure was dose- and functionalization-

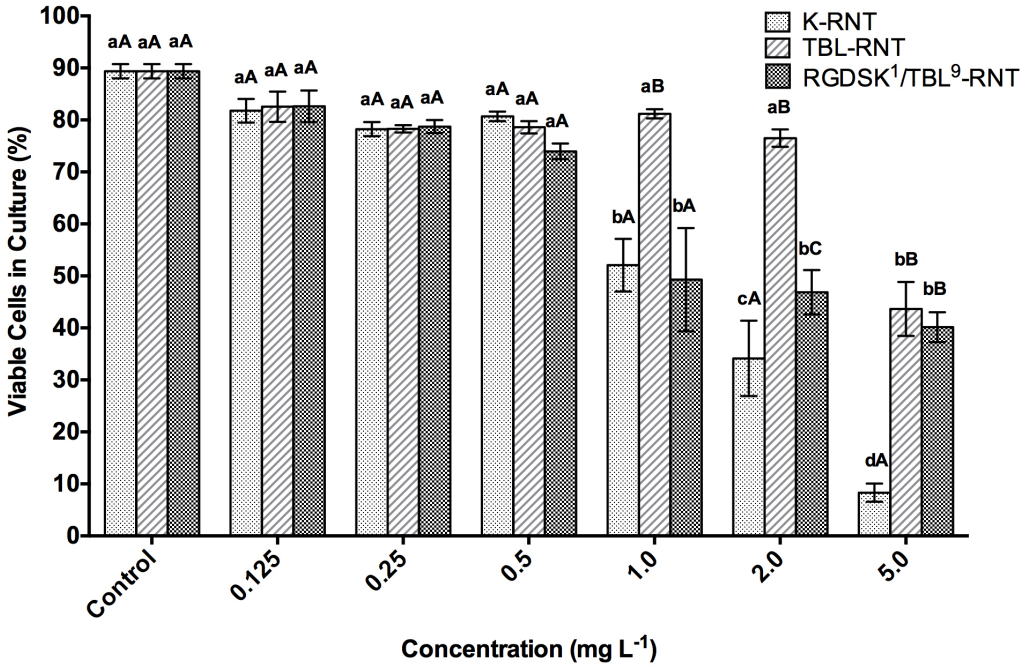
K-RNT
TBL-RNT
RGDSK[1]/TBL[9]-RNT
Viable Cells in Culture (%)
Concentration (mg L-1)
Control
0.125
0.25
0.5
1.0
2.0
5.0

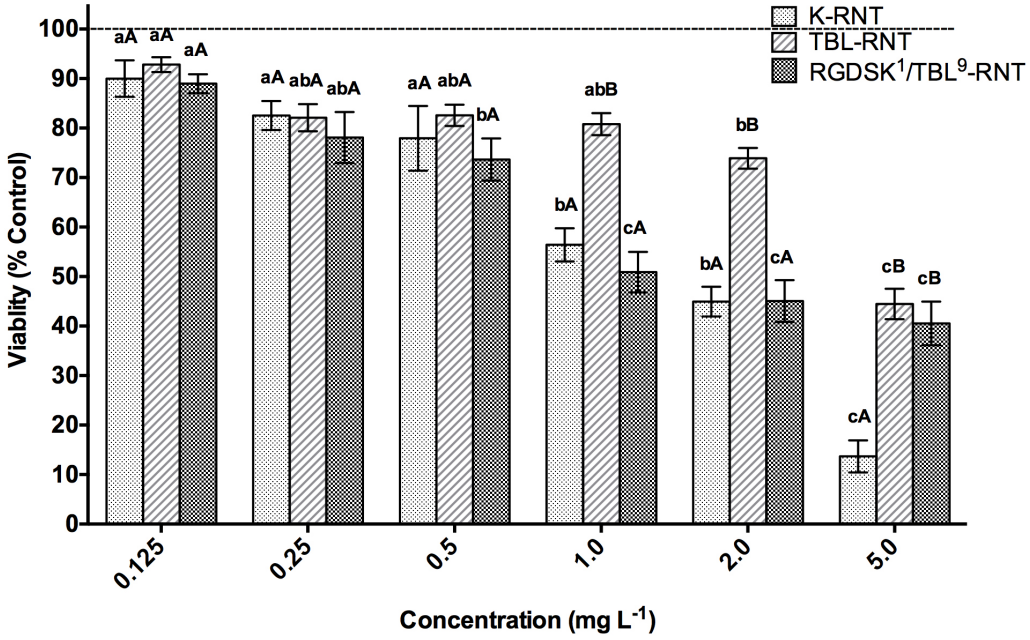
K-RNT
TBL-RNT
RGDSK[1]/TBL[9]-RNT
Viablity (% Control)
Concentration (mg L-1)
0.125
0.25
0.5
1.0
2.0
5.0

Figure 2-3. RNT exposure has a significant effect on channel catfish B-cell-like 1G8 viability and depends upon functionalization. $2.0x10^4$ 1G8 cells were incubated with 0.125, 0.25, 0.5, 1.0, 2.0 or 5.0 mg L^{-1} RNT (K-, TBL- or $RGDSK^1/TBL^9$-) for 24 h. Summarized flow cytometric viability data (A) and MTS viability data (B) demonstrate a dose- and functionalization-dependent response to RNT exposure. Data were analyzed by two-way ANOVA with a Tukey's *post hoc* test. Lowercase letters (a,b,c) denote significant differences between concentrations tested for each RNT-functionalization. Uppercase letters (A,B,C) denote significant differences between K-, TBL- or $RGDSK^1/TBL^9$-functionalizations for each concentration tested ($p<0.05$). Means ± SE are shown, n=5.

dependent **(Figure 2-4)**. Flow cytometric analysis revealed that 28S.3 cells exposed to K-RNTs at 2 and 5 mg L^{-1} had the greatest decline in viability after 24 h exposure resulting in 53.6±5 % and 44.4±8 % viable cells, respectively **(Figure 2-4A)**. A similar trend was found using the MTS assay; 28S.3 cells exposed to 2 and 5 mg L^{-1} K-RNT had viability decline to 60.5±3 % and 50.3±5 % compared to control, respectively **(Figure 2-4B)**. The declines in 28S.3 viability after K-RNT exposure was significantly greater compared to TBL- and $RGDSK^1/TBL^9$-functionalizations. TBL-RNT exposure had the least effect on 28S.3 viability. Significant declines in 28S.3 viability only occurred at the highest dose examined. There were no significant differences in viability of 28S.3 cells exposed to either TBL- or $RGDSK^1/TBL^9$-functionalized RNTs at 2 or 5 mg L^{-1} **(Figure 2-4)**.

2.3.2.4 Comparison between cell lines

A comparison between 3B11, 1G8 and 28S.3 cells was generated by three way ANOVA ($p<0.05$). This analysis revealed that the response to RNT exposure was also cell line-dependent. Flow cytometric data grouped by functionalization allows a more direct comparison between cell-lines and the results are shown in **Supplemental Figure S2-2**. When cells are exposed to 1, 2 or 5 mg L^{-1} RNTs there were no significant differences in the percentage of viable cells in culture between 3B11 and 1G8 cell lines (for example, 52.1±5 versus 50.1±7, 34.1±7 versus 28.9±6, 9.5±3 versus 8.3±2 for 1, 2 or 5

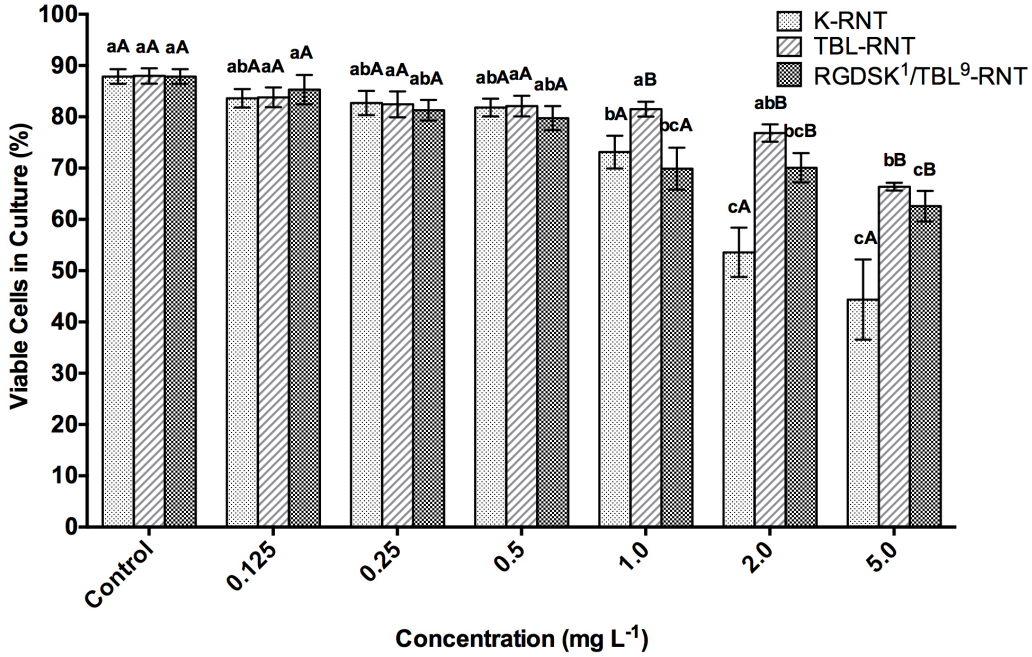
K-RNT
TBL-RNT
RGDSK[1]/TBL[9]-RNT
Viable Cells in Culture (%)
Concentration (mg L-1)
Control
0.125
0.25
0.5
1.0
2.0
5.0

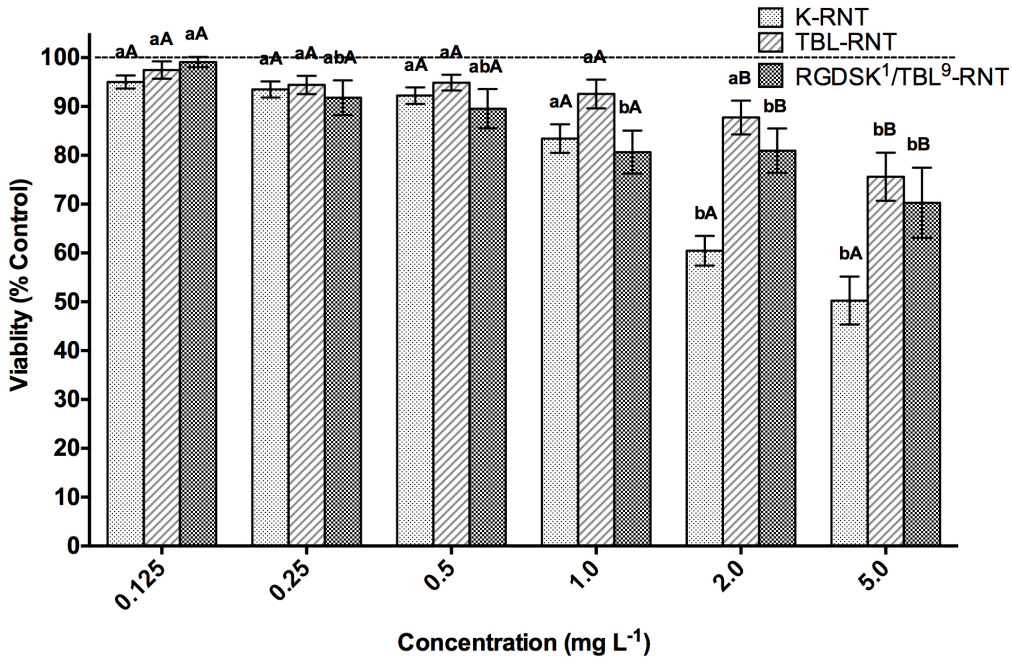
K-RNT
TBL-RNT
RGDSK[1]/TBL[9]-RNT
Viablity (% Control)
Concentration (mg L-1)
0.125
0.25
0.5
1.0
2.0
5.0

Figure 2-4. RNT exposure has a significant effect on channel catfish T-cell-like 28S.3 viability and depends upon functionalization. $2.0x10^4$ 28S.3 cells were incubated with 0.125, 0.25, 0.5, 1.0, 2.0 or 5.0 mg L^{-1} RNT (K-TBL- or $RGDSK^1/TBL^9$-) for 24 h. Summarized flow cytometric viability data (A) and MTS viability data (B) demonstrate a dose- and functionalization-dependent response to RNT exposure. Data were analyzed by two-way ANOVA with a Tukey's *post hoc* test. Lowercase letters (a,b,c) denote significant differences between concentrations tested for each RNT-functionalization. Uppercase letters (A,B) denote significant differences between K-, TBL- or $RGDSK^1/TBL^9$-functionalizations for each concentration tested ($p<0.05$). Means ± SE are shown, n=5.

mg L^{-1} K-RNT exposure, respectively, in 3B11 versus 1G8) (compare **Figure 2-2E** and **Figure 2-3A; Supplemental Figure S2-2**). In contrast, there was a significant difference in the percentage of viable 28S.3 cells remaining in culture after 1, 2 or 5 mg L^{-1} RNT exposure when compared to both 3B11 and 1G8 cell lines. In general, 28S.3 cells were found to be less susceptible to RNT exposure, with more viable cells remaining in culture after 24 h of RNT exposure compared to both 3B11 and 1G8 cells (compare **Figure 2-2E, 2-3A** with **Figure 2-4A; Supplemental Figure S2-2**).

2.3.3 Effect of RNT exposure on IpLITR/IpFcRγ-L mediated phagocytosis

Given the effect of RNTs on catfish lymphocytes above, we wished to examine the potential effect of differentially functionalized RNTs on immune cell effector responses such as phagocytosis. To accomplish this, we used a rat basophilic cell line (RBL)-2H3 transfected with the catfish leukocyte immune type receptor (IpLITR) and examined both viability and the ability to phagocytose upon stimulation. Exposure to each of the functionalized RNTs for 2 h during the phagocytosis protocol significantly reduced the viability of RBL-2H3 cells transfected with the chimeric teleost receptor IpLITR/IpFcRγ-L, although the dose required for reduction in RBL-2H3 cell viability was higher compared to catfish cell lines. A representative flow cytometric plot for transfected RBL-2H3 cells exposed to 25 mg L^{-1} K-RNT shows a significant reduction in cell viability, as indicated through increased PI fluorescence, **(Figure 2-5B)** compared to control **(Figure 2-5A)**. Combined flow

cytometric viability data for transfected RBL-2H3 cells is shown in **Figure 2-5C**. RBL-2H3 cells exposed to 15, 20 and 25 mg L^{-1} K-RNTs for 2 h had a significant decline in the percentage of viable cells in culture compared to vehicle control (81.0±4.1, 75.9±4.2, 65.7±4.7 %, respectively). RBL-2H3 viability was significantly affected by 25 mg L^{-1} TBL- and $RGDSK^{1}/TBL^{9}$-RNTs exposure, with the percentage of viable cells in culture declining to 77.8±4 and 77.4±5%, respectively.

Exposure of cells to K-, TBL- or $RGDSK^{1}/TBL^{9}$-RNT significantly reduced the ability of cells to phagocytose via the IpLITR/IpFcRγ-L receptor. Representative flow cytometric plots for RBL-2H3 cells expressing IpLITR/IpFcRγ-L chimeric receptor is shown in **Figure 2-6A-C**. A large proportion of RBL-2H3 cells expressing IpLITR/IpFcRγ-L internalized anti-HA m-Ab-coated fluorescent beads, represented by a large shift in FL1 fluorescence **(Figure 2-6A)**. In general, this response was diminished with 2 h exposure to high doses of RNTs **(Figure 2-6B)** but unaffected at lower doses of RNTs **(Figure 2-6C)**. Specifically, cells exposed to K-RNT for 2 h had a dose-dependent decrease in phagocytosis **(Figure 2-6D)**. Compared to control (57.8±2 %), the percentage of cells that internalized one or more beads significantly decreased when exposed to 10 mg L^{-1} (45.8±2 %), 15 mg L^{-1} (42.6±2 %), 20 mg L^{-1} (36.7±2 %) or 25 mg L^{-1} (29.2±3 %) K-RNT. RBL-2H3 cells exposed to TBL- or $RGDSK^{1}/TBL^{9}$-RNTs for 2 h had significant decreases in phagocytosis at exposure concentrations of 20 and 25 mg L^{-1}

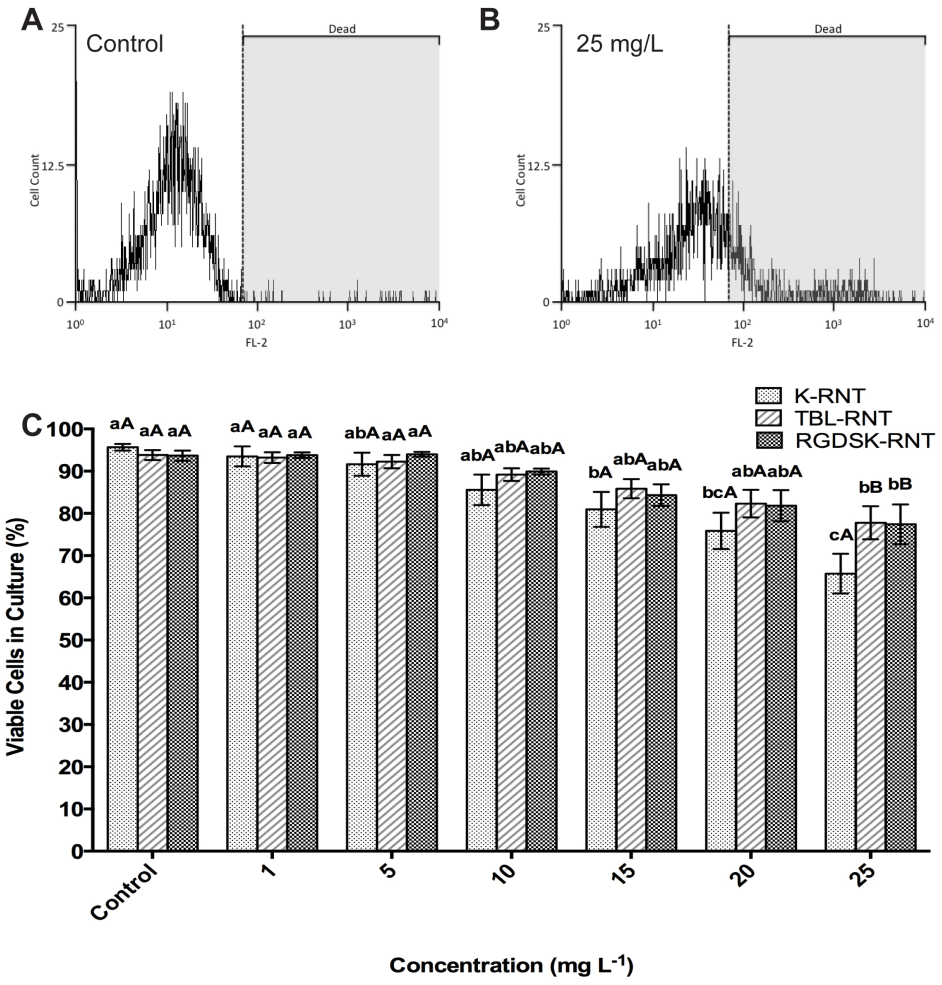

Figure 2-5. RNT exposure had a significant effect on IpLITR/IpFcRγ-L expressing RBL-2H3 cell viability. RBL-2H3 cells expressing IpLITR/IpFcRγ-L at a density of 1 x 10^5 cells were exposed to 1, 5, 10, 15, 20, 25 mg L^{-1} RNT (K-, TBL- or $RGDSK^1$/TBL^9-) for 2 h. Representative flow cytometric plots of RBL 2H3 cells exposed to 25 mg L^{-1} K-RNT had a shift in FL2 fluorescence indicative of increased PI staining and declining viability (A) when compared to cells exposed to vehicle control (B). Summarized flow cytometric viability data (C) demonstrate a dose- and functionalization-dependent response to RNT exposure. Data were analyzed by two-way ANOVA with a Tukey's *post hoc* test. Lowercase letters (a,b,c) denote significant differences between concentrations tested for each RNT-functionalization. Uppercase letters (A,B) denote significant differences between K-, TBL- or $RGDSK^1$/TBL^9-functionalizations for each concentration tested ($p<0.05$). Means ± SE are shown, n=5.

(Figure 2-6E, F). Compared to control (56.3±3 %), the percentage of cells that internalized one or more bead significantly decreased to 43.0±3 % or 41.5±3 % after 20 or 25 mg L^{-1} TBL-RNT exposure **(Figure 2-6E)**. Similarly, cells exposed to $RGDSK^{1}/TBL^{9}$-RNTs had a significant decrease in the percentage of cells that internalized one or more bead after exposure to 20 mg L^{-1} (41.5±3 %) or 25 mg L^{-1} (41.8±3 %) compared to control (55.9±4 %) **(Figure 2-6F)**.

2.4 DISCUSSION

To our knowledge, this study is the first report on the effects of NMs on fish lymphocytes, cells that mediate the humoral and cell-mediated responses of adaptive immunity. The data presented herein indicate that RNTs can affect the viability teleost immune cells and affect the function of teleost immune receptors *in vitro.* Moreover, functionalization was found to be an important determinate of immunotoxicity, with fish leukocyte viability varying significantly after exposure to one of three differentially functionalized RNTs. In addition, RNT functionalization differentially affected fish immune receptor function; inhibition of IpLITR induced phagocytosis was functionalization dependent and occurred at sub-lethal levels of RNT exposure. We also found that different classes of lymphoid cells (*e.g.,* B- or T-cells) have distinct dose dependent responses to RNT exposures. Channel catfish lymphoid cells were particularly sensitive to NM exposure, with significant changes in viability after RNT exposure at

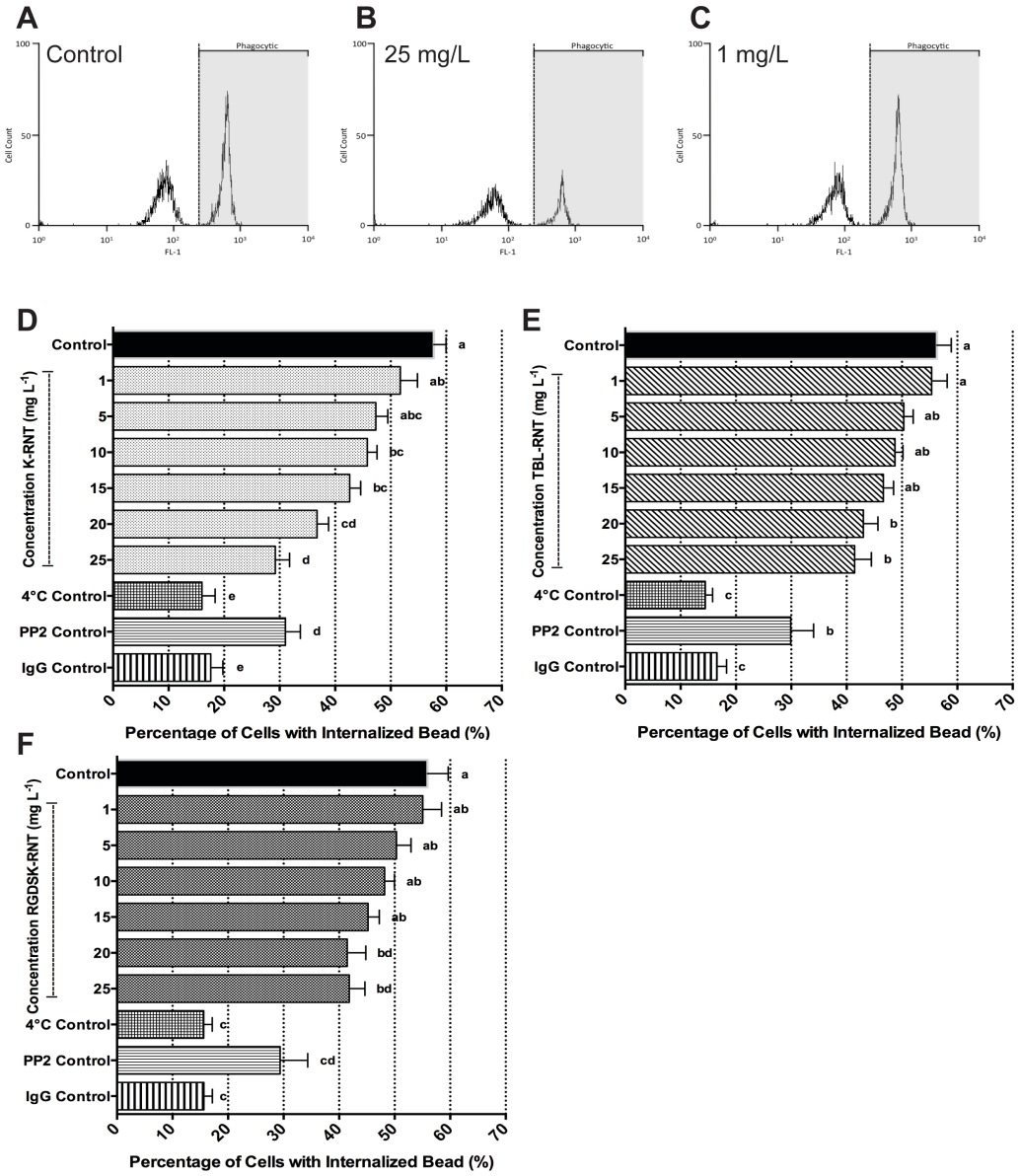
A
Control
Phagocytic
Cell Count
FL-1
B
25 mg/L
Phagocytic
C
1 mg/L
Phagocytic
D
Concentration K-RNT (mg L-1)
Control
1
5
10
15
20
25
4°C Control
PP2 Control
IgG Control
a
ab
abc
bc
bc
cd
d
e
d
e
Percentage of Cells with Internalized Bead (%)
E
Concentration TBL-RNT (mg L-1)
a
a
ab
ab
ab
b
b
c
b
c
Percentage of Cells with Internalized Bead (%)
F
Concentration RGDSK-RNT (mg L-1)
a
ab
ab
ab
ab
bd
bd
c
cd
c
Percentage of Cells with Internalized Bead (%)

Figure 2-6. RNT exposure had a significant effect on IpLITR/IpFcRγ-L mediated phagocytosis in RBL-2H3 cells. RBL-2H3 cells expressing IpLITR/IpFcRγ-L at a density of 1 x 10^5 cells were exposed to 1, 5, 10, 15, 20, 25 mg L^{-1} RNT (K-, TBL- or $RGDSK^1/TBL^9$-) for 2 h. A large shift in FL1 fluorescence indicates the increased proportion of RBL-2H3 cells that have internalized anti-HA m-Ab-coated fluorescent beads (A); in general, this response was diminished with 2 h exposure to high doses of RNTs (representative 25 mg L^{-1} flow cytometric trace) (B) but unaffected at lower doses of RNTs (representative 1 mg L^{-1} flow cytometric trace) (C). Summarized flow cytometric phagocytosis data demonstrate that K-RNT (D), TBL-RNT (E) and $RGDSK^1/TBL^9$-RNT (F) exposure impacts the ability of RBL 2H3 cells to elicit IpLITR/IpFcRγ-L mediated phagocytosis after 2 h. Data were analyzed by one-way ANOVA with a Tukey's *post hoc* test. Lowercase letters (a,b,c,d) denote significant differences between concentrations tested for each RNT-functionalization ($p<0.05$). Means ± SE are shown, n=5.

concentrations that were an order of magnitude lower when compared with mammalian myeloid (*i.e.* granulocytes and monocyte) cells (**Chapter 4**). Together, these results suggest that surface functionalization is a major determinate of NM immunotoxicity, with channel catfish being a particularly sensitive model to examine the effects of NM exposure in fish.

2.4.1 Differential response of catfish lymphocytes to RNT exposure

The classes of lymphoid cells investigated here responded differently to RNT exposure. The two channel catfish B-cell-like lines tested, 1G8 and 3B11, share similar toxicity profiles after RNT exposure and had significantly greater declines in viability compared to the T-cell-like line tested, 28S.3. If the cell lines responsible for carrying out the effector functions of the two arms of adaptive immunity in fish are differentially susceptible, this has important implications. B-cells, which are responsible for antibody production and important in humoral immunity, appear to be more sensitive to RNTs in contrast to T-cells, which are responsible for cell-mediated immunity (Zapata et al., 2006). In addition to the noted differences in sensitivity between B- and T-cells, we observe that these cell lines are an order of magnitude more sensitive to nanomaterial exposure than mammalian cell lines tested (**Chapter 4**). This suggests that mammalian data may not be indicative of the effects of NM exposure in fish.

There are many physiological factors that may account for differences in cell line sensitivities. Metabolic rates, types of internalization pathways,

rates of cellular internalization, antioxidant capacities and detoxification capacities have all been implicated in contributing to the level of resiliency in cells exposed to toxicants (Chang et al., 2007; Horev-Azaria et al., 2013; Kroll et al., 2011; Lanone et al., 2009; Riley et al., 2005). For example, in a comparison of sensitivities between macrophage and epithelial cell lines exposed to combustion derived metals, macrophages were found to be an order of magnitude more sensitive to metal exposure. This increased sensitivity was attributed to higher rates of phagocytosis and internalization in macrophages (Riley et al., 2005). Future studies examining the mechanisms accounting for these noted differences in catfish lymphoid sensitivities to NM exposure are required.

2.4.2 Different functionalization impacts the effect of RNT exposure

The increasing numbers of NMs being manufactured that differ in chemical composition, surface functionalization and size makes toxicity testing of every material technically unfeasible. RNTs provide an ideal platform to investigate the effects of altering NM surface functionalization in high aspect ratio NMs while immunotoxicity can provide a more sensitive and cost efficient approach to environmental toxicity assessment.

Despite the differences in sensitivities between catfish lymphoid B-cell-like and T-cell-like lines to RNT exposure noted above, the relationship between RNT physico-chemical characteristics and cytotoxicity was conserved across all cell lines examined. Although the overall change in

viability was cell line specific, for all catfish lymphocytes examined, K-functionalized RNT exposure caused greater declines in viability while TBL-functionalized RNT exposure resulted in the smaller declines in viability. For the surface functionalizations examined, lymphocyte viability was most greatly affected, in descending order, by exposure to K-RNT > RGDSK[1]/TBL[9]-RNTs > TBL-RNT. Results from this study corroborate other reports suggesting NM surface functionalization is an important determinate of immunotoxicity (Goodman et al., 2004). For example, trout macrophages were differentially stimulated by single-walled carbon nanotubes (SWCNTs) and multi-walled carbon nanotubes (MWCNTs) covalently functionalized with sulfonate groups (anionic functionalization), poly-ethylene glycol groups (neutral functionalization) and m-polyaminobenzene sulfonic acid groups (Klaper et al., 2010).

Two physicochemical properties that could influence the toxicity of K- and TBL-RNTs are charge and functionalization density. Computer simulations of NM exposure suggest that the sign (positive or negative) and density of surface charges have important implications on NM interactions with lipid membranes (Lin et al., 2010). Functionalizing Au NP with positive surface charges resulted in increased bilayer adherence when compared with negative and hydrophobic surface charges with potential consequences on viability (Lin et al., 2010). In concordance, positively-charged Au NPs were internalized by mammalian cell lines while negatively-, neutral- and zwitterionic-charged NPs were not (Arvizo et al., 2010). Increased

association of NMs with cellular membranes can affect cell viability. For example, the interaction of positively-charged Au NPs resulted in membrane depolarization and a concomitant increase in intracellular calcium that effected cell proliferation and induced apoptosis (Arvizo et al., 2010). In our study, while both K-RNTs and TBL-RNTs are positively charged, K-RNTs have a more positive ζ-potential. This would suggest increased membrane association and internalization of K-RNTs. Increased affiliation with the cellular membrane could contribute to the greater toxicity we observed for K-functionalized RNTs.

Computer simulated exposures also suggest that surface charge density has significant impacts on NM penetration and membrane disruption whereby increasing cationic surface charge density from 10 to 100% resulted in increased membrane penetration and a concomitant disruption of modeled bilayers that significantly affect cell viability (Lin et al., 2010). K- and TBL-RNTs have significant differences in functionalization density; K-RNTs being a single-based rosette nanotube, have a precursor unit consisting of one G□C motif covalently attached to a single K-group. In contrast, TBL-RNTs are twin-based (TB) rosette nanotubes, with a precursor unit consisting of two G□C motifs covalently attached to a single aminobutyl group. This effectively results in TBL-RNTs having half the functionalization density compared to K-RNTs. K-RNTs, with their increased density of positively charged surface groups, may exhibit increased penetration and disruption of cell membranes compared to TBL-RNTs and provides a possible

explanation for the greater declines in catfish lymphocyte viability we observed after K-RNT exposure. Taken together, we propose that the increased charge and density of K-RNTs (compared to TBL-RNTs) may contribute to the differences in viability we observed.

RNTs are polyelectrolytes that are very soluble in aqueous media and generally have little affinity for proteins; however, their overall positive charge could attract a variety of anionic biomolecules such as nucleic acids. This in turn could influence RNT surface properties, affiliation with proteins, charge, aggregation and size in solution (Lundqvist et al., 2008). The differential affiliation with various biomolecules such as proteins could be another factor influencing the variation in toxicity observed between K- and TBL-functionalized RNTs. Recent reports suggest that altering the functionalization of NMs alters the composition of bound proteins. For example, varying the charge and size of polystyrene NMs led to changes in immunoglobulin proteins, apolipoproteins, complement proteins, acute-phase proteins and coagulation factors that were bound to NMs (Lundqvist et al., 2008). The density of surface functionalizations also has significant impacts on the composition of bound proteins. For example, it has been demonstrated that different complement pathways are activated upon NM exposure in human serum when the density of functionalized polymers is altered (Hamad et al., 2010; Sim and Wallis, 2011). Given that K- and TBL-RNTs vary in both surface charge and functionalization density, it is likely

that there are differences in bound biomolecules and this could contribute to the observed differences in toxicity.

While there are significant differences in surface charge and functionalization density between K- and TBL-RNTs, the co-assembly of TB-RGDSK and TB-TBL resulted in RGDSK^{1}/TBL^{9}-RNTs expressing the RGDSK-peptide, while maintaining a solubility and surface charge profile similar to TBL-RNTs. Despite this similarity, the introduction of a peptide ligand, RGDSK-, to the surface of RNTs caused greater declines in viability compared to TBL-RNTs at 1.0 and 2.0 mg L^{-1} exposures. This suggests that in addition to functionality causing differential toxicity based on physicochemical parameters, toxicity can also be tailored with biologically active peptides. In support, Suri et al. (2009) found that exposure to RNTs functionalized with the RGDSK-peptide caused phosphorylation of p38 mitogen-activated protein kinase (MAPK) in Calu-3 cells. Activation of p38 MAPK led to increased TNF-α secretion, activation of caspase-3 and ultimately induced apoptosis (Suri et al., 2009). Taken together, this supports the use of RNTs as a therapeutic to deliver targeted ligands to cells.

2.4.3 RNT exposure affects IpLITR/IpFcRγ-L mediated phagocytosis

Results demonstrate that sub-lethal levels of RNT exposure affect the ability of immune cells to elicit effector responses *in vitro* and was concentration- and functionalization-dependent. Significant inhibition of IpLITR/IpFcRγ-L mediated phagocytosis occurred after exposure to 10, 15,

20, 25 mg L^{-1} K-functionalized RNTs. TBL- and $RGDSK^{1}/TBL^{9}$-functionalized RNTs inhibited IpLITR/IpFcRγ-L mediated phagocytosis to a lesser extent, with significant declines noted at 20 and 25 mg L^{-1}.

Our finding that sub-lethal exposures of RNTs inhibit the ability of the chimeric teleost immune receptor IpLITR/IpFcRγ-L to phagocytose is of special interest. Altered immune function can affect an organism's ability to fight against bacterial, viral, fungal and parasitic infections. The fact that we observe these changes before significant declines in cell viability suggests that using cell effector functions to gauge toxicity is an important aspect to consider in aquatic nanotoxicology.

Interestingly, RNT functionalization differentially affected phagocytosis. As phagocytosis is receptor-mediated through IpLITR/IpFcRγ-L, interactions between RNTs and the cell membrane likely are influencing the ability of this receptor to elicit effector responses. Since NMs have been shown to interact with proteins in solutions, it is possible that RNTs are binding the chimeric receptor IpLITR/IpFcRγ-L or its antigen, the α-HA mAb. Such changes could ultimately change receptor engagement with its ligand and could be responsible for the decreased phagocytosis observed (Nel et al., 2009). NM association with biomolecules (including proteins) is functionalization dependent and may account for the observed differences in inhibition of phagocytosis between RNT functionalizations. The exact mechanism of how our different functionalizations impact phagocytosis

remains unclear but has important implications for both innate and acquired immunity in fish.

2.5 CONCLUSIONS

Our results indicate that surface functionalization is an important determinate of nanotoxicity. RNTs with a higher density of positively charged surface moieties (K-RNTs) caused greater declines in lymphocyte viability and impaired the ability of cells to phagocytose through the fish immune receptor, IpLITR. To our knowledge, this is the first study examining the effect of NM exposure on fish lymphoid cell lines. We demonstrate that channel catfish lymphocytes are particularly sensitive to NM exposure *in vitro*, displaying significant declines in viability at concentrations of NMs that are an order of magnitude lower than mammalian cell lines. In addition, channel catfish lymphocytes responded differentially to RNT exposure. The B-cell-like lines, 1G8 and 3B11, and had significantly greater declines in viability compared to the T-cell-like line, 28S.3. The sensitivity of channel catfish lymphocytes, the availability of several distinct immune cell types *in vitro* and an array of available endpoints to examine immune function make channel catfish a versatile model for future immunotoxicology studies in fish. Future studies should continue to focus on the physico-chemical parameters that may contribute to NM immunomodulation and the mechanisms through which NMs may be exerting their effects.

CHAPTER 3

Acid functionalized carbon nanotubes affect channel catfish (*Ictalurus punctatus*) lymphocyte viability and function

3.1 INTRODUCTION

Carbon nanotubes (CNTs) are seamless cylinders comprised of one (single-walled CNTs) or more (multi-walled CNTs) rolled sheets of graphene. These materials have a high aspect ratio, with single walled CNTs having a diameter ranging from 0.8 – 2 nm while their length can range from less than 100 nm to several centimeters long (De Volder et al., 2013). Carbon nanotubes (CNTs) have unique mechanical, thermal, optical, electrical and chemical properties that have been utilized for many commercial applications including energy storage, water treatment, composite materials, electronics and biotechnology (De Volder et al., 2013). Increased commercial demand has been met with increased CNT production and from 2006 to 2011 the worldwide production of carbon nanotubes increased 10 fold, with production exceeding 4.5 kilotons per year (De Volder et al., 2013). This large increase in production driven by commercial demand has been facilitated by new high volume CNT manufacturing techniques such as the chemical vapour deposition (CVD) technique and the induction thermal plasma (ITP) process (De Volder et al., 2013; Kim et al., 2009). With increased production and incorporation into commercial products, a concomitant increase in the environmental release of CNTs is expected. Initial models predicting the environmental concentrations of CNTs suggest these materials are already accumulating in terrestrial and aquatic environments. For example, Sun et al. (2014) predicted an environmental concentration of CNTs in effluent of 4.0 ng L^{-1} and given rising production,

environmental accumulation is expected rise. This has led to concerns over the environmental hazard of CNTs on aquatic ecosystems including the health of aquatic organisms such as fish (Handy et al., 2011; Petersen et al., 2011). Cheng *et al*. (2012) observed severe developmental toxicity in zebrafish embryos exposed to CNTs (Cheng and Cheng, 2012) and rainbow trout exposed to CNTs had significant gill injury and associated respiratory distress at exposure concentrations as low as 1 mg L^{-1} (Smith et al., 2007). However, significant gaps in the literature have been identified, including the sub-lethal effects of CNT exposure in fish and the potential effects of CNT exposure on fish immunity (Jovanović and Palić, 2012; Petersen et al., 2011).

Changes in the function of the immune system, comprised of a complex network of molecules, cells and tissues, can have important effects on the ability of fish to fight bacterial, viral, fungal and parasitic infections. Immune cells are some of first cells to encounter and respond to foreign materials, such as nanomaterials, making them important in the evaluation of nanotoxicity. Myeloid cells (*i.e.* macrophages and granulocytes) are important mediators of innate immunity and to date, few studies have examined the response of fish myeloid cells to CNT exposure. Klaper et al. (2010) described one of the first studies examining differentially functionalized CNT exposure to trout primary macrophages and found that sub-lethal CNT exposures caused the expression of the pro-inflammatory mediator IL-1β. Lymphoid cells (*i.e.* B-cells and T-cells) are important in

acquired immunity and to date, no studies have reported on the response of fish lymphoid cells to CNT exposure.

Here we examine the toxicity of unfunctionalized CNTs (U-CNTs) produced directly from induction thermal plasma process on fish lymphocyte viability and function. We also examine the effect of purified and acid functionalization CNTs (AF-CNTs) on fish lymphocyte viability and function following exposure to three differentially AF-CNTs: CNT-30, CNT-40 and CNT-50. We hypothesize that acid functionalization of CNTs, and the corresponding increase in solubility, will increase the biological interaction of CNTs and ultimately increase their toxicity *in vitro*. To complete these studies, we utilized channel catfish (*Ictalurus punctatus*) lymphoid cells including two B-cell-like (3B11, 1G8) and one T-cell-like (28S.3) cell line. To examine the effect of CNT exposure on lymphoid cell function, we examined channel catfish leukocyte immune-type receptor (IpLITR) mediated phagocytosis following CNT exposure. IpLITRs are surface receptors expressed on myeloid and lymphoid cells with stimulatory and inhibitory forms that regulate a variety of immune responses including phagocytosis and degranulation (Cortes et al., 2012). The availability of *in vitro* lymphoid cell lines and the extensive characterization of IpLITRs make catfish a powerful model to examine the effects of CNT exposure on fish lymphoid viability and function.

3.2 MATERIALS AND METHODS

3.2.1 Synthesis and physico-chemical characterization of CNTs

U-CNTs were produced from commercial carbon black (Columbian Inc.) using the induction thermal plasma technique with nickel, cobalt and yttrium oxides as catalysts. CNTs were produced at the Steacie Institute for Molecular Sciences and a detailed report on their synthesis and characterization can be found in Kim et al. (2007). Purification and acid-functionalization of U-CNTs was completed in a nitric acid/sulfuric acid (HNO_3/H_2SO_4) solution for 2 h at 30, 40 or 50 °C to yield CNT-30, CNT-40 or CNT-50, respectively. Price et al. (2009) reports details on the purification and acid-functionalization of U-CNTs. Increasing the oxidation temperature produces progressively shorter CNTs functionalized with carboxylic acid groups. U-CNT, CNT-30, CNT-40 and CNT-50 were suspended in double distilled water (ddH_2O) at a final concentration of 1000 mg L^{-1} to create the stock suspensions used in this study.

We have previously reported on the characterization of U-CNT, CNT-30, CNT-40 and CNT-50 and a summary of these findings is provided in the Supplemental Information. Transmission electron microscopy (TEM) micrographs of U-CNTs were completed on a H-750 electon microscope (Hitachi High-Technologies Corporation, Japan) and are provided in **Supplemental Figure S3-1**. Dynamic light scattering measurements of hydrodynamic diameter, polydispersity index and zeta potential for CNT-30, CNT-40 and CNT-50 at concentrations of 10, 50, 100 and 250 mg L^{-1} were

completed using a Malvern Zetasizer (Malvern Instruments, UK) and are provided in **Supplemental Table S3-1**. Measurements of hydrodynamic diameter and zeta potential for U-CNTs could not be completed due to their poor solubility; characterization of AF-CNTs at concentrations below 10 mg L^{-1} was below accurate limits of detection using DLS. In addition, it was not possible to collect reproducible data of CNTs in cell culture media using DLS. Infrared and Raman spectroscopy were used to verify that the oxidation procedure introduced carboxylic acid groups to the ends and sidewalls of U-CNTs and the spectra of U-CNT and CNT-30 are provided in **Supplemental Figure S3-2**. Using inductively coupled plasma atomic emission spectroscopy (ICP-AES) we verified the degree of carboxylic acid group functionalization by weight and calculated the functionalization degree (mole %) of CNT-30, CNT-40 and CNT-50, these results are presented in **Supplemental Table S3-2**.

3.2.2 Cell culture

Channel catfish lymphocyte cell lines 3B11, 1G8 and 28S.3 were cultured in filter sterilized (0.22 μm filter; Corning) AL media (1:1, AIM-V medium:L-15 medium; Gibco) supplemented with 0.5 g sodium bicarbonate (Sigma), 0.05 M 2-mercaptoethanol, 100 units mL^{-1} penicillin (Gibco), 100 μg mL^{-1} streptomycin (Gibco) and 3% catfish serum at 27 °C and 5% CO_2. 3B11, 1G8 and 28S.3 were passaged when 80% confluence was reached (~3-5 days).

RBL-2H3 cells were cultured in filter sterilized (0.22 μm filter; Corning) minimum essential media (MEM/EBSS; Hyclone) with 2 mM L-glutamine (Gibco), 100 units mL^{-1} penicillin (Gibco), 100 μg mL^{-1} streptomycin (Gibco) and 10% heat inactivated fetal bovine serum (FBS; Hyclone) supplemented with G418 selection reagent at 37 °C and 5% CO_2. Cells were passaged when 80% confluence was reached (~3-4 days).

3.2.3 Determining channel catfish lymphocyte viability following CNT exposure

For comparison and accuracy, channel catfish lymphocyte viability following CNT exposure was measured using both the MTS assay and flow cytometric analysis. U-CNT, CNT-30, CNT-40 or CNT-50 exposure solutions (0.25, 0.5, 1, 5, 10, 25, 50 mg L^{-1}) in cell culture media were created from serially diluted CNT stock suspensions following vortexing for 30 seconds and subsequently sonicating for 30 seconds using a Sonifer Cell Disruptor (Branson Ultrasonics, USA). Control exposures received AL culture media alone (negative control) or AL3 media containing CNT stock solution supernatant (vehicle control) obtained by centrifuging U-CNT stock solution and subsequently filtering the collected supernatant through a 0.22 μm filter (Corning). The vehicle control was run to determine if any trace metal contaminants that might remain in CNT stock solutions affect cell viability.

The MTS assay was completed in round-bottom 96 well plates (Becton Dickinson) using the Cell Titer 96 Aqueous Non-Radioactive Cell Proliferation

Kit (Promega). MTS [3-(4,5-dimethylthiazol-2-yl)-5-(3-carboxymethoxyphenyl)-2-(4-sulfophenyl)-2H-tetrazolium] is a tetrazolium salt that undergoes a color change when bioreduced by viable cells in culture and can be used to gauge relative cell viability by measuring the change in absorbance at 490 nm. Briefly, 3B11, 1G8 and 28S.3 cells were seeded at a density of 20,000 cells per well and exposed to 0.25, 0.5, 1, 5, 10, 25, 50 mg L^{-1} U-CNT, CNT-30, CNT-40 or CNT-50, negative control or vehicle control solutions for 6, 24 or 48 h at 27 °C and 5% CO_2. Following exposure, prepared kit reagents were added to each well and the plate was incubated at 27 °C and 5% CO_2 for 3 h. Cell solutions were then transferred to a flat-bottom 96 well plate (Becton Dickinson) and absorbance was measured at 490 nm on a Wallac 1420 microplate reader (Perkin Elmer). To account for interference by CNTs, the absorbance of wells containing 0, 0.25, 0.5, 1, 5, 10, 25 or 50 mg L^{-1} U-CNT, CNT-30, CNT-40 or CNT-50 in AL media without cells was measured. Viability was calculated based on the following formula:

Viability (% Control) = [(CNT exposed cells absorbance)-(Background CNT absorbance)] / [(Control exposed cells absorbance)-(Background control absorbance)]

Catfish lymphocyte viability following CNT exposure was also determined with flow cytometric analysis. Briefly, 3B11, 1G8 and 28S.3 cells were seeded at a density of 20,000 cells per well in a 96-well round bottom plate (Becton Dickinson) and exposed to 0.25, 0.5, 1, 5, 10, 25, 50 mg L^{-1} U-CNT, CNT-30, CNT-40 or CNT-50, negative control or vehicle control solutions for 6, 24 or 48 h at 27 °C and 5% CO_2. Following exposure, cells

were stained with propidium iodide (PI, 100 μg mL^{-1}) and analyzed by flow cytometry (Quanta SC, Beckman Coulter). PI, a fluorescent marker for cell death, can only penetrate dead, necrotic and apoptotic cells where it intercalates with nucleic acids and fluoresces (Brana et al., 2002). Whole cell populations for 3B11, 1G8 and 28S.3 were gated using side scatter (SS) and forward scatter (FS) metrics and subsequently analyzed for PI fluorescence using the FL2 filter to separate viable from non-viable cells. The percentage of viable cells in culture was calculated from the number of cells within the whole population gate with low levels of PI fluorescence. All gates were established with negative control treated cells.

3.2.4 Examination of IpLITR/IpFcRγ-L induced phagocytosis following CNT exposure

To examine the effect of CNT exposure on the ability of immune cells to elicit appropriate effector functions, we examined the ability of cells to phagocytose following U-CNT, CNT-30, CNT-40 and CNT-50 exposure. For these studies, we examined phagocytic ability using channel catfish (*Ictalurus punctatus)* leukocyte immune-type receptors (IpLITRs). To target this receptor, an N-terminal HA epitope tagged IpLITR/IpFcRγ-L chimeric receptor was constructed from fusing the extracellular domain of IpLITR with the transmembrane region and cytoplasmic tail of its adaptor protein, IpFcRγ-L. For full details on the construction and cloning of this chimeric

receptor into pDISPLAY vector (Invitrogen) see Cortes *et al.,* (2012) and Mewes *et al*., (2009).

We subsequently transfected RBL-2H3 cells with the IpLITR/IpFcRγ-L construct as described previously (Cortes et al., 2012; Mewes et al., 2009). Briefly, RBL-2H3 cells were seeded at a density of 1.25 x 10^5 cells per well and allowed to attach to the substrate at 37 °C and 5% CO_2. We transfected 1 µg of pDISPLAY IpLITR/IpFcRγ-L plasmid using Xfect transfection reagent (Clontech) in OptiMEM (Hyclone) for 4 h at 37 °C and 5% CO_2. Cells were then incubated overnight (37 °C and 5% CO_2) in fresh culture media. Cell selection was completed in culture media supplemented with G418 disulfate salt (Sigma-Aldrich) for 4 days (37 °C and 5% CO_2) before washing cells and selecting for an additional 8-12 days until confluence was reached.

We utilized flow cytometry to confirm the surface expression of IpLITR/IpFcRγ-L in RBL-2H3 cells. IpLITR/IpFcRγ-L was labeled with anti-hemagglutinin (HA) monoclonal antibody (mAb; Cedarlane Laboratories) and PE-conjugated goat anti-mouse immunoglobulin (Ig) G polyclonal antibody (pAb; Beckman Coulter) and sorted into HA-positive and HA-negative populations (FACSAria, Becton Dickinson). The IpLITR/IpFcRγ-L positive RBL-2H3 cells were subsequently cultured in culture media supplemented with G418 selection reagent and maintained for phagocytosis studies.

Phagocytosis assays utilized flow cytometry to measure the internalization of fluorescent beads opsonized with anti-HA mAb to target IpLITR/IpFcRγ-L and was based on methods described by Cortes *et al.*

(2012). To generate HA mAB opsonized fluorescent beads, 1.25 x 10^8 fluorescent beads (Fluoresbrite Carboxy YG 4.5 micron microspheres; Polysciences) were incubated at room temperature with 200 µg of protein A (*Staphylococcus aureus* origin, Sigma-Aldrich) in borate buffer. Two types of opsonized beads were created, incubating the protein A absorbed beads (4 °C for 3 h) with 20 µg mL^{-1} of either anti-HA mAb or mouse IgG3 isotype antibody (Beckman Coulter). Opsonized beads were subsequently washed with 10 mg mL^{-1} BSA in 1x phosphate buffered saline (PBS).

To examine the effect of CNT exposure on IpLITR/IpFcRγ-L mediated phagocytosis, RBL-2H3 cells expressing IpLITR/IpFcRγ-L were suspended in 100 µL culture media containing 0.25, 0.5, 1, 5, 10, 25, 50 mg L^{-1} U-CNT, CNT-30, CNT-40 or CNT-50 at a density of 1 x 10^5 cells for 2 h at 37 °C and 5% CO_2. Control treatments were exposed to CNT stock solution supernatant (vehicle). Following CNT exposure, cells were split and underwent one of two separate protocols: viability and phagocytosis. To determine RBL-2H3 cellular viability following CNT exposure, cells were analyzed by flow cytometry after being stained with PI (100 µg mL^{-1}) as described above (see section 3.3). For the phagocytosis protocol, CNT exposed RBL-2H3 cells expressing IpLITR/IpFcRγ-L were incubated with 4 µL of anti-HA mAb opsonized beads for 1 h at 37 °C and 5% CO_2. Cells were then centrifuged (5000 *g*; 1 min) and the supernatant was aspirated. Cells were then resuspended and incubated in 100 µL 1x PBS containing 0.05% trypsin, 1 mM EDTA for 15 min on ice to detach non-internalized beads bound to the

cell membrane. Cells were washed with 250 µL 1x PBS containing 0.5% BSA, 2 mM EDTA before being suspended in 300 uL 1% paraformaldehyde (PFA) in 1x PBS. To gauge IpLITR/IpFcRγ-L-mediated phagocytosis following CNT exposure, cells were analyzed by flow cytometry (Quanta SC, Beckman Coulter) for FL-1 fluorescence, with an increase in FL-1 fluorescence indicating the internalization of one or more beads. Our positive control, exposed to vehicle alone and incubated with anti-HA mAb opsonized beads at 37 °C and 5% CO_2 represents a normal phagocytic response through IpLITR/IpFcRγ-L engagement. Incubation with anti-HA mAb opsonized beads at 4 °C (4 °C Control) was run to determine that phagocytosis was occurring through an active cell process requiring ATP hydrolysis. Isotype control, incubation of cells with IgG3 Ab opsonized beads at 37 °C, was run to verify phagocytosis was occurring through IpLITR/IpFcRγ-L engagement. The PP2 control treatment consisted of pre-treating cells with 10 µM of PP2 (EMD Biosciences) for 30 min before incubating cells with anti-HA mAb opsonized beads for 1 h at 37 °C and 5% CO_2. Treatment with PP2 inhibits Src kinases, known downstream signaling intermediates of IpLITRs (Cortes et al., 2012) and was also used to verify that the route of bead internalization was through IpLITR/IpFcRγ-L engagement.

3.2.5 Statistical analysis

Statistical analysis were performed with GraphPad 6.0 statistical software with significance set at $p<0.05$. To investigate the effects of CNT

exposure on catfish lymphocyte viability a two-way analysis of variance (ANOVA) with Tukey post hoc test was performed. To compare toxicity profiles between catfish cell lymphocytes (3B11, 1G8, 28S.3), CNT functionalization and CNT concentration, a three-way ANOVA followed by post-hoc Holm-Sidak test was performed. To investigate the effects of CNT exposure on IpLITR/IpFcRγ-L mediated phagocytosis, a two-way analysis of variance (ANOVA) with Tukey post hoc test was performed. All data is presented as mean ± standard error of the mean (SE) unless indicated otherwise.

3.3 RESULTS

3.3.1 Effect of CNT exposure on channel catfish lymphocyte viability

3.3.1.1 Effect of CNT exposure on 3B11 viability

3B11 cells exposed to CNTs had significant declines in viability that were dose- and time-dependent but not functionalization-dependent. Combined flow cytometric results for 3B11 cells exposed to varying concentrations of CNTs for 6 h revealed a dose-dependent decrease in cell viability (**Figure 3-1A**). Significant declines in the number of viable 3B11 cells in culture were found after exposure to 25 and 50 mg L^{-1} U-CNT, CNT-30, CNT-40 and CNT-50 for 6 h.

CNT functionalization was not a significant determinant of toxicity, with similar declines in 3B11 viability for U-CNT, CNT-30, CNT-40 and CNT-

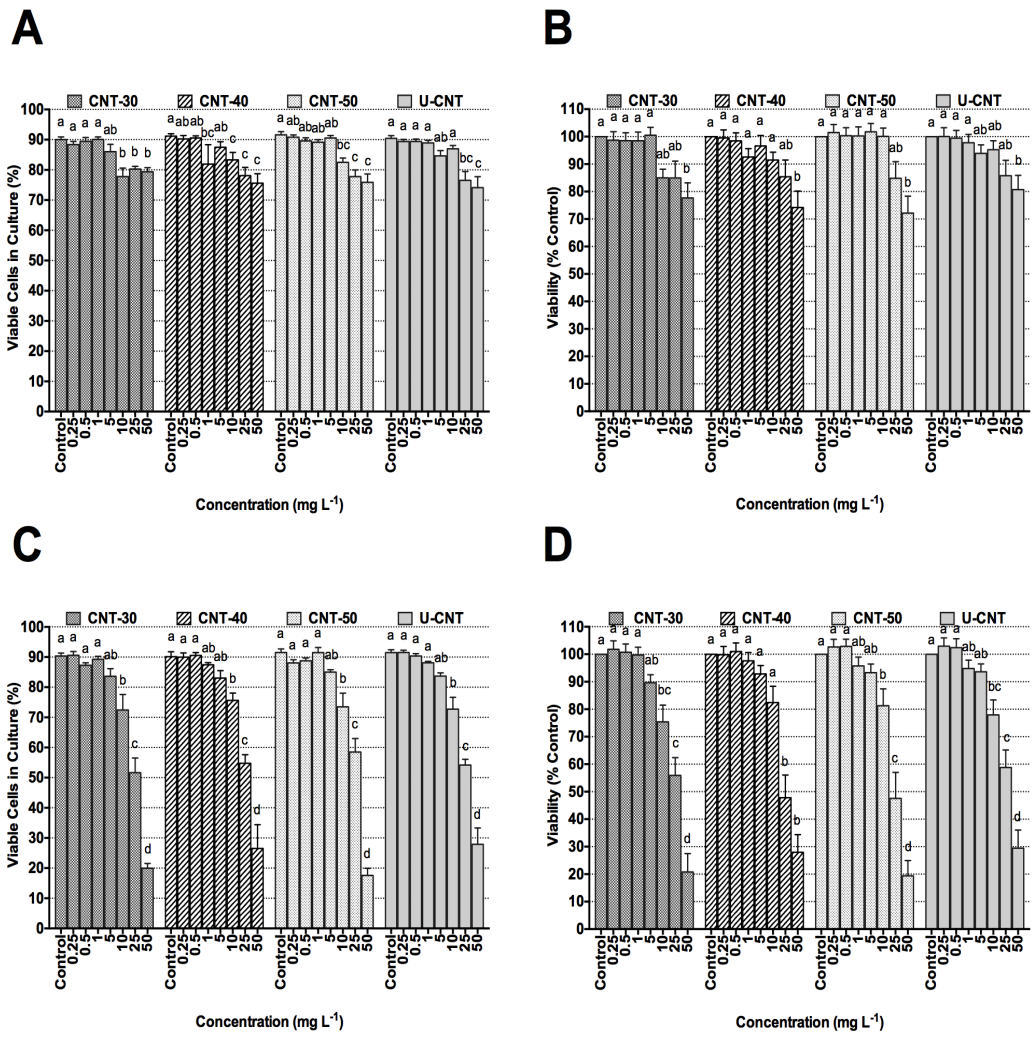

Figure 3-1. CNT exposure had a significant effect on channel catfish 3B11 cell viability. 3B11 cells ($2.0x10^4$ cells $well^{-1}$) were incubated with 0.25, 0.5, 1, 5, 10, 25, 50 mg L^{-1} U-CNT, CNT-30, CNT-40 or CNT-50 for 6 (A, B) or 24 h (C, D). Summarized flow cytometric viability data (A, C) and MTS viability data (B, D) demonstrate a dose- and time-dependent decline in 3B11 viability following CNT exposure. Data were analyzed by two-way ANOVA followed by Tukey's *post hoc* test. Letters denote significant differences in viability between concentrations tested for each CNT. Means±SE are shown.

50. For example, 3B11 cells exposed to 25 mg L^{-1} U-CNT, CNT-30, CNT-40 or CNT-50 for 6 h had (n=5) 77±3%, 80±1%, 78±3% or 78±2% viable cells in culture, respectively (**Figure 3-1A**). Verifying our flow cytometric data, similar declines in 3B11 viability were measured with the MTS assay following 6 h of CNT exposure. Significant declines in 3B11 viability were noted after 6 h exposure to 50 mg L^{-1} U-CNT, CNT-30, CNT-40 and CNT-50 (**Figure 3-1B**) with similar declines in 3B11 viability for all CNT functionalization examined.

Changes in 3B11 viability following CNT exposure was also time-dependent, with significantly greater overall declines in viability after 24 h exposure to 10, 25 and 50 mg L^{-1} CNTs compared to 6 h exposures (**Figure 3-1C**). After 24 h exposure to 50 mg L^{-1} U-CNT, CNT-30, CNT-40 or CNT-50 the number of viable 3B11 cells in culture declined to (n=5) 28±5%, 20±2%, 27±8% or 18±3%, respectively. This represents a more significant decline in viability compared to the number of viable 3B11 cells that remained in culture after 6 h exposure to 50 mg L^{-1} CNT (74±4%, 79±1%, 76±3% or 76±3% for U-CNT, CNT-30, CNT-40 or CNT-50, respectively). However, similar to the 6 h time point, functionalization was not a significant determinant of CNT toxicity, with similar declines noted for U-CNT, CNT-30, CNT-40 and CNT-50 at each concentration (**Figure 3-1C**). Similar results were obtained with the MTS assay, with significantly greater declines in

viability after 24 h exposure to 10, 25 and 50 mg L^{-1} CNT and no significant differences between the CNT functionalization examined (**Figure 3-1D**).

3.3.1.2 Effect of CNT exposure on 1G8 viability

Similar to 3B11 cells, 1G8 cells had significant declines in viability after 6 and 24 h of exposure to CNTs that was dose- and time-dependent; CNT functionalization was not a significant determinant of toxicity in 1G8 cells. After 6 h of CNT exposure, declines in 1G8 cell viability was dose-dependent with significant declines in the number of viable cells in culture for all CNT functionalizations examined at concentrations of 25 mg L^{-1} and 50 mg L^{-1}. Exposure to 50 mg L^{-1} U-CNT, CNT-30, CNT-40 or CNT-50 for 6 h reduced the percentage of viable 1G8 cells in culture to 73±3%, 76±3%, 77±3% or 77±3%, respectively (**Figure 3-2A**). Exposure to 50 mg L^{-1} U-CNT, CNT-30, CNT-40 or CNT-50 for 24 h further reduced 1G8 viability, declining to 28±6%, 35±8%, 28±8%, 20±5% viable cells in culture, respectively (**Figure 3-2C**). In addition, significant declines in 1G8 viability occurred at lower doses of CNTs after 24 h of exposure. 1G8 cells exposed to CNTs had significant declines in viability at concentrations of 10, 25 and 50 mg L^{-1} for all CNT functionalizations examined.

MTS measurements of 1G8 viability following CNT exposure verified our flow cytometric results. CNT exposure reduced 1G8 viability in a dose- and time-dependent manner. Exposure to CNTs for 6 h caused significant reductions in 1G8 viability (**Figure 3-2C**). Further reductions in viability

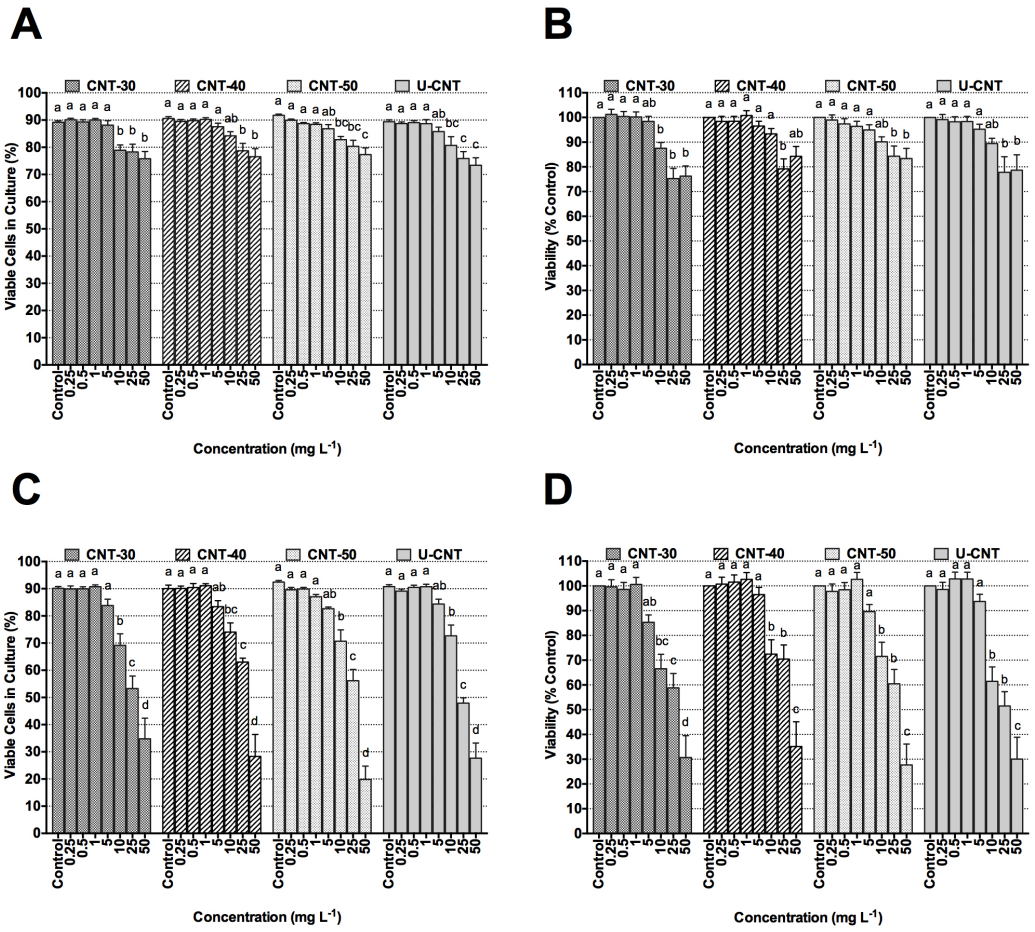

Figure 3-2. CNT exposure had a significant effect on channel catfish 1G8 cell viability. 1G8 cells ($2.0x10^4$ cells $well^{-1}$) were incubated with 0.25, 0.5, 1, 5, 10, 25, 50 mg L^{-1} U-CNT, CNT-30, CNT-40 or CNT-50 for 6 (A, B) or 24 h (C, D). Summarized flow cytometric viability data (A, C) and MTS viability data (B, D) demonstrate a dose- and time-dependent decline in 1G8 viability following CNT exposure. Data were analyzed by two-way ANOVA followed by Tukey's *post hoc* test. Letters denote significant differences in viability between concentrations tested for each CNT. Means±SE are shown.

occurred after 24 h CNT exposure, with significant declines in 1G8 viability at concentrations of 10, 25, and 50 mg L^{-1} (**Figure 3-2D**).

3.3.1.3 Effect of CNT exposure on 28S.3 viability

Lastly, the effect of CNT exposure on 28S.3 cell viability was examined. Unlike 3B11 and 1G8 catfish lymphocytes, there was no significant decrease in 28S.3 viability compared to control after 6 h of U-CNT, CNT-30, CNT-40 or CNT-50 exposure as determined by flow cytometric analysis and the MTS assay (**Figure 3-3 A,B**). However, after 24 h of exposure, the declines in 28S.3 lymphocyte viability were dose-dependent with significant reductions in viability after exposure to 25 or 50 mg L^{-1} U-CNT, CNT-30, CNT-40 or CNT-50 (**Figure 3-3C,D**). Flow cytometric analysis revealed that exposure to 50 mg L^{-1} U-CNT, CNT-30, CNT-40 or CNT-50 for 24 h reduced the percentage of viable 28S.3 cells in culture to 70±4%, 63±5%, 69±35% or 73±5%, respectively (**Figure 3-3C**). Flow cytometric analysis and the MTS assay found that CNT functionalization was not a major determinant of toxicity in 28S.3 lymphocytes (**Figure 3-3**).

3.3.1.4 Comparison of CNT toxicity between catfish lymphocyte cell lines

To compare the effects of CNT exposures on 3B11, 1G8 and 28S.3 cells, we utilized a three-way ANOVA followed by Holm-Sidak post hoc tests. Flow cytometric and MTS assay data grouped for all three catfish lymphocyte cell lines following 48 h exposure to U-CNT, CNT-30, CNT-40 and CNT-50 is

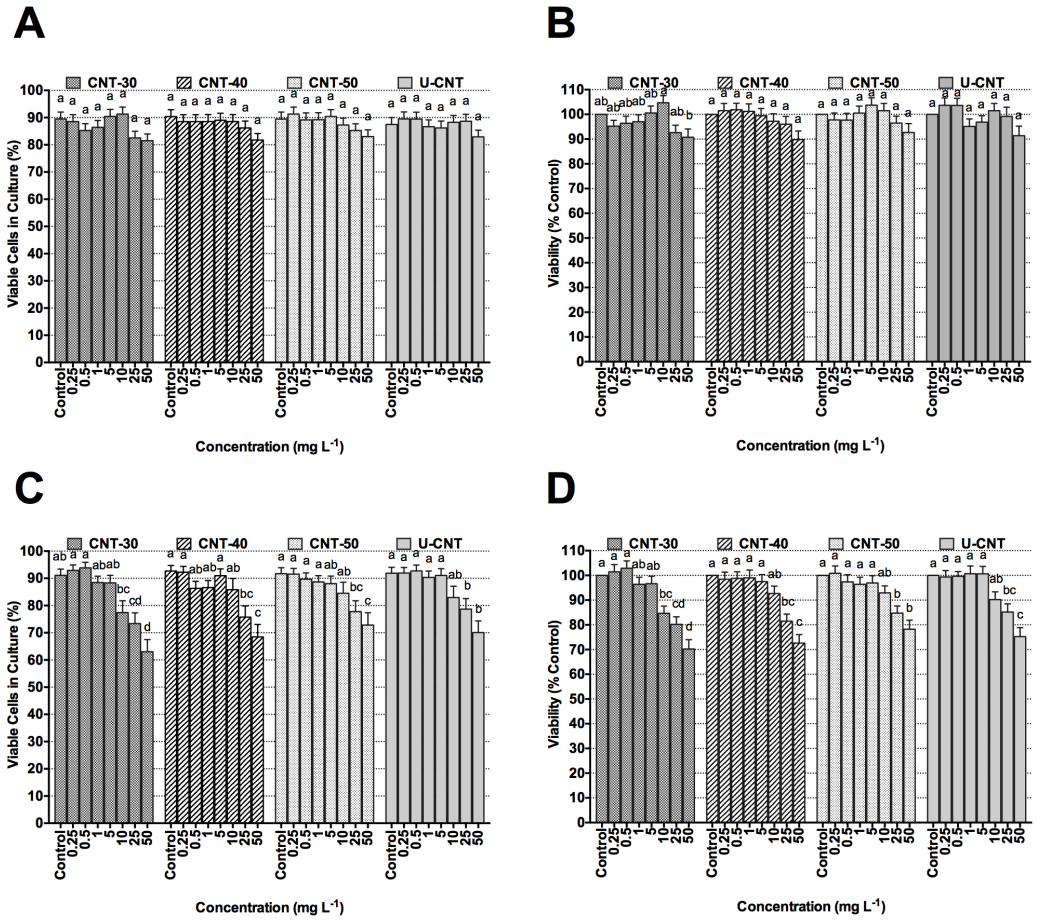

Figure 3-3. CNT exposure had a significant effect on channel catfish 28S.3 cell viability. 28S.3 cells ($2.0x10^4$ cells $well^{-1}$) were incubated with 0.25, 0.5, 1, 5, 10, 25, 50 mg L^{-1} U-CNT, CNT-30, CNT-40 or CNT-50 for 6 (A, B) or 24 h (C, D). Summarized flow cytometric viability data (A, C) and MTS viability data (B, D) demonstrate a dose- and time-dependent decline in 28S.3 viability following CNT exposure. Data were analyzed by two-way ANOVA followed by Tukey's *post hoc* test. Letters denote significant differences in viability between concentrations tested for each CNT. Means±SE are shown.

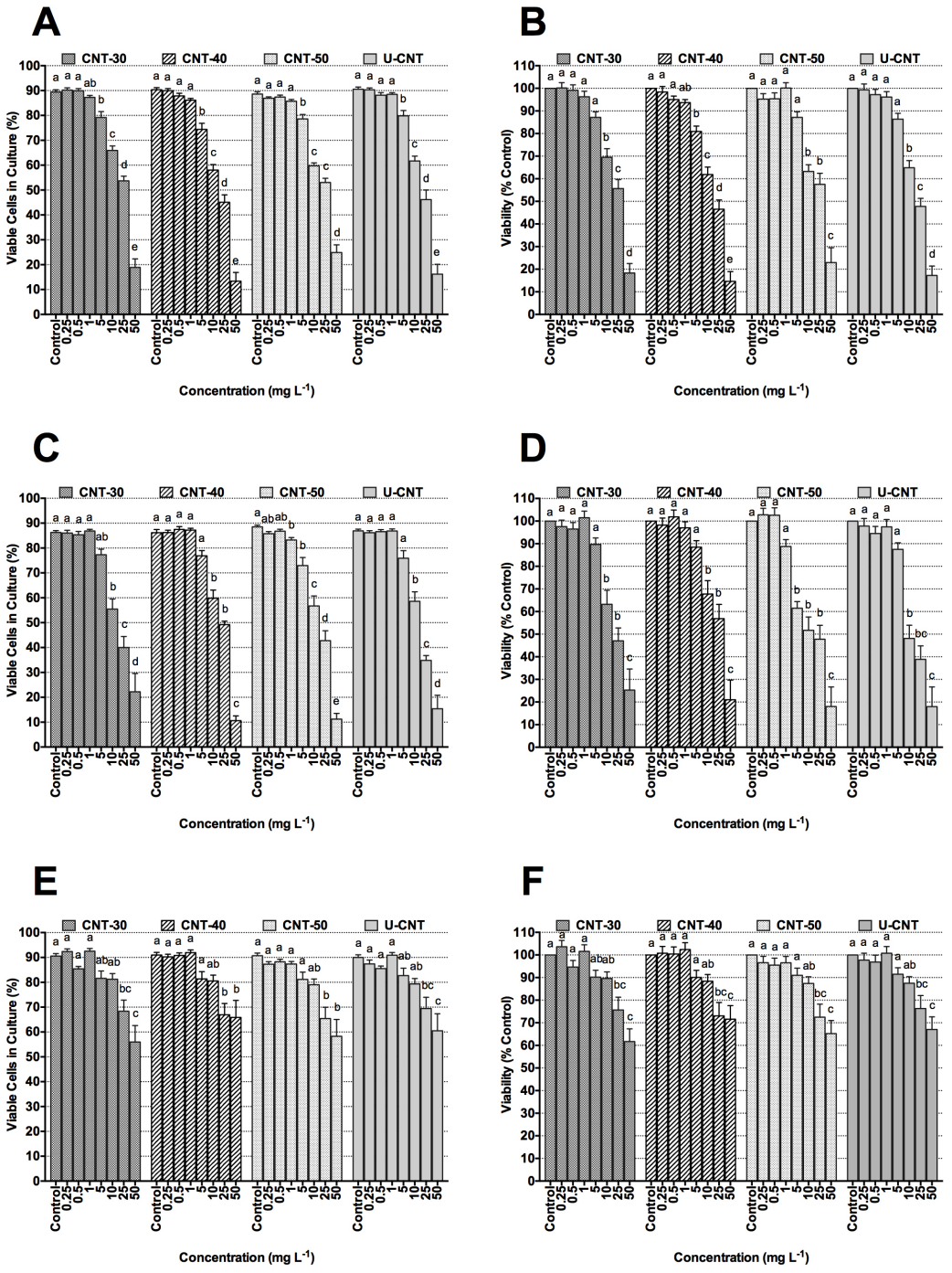
A
B
C
D
E
F
CNT-30
CNT-40
CNT-50
U-CNT
Viable Cells in Culture (%)
Viability (% Control)
Concentration (mg L-1)
Control
0.25
0.5
1
5
10
25
50

Figure 3-4. Declines in channel catfish lymphocyte viability following CNT exposure was cell line dependent. 3B11 (A, B), 1G8 (C, D) and 28S.3 (E, F) cells ($2.0x10^4$ cells $well^{-1}$) were incubated with 0.25, 0.5, 1, 5, 10, 25, 50 mg L^{-1} U-CNT, CNT-30, CNT-40 or CNT-50 for 48 h. Summarized flow cytometric viability data (A, C, E) and MTS viability data (B, D, F) demonstrate a dose-dependent decline in channel catfish lymphocyte viability following CNT exposure. 3B11 and 1G8 cells had similar, and significantly greater, declines in viability compared to 28S.3 cells. Data were analyzed by three-way ANOVA followed by Holm-Sidak *post hoc* test. Letters denote significant differences in viability between concentrations tested for each CNT. Means±SE are shown.

shown in **Figure 3-4** to allow a more direct comparison between lymphocytes. In general, 3B11 and 1G8 lymphocytes response to CNT exposure were not significantly different, with similar declines in viability following 48 h CNT exposure. For example, exposure of 3B11 cells to 50 mg L^{-1} U-CNT, CNT-30, CNT-40 or CNT-50 for 48 h resulted in 16±4%, 19±3%, 13±3% or 25±3% viable cells in culture, respectively, as determined by flow cytometric analysis (**Figure 3-4A**). This response was not significantly different from 1G8 cells which had 15±5%, 22±7%, 11±2% or 11±3% viable cells in culture following 48 h exposure to 50 mg L^{-1} U-CNT, CNT-30, CNT-40 or CNT-50, respectively (**Figure 3-4C**). In contrast, 28S.3 cells were significantly more robust with reduced toxicity compared to 3B11 and 1G8 lymphocytes following CNT exposure. Following 48 h exposure to 50 mg L^{-1} U-CNT, CNT-30, CNT-40 or CNT-50, the percentage of viable 28S.3 cells remaining in culture were 60±7%, 56±6%, 66±7% or 58±7%, respectively (**Figure 3-4E**).

3.3.2 Effect of CNT exposure on IpLITR/IpFcR γ -L mediated phagocytosis

With demonstrated declines in channel catfish lymphocyte viability following CNT exposure, we wished to examine if the ability of lymphoid cells to elicit appropriate effector responses, such as phagocytosis, would be affected following CNT exposure. We utilized transfected channel catfish (*Ictalurus punctatus)* leukocyte immune-type receptors (IpLITRs) to examine

phagocytosis through IpLITR/IpFcRγ-L following U-CNT, CNT-30, CNT-40 or CNT-50 exposure.

Exposure to CNTs for 2 h during the phagocytosis protocol had no significant effect on the viability of IpLITR/IpFcRγ-L transfected RBL-2H3 cells. Representative flow cytometric plots of cells exposed to vehicle control (**Figure 3-5A**) or 250 mg L^{-1} U-CNT (**Figure 3-5B**) shows no significant reduction in cell viability as indicated through PI fluorescence. Combined flow cytometric viability data for IpLITR transfected cells shows that exposure to CNT-30 (**Figure 3-5C**), CNT-40 (**Figure 3-5D**), CNT-50 (**Figure 3-5E**) or U-CNT (**Figure 3-5F**) had no significant effect on the percentage of viable cells in culture.

Although exposure to CNTs did not affect cell viability, CNT exposure did significantly reduce the ability of cells to phagocytose through IpLITR/IpFcRγ-L. Representative flow cytometric plots for control and isotype control treatments are shown in **Figure 3-6**. Control treated cells shows a large proportion of the population internalizing anti-HA m-Ab coated fluorescent beads, indicated by the shift in FL-1 fluorescence and represents a normal phagocytic response (**Figure 3-6A**). The isotype control, consisting of incubation with IgG Ab coated fluorescent beads, is unable to bind IpLITR and has a diminished proportion of cells that internalized a fluorescent bead and represents the background level of phagocytosis (**Figure 3-6B**). In general, CNT exposure significantly reduced IpLITR internalization of anti-HA m-Ab coated fluorescent beads compared

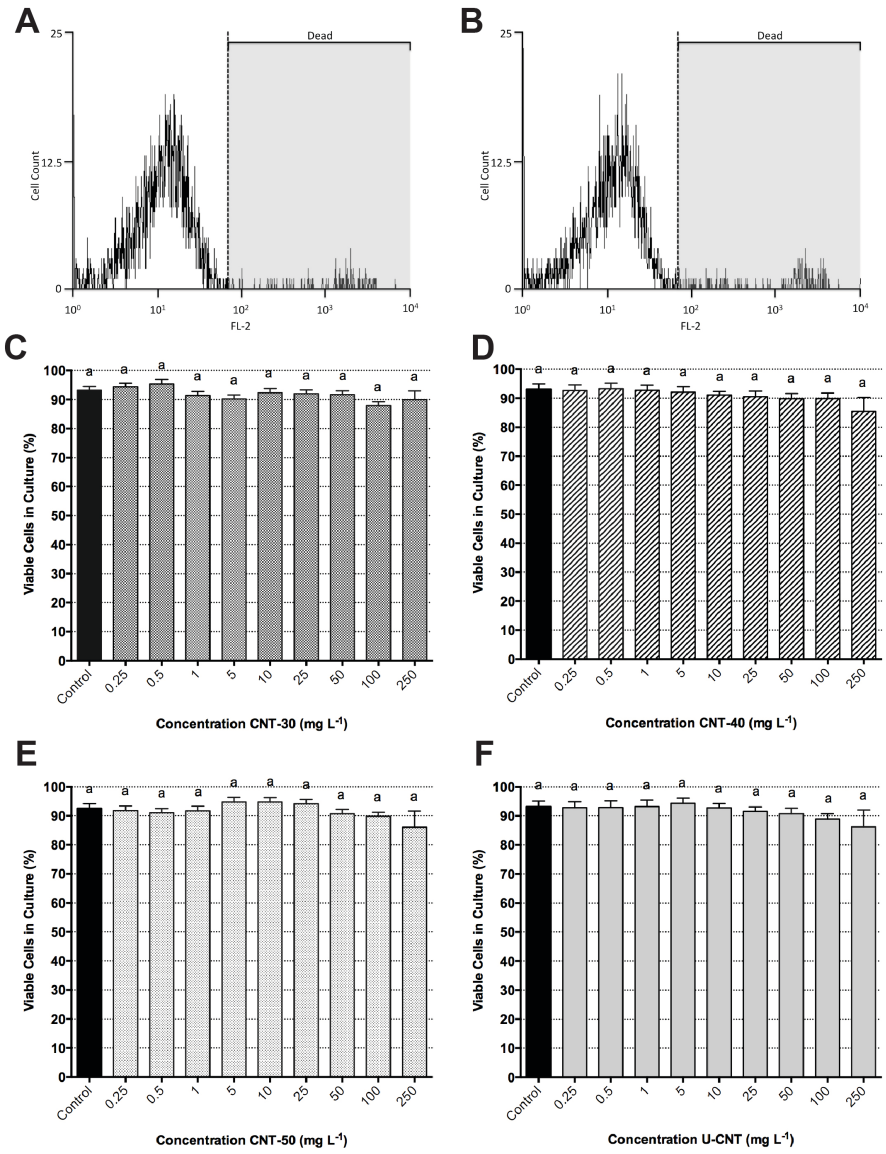
A
B
Dead
Cell Count
FL-2
C
D
E
F
Viable Cells in Culture (%)
Control
0.25
0.5
1
5
10
25
50
100
250
Concentration CNT-30 (mg L-1)
Concentration CNT-40 (mg L-1)
Concentration CNT-50 (mg L-1)
Concentration U-CNT (mg L-1)

Figure 3-5. CNT exposure did not significantly affect the viability of RBL-2H3 cells expressing IpLITR/IpFcRγ-L. RBL-2H3 cells expressing IpLITR/IpFcRγ-L at a density of $1.0x10^5$ cells $well^{-1}$ were exposed to 0.25, 0.5, 1, 5, 10, 25, 50, 100, 250 mg L^{-1} CNT-30, CNT-40, CNT-50 or U-CNT for 2 h. Representative flow cytometric plots of RBL-2H3 cells exposed to (A) vehicle control or (B) 250 mg L^{-1} U-CNT shows low levels of PI fluorescence (100 μg mL^{-1}) indicating no significant reduction in cell viability. Summarized flow cytometric viability data for RBL-2H3 cells exposed to (C) CNT-30, (D) CNT-40, (E) CNT-50 or (F) U-CNT for 2 h show no significant effect of CNT exposure on RBL-2H3 viability. Data were analyzed by two-way ANOVA followed by *post hoc* Tukey test. Letters denote no significant differences in viability for concentrations tested. Mean±SE are shown.

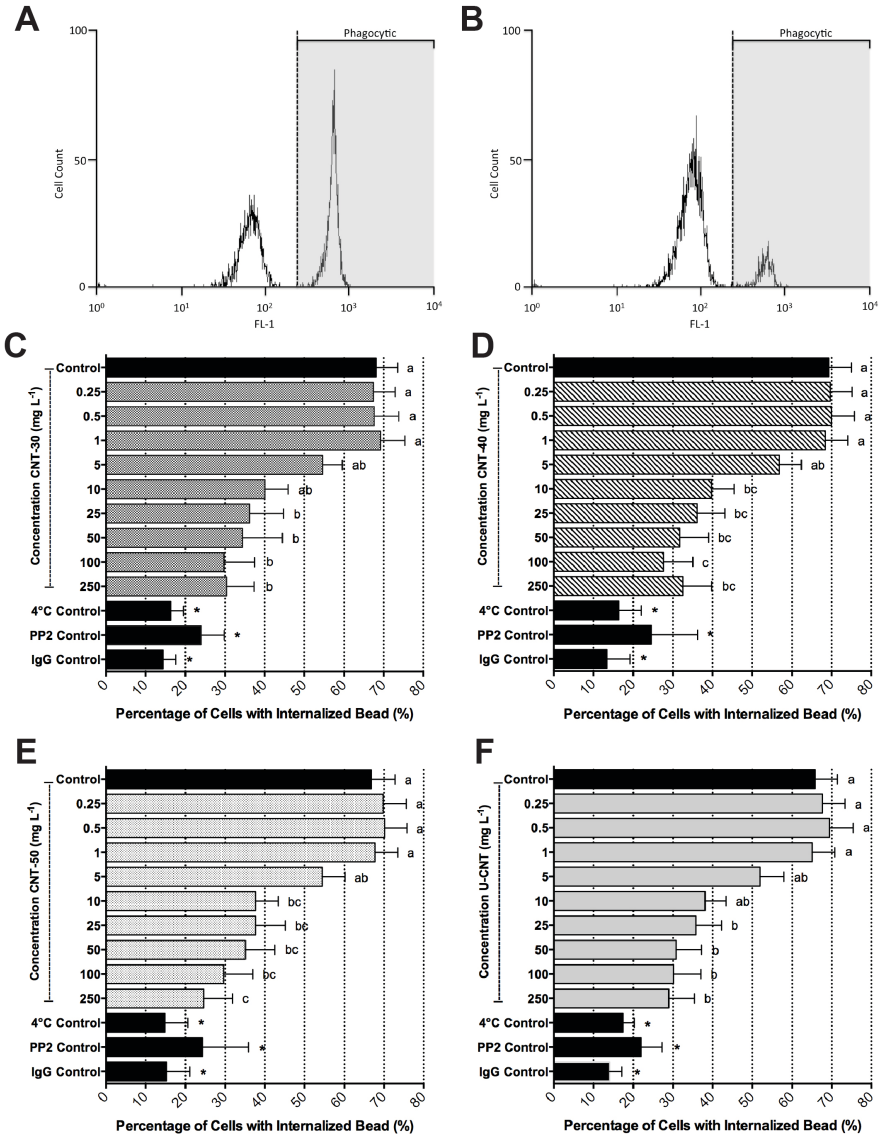
A
B
Phagocytic
Cell Count
FL-1
C
D
E
F
Concentration CNT-30 (mg L-1)
Concentration CNT-40 (mg L-1)
Concentration CNT-50 (mg L-1)
Concentration U-CNT (mg L-1)
Control
0.25
0.5
1
5
10
25
50
100
250
4°C Control
PP2 Control
IgG Control
Percentage of Cells with Internalized Bead (%)

Figure 3-6. CNT exposure significantly reduced IpLITR/IpFcRγ-L mediated phagocytosis. RBL-2H3 cells expressing IpLITR/IpFcRγ-L at a density of $1.0x10^5$ cells $well^{-1}$ were exposed to 0.25, 0.5, 1, 5, 10, 25, 50, 100, 250 mg L^{-1} CNT-30, CNT-40, CNT-50 or U-CNT for 2 h before being incubated with anti-HA mAb coated fluorescent beads. Representative flow cytometric plot of (A) control treated cells have a large shift in FL-1 fluorescence, indicating an increased proportion of RBL-2H3 cells that have internalized one or more fluorescent bead compared to (B) isotype control treated cells. Summarized flow cytometric data show diminished IpLITR/IpFcRγ-L mediated phagocytosis after 2 h exposure to (C) CNT-30, (D) CNT-40, (E) CNT-50 or (F) U-CNT. Data were analyzed by two-way ANOVA followed by Tukey *post hoc* test. Letters denote significant differences between concentrations tested for each CNT-functionalization, asterisks indicate significant differences compared to control. Means±SE are shown.

to control. Cells exposed to CNT-30 (**Figure 3-6C**), CNT-40 (**Figure 3-6D**), CNT-50 (**Figure 3-6E**) or U-CNT (**Figure 3-6F**) for 2 h had a dose-dependent decrease in IpLITR/IpFcRγ-L mediated phagocytosis, with significant reductions in the percentage of cells with one or more internalized beads after exposure to 25, 50, 100 or 250 mg L^{-1}. For example, compared to control (68±5%) the percentage of cells with an internalized bead significantly decreased to 36±8%, 34±10%, 30±8% or 30±4% after 2 h exposure to 25, 50, 100 or 250 mg L^{-1} CNT-30, respectively (**Figure 3-6C**). The inhibition of IpLITR/IpFcRγ-L-mediated phagocytosis did not vary significantly with CNT functionalization, similar declines in bead internalization were found after CNT-30, CNT-40, CNT-50 and U-CNT exposure.

3.4 DISCUSSION

3.4.1 Response of catfish lymphocytes to CNT exposure

The two types of teleost lymphoid cells examined here (B-cell-like and T-cell-like) were differentially susceptible to CNT exposure. B-cells, major contributors to humoral immunity and responsible for antibody production had larger declines in viability following CNT exposure compared to T-cells, important in cell-mediated immunity. In addition, channel catfish leukocytes appear to be more sensitive to CNT exposure compared to mammalian leukocytes; the lowest concentration to significantly impact fish lymphocyte

viability after 6 h of exposure occurred at concentrations of 10 mg L^{-1} while no significant declines in mammalian myeloid cell viability was found at concentrations up to 250 mg L^{-1} after 6 h of exposure (**Chapter 5**). These findings are in agreement with previous reports on the toxicity of helical rosette nanotubes which found 3B11 and 1G8 cell lines had larger declines in viability following RNT exposure compared to 28S.3 and that channel catfish lymphocytes were much more sensitive to exposure compared to mammalian cell lines (**Chapter 2, Chapter 4**).

Interestingly, altering CNT surface functionalization did not impact the effect of CNTs on channel catfish lymphocyte viability with U-CNT, CNT-30, CNT-40 and CNT-50 all causing similar declines in viability post exposure. This finding is in contrast to several studies utilizing mammalian models that found AF-CNTs cause differential changes in viability compared to U-CNTs. Increased toxicity of AF-CNTs was reported in LA4 mouse epithelial cells compared to U-CNTs, with significant declines at exposures as low as 5 mg L^{-1} (Saxena et al., 2009). However, in general, AF-CNTs are associated with reduced toxicity compared to U-CNTs (Fadel and Fahmy, 2014). Human monocyte macrophages readily internalized AF-CNTs but showed no toxicity at concentrations up to 100 mg L^{-1} (Witasp et al., 2009). Delogu *et al.* (2012) examined the viability of human peripheral blood mononuclear cells *ex vivo* exposed to 100 mg L^{-1} AF-CNTs for 24 h but found no change in viability or the number of apoptotic cells in culture (Delogu et al., 2012).

In this study, U-CNTs were the direct product of the induction thermal plasma process and TEM analysis indicated the presence of amorphous carbon in addition to CNT bundles (**Supplemental Figure S3-1**). AF-CNTs were produced from U-CNTs following purification and oxidation and contained very little amorphous carbon. This suggests that by weight, U-CNT exposures, consisting of both amorphous carbon and CNTs in solution, contain fewer CNTs and may have masked differences in the toxicity of CNT functionalizations. Nevertheless, testing U-CNTs produced from commercial high production techniques such as induction thermal plasma process is important given their high likelihood of environmental exposure.

3.4.2 Effect of CNT exposure on IpLITR/ IpFcR γ -L mediated phagocytosis

CNT exposure significantly reduced IpLITR/IpFcRγ-L -mediated phagocytosis and was dose-dependent with no discernable difference between the level of inhibition between U-CNT, CNT-30, CNT-40 or CNT-50. These effects occurred at sub-lethal levels of exposure and suggest that CNTs can diminish the ability of fish leukocyte receptors to mediate appropriate effector responses. Few studies to date have examined the immunomodulatory effects of CNTs in fish. Klaper et al., (2010) investigated the response of trout macrophages to differentially functionalized CNT exposure. CNTs functionalized with either sulfonate groups, poly-ethylene glycol groups or m-polyaminobenzene sulfonic acid groups, differentially

induced the expression of IL-1β in trout macrophages and suggested proinflammatory potential of CNT exposure in fish. Other studies utilizing mammalian models have suggested CNT exposure can cause immunomodulatory effects in various immune cells with both immunoactivation and immunosuppression described. Immunoactivation was described by Brown et al*.,* (2007) in monocytes exposed to U-CNTs that resulted in the release of proinflammatory mediators. Similarly, monocytes and NK-cells were activated *ex vivo* following exposure to AF-CNTs (Delogu et al., 2012). In contrast, other reports suggest that CNT exposure can cause immunosuppression. Mitchel et al., (2009) reported a decreased T-cell dependent antibody response in mice following U-CNT exposure while Alam et al., (2013) described a suppressed cytotoxic T-cell response in a mixed lymphocyte reaction following AF-CNT exposure. Results from this study add to reports of immunosuppression following CNT exposure with sub-lethal exposures to U-CNT, CNT-30, CNT-40 and CNT-50 significantly reducing the ability of a fish leukocyte receptor, IpLITR, to phagocytose.

CNTs have been shown to bind a variety of proteins in solution and affiliate directly with cellular membranes (Lelimousin and Sansom, 2013; Rybak-Smith and Sim, 2011). When NMs interact with proteins in solution, they have been demonstrated to induced conformational changes that can alter protein function, hide epitopes and thus change protein affinity or avidity for potential receptors (Stueker et al., 2014). As such, the reduced phagocytosis reported here could be a result of CNT exposure reducing

IpLITR engagement with its ligand, either by binding the IpLITR receptor, the α-HA mAb antigen or both. In support, immunosuppression in rat basophilic leukemia (RBL)-2H3 cells following CNT exposure has been reported for another receptor-mediated effector response, degranulation. CNT exposure resulted in a diminished IgE-FcεR1 mediated degranulatory response in RBL-2H3 cells by interfering with the receptor binding its ligand (**Chapter 5**).

3.5 CONCLUSIONS

This study is the first to examine the effect of CNT exposure on fish lymphocytes, cells that contribute to the humoral and cell-mediated responses of adaptive immunity. CNT exposure to catfish lymphocytes caused a dose- and time-dependent decline in cell viability. The two types of lymphoid cells examined, B-cell-like or T-cell-like, had significantly different responses to CNTs with B-cells being significantly more susceptible to exposure. We also demonstrate that IpLITR/IpFcRγ-L-mediated phagocytosis is significantly diminished at sub-lethal levels of CNT exposure. Interestingly, functionalization was not a major determinant of cytotoxicity or impaired immune function; pristine (U-CNT) and AF-CNTs (CNT-30, CNT-40, CNT-50) all had similar effects *in vitro*.

CHAPTER 4

Rosette nanotubes alter degranulation in the rat basophilic leukemia (RBL)-2H3 cell line

4.1 INTRODUCTION

Biologically-inspired rosette nanotubes (RNTs) are a self-assembling nanomaterial (NM) formed in solution from a guanine□cytosine (G□C) hybrid motif through a hierarchical, entropically-driven process (Fenniri et al., 2002b; 2001; Moralez et al., 2005). The fundamental self-assembling building block of the RNTs can be synthesized to feature either one (**Figure 4-1A**) or two G□C units (**Figure 4-1D-E**). This leads to the formation of hexameric rosettes, which are maintained by either 18- or 36-hydrogen bonds, respectively. The resulting large and substantially hydrophobic supermacrocycles (**Figure 4-1B**) subsequently stack upon one another to form a stable tubular nanostructure (**Figure 4-1C, F-H**), which can be up to several hundred micrometers long.

RNTs hold potential in a variety of biomedical applications including targeted drug delivery, improved vascular implants, tissue engineering and enhanced orthopedics (Fine et al., 2009; Song et al., 2011; Sun et al., 2012). RNTs are also metal-free, hydrophilic and can be dispersed in polar media, and thus offer advantages for these applications compared to many other engineered NMs (Fenniri et al., 2002b; 2001). Moreover, RNTs have tunable dimensions and can be engineered to express a diverse range of functional groups on their outer surface through covalent functionalization of the G□C molecule (Borzsonyi et al., 2010; Chhabra et al., 2009; Fenniri et al., 2002a; Tikhomirov et al., 2008). This allows for the manipulation of both their physical and biological properties (Fenniri et al., 2002a; Fine et al., 2009; Sun

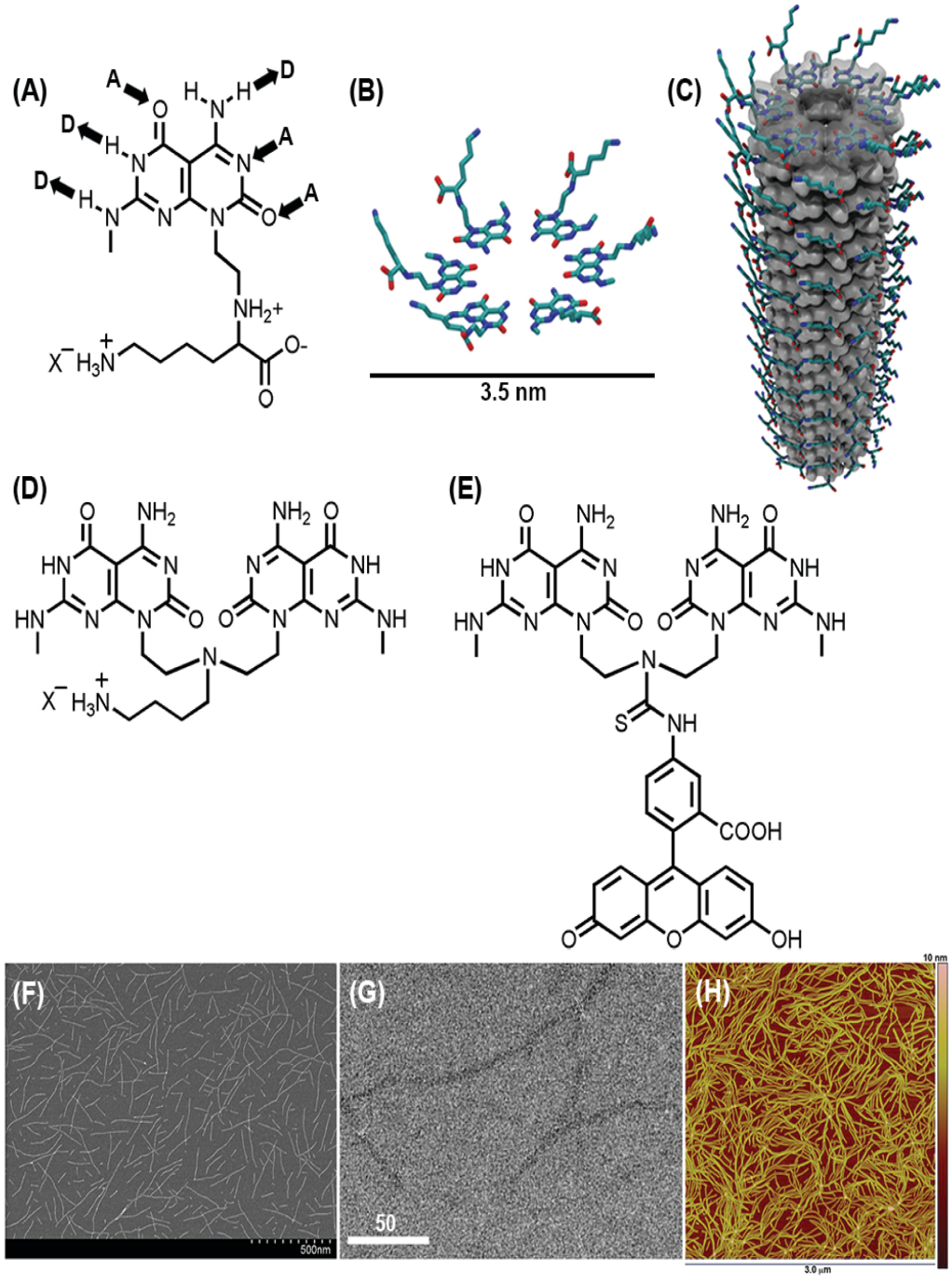
(A)
(B)
3.5 nm
(C)
(D)
(E)
COOH
OH
(F)
500nm
(G)
50
(H)
10 nm
3.0 µm

Figure 4-1. (A) Lysine-functionalized G□C motif featuring the donor (D) and acceptor (A) hydrogen bonding arrays of guanine and cytosine self-assembles into (B) hexameric rosettes, which further stack to form (C) K-RNTs having a tubular architecture. Structures of the twin-G□C motifs functionalized with (D) butylamine (termed TB-TBL) and (E) FITC (termed TB-FITC) which were co-assembled to form the FITC^{1}/TBL^{19}-RNTs. (F-H) SEM, TEM and AFM images of K-RNTs which have an outer diameter of *ca.* 3.5 nm. Scale bar is in nm.

et al., 2012). Given the potential utility of RNTs, a thorough assessment of their potential interaction with cells, tissues and systems is necessary.

A critical factor to consider when assessing the biocompatibility and toxicity of new materials are their interactions with various *in vivo* processes such as those facilitated by the immune system (Remes and Williams, 1992). Recent data has demonstrated that NMs may adversely influence immune cell responses *in vivo* during inadvertent exposure and following deliberate pulmonary, subcutaneous, intraperitoneal and intravenous introduction (Chen et al., 2010; Gustafsson et al., 2011; Kolosnjaj-Tabi et al., 2010; Meng et al., 2011; Song et al., 2009). For example, fullerenes have been demonstrated to act as potent antigens, stimulating the production of fullerene-specific IgG antibodies, but have also been shown to be immunosuppressive, suppressing the inflammatory response of peripheral blood basophils and mast cells by inhibiting the activation of signaling intermediates required for exocytosis of immunogenic mediators (Braden et al., 2000; Chen et al., 1998; Ryan et al., 2007). In addition, even subtle changes in NM structure can alter their biological effects; for example, changing the density of functionalized polymers on NMs can switch the complement pathways that are activated upon NM exposure in human serum (Hamad et al., 2010; Sim and Wallis, 2011).

It is important to understand the response of immune cells occupying 'sentinel locations' within tissues and at interfaces between the body and environment. Myeloid cells (*i.e.* macrophages and granulocytes) are found

throughout body tissues including respiratory, intestinal, and mucosal epithelia and are one of the first activators of the inflammatory response (Passante and Frankish, 2009). Granulocytes (*i.e.* neutrophils and mast cells) contain granules in their cytoplasm, which when stimulated are released via a process called degranulation and include various mediators of immunity. In this study, we investigate the cellular response of rat basophilic leukemia (RBL)-2H3 cells, a granulocyte cell line used extensively in studies of allergy and inflammation, to understand the impact of K-RNT exposure. RBL-2H3 cells express an endogenous, high affinity Fcε receptor (FcεRI), which when bound by IgE in a process called sensitization and subsequently cross-linked by dinitrophenyl-human serum albumin (DNP-HSA), induces degranulation (Gilfillan and Tkaczyk, 2006). Degranulation releases a variety of chemical mediators including histamine, serotonin and β-hexosaminidase providing a sensitive endpoint to examine the effects of K-RNT exposure on immune effector functions (Huang et al., 2009).

Herein, we examined the influence of K-RNT exposure on RBL-2H3 viability and using the IgE-DNP model, assess the direct effects of RNT exposure on IgE/FcεRI-mediated degranulation to determine if they alter the activation of innate immune responses. As well, using a reporter array, we examined various cell signaling pathways related to cellular toxicity in order to elucidate the cellular mechanisms that mediate cell death reported here and in previous studies. Finally, confocal microscopy studies were performed in order to gain insight into the physical interactions between

RBL-2H3 cells and RNTs. For this purpose, a RNT termed FITC^{1}/TBL^{19}-RNT, was synthesized through a co-assembly process of TB-FITC (**Figure 4-1D**) and TB-TBL (**Figure 4-1E**) in a 1:19 molar ratio, in order to express the fluorescent marker fluorescein isothiocyanate (FITC), while maintaining a solubility and surface charge profile similar to K-RNTs (Fenniri et al., 2001). We hypothesize that K-RNTs will affiliate with RBL-2H3 cells resulting in reduced cell viability and interfering with the ability of these cells to elicit appropriate effector functions *in vitro*.

4.2 MATERIALS AND METHODS

4.2.1 RNT synthesis and characterization

The synthesis of the lysine functionalized G□C motif (**Figure 4-1A**) and self-assembly into a stock solution of K-RNTs (1 g L^{-1}) (**Figure 4-1C**) in nanopure water was performed and extensively characterized according to a previously reported procedure (Fenniri et al., 2002b; 2001). The synthesis of TB-TBL (**Figure 4-1D**) has also been previously reported, while the preparation of TB-FITC (**Figure 4-1E**) will be described in due course. For the preparation of the stock solution of co-assembled FITC^{1}/TBL^{19}-RNTs (1:19 molar ratio, 385 mg L^{-1} total), a solution of TB-TBL in nanopure water was sonicated for 30 s and then transferred to a vial containing TB-FITC. The suspension was sonicated for 5 min, vortexed for 5 s, followed by heating using a heat gun (on high setting) for 1 min. This procedure was repeated

twice, or until no further dissolution occurred. The yellow suspension was allowed to stand at room temperature in the dark for 2 days to allow for the growth of the RNTs and sedimentation of any undissolved TB-FITC. The yellow supernatant was then transferred into another glass vial and was stored in the fridge in the dark. Aliquots from this stock solution of $FITC^{1}/TBL^{19}$-RNTs were diluted and used for the cell studies.

The hydrodynamic diameter and zeta-potentials of K-RNTs and $FITC^{1}/TBL^{19}$-RNTs at concentrations of 1, 10, 50 mg L^{-1} and 10, 50 mg L^{-1}, respectively, were determined using dynamic light scattering (DLS; Malvern Instrument Zetasizer Nano ZS, Westborough, MA). Hydrodynamic radii were measured using 173° backscattering mode and reported as the peak value of >99% intensity. Extensive characterization details of RNTs under a variety of physiological conditions and with various side-group functionalizations have been previously reported and the reader is directed to previous studies by Fenniri *et al.* (2001, 2002) and Moralez *et al.* (2005) for full details. However, a summary profile with pertinent information for this study has been included as **Supplemental Table S2-1**.

4.2.2 Cell culture

RBL-2H3 cells were cultured at 37°C and 5% CO_2 in filter sterilized (0.22μm, Corning) Minimum Essential Media (MEM; Hyclone) containing 10% heat-inactivated fetal bovine serum (FBS) (characterized; Hyclone) supplemented with 2mM L-glutamine (Gibco), 100 units mL^{-1} penicillin

(Gibco), and 100μg mL^{-1} streptomycin (Gibco) as described previously (Cortes et al., 2014).

HEK 293T cells were cultured at 37°C and 5% CO_2 in filter sterilized (0.22μm, Corning) DMEM/High glucose (Hyclone) containing 10% heat-inactivated FBS (characterized; Hyclone) supplemented with 2mM L-glutamine (Gibco), 100 units mL^{-1} penicillin (Gibco), 100 μg mL^{-1} streptomycin (Gibco), 1mM sodium pyruvate (Gibco), and 1% MEM non-essential amino acid solution (Gibco) as described previously (Montgomery et al., 2009).

4.2.3 Examination of RBL-2H3 and HEK-293T viability after exposure to K-RNTS

RBL-2H3 cells were seeded in a 96 well plate at a density of 40,000 cells per well and allowed to attach for 1 h (37°C, 5% CO_2) before dosing with 1, 10, 50, 100 or 200 mg L^{-1} K-RNT in MEM for 2, 4, or 24 h (37°C, 5% CO_2). We recognize that several dosing metrics have been identified for NMs and provide the conversions between mass per volume, particles per volume and surface area per volume in **Supplemental Table S2-2**. Control wells received MEM alone (negative control) or 40 μL of nanopure water (vehicle control). Following exposure, cells were harvested, washed twice with 1x PBS, and re-suspended in 200 μL of 1x PBS/propidium iodide (PI) (100 μg mL^{-1}) and analyzed by flow cytometry (Quanta SC, Beckman Coulter). An increase in PI fluorescence, indicative of cell death, was detected using the

FL2 filter. Viability is expressed relative to negative controls, calculated as a percentage of viable RNT-exposed cells to viable unexposed cells.

The effects of RNTs on cell viability were also studied using a non-radioactive cell proliferation assay performed according to the manufacturer's instructions (Cell Titer 96 Aqueous Non-Radioactive Cell Proliferation Assay Kit, Promega, WI, USA). MTS [3-(4,5-dimethylthiazol-2-yl)-5-(3-carboxymethoxyphenyl)-2-(4-sulfophenyl)-2H-tetrazolium] when bioreduced by cells can gauge cell number by recording a change in absorbance at 490nm. RBL-2H3 cells were seeded in a 96 well plate at a density of 40,000 cells per well and allowed to attach for 1 h (37°C, 5% CO_2) before dosing with 1, 10, 50, 100 or 200 mg L^{-1} K-RNT in MEM for 2, 4, or 24 h (37°C, 5% CO_2). HEK-293T cells were seeded in a 96 well plate at a density of 25,000 cells per well. Cells were allowed to attach for 2 h before exposing them to 0.5, 1, 5, 10, 50, or 100 mg L^{-1} K-RNT in DMEM for 6 h (37°C, 5% CO_2), which was the exposure time used for the luciferase reporter assay (see section 2.4 below). Following the exposures, RBL-2H3 or HEK-293T cells were washed with complete media (MEM or DMEM, respectively) and prepared kit reagents were added to the plate for an additional 1 h (37°C, 5% CO_2). Absorbance at 490 nm was then measured using a microplate reader (WALLAC 1420, PerkinElmer, MA, USA). Viability is expressed relative to negative controls, calculated as a percentage of viable RNT-exposed cells absorbance to viable unexposed cells absorbance. Pair-wise RNT controls were used to account for background absorbance from NMs.

4.2.4 Effects of K-RNT exposure on intracellular toxicity-related signaling pathways

To investigate the intracellular signaling events underlying the toxicity observed at higher doses of K-RNTs, highly transfectable human embryonic kidney (HEK)-293T cells were employed and a transfected reporter array was used to identify changes in 10 broad intracellular toxicity-related signaling pathways using Cignal Finder Toxicity 10-Pathway Reporter Array (SABiosciences). This luciferase-based reporter measures changes in intracellular signaling of ten toxicity-related signaling pathways: 1) p53/DNA damage, 2) hypoxia, 3) NFκβ, 4) glucocorticoid receptor, 5) cell cycle/pRB-E2F, 6) MAPK/ERK, 7) MAPK/JNK, 8) PKC/Ca^{2+} 9) TGFβ and 10) Myc/Max. Each reporter also consists of a constitutively expressing *Renilla* construct allowing for transfection efficiencies to be normalized. In addition, the kit includes a negative control (non-inducible reporter) and a positive control (constitutively expressing both firefly lucifererase and a GFP construct).

Transfections were performed according to the manufacturer's instructions using HEK-293T cells seeded in a 96-well plate. Cells were seeded at a density of 25,000 cells/well in 200 µL complete DMEM and incubated overnight (37°C and 5% CO_2). Cells were then transfected with 100ng of Cignal Reporter Constructs. For all 12 Cignal Reporters, a master mix was created consisting of 400 ng of Cignal Reporter, 20 µL of OptiMEM (Invitrogen) and 0.4 µL of Turbofect (Fermentas) per well. This solution was gently mixed and allowed to sit at room temperature for 15 min. Next, 21 µL of master mix was added to each well and the cells were incubated for 24 h

(37°C and 5% CO_2) at which time, the media was removed and cells were exposed to 50 or 100 mg L^{-1} K-RNT in complete DMEM for 6 h (37°C and 5% CO_2). Cells were then assayed for firefly and *Renilla* luciferase activity using Dual-Glo Luciferase Assay System (Promega).

A ratio of luminescence from the experimental reporter (firefly luminescence) to the control reporter (*Renilla* luminescence) was used to control for transfection efficiency. A quotient of the firefly:*Renilla* ratio for cells treated with K-RNTs (firefly:*Renilla*^{txt}) to the firefly:*Renilla* ratio for control treatments (firefly:*Renilla*^{ctrl}) was calculated and represents a change in luminescence for RNT exposure compared to control.

4.2.5 Examination of RBL-2H3 degranulation in the presence of K-RNTs

RBL-2H3 degranulation was measured using the β-hexosaminidase release assay as described previously (Cortes et al., 2012). Briefly, RBL-2H3 cells were seeded into a flat bottom 96-well plate (Costar) at a density of 40,000 cells per well and allowed to attach for 2 h in complete MEM (37°C, 5% CO_2). Next, cells were sensitized with 0, 12.5, 25, 50 or 100 ng mL^{-1} of mouse anti-DNP IgE mAb (Sigma-Aldrich) in incomplete Tyrodes buffer (25 mM HEPES, 140 mM NaCl, 1.8 mM $CaCl_2$, 5.6 mM D-glucose, 12 mM $NaHCO_3$, 0.37 mM NaH_2PO_4 and $MgCl_2$, pH 7.4) for 1 h at 37 °C and 5% CO_2. Solutions were then removed and the cells washed with 200 μL of Tyrodes buffer containing 0.1% BSA. Cells were then stimulated to degranulate with 0.05 μg mL^{-1} DNP-HSA in Tyrodes/BSA buffer heated to 37°C. Negative controls

were exposed to Tyrodes buffer alone to measure non-specific background signal. The efficacy of the assay was verified by use of a positive control, 0.625 μM calcium ionophore A23187 (Sigma-Aldrich). Cells were placed in the incubator for 1 h at 37°C and 5% CO_2 and the amount of β-hexosaminidase released by RBL-2H3 cells was then assayed by removing 25 μL of the supernatant and combining it with 100 μL of β-hexosaminidase substrate buffer (2 mM 4-methylumbelliferyl N-acetyl-b-D-glucosaminide (Sigma–Aldrich), 100 mM citrate, pH 4.5) for 30 min at 37 °C and 5% CO_2. The reaction was quenched by adding 150 μL of 200 mM L-glycine, pH 10.7. The cleavage of the substrate 4-methylumbelliferyl N-acetyl-b-D-glucosaminide by β-hexosaminidase was measured using a microplate reader with 360 nm excitation and 450 nm emission filters (WALLAC 1420, PerkinElmer, MA, USA). The relative fluorescence units (RFUs) for the treatments were standardized to our negative control (non-specific background).

Using the above protocol, two experimental approaches were devised to investigate different mechanisms by which K-RNTs may affect the degranulatory response of RBL-2H3 cells. The first experiment examined if pre-exposing RBL-2H3 cells to K-RNTs affected degranulation when subsequently sensitized and stimulated, thereby examining if K-RNT exposure could affect the long-term function of immune cells to elicit the appropriate immunological responses. Here, cells were first exposed to 50 or 100 mg L^{-1} K-RNT solutions in complete MEM for 2 h (37°C, 5% CO_2) and

washed thrice with complete Tyrodes buffer prior to sensitization with IgE. Cells were then stimulated and degranulation was assessed. Control treatments consisted of a 2 h exposure to the ultra pure water vehicle.

In the second experiment, cells were co-exposed to either 50 or 100 mg L^{-1} K-RNTs and IgE to examine if the presence of K-RNTs interferes with IgE binding FcεRI during sensitization, a step required to elicit IgE/FcεRI-mediated degranulation in RBL-2H3 cells. Here, during sensitization with 0, 12.5, 25, 50 or 100 ng mL^{-1} IgE, cells were simultaneously exposed to 50 and 100 mg L^{-1} K-RNT for 1 h at 37°C and 5% CO_2. Solutions were then removed and the cells were washed with 200 µL of complete Tyrodes buffer and the protocol was followed as described above. Control treatments consisted of a simultaneous vehicle (ultrapure water) and IgE exposure.

4.2.6 Examination of $FITC^{1}/TBL^{19}$-RNT interaction with RBL-2H3 cells by confocal microscopy

$FITC^{1}/TBL^{19}$-RNTs were used to investigate the cellular association of RNTs with RBL-2H3 cells. Glass coverslips (Fisher Scientific) were treated with 70% ethanol, washed with 1x PBS and subsequently UV-irradiated. RBL-2H3 cells were seeded on coverslips in a 6-well plate at a density of $1x10^{5}$ and allowed to grow for 48 h (37°C, 5% CO_2). After incubation, cells were exposed to 10 mg L^{-1} $FITC^{1}/TBL^{19}$-RNTs for 2, 4 or 6 h. Cells were washed with antibody staining buffer (phosphate buffered saline, 0.5% bovine serum albumin) (ASB). Coverslips were then placed on parafilm

containing ASB with 100 ng mL^{-1} IgE mAb for 30 min over ice. Cells were washed with ASB and then placed on parafilm containing ASB with 50 ng mL^{-1} goat anti-mouse IgG PE-conjugated staining antibody (Beckman Coulter) at 4 °C for 30 min in the dark. Cells were subsequently washed with ASB before being placed in Fixation Buffer (BioLegend) for 20 min at room temperature in the dark. Finally, cells were washed with ASB and mounted on slides using mounting media containing DAPI. Slides were viewed with a Laser Scanning Confocal Microscope (Zeiss LSM 710, objective 40x 1.3 oil plan-Apochromat) at the Cross Cancer Institute Cell Imaging Facility, Edmonton, Alberta. Images were collected with Zen 2011 software and processed with LSM Image Browser (v. 4.2.0.121, Carl Zeiss). Surface rendering and three-dimensional (3D) reconstruction of Z-stack images were performed using Imaris software (v. 6.2.2, Bitplane).

4.2.7 Statistical analysis

To investigate the effect of RNT exposure on RBL-2H3 viability, two-way Analysis of Variance (ANOVA) followed by post-hoc Bonferroni test were performed. To determine the effect of RNT exposure on RBL-2H3 degranulation, two-way ANOVA were performed to determine differences between experimental and control treatments followed by post-hoc Sidak's test. To investigate the effect of RNT exposure on HEK 293T viability, a one-way ANOVA followed by post-hoc Dunnett's test were performed. All

statistical analyses were performed using GraphPad 6.0 statistical software program. Statistical significance was set at $p<0.05$.

4.3 RESULTS

4.3.1 Sample characterization

For this study, K-RNTs self-assembled from the lysine-functionalized G□C motif were characterized as previously described (Fenniri et al., 2001). Representative SEM, TEM and AFM images of the nanotubes are shown in **Figure 4-1F-H**, which have an average outer diameter of *ca.* 3.5 nm (Fenniri et al., 2001). Dynamic light scattering (DLS) measurements shown in **Table 4-1** revealed that the hydrodynamic radii of K-RNTs at concentrations of 10 and 50 mg L^{-1} in ultra pure water were (mean±SD, n=4) 397±136 and 405±122 nm, respectively. The measured ζ-potential of K-RNTs at 10 mg L^{-1} was 71±3 mV and this value did not change at a higher concentration of 50 mg L^{-1} (72±2 mV). Unfortunately, it was not possible to characterize RNTs in cell culture media using currently available common techniques such as DLS since the concentrations tested in this complex matrix were below the instruments detection limit. To give the reader additional RNT characterization, **Supplemental Table S2-1** summarizes data from several publications. In our analysis, we use gravimetric measures as an indicator of dose. Since these high aspect ratio RNT materials do not increase in either individual diameter or length with increasing dose, both surface area and

Table 4-1. Physiochemical characterization of K- and FITC^{1}/TBL^{19}-RNTs showing hydrodynamic diameter (nm) and zeta potential (mV) diluted to 1, 10, and 50 mg L^{-1} in ultra pure H_2O reported as mean±standard deviation.

Material	Hydrodynamic diameter [nm]			Zeta potential [mV]	
	1 mg L^{-1}	10 mg L^{-1}	50 mg L^{-1}	10 mg L^{-1}	50 mg L^{-1}
K-RNT	280±169	397±136	405±122	71±3	72±2
FITC^{1}/TBL^{19}-RNT		312±133		17±2	

molarity will increase linearly with gravimetric dose. The conversion factors for recalculation of dose as either surface area or molarity is provided in **Supplemental Table S2-2**.

4.3.2 Effects of K-RNTs on RBL-2H3 viability

Exposure to K-RNTs resulted in a significant change in adherent RBL-2H3 viability, with both dose- and time-dependent effects observed. Flow cytometric analysis revealed no significant change in viability for 2, 4 or 24 h exposure to 1, 10 and 50 mg L^{-1} K-RNT (**Figure 4-2A**). However, while exposure to 100 mg L^{-1} K-RNT for 2 and 4 h did not result in a significant change in viability, there was a significantly decreased viability after 24 h of exposure (mean ± SE, n=4; 84.4±2%) compared to control (**Figure 4-2A**). At 200 mg L^{-1} effects of K-RNTs appeared earlier during the exposure with viability significantly decreased to: 81.4±3%, 83.1±3% and 74.8±3% of control at 2, 4 and 24 h respectively (**Figure 4-2A**).

Results using the MTS assay to measure cell proliferation and verify viability results demonstrated that exposure to K-RNTs caused a significant decline in cell viability that was both dose- and time-dependent (**Figure 4-2B**). Similar to the flow cytometric viability analysis (**Figure 4-2A**), there was no significant change in RBL-2H3 viability after 2, 4 or 24 h at exposure levels of 1, 10 or 50 mg L^{-1} K-RNT. However, 100 mg L^{-1} of K-RNT after 2, 4 and 24 h resulted in significant declines in viability, compared to controls. Cells exposed to 100 mg L^{-1} had viability significantly decreased to (mean ±

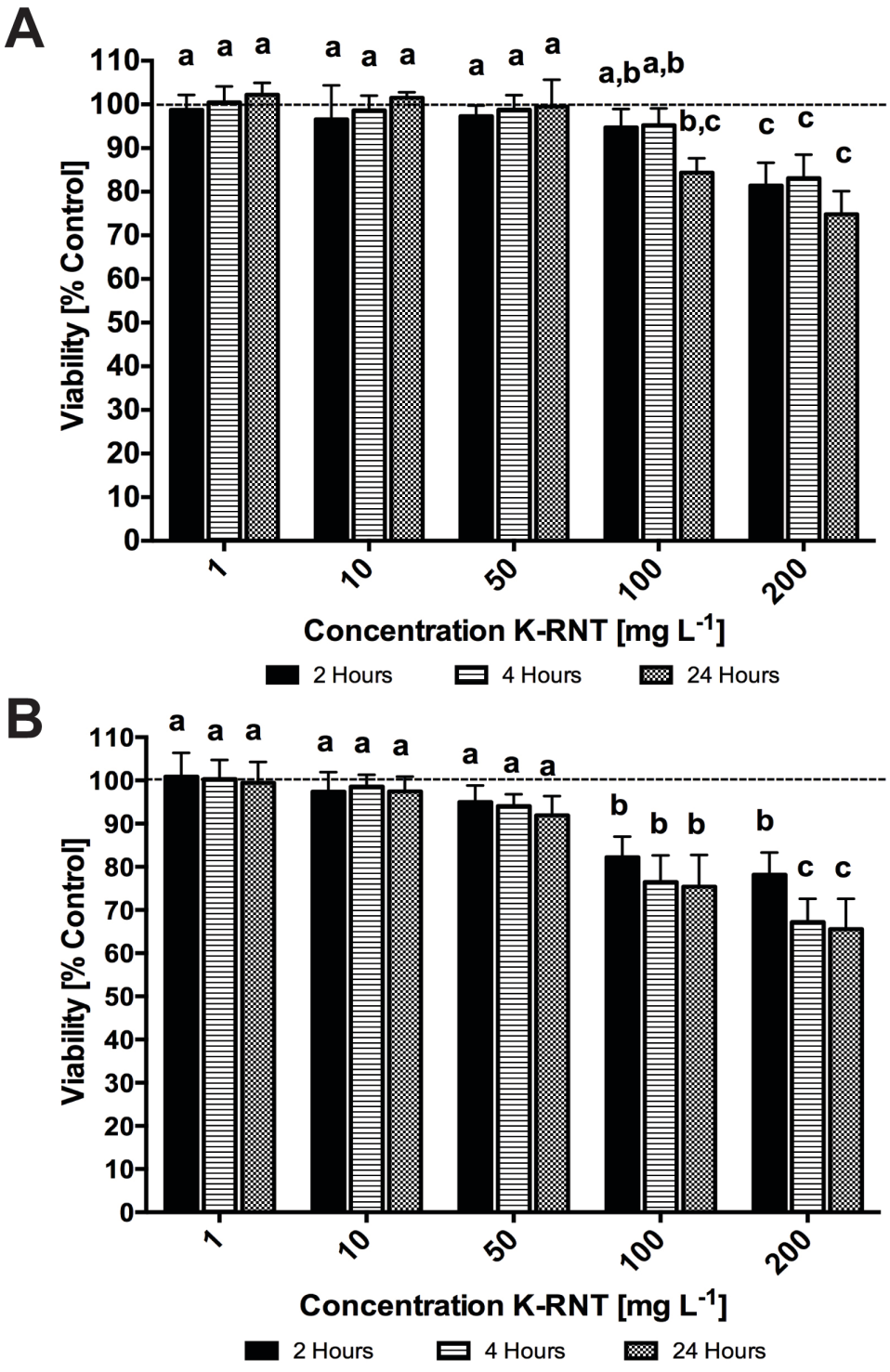
A
a a a a a a a a a a,b a,b b,c c c c
110 100 90 80 70 60 50 40 30 20 10 0
Viability [% Control]
1 10 50 100 200
Concentration K-RNT [mg L-1]
2 Hours
4 Hours
24 Hours
B
a a a a a a a a a b b b b c c
110 100 90 80 70 60 50 40 30 20 10 0
Viability [% Control]
1 10 50 100 200
Concentration K-RNT [mg L-1]
2 Hours
4 Hours
24 Hours

Figure 4-2. Exposure to K-RNTs significantly affected RBL-2H3 viability. (A) 4 x 10^4 RBL 2H3 cells were exposed to 1, 10, 50, 100 or 200 mg L^{-1} K-RNT for 2, 4 or 24 h. Cells were stained using propidium iodide (100 μg mL^{-1}) and analyzed by flow cytometry using FL2 to distinguish between viable and non-viable cells. Viability is expressed relative to negative controls, calculated as a percentage of viable RNT-exposed cells to viable unexposed cells. Values are means ± SE (n=4) (B) 4 x 10^4 RBL-2H3 cells were exposed to 1, 10, 50, 100 or 200 mg L^{-1} K-RNT for 2, 4 or 24 h. Metabolic activity, as an indicator of cell viability, was measured in cells after exposure using the MTS assay. Absorbance values were measured at 490 nm and compared to control to calculate percent cell viability. Values are means ± SE (n=8). Letters indicates significantly different values ($p<0.05$, ANOVA followed by Dunnett's post-hoc comparison).

SE, n=8): 82.2±2%, 76.5±6%, and 75.4±7% of control after 2, 4 and 24 h, respectively (**Figure 4-2B**). Exposure to 200 mg L^{-1} K-RNT further reduced RBL-2H3 viability at 4 and 24 h with 67.2±5%, and 66.3±8% viability compared to controls (**Figure 4-2B**).

4.3.3 Characterizing changes in intracellular signaling toxicity-related pathways upon K-RNT exposure

We sought to investigate the intracellular signaling events underlying the toxicity observed at higher doses of K-RNTs **(Figure 4-3)**. To accomplish this, HEK-293T cells were transfected with a series of luciferase-based reporters, each specific for monitoring the transcriptional activity of ten intracellular signaling pathways related to toxicity. First, we verified that the viability of HEK-293T exposed to K-RNTs for 6 h was similar to that observed for RBL-2H3 cells. HEK-293T cells showed a decrease in viability upon exposure to K-RNTs at doses of 50 (mean ± SE, n=5; 89±3%) and 100 mg L^{-1} (72±2%) (**Figure 4-3A**)**.** Examination of the luciferase activity after 6 h exposure to 50 mg L^{-1} K-RNT revealed a general down-regulation of multiple toxicity-related pathways with the exception of hypoxia inducible factor, which remained unchanged (**Figure 4-3B**).

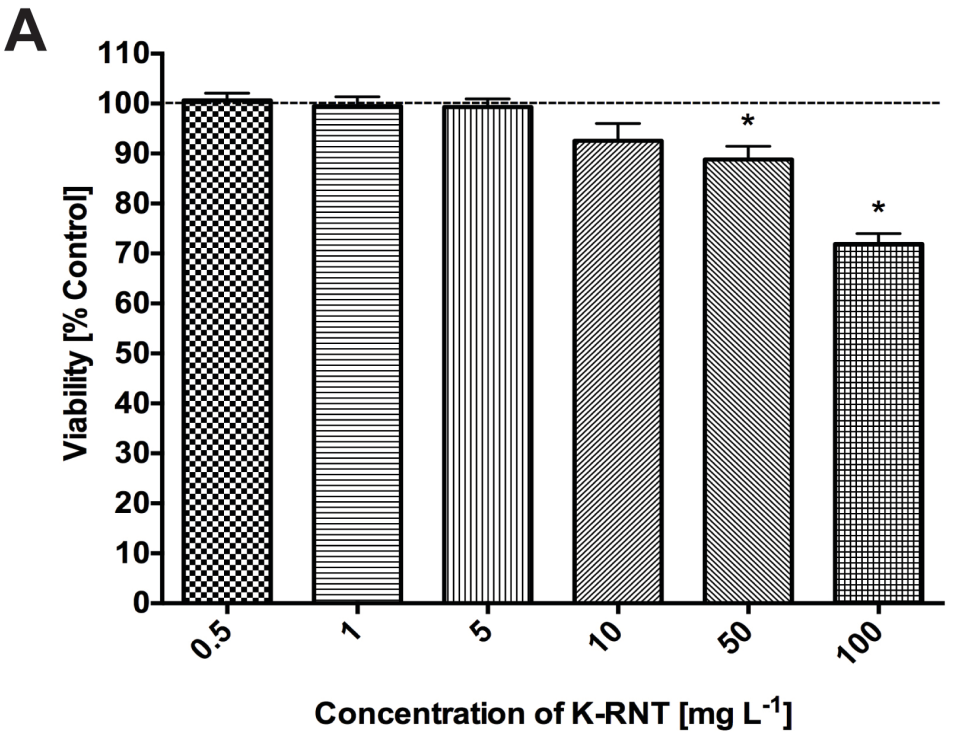
A
Viability [% Control]
110
100
90
80
70
60
50
40
30
20
10
0
*
*
0.5
1
5
10
50
100
Concentration of K-RNT [mg L-1]

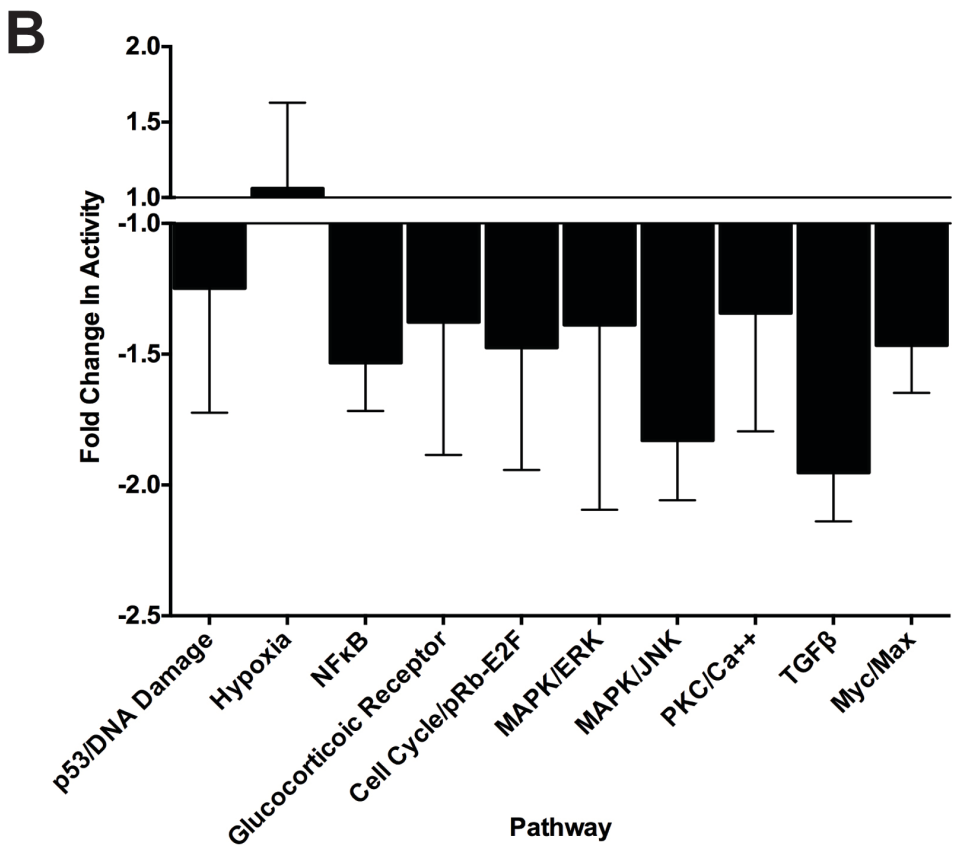
B
Fold Change In Activity
2.0
1.5
1.0
-1.0
-1.5
-2.0
-2.5
p53/DNA Damage
Hypoxia
NFκB
Glucocorticoic Receptor
Cell Cycle/pRb-E2F
MAPK/ERK
MAPK/JNK
PKC/Ca++
TGFβ
Myc/Max
Pathway

Figure 4-3. Exposure to K-RNTs did not change the transcriptional activity of 10 toxicity-related signaling pathways in HEK 293T cells. (A) 2.5 x 10^4 HEK 293T cells were exposed to 0.5, 1, 5, 10, 50, or 100 mg L^{-1} K-RNT for 6 h. Metabolic activity, as an indicator of cell viability, was measured in cells after exposure using the MTS assay. Absorbance values were measured at 490 nm and compared to control to calculate percent cell viability. Values are means ± SE (n=8). Letters indicates significantly different values ($p<0.05$, ANOVA followed by Dunnett's post-hoc comparison). (B) 2.5 x 10^4 HEK 293T cells were transfected with one of ten Cignal Reporter Constructs for 24 h. Constructs represent a luciferase reporter gene linked to a specific transcriptional response element for ten broad, intracellular toxicity-related signaling pathways. Cells were exposed to 50 mg L^{-1} K-RNT in growth media for 6 h. Cells were then assayed for luciferase activity as an indicator of intracellular signaling activation. K-RNT treatment is standardized to vehicle control treatment and is expressed as fold-change in luminescence activity. Asterisk indicates significantly different values compared to control (n=5, $p<0.05$, ANOVA followed by Dunnett's post-hoc comparison).

4.3.4 IgE/FcεRI-mediated degranulation of RBL-2H3 cells in response to K-RNT exposure

In the first series of experiments, RBL-2H3 cells were simultaneously sensitized with 0, 12.5, 25, 50 or 100 ng mL^{-1} IgE and exposed to 50 or 100 mg L^{-1} K-RNTs. In all treatments tested, there was an increase in the degranulatory response of the cells (**Figure 4-4A-C**). This effect was observed irrespective of the concentration of IgE (12.5, 25, 50, or 100 ng mL^{-1}) or concentration of K-RNT (50 or 100 mg L^{-1}) tested (**Figure 4-4A,B**). The presence of K-RNTs at either 50 or 100 mg L^{-1} resulted in an increased IgE/FcεRI-mediated degranulatory response, ranging from (mean ± SE, n=5) 119±4% to 140±7% of controls (**Figure 4-4C**). It should be noted that when IgE was not present (0 ng mL^{-1}), exposure to either 50 or 100 mg L^{-1} K-RNT still resulted in a significantly elevated β-hexosaminidase release (126.6±4% and 120±4%, respectively).

The second experiment examined if pre-exposure to either 50 or 100 mg L^{-1} of K-RNTs for 2 h affects the ability of IgE/FcεRI-mediated degranulation in RBL-2H3 cells. Pre-exposure to 50 mg L^{-1} of K-RNT showed a potentiated IgE/FcεRI-mediated degranulatory response starting at higher doses of IgE (25 mg L^{-1} and above), relative to controls (**Figure 4-5A**). Cells pre-exposed to 100 mg L^{-1} of K-RNT for 2 h displayed a potentiated degranulatory response at all concentrations of IgE tested ((mean ± SE, n=5) 12.5 ng mL^{-1}: 123±4%; 25 ng mL^{-1}: 129±4%; 50 ng mL^{-1}: 126±2%; and 100 ng mL^{-1}: 123±2%) (**Figure 4-5B**). Of note, cells that were pre-exposed to 50 and 100 mg L^{-1} K-RNT but were not sensitized with IgE (0 ηg mL^{-1} IgE) did

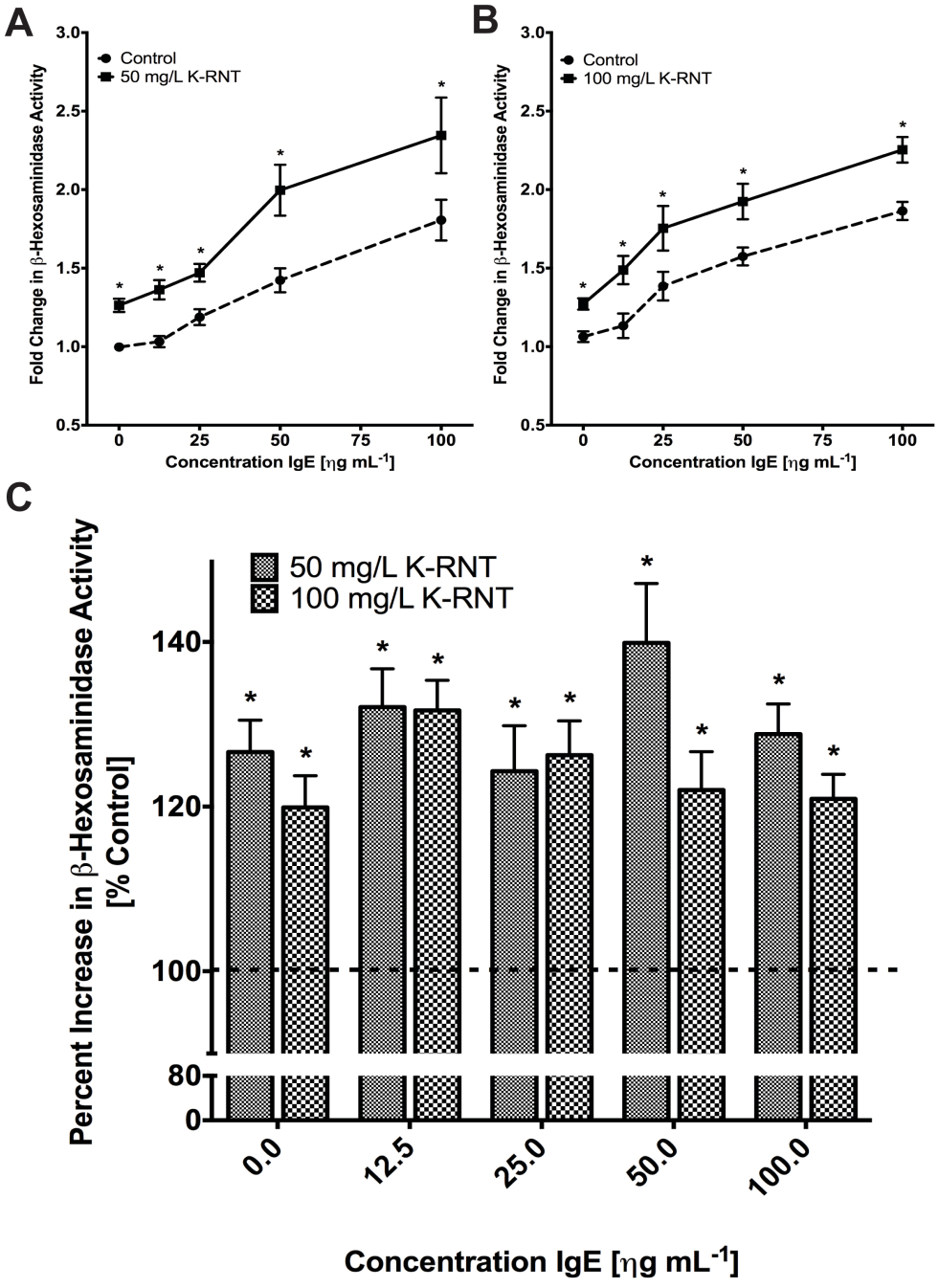
A
B
C
Control
50 mg/L K-RNT
100 mg/L K-RNT
Fold Change in β-Hexosaminidase Activity
Concentration IgE [ηg mL-1]
Percent Increase in β-Hexosaminidase Activity [% Control]
0.0
12.5
25.0
50.0
100.0

Figure 4-4. RBL-2H3 cells increased release of β-hexosaminidase when co-exposed to K-RNTs during IgE sensitization. RBL-2H3 cells were seeded at 4 x 10^4 into a 96-well plate and allowed to rest for 2 h. Cells were simultaneously sensitized with IgE (0, 12.5, 25, 50, or 100 ng mL^{-1}) and exposed to either (A) 50 or (B) 100 mg L^{-1} K-RNT. Control cells were simultaneously sensitized with IgE (0, 12.5, 25, 50 or 100 ng mL^{-1}) and exposed to vehicle (ultra pure H_2O). Negative controls were exposed to Tyrodes buffer alone (no IgE) to measure non-specific background signal. After washing, cells were subsequently stimulated to degranulate with DNP-HSA. Supernatant was collected and β-hexosaminidase activity assayed. The relative fluorescent units (RFUs) for each treatment was standardized to our negative control to calculate the fold change in β-hexosaminidase activity over background. (C) Summary, showing the percent increase in β-hexosaminidase activity for K-RNT treatment compared to control for each level of IgE sensitization. Values are means ± SE (n=5). Asterisk indicates significantly different values compared to control ($p<0.05$, ANOVA followed by Dunnett's post-hoc comparison).

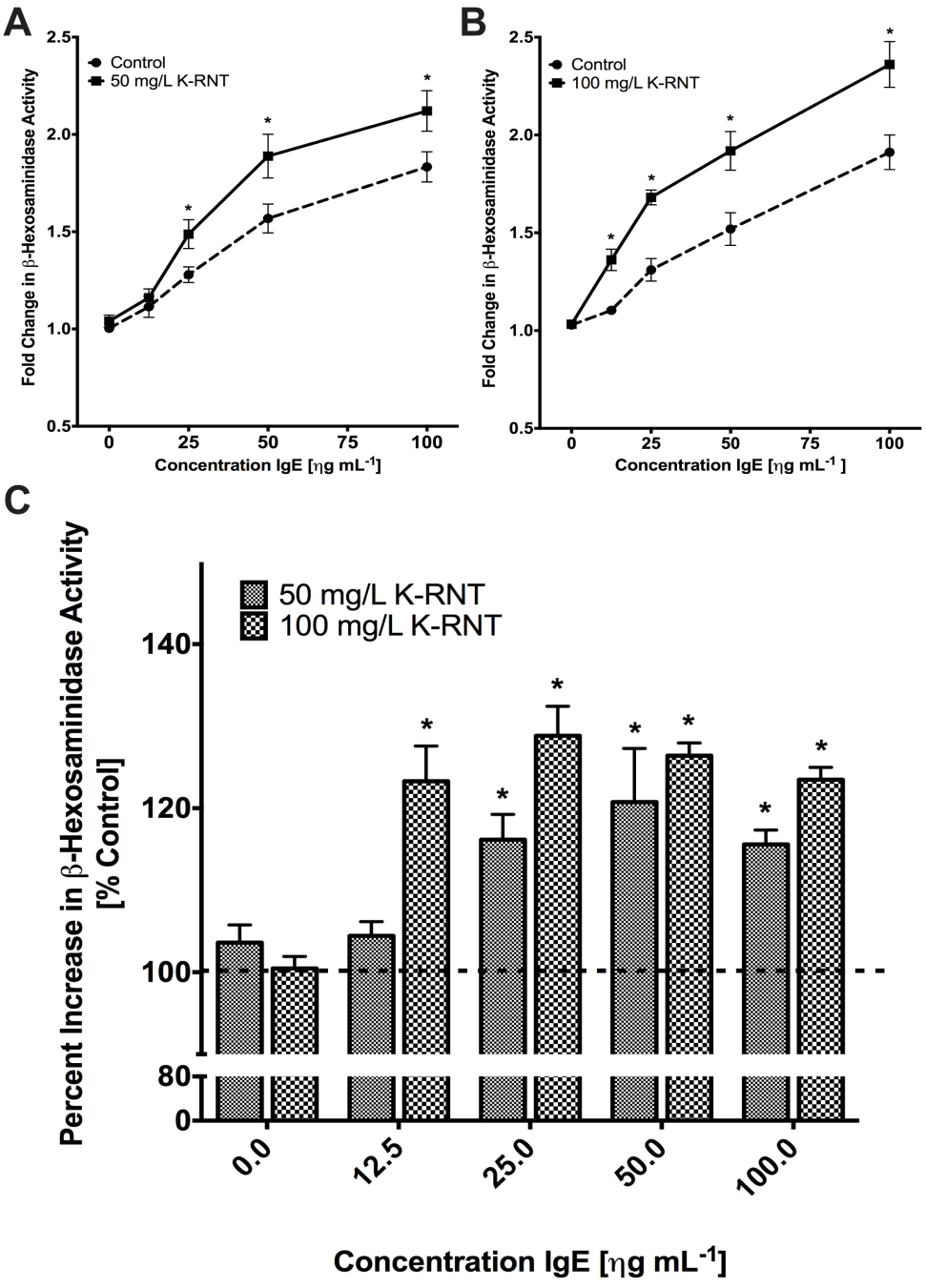
A
Control
50 mg/L K-RNT
Fold Change in β-Hexosaminidase Activity
Concentration IgE [ηg mL-1]
B
Control
100 mg/L K-RNT
Fold Change in β-Hexosaminidase Activity
Concentration IgE [ηg mL-1]
C
50 mg/L K-RNT
100 mg/L K-RNT
Percent Increase in β-Hexosaminidase Activity [% Control]
Concentration IgE [ηg mL-1]

Figure 4-5. RBL-2H3 cells showed increased degranulation after pre-exposure to K-RNTs. RBL-2H3 cells were seeded at 4 x 10^4 into a 96-well plate and allowed to rest for 2 h. Cells were then exposed to (A) 50 or (B) 100 mg L^{-1} K-RNT for 2 h. Cells were washed to remove K-RNTs before sensitization with 0, 12.5, 25, 50, or 100 ng mL^{-1}IgE and subsequent treatment with DNP-HSA to stimulate degranulation. Supernatant was collected and β-hexosaminidase activity assayed. The relative fluorescent units (RFUs) for each treatment was standardized to our negative control to calculate the fold change in β-hexosaminidase activity over background. (C) Summary, showing the percent increase in β-hexosaminidase activity compared to control. Values are means ± SE (n=5). Asterisk indicates significantly different values compared to control ($p<0.05$, ANOVA followed by Dunnett's post-hoc comparison).

not have an elevated degranulatory response (**Figure 4-5C**). This contrasts with the previous experiment when K-RNT and IgE were exposed simultaneously during sensitization (**Figure 4-4C** and **Figure 4-5C**).

4.3.5 Examination FITC^{1}/TBL^{19}-RNT interaction with RBL-2H3 cells by confocal microscopy

Confocal laser scanning microscopy of FITC^{1}/TBL^{19}-RNTs demonstrated that RNTs bind to RBL-2H3 cells. When RBL-2H3 cells were exposed to 10 mg L^{-1} FITC^{1}/TBL^{19}-RNTs for 4 or 6 h, extensive co-localization between RNTs and FcεR was observed (**Figure 4-6**). Micrographs showing DAPI fluorescence (**Figure 4-6A-C**), FcεRI fluorescence (**Figure 4-6D-F**), and FITC^{1}/TBL^{19}-RNT fluorescence (**Figure 4-6G-I**) suggest that FITC-RNTs are highly associated with FcεR in particular and the cell membrane in general as demonstrated through co-localized fluorescence (**Figure 4-6J-O**). This association remained despite the extensive washing of RBL-2H3 cells during confocal preparation, suggesting a strong affiliation between the two.

Using the fluorescence of labeled FcεR, a surface expressed receptor, as a reference point for the cellular membrane, FITC^{1}/TBL^{19}-RNT fluorescence is observed within the cell interior, visualized through 3D reconstruction of Z-stack images (**Figure 4-6P**). This suggests FITC^{1}/TBL^{19}-RNTs can be internalized by RBL-2H3 cells after just 2 h of exposure. Using the fluorescence of DAPI, a nucleic stain, as a reference point for the

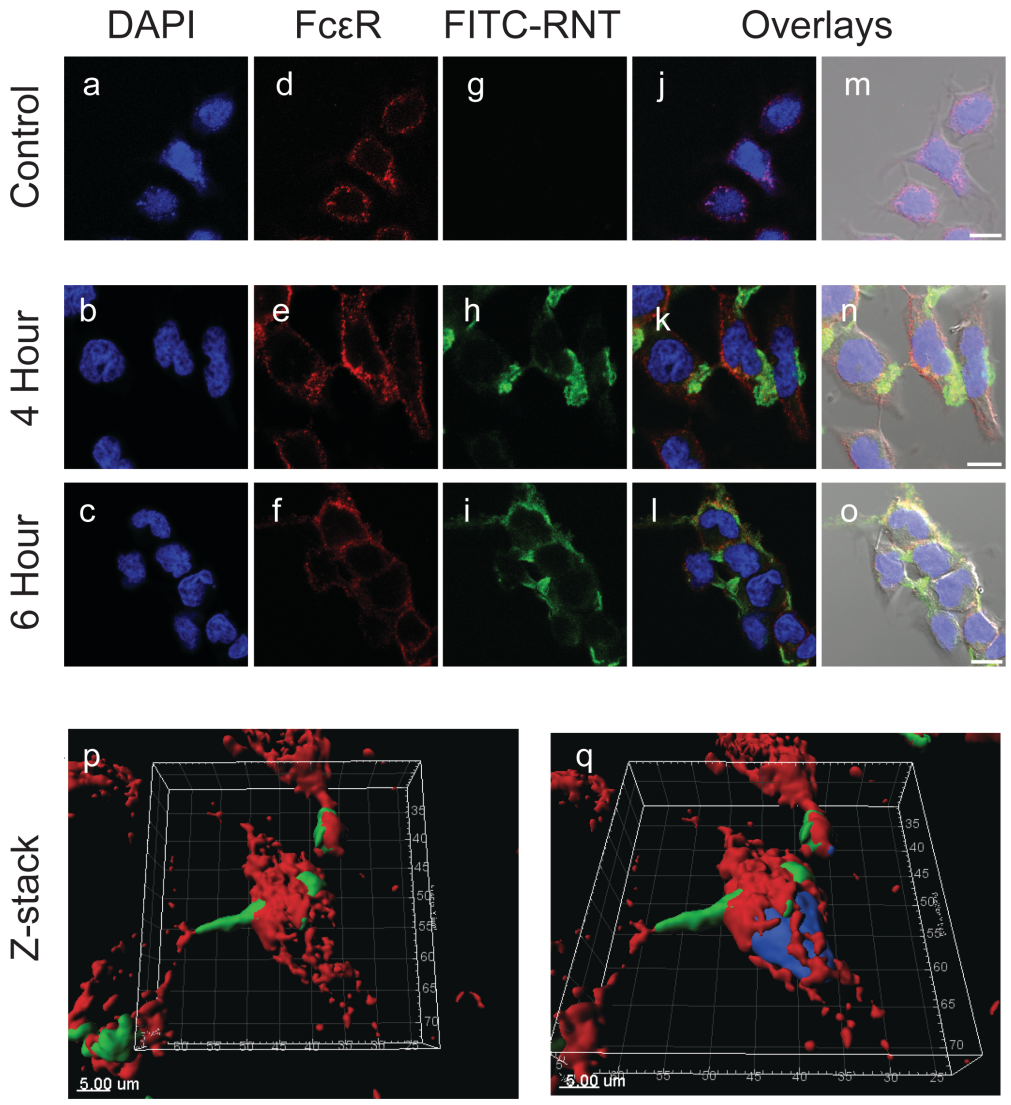
DAPI
FcεR
FITC-RNT
Overlays
Control
4 Hour
6 Hour
Z-stack
a
b
c
d
e
f
g
h
i
j
k
l
m
n
o
p
q
5.00 um
5.00 um

Figure 4-6. Confocal micrographs showing association of FITC[1]/TBL[19]-RNTs with RBL-2H3 cells. Cells were stained for FCεR using IgE primary antibody and goat anti-mouse IgG PE-conjugated secondary antibody before being fixed. Nuclei were stained using DAPI. Laser scanning confocal micrographs with DAPI fluorescence (a, b, c), FCεR fluorescence (d, e, f), FITC-RNT fluorescence (g, h, i), fluorescence overlay (j, k, l), and bright-field overlay (m, n, o) of RBL-2H3 cells exposed to vehicle control for 4 h (top) or 10 mg L-1 FITC1/TBL19 for 4 (middle) or 6 (bottom) h. Scale bars are 10 μm. Surface rendering and three-dimensional reconstruction of Z-stack images suggest FITC-RNTs are internalized in RBL-2H3 cells after 2 h of exposure. (p, q) RBL-2H3 cells were exposed to 10 mg L-1 FITC1/TBL19-RNTs for 2 h and subsequently washed, stained for FCεR using IgE primary antibody and goat anti-mouse IgG PE-conjugated secondary antibody before being fixed. Nuclei were stained with DAPI. Surface rendering and three-dimensional reconstruction of z-stack fluorescence was performed using Imaris software. FCεR fluorescence (red) and FITC1/TBL19-RNT fluorescence (green) shown without (p) and with (q) DAPI fluorescence (blue).

intracellular compartment in 3D reconstruction of Z-stack images confirmed the intracellular presence of FITC^{1}/TBL^{19}-RNT (**Figure 4-6Q**).

4.4 DISCUSSION

4.4.1 Effects of K-RNTs on immune cell viability

Cell viability was assessed through a combination of flow cytometric analysis and the MTS assay. RBL-2H3 cells showed a dose dependent decrease in cell viability with increasing doses of K-RNTs after 2 and 4 h of exposure with significant decreases in viability at 100 and 200 mg L^{-1} K-RNT. By comparison, Journeay et al., (2008) demonstrated a significant reduction in the viability of the pulmonary epithelial cell line Calu-3 after a 24 h exposure to 50 mg L^{-1} K-RNTs. Similarly, a human macrophage cell line, U937, demonstrated a significant decrease in viability after 24 h exposure to 50 mg L^{-1} K-RNTs (Journeay et al., 2009). While a significant change in RBL-2H3 cell viability at 50 mg L^{-1} K-RNT was not observed, the epithelial cell line HEK 293T did exhibit a significant decrease in cell viability after 6 h of exposure to 50 and 100 mg L^{-1} K-RNTs. Differential susceptibility of several cell lines has been reported in studies on metal toxicity (Tan et al., 2008). Pfaller et al., (2009) in their investigation of immunomodulatory effects of NMs noted significant differences in sensitivity of A549, Jurkat, and THP-1 cell lines. Our results, together with previous findings, highlight the need to

use a variety of models and viability assays when investigating the biocompatibility of new materials (Zhao et al., 2013).

With demonstrated changes in viability upon K-RNT exposure, an investigation into the mechanisms of observed cell death was warranted. The use of a luciferase-based reporter system has been used with success to survey a broad list of potential mechanisms of zinc oxide and platinum nanoparticle toxicity for further study (Rallo et al., 2011). In general, it was found that after 6 h of K-RNT exposure, the transcriptional activity related to a broad variety of intracellular signaling pathways was down-regulated with the exception of hypoxia inducible factor, which remained unchanged. However, no significant changes in transcriptional activity were observed. Many of these candidate signaling pathways play important roles in apoptosis including PKC/Ca^{2+}, Myc/Max and p53/DNA damage. The lack of induction of these pro-apoptotic pathways by K-RNT exposure suggests the possibility of non-apoptotic mechanisms of cell death such as regulated or unregulated necrosis (Sun and Wang, 2014).

Using $FITC^{1}$/TBL^{19}-RNTs, the cellular association and subsequent internalization of the nanotubes in RBL-2H3 cells was confirmed. This is the first demonstration of the cellular uptake of RNTs using confocal imaging. Confocal micrographs show co-localization between IgE labeled FcεR and $FITC^{1}$/TBL^{19}-RNTs, suggesting these NMs are associating with the cellular membrane. The presence of $FITC^{1}$/TBL^{19}-RNTs, despite extensive washing, demonstrates a strong association between this material and the cell

membrane. In computer simulations, functionalizing gold NMs with positive surface charges resulted in increased lipid bilayer adherence when compared with negative and hydrophobic surface functionalizations (Lin et al., 2010). It is likely that the high level of $FITC^{1}/TBL^{19}$-RNT and cell membrane interaction results from the attraction between the positively charged nanotubes (**Table 4-1**) and negatively charged cell membranes. 3D reconstruction and surface renderings of Z-stacks also suggest the internalization of $FITC^{1}/TBL^{19}$-RNTs after 2 h exposure. Such strong affiliation of RNTs with the membrane could potentially contribute to a loss of membrane integrity, causing cell death through a non-regulated necrotic process. With a lack of candidates identified from the reporter assay, our lab is currently investigating if necrosis could be the mechanism of RNT toxicity observed at higher doses.

4.4.2 Effects of K-RNT on RBL-2H3 cell degranulation

Endpoints beyond viability are being recognized as important in the toxicological evaluation of NMs (Ortega et al., 2013). Here we demonstrate for the first time an immediate degranulatory event by RBL-2H3 cells when exposed to K-RNTs. Interestingly, exposure to K-RNTs increased β-hexosaminidase release, with and without IgE sensitization (**Figure 4-4C**) suggesting these materials can augment IgE-mediated release of granular products, but can also induce degranulation in RBL-2H3 cells independent of IgE/FcεRI. Previous reports in Calu-3 pulmonary epithelial cells and U937

cells, a human macrophage cell line, demonstrated that exposure to 50 mg L^{-1} K-RNT for 1 and 6 h induced cytokine secretion (Journeay et al., 2008). Together these findings suggest K-RNTs may be proinflammatory, capable of eliciting an immune response through the above endpoints. Similar proinflammatory effects on mast cells have been reported for other high-aspect ratio NMs, including multi-wall carbon nanotube (MWCNT) (Katwa et al., 2012). RBL-2H3 cells have also been demonstrated to degranulate due to a variety of non-immunological stimuli (Passante and Frankish, 2009). For example, Fowlkes *et al.* (2013) showed that mechanical loading in RBL-2H3 cells accomplished through RGD-binding integrin receptors caused secretion of β-hexosaminidase. With our confocal results demonstrating an interaction with RBL-2H3 cell membranes, the observed increase in degranulation upon K-RNT exposure could be attributed to such physical stimulation.

To further investigate the proinflammatory response to K-RNTs, we tested the effect of pre-exposing RBL-2H3 to K-RNT and examined their ability to degranulate. In contrast to the previous experiment, residual unbound K-RNT was washed-off prior to sensitization with IgE. This step was essential to establish whether unbound K-RNTs were interfering with IgE binding its receptor, FcεRI. It is well known that many NMs non-specifically bind to proteins in solution and thereby alter either their activity or affect their ability to bind to their cognate receptors (Maccormack et al., 2012; Stueker et al., 2014). Moreover, with confocal microscopy demonstrating a strong affiliation of K-RNTs with the cellular membrane, we

wanted to determine if the noted effects were most likely due to K-RNTs remaining bound to the cells. We found that following 2 h pre-exposure to K-RNTs and subsequently washing away unbound K-RNT, cells were still able to elicit an IgE/FcεRI-mediated degranulatory response. However, unexpectedly, the cells demonstrated a significant increase in IgE/FcεRI-mediated release of β-hexosaminidase compared to untreated cells.

To date, a variety of stimuli have been shown to induce degranulation in RBL-2H3 cells. It is possible that RNTs could be affecting membrane integrity in RBL-2H3 cells. Carbon NMs have been implicated in several studies to destabilize cellular membranes (Tahara et al., 2012). If such a mechanism occurs in RBL-2H3 cells, the release of a variety of intracellular components, including β-hexosaminidase would result. However, since cells were washed prior to sensitization, we removed these factors and therefore suggest that K-RNTs are acting directly on the cell membrane and eliciting a potentiation of the IgE/FcεRI-mediated degranulatory response. Our confocal microscopy demonstrated co-localization of RNTs with FcεRI. Therefore, it is possible RNTs potentiate the IgE/FcεRI-mediated degranulatory response by increasing FcεRI crosslinking. Previous reports have suggested NMs can alter receptor crosslinking in RBL-2H3 cells, either promoting or inhibiting degranulation based largely on NM architecture. For example, gold nanoparticles larger than 19.8 nm, and coated with cell-activating antigens, promoted IgE/FcεRI crosslinking and activation and were potent effectors of RBL-2H3 degranulation; alternatively, antigen-

coated gold NMs smaller than 19.8 nm competitively inhibited degranulation (Huang et al., 2009). Interestingly, gold NMs alone did not elicit or alter a degranulatory response. RNTs are a high-aspect ratio NM with a diameter of 3.5 nm; however, they can be up to several hundred micrometers long. Given this large architecture, it is possible RNTs could be promoting IgE/FcεRI crosslinking and inducing degranulation in RBL-2H3 cells.

4.5 CONCLUSIONS

In conclusion, we have demonstrated that K-RNTs interact directly with the membrane of immune cells and can be internalized after exposure. These interactions affect viability and alter the ability of these cells to elicit receptor-mediated responses such as IgE/FcεRI-mediated degranulation. In addition, at high doses, K-RNTs can elicit degranulatory responses irrespective of IgE mediated stimulation. Currently, we are trying to elucidate the nature of this interaction, the relative importance of membrane associated versus internalized K-RNTs, and the mechanism mediating this response.

CHAPTER 5

Carbon nanotubes diminish degranulation in the rat basophilic leukemia (RBL)-2H3 cell line

5.1 INTRODUCTION

Carbon nanotubes (CNTs) have unique mechanical, optical, magnetic, thermal, electrical and chemical properties that have contributed to their increased production and incorporation into numerous commercial applications including composite materials, microelectronics and industrial coatings (De Volder et al., 2013). CNTs are rolled sheets of graphene forming a cylinder with a high aspect ratio. CNTs can exist as a single rolled sheet of graphene, termed single-wall carbon nanotube (SWCNT) or as multiple graphene sheets termed multiwall carbon nanotubes (MWCNT). Pristine carbon nanotubes have all carbons bound in a hexagonal lattice and can be produced through several techniques including arc discharge and chemical vapour deposition; purification and covalent functionalization of CNTs introduces defects into the sidewalls. New covalent and non-covalent functionalization strategies have increased the solubility of CNTs and was a crucial step in creating a wave of new biomedical applications including drug and vaccine delivery, cancer and gene therapies, as well as novel imaging techniques (Fadel and Fahmy, 2014; Vardharajula et al., 2012). The safe utilization of CNTs for these biomedical applications requires a comprehensive assessment of their biocompatibility.

In assessing the biocompatibility of new materials it is important to examine the response of the immune system to exposure (Remes and Williams, 1992). The tissues, cells and molecules comprising the innate immune system form one of the earliest barriers to entry and as such are

some of the first cells to encounter and respond to NM exposure. Given that CNTs have been demonstrated to affiliate with cellular membranes (Lelimousin and Sansom, 2013) as well as bind and alter the function of soluble proteins (Maccormack et al., 2012; Rybak-Smith and Sim, 2011; Stueker et al., 2014), the potential to disturb immune function has serious implications for biocompatibility. Recent investigations into CNTs interaction with the tissues, cells and molecules of innate immunity suggest that the level of biocompatibility is highly dependent on surface chemistry (Fadel and Fahmy, 2014). For example, acid functionalizing CNTs (AF-CNTs) appears to lower the cytotoxicity of CNTs in human monocyte derived macrophage cells compared to pristine CNTs (P-CNTs) (Porter et al., 2009). However, studies have suggested that exposure to AF-CNTs can still cause the release of pro-inflammatory mediators. For example, in mice intravenously exposed to acid treated SWCNTs, histopathological observation of pulmonary tissue revealed general inflammation indicated through inflammatory cell infiltration (Yang et al., 2008). The level of inflammation induced by CNT exposure has been shown to vary depending on surface chemistry, metal content, solubility and architecture; given that inflammation has important pathological consequences, further investigations into CNT biocompatibility is required (Fadel and Fahmy, 2014).

The immune system is a complex network of tissues, cells and molecules all working in concert to provide defense against infection. Myeloid cells (i.e. macrophages and granulocytes) are important mediators of

innate immunity and one of the first activators of the inflammatory response. Granulocytes, including neutrophils and mast cells, harbor granules in their cytoplasm which can be released and contain various mediators of immunity. Mast cells in particular, often located at interfaces of the body with the external environment, are one of the first immune cells likely to encounter and respond to NM exposure (Passante and Frankish, 2009). Through the release of a variety of cytokines and chemoattractants for other immune cells such as neutrophils and macrophages, mast cells are one of the first to initiate the inflammatory response (Passante and Frankish, 2009).

Mast cells express high affinity surface membrane Fcε receptors (FcεRI) which engage immunoglobulin E (IgE) antibodies to detect foreign antigens. Antigen-dependent mast cell activation results following FcεRI aggregation induced by antigen-bound IgE antibodies and results in a complex series of intracellular signaling processes. Membrane bound and receptor associated Src-family kinases (e.g. LYN, SYK) phosphorylate the immunoreceptor tyrosine-based activation motif (ITAM) located on FcεRI to initiate signal transduction. Signal propagation includes the downstream activation of calcium channels and other signaling kinases such as extracellular signal-related kinases (ERK) that ultimately stimulates degranulation (Gilfillan and Tkaczyk, 2006). The rat basophilic leukemia (RBL)-2H3 cell line expresses FcεRI which can bind IgE in a processes termed sensitization. When subsequently cross-linked by dinitrophenyl-human serum albumin (DNP-HSA), degranulation is stimulated and includes the

extracellular release of a variety of chemical mediators including histamine, serotonin and β-hexosaminidase (Huang et al., 2009). RBL-2H3 cells have been utilized as an *in vitro* model to investigate mast cell-like immune function and they have been used extensively in studies of allergy and inflammation.

The aim of the present study was to investigate the impact of several differentially functionalized CNTs, including pristine, unfunctionalized CNTs (U-CNTs) produced directly from the induction thermal plasma process as well as AF-CNTs that were purified and differentially carboxy-functionalized (CNT-30, CNT-40 and CNT-50), on RBL-2H3 cells. We examine this cells ability to degranulation by utilizing the IgE-DNP model to assess the effects of CNT exposure on IgE-FcεRI-mediated degranulation. We also examine the effect of CNT exposure on the underlying signaling activation required to elicit IgE-FcεRI-mediated degranulation to gauge potential mechanisms of CNT immunomodulation. The removal of metal impurities, increasing CNT solubility, and decreasing the length of CNTs, all associated with AF-CNTs has been suggested as factors for reducing cytotoxicity (Liu et al., 2012). Our hypothesis is that exposure to purified and AF-CNTs (CNT-30, CNT-40 and CNT-50) will have reduced cytotoxicity and immunomodulation in RBL-2H3 cells compared to U-CNTs.

5.2 MATERIALS AND METHODS

5.2.1 CNT synthesis and characterization

CNTs used in this study were synthesized and characterized at the Steacie Institute for Molecular Sciences. Detailed reports of their production have been published (Kim et al., 2007; Price et al., 2009). Briefly, U-CNT were produced using the induction thermal plasma process using commercial carbon black (Columbian Inc.) and nickel (Ni), cobalt (Co) and yttrium oxides (Y_2O_3) as catalysts. U-CNTs were subsequently oxidized in a nitric acid/sulfuric acid (HNO_3/H_2SO_4) solution for 2 h at 30, 40 or 50 °C. Increasing the temperature of the oxidation treatment yields progressively shorter CNTs with mostly carboxylic acid groups covalently bound to the sidewall and ends. CNTs oxidized at 30, 40 or 50 °C were termed CNT-30, CNT-40 and CNT-50, respectively. Stock suspensions at a final concentration of 1000 mg L^{-1} were prepared by suspending U-CNT, CNT-30, CNT-40 and CNT-50 in double distilled water (ddH_2O).

Test suspensions were created by vortexing stock suspension for 30 seconds followed by sonication for 30 seconds (Sonifer Cell Disruptor, Branson Ultrasonics Corporation, USA) and subsequently serially diluting in ultrapure water and in RBL-2H3 culture media (see "Cell culture" section below). CNTs were characterized with transmission electron microscopy (TEM) analysis using a H-750 electron microscope (Hitachi High-Technologies Corporation, Japan). In addition, the hydrodynamic diameter, polydispersity index and zeta potential of CNTs at experimental concentrations of 10, 50, 100, 250 mg L^{-1} in ultrapure water were determined

using dynamic light scattering (DLS; Malvern Zetasizer, Malvern Instruments Inc., UK). Hydrodyamic radii were measured using 173° backscattering mode and are reported as the peak value of >99% intensity. Concentrations below 10 mg L^{-1} were below accurate limits of detection using DLS. It was not possible to gather reproducible data of hydrodynamic diameter, polydispersity index and zeta potential of CNTs in RBL-2H3 cell culture media.

5.2.2 Cell culture

RBL-2H3 cells were grown to confluence at 37 °C and 5% CO_2 in culture media consisting of filter sterilized (0.22 μm, Corning) minimum essential medium (MEM; Hyclone) containing 10% heat-inactivated fetal bovine serum (FBS; Hyclone) supplemented with 2 mM L-glutamine (Gibco), 100 units mL^{-1} penicillin (Gibco), and 100 μg mL^{-1} streptomycin (Gibco) as described previously (Cortes et al., 2014). Upon reaching confluence, RBL-2H3 cells were harvested by incubating in RBL-2H3 harvest buffer (1.5 mM EDTA, 135 mM NaCl, 20 mM HEPES, 5 mM KCl, pH 7.4) at 37 °C and 5% CO_2 for 10 min followed by pipetting to detach cells from their substrate. Cells were subsequently seeded into new culture plates (BD Biosciences) containing fresh culture media and grown to confluence (37 °C and 5% CO_2).

5.2.3 Examination of RBL-2H3 viability following CNT exposure by flow cytometry

Harvested RBL-2H3 cells were enumerated and seeded in a 96 well plate (Costar) at a density of 40,000 cells per well. Cells were incubated at 37 °C and 5% CO_2 for 1 h to allow them to adhere to the substrate. Subsequently, cells were dosed with either U-CNT, CNT-30, CNT-40 or CNT-50 at a concentration of 1, 5, 10, 50, 100 or 250 mg L^{-1} in RBL culture media for 2, 6 or 24 h. Control wells received RBL culture media alone (negative control) or 40 µL of CNT stock solution supernatant (vehicle control). The vehicle control was run to determine if any trace metal contaminants present in CNT stock solutions affect cell viability and was obtained by centrifuging U-CNT stock solution and subsequently filtering the collected supernatant (0.22 µm, Corning).

Following CNT exposure, cells were washed twice with 1x PBS and harvested using RBL harvest buffer. Harvested cell suspensions were washed twice with 1x PBS and re-suspended in 200 µL of 1x PBS containing propidium iodide (PI; 100 µg mL^{-1}) and analyzed by flow cytometry (Quanta SC, Beckman Coulter). PI fluorescence, indicating cell death, was detected using the FL2 filter and was used to calculate the percentage of viable cells in culture for each exposure.

5.2.4 Examination of RBL-2H3 viability following CNT exposure using the MTS assay

To complement the viability data collected using flow cytometric analysis, the effect of CNT exposure on RBL-2H3 viability was also investigated using the MTS assay. MTS [3-(4,5-dimethylthiazol-2-yl)-5-(3-carboxymethoxyphenyl)-2-(4-sulfophenyl)-2H-tetrazolium] is a tetrazolium salt that undergoes a colour change when bioreduced by cells and can be used to gauge the number of respiring cells in culture.

Harvested RBL-2H3 cells were enumerated, seeded and exposed to CNTs in a 96 well plate following the same protocol above (see section 2.3). Following 2, 6 or 24 h CNT exposure, the MTS cell proliferation assay was performed according to the manufacturer's instructions (Cell Titer 96 Aqueous Non-Radioactive Cell Proliferation Assay Kit, Promega, USA). Briefly, cells were washed twice with 1x PBS before being replenished with 100 μL of fresh culture media. Prepared kit reagents were added to each well and the plate was incubated at 37 °C and 5% CO_2 for 1 h; subsequently, absorbance at 490 nm was measured for each treatment using a microplate reader, (WALLAC 1420, PerkinElmer, USA). After correcting for background absorbance of materials, viability was calculated by dividing the absorbance of CNT exposed cells by the absorbance of vehicle-only exposed cells and expressed as percent control.

5.2.5 Examination of IgE-FcεRI-mediated degranulation following CNT exposure

Degranulation, the release of a variety of chemical mediators including histamine, serotonin and β–hexosaminidase, was used as a marker of cellular activation (Huang et al., 2009). To assess overall degranulation, the activity of released β–hexosaminidase was assayed using the β–hexosaminidase release assay as described previously (Naal et al., 2004). Briefly, RBL-2H3 cells were seeded at a density of 4.0×10^4 cells per well into a 96-well flat-bottom plate (Costar) in cell culture media. Seeded cells were incubated at 37 °C and 5% CO_2 for 2 h to allow for cell attachment to the substrate. Cells were then sensitized by incubating with 100 ng mL^{-1} of mouse anti-DNP IgE mAb (Sigma-Aldrich) in incomplete Tyrodes buffer (25 mM HEPES, 140 mM NaCl, 1.8 mM $CaCl_2$, 5.6 mM D-glucose, 12 mM $NaHCO_3$, 0.37 mM NaH_2PO_4 and $MgCl_2$, pH 7.4) for 1 h at 37 °C and 5% CO_2. Following sensitization, cells were washed with 200 µL of Tyrodes buffer containing 0.1% bovine serum albumin (BSA; Sigma-Aldrich). Sensitized cells were stimulated to degranulate with the addition of 0.05 µg mL^{-1} DNP-HSA (Biosearch Technologies Inc.) in 0.1% BSA/Tyrodes buffer warmed to 37 °C. For this assay, negative controls were exposed to 0.1% BSA/Tyrodes buffer alone to measure background activity without DNP-HSA stimulation. Positive controls were exposed to 0.625 µM calcium ionophore A23187 (Sigma-Aldrich) in 0.1% BSA/Tyrodes buffer. All treatments were incubated for 1 h at 37 °C and 5% CO_2. The activity of released β–hexosaminidase was measured by removing 25 µL of supernatant from each treatment and combining it with 100 µL of β–hexosaminidase substrate buffer (2 mM 4-

methylumbelliferyl N-acteyl-b-D-glucosaminide (Sigma-Aldrich), 100mM citrate, pH 4.5). Following a 30 min incubation at 37 °C and 5% CO_2, the reaction was quenched with the addition of 150 uL quench buffer (200 mM L-glycine, pH 10.7) and sample fluorescence, measuring cleavage of the substrate by β–hexosaminidase, was measured with a microplate reader with 360 nm excitation and 450 nm emission filter (WALLAC 1420, Perkin Elmer, USA).

Using the above protocol, RBL-2H3 cells were exposed to CNTs and subsequently sensitized and stimulated to degranulate to determine if the ability of cells to elicit appropriate functional responses was affected following nanomaterial (NM) exposure. After seeding cells into 96 well plates and subsequent 2 h incubation, cells were exposed to 1, 5, 10, 50, 100 or 250 mg L^{-1} of U-CNT, CNT-30, CNT-40 or CNT-50 for either 2, 4 or 6 h at 37 °C and 5% CO_2. Vehicle control treatments consisted CNT stock solution supernatant exposure for either 2, 4 or 6 h (see section 2.2). Following CNT exposure, cells were sensitized and stimulated and the β–hexosaminidase release assay was completed as described above.

5.2.6 Examination of IgE-FcεRI-mediated degranulatory recovery following CNT exposure

To determine if the reduction in degranulation observed after CNT exposure could be rescued, a second protocol was developed that introduced a wash-step to remove CNTs post exposure. RBL-2H3 cells were exposed to

U-CNT, CNT-30, CNT-40 or CNT-50 as described above. Following CNT exposure, cells were washed three times with 0.1% BSA/Tyrodes buffer to remove residual and unbound CNTs. Following the wash step the degranulation assay was subsequently conducted as previously described. All control treatments also received the introduced wash step.

5.2.7 Examination of stimulated RBL-2H3 MAPK ERK1(p44)/ERK2(p42) cell signaling following CNT exposure

To assess if the reduced degranulatory response observed with CNT exposure caused a corresponding change in the signal transduction pathways leading to degranulation, mitogen activated protein kinase (MAPK) signaling of extracellular signal-related kinases (ERK) was used as a biomarker (MAPK/ERK). RBL-2H3 cells were seeded in 6-well plates (Costar) at a density of 5.0 x 10^5 cells per well. Cells were cultured at 37 °C and 5% CO_2 for ~2 days until confluence was reached. Cells were then exposed to 1, 10, 50, 100 or 250 mg L^{-1} of U-CNT or CNT-30 for either 2 or 6 h at 37 °C and 5% CO_2. Vehicle controls received CNT stock solution supernatant, positive and negative controls received sterile ddH_2O. In the first experiment, after 2 or 6 h, exposure solutions were removed and CNT exposed cells and vehicle control cells were sensitized with 100 ng mL^{-1} of mouse anti-DNP IgE mAb in Tyrodes buffer for 1 h at 37 °C and 5% CO_2. In the second experiment, after 2 or 6 h, exposure solutions were removed and CNT exposed cells and vehicle control cells were washed three times with 0.1% BSA/Tyrodes buffer to

remove residual and unbound CNTs. RBL-2H3 cells were then sensitized with 100 ng mL^{-1} of mouse anti-DNP IgE mAb in Tyrodes buffer for 1 h at 37 °C and 5% CO_2. In both experiments, negative and positive control treatments were not sensitized with IgE. Following IgE sensitization, cells were stimulated with the addition of 0.05 μg mL^{-1} DNP-HSA for 8 min. A DNP-HSA exposure of 8 min was determined to maximally induce ERK signaling over a 30 min period. Positive control treatments were stimulated with the addition of 0.625 μM calcium ionophore A23187; negative controls were left undisturbed. All treatments were subsequently washed with PBS and lysed with mechanical disruption using 200 μL of ice-cold lysis buffer (1% Triton X-100, 150 mM NaCl, 50 mM Tris, phosphatase and protease inhibitors (Roche), pH 8.0).

To prepare for western blotting, samples were diluted 1:1 in 2x Laemmli buffer (0.5M Tris, 10% glycerol, 10% SDS. 1% bromophenol blue, 5% b-mercaptoethanol) and subsequently heating to 95 °C for 10 min. Sample proteins were separated on a SDS-PAGE gel (10% acrylamide, 10% SDS, 1.5 M Tris separating buffer) for 1 h at 150 V and then transferred to a nitrocellulose membrane in transfer buffer (Tris base, glycine with 20% methanol) for 1 h at 100 V. Membranes were blotted with anti-ERK1(p44)/ERK2(p42) MAPK (L34F12) and anti-phospho-p44/p42 MAPK (Erk1/2) mouse mAb (Cell Signaling Technologies) diluted 1:5,000 (v/v). To detect immunoreactive bands, membranes were subsequently blotted with goat anti-rabbit IgG (H+L) HRP-conjugated pAb (Bio-Rad) diluted 1:5,000

(v/v). Membranes were developed with SuperSignal West Pico Chemiluminescent Substrate kit (Pierce Biotechnology) and visualized on authoradiography film (GE Healthcare). Band intensity was analyzed and quantified using ImageJ v1.47 and expressed relative to our vehicle control.

5.2.8 Examination of CNT interactions with RBL-2H3 cells by confocal microscopy

To investigate how CNTs are interacting with RBL-2H3 cells confocal microscopy experiments were performed. Glass coverslips (Fisher Scientific) were sterilized with 70% ethanol, washed with PBS and UV irradiated. Coverslip were placed in the bottom of each well on a 6 well plate (Costar) and subsequently seeded with RBL-2H3 cells at a density of 1×10^5 in culture media. Coverslips were incubated at 37 °C and 5% CO_2 for ~ 2 days. When confluence was reached, cells were dosed with 250 mg L^{-1} U-CNT or CNT-30 for 6 h. Vehicle control was dosed with CNT stock solution supernatant for 6 h. Subsequently, coverslips were inverted on parafilm containing 100 ng mL^{-1} IgE mAb in antibody staining buffer (ASB; phosphate buffered saline, 0.5% bovine serum albumin) for 30 min over ice. Coverslips were placed back in 6 well plates and washed twice with ASB. Cells were then inverted on parafilm containing 50 ng mL^{-1} goat anti-mouse IgG PE-conjugated staining antibody (Beckman Coulter) in ASB at 4 °C for 30 min in the dark. Coverslips were again placed back in 6 well plate and washed twice with ASB before being treated with Fixation Buffer (BioLegend) for 20 min at room temperature.

Fixed cell preparations were washed with ASB and then mounted on glass slides using mounting media. Slides were imaged with a Zeiss LSM 710 Laser Scanning Confocal Microscope (objective 40x 1.3 oil plan-Apochromat), collected with Zen 2011 software and processed with LSM Image Browser (v. 4.2.0.121, Carl Zeiss).

5.2.9 Statistical analysis

A two-way Analysis of Variance (ANOVA) followed by post-hoc Tukey test was performed to analyze the effect of CNT exposure on RBL-2H3 viability. To examine the effect of CNT exposure on RBL-2H3 degranulation, two-way ANOVA followed by post-hoc Tukey test was performed. To compare the effect of U-CNT with CNT-30 exposure on RBL-2H3 degranulation, a two-way ANOVA followed by Sidak's post-hoc test was performed. A one-way ANOVA followed by a post-hoc Dunnett test was utilized to analyze changes in intracellular signaling due to CNT exposure. Statistical analyses were performed using GraphPad 6.0 statistical software program with significance set at $p<0.05$.

5.3 RESULTS

5.3.1 CNT physico-chemical characterization

For this study, single walled carbon nanotubes (CNTs) were produced and characterized as previously described yielding U-CNTs (Kim et al., 2007;

Price et al., 2009). TEM analysis revealed U-CNTs formed parallel bundles in solution that ranged between 10 and 30 nm in diameter; individual U-CNTs had a diameter of ~1.5-1.6 nm **(Supplemental Figure S3-1)**. Parallel bundles of U-CNTs extended up to several micrometers in length; however, the presence of amorphous carbon within the matrix prevented their exact measurement **(Supplemental Figure S3-1).**

U-CNTs were subsequently purified and oxidized in nitric acid/sulfuric acid (HNO_3/H_2SO_4) solution at 30, 40 or 50 °C producing AF-CNTs termed CNT-30, CNT-40 and CNT-50, respectively. For a schematic of the production see **Supplemental Figure S5-1**. The purification procedure removed residual metal catalyst and non-CNT carbon material in the sample (Price et al., 2009). The oxidation process introduced carboxylic acid groups to the ends and sidewalls of U-CNTs and was verified with infrared and Raman spectroscopy; Fourier transformed infrared and Raman spectra of U-CNT and CNT-30 are provided in **Supplemental Figure S3-2**. Inductively coupled plasma atomic emission spectroscopy (ICP-AES) analysis of oxidized CNTs revealed CNT-30, CNT-40 and CNT-50 were 22.46, 28.86 and 36.9% carboxylic acid group by weight, corresponding to a functionalization degree (mole %) of 4.0, 5.5 and 7.8 respectively **(Supplemental Table S3-2)**. Dynamic light scattering (DLS) measurements of oxidized CNTs revealed hydrodynamic diameters ranging from 6719±572 nm to 7018±462 nm for CNT-30, 4197±332 nm to 4463±429 nm for CNT-40 and 3044±349 nm to 3248±512 nm for CNT-50 **(Supplemental Table S3-1)**. Measured zeta

potentials of oxidized CNTs (CNT-30, CNT-40 and CNT-50) revealed an overall negative charge ranging from -13.76±0.61 mV to -15.94±0.27 mV and indicates a relatively stable colloid suspension. Accurate DLS measurements for U-CNTs including hydrodynamic diameter and zeta potential was not possible due to their poor solubility and dispersibility in water; DLS measurements of U-CNT, CNT-30, CNT-40 and CNT-50 in cell culture media were not possible.

5.3.2 Effect of CNT exposure on RBL-2H3 viability

Exposure to CNTs caused a significant decline in RBL-2H3 viability that was functionalization-, dose- and time-dependent. Flow cytometric analysis revealed no significant decrease in the number of viable cells in culture after exposure to CNT-30, CNT-40, CNT-50 or U-CNT for 2 or 6 h **(Figure 5-1A,B)**. Following 24 h of exposure to 50, 100 or 250 mg L^{-1} acid functionalized CNTs (CNT-30, CNT-40 and CNT-50), a significantly decreased in the number of viable cells in culture was observed; in contrast, U-CNTs only caused a significant decline in RBL-2H3 viability after 24 h at a concentration of 250 mg L^{-1} **(Figure 5-1C)**. Significant declines in cell viability were greater following exposure to acid functionalized CNTs compared to U-CNTs for any given concentration tested. For example, after exposure to 250 mg L^{-1} CNTs for 24 h, CNT-30, CNT-40 and CNT-50 exposures had (mean±SE, n=4) 55.4±4%, 58.4±3% and 55.8±4% viable cells in culture while U-CNT exposures had 78.5±3% viable cells remaining in

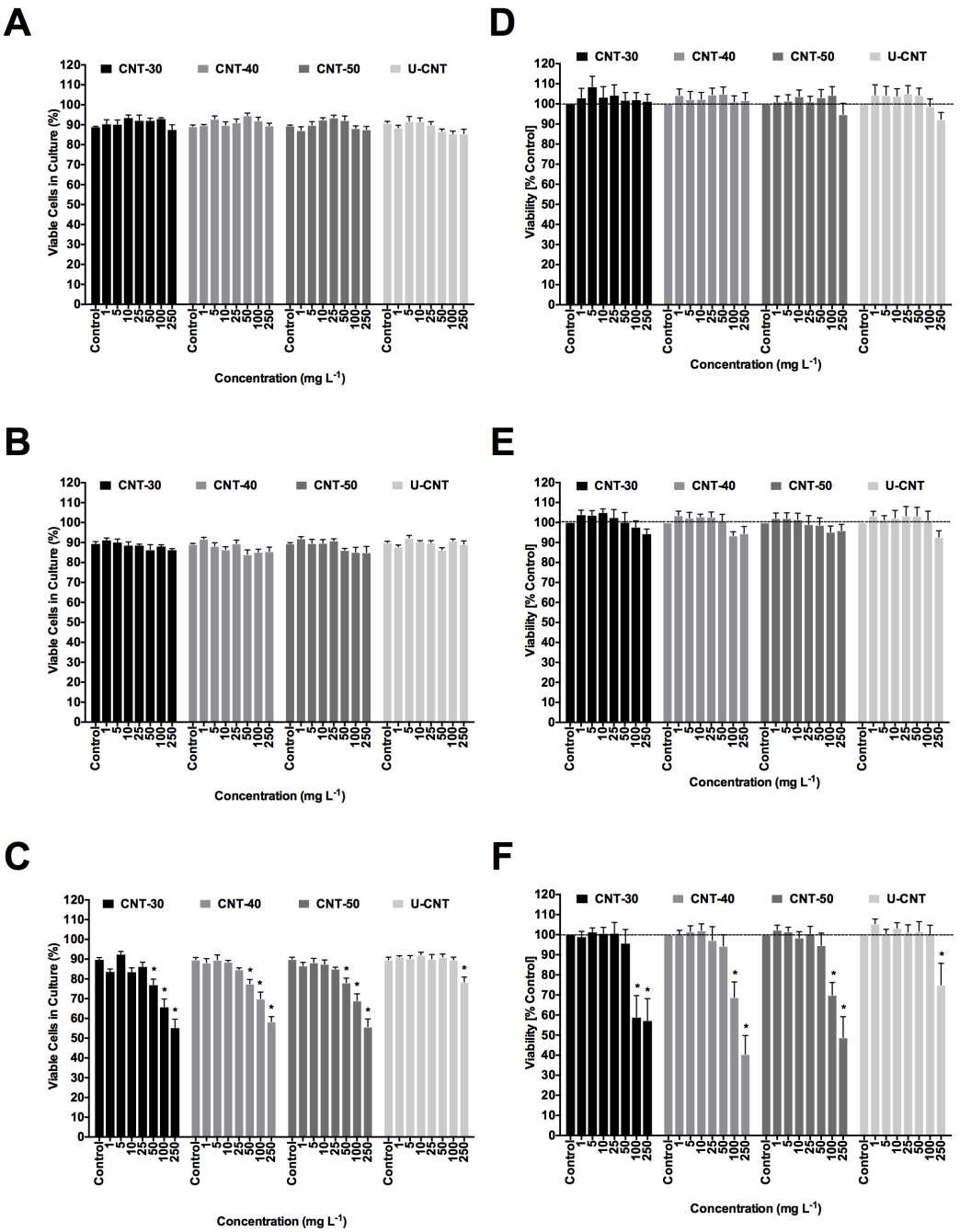
A
B
C
D
E
F
CNT-30
CNT-40
CNT-50
U-CNT
Viable Cells in Culture (%)
Viability [% Control]
Concentration (mg L-1)
Control
1
5
10
25
50
100
250

Figure 5-1. Exposure to CNTs significantly affected RBL-2H3 viability after 24 h of exposure. RBL-2H3 cells at a density of 4 x 10^4 were exposed to 1, 5, 10, 25, 50, 100 or 250 mg L^{-1} of U-CNT, CNT-30, CNT-40 or CNT-50 for 2 (A), 6 (B) or 24 (C) h. Cells were stained with propidium iodide (100 µg mL^{-1}) and analyzed by flow cytometry to distinguish between viable and non-viable cells. Viability is expressed as the percentage of viable cells in culture for each exposure. Values are means ± SE (n=4). RBL-2H3 cells at a density of 4 x 10^4 were exposed to 1, 5, 10, 25, 50, 100 or 250 mg L^{-1} of U-CNT, CNT-30, CNT-40 or CNT-50 for 2 (D), 6 (E) or 24 (F) h. Metabolic activity was used to gauge cell viability using the MTS assay. Absorbance values were measured at 490 nm and cell viability was expressed relative to control values. Values are means ± SE (n=4). Asterisk indicates significantly different values compared to control ($p<0.05$, two-way ANOVA followed by Tukey post-hoc comparison).

culture. There were no significant changes in RBL-2H3 viability following exposure to 1, 5, 10 or 25 mg L^{-1} of CNT-30, CNT-40 or CNT-50 for 2, 6 or 24 h. No significant changes in RBL-2H3 viability was found for 1, 5, 10, 25, 50 or 100 mg L^{-1} U-CNT at any time point examined **(Figure 5-1A,B,C)**.

To verify the effects of CNT exposure on viability, the MTS assay was performed. Similar to flow cytometric analysis, changes in RBL-2H3 viability after CNT exposure was dose- and time-dependent. No changes in viability were found for any CNTs tested after 2 or 6 h of CNT exposure **(Figure 5-1D,E)**. Following 24 h of exposure, acid functionalized CNTs (CNT-30, CNT-40 and CNT-50) caused significant reductions in viability at concentrations of 100 and 250 mg L^{-1} while exposure to U-CNTs only reduced viability at the highest dose examined **(Figure 5-1F)**. Exposure to 250 mg L^{-1} acid functionalized CNTs for 24 h reduced RBL-2H3 viability to 57.3±11%, 40.6±9% or 48.8±10% viability compared to controls for CNT-30, CNT-40 or CNT-50 respectively. In comparison, 250 mg L^{-1} U-CNT exposure for 24 h only reduced RBL-2H3 viability to 75.0±11% viability compared to control.

5.3.3 IgE-FcεRI-mediated degranulation following CNT exposure

RBL-2H3 cells were exposed to CNT-30 or U-CNT for 2, 4 or 6 h and subsequently sensitized and stimulated to degranulate. After 2 h, a significant decrease in IgE-FcεRI-mediated degranulation was observed in RBL-2H3 cells exposed to 50, 100 or 250 mg L^{-1} U-CNT. Inhibition of IgE-FcεRI-mediated degranulation occurred at lower doses for U-CNT compared

to CNT-30 exposure which caused a decreased degranulatory response only at the highest dose examined after 2 h of exposure **(Figure 5-2A)**. A similar trend was observed in RBL-2H3 cells exposed to U-CNT or CNT-30 for 4 h. U-CNT exposure inhibited IgE-FcεRI-mediated degranulation at lower doses compared to acid functionalized CNT-30, which inhibited RBL-2H3 degranulation at a concentration of 250 mg L^{-1} **(Figure 5-2B)**. The greatest change in degranulation was observed after 6 h CNT exposure. RBL-2H3 cells exposed to 10, 50, 100 and 250 mg L^{-1} U-CNT had a significantly lowered IgE-FcεRI-mediated degranulatory response, falling to 72.4±5%, 67.0±5%, 59.6±9% and 62.8±12% compared to control, respectively. In comparison, 6 h exposure to acid functionalized CNT-30 only significantly inhibited RBL-2H3 degranulation at concentrations of 100 and 250 mg L^{-1}, falling to 73.9±6% and 75.3±6% compared to control, respectively.

5.3.4 IgE-FcεRI-mediated degranulatory recovery following CNT exposure

RBL-2H3 cells exposed to 250 mg L^{-1} CNT-30 for 2, 4 or 6 h had their IgE-FcεRI-mediated degranulatory response significantly decrease to (mean±SE, n=4) 70.5±7%, 67.2±8% and 70.5±7% of control, respectively **(Figure 5-3A, B, C)**. The diminished degranulation following CNT-30 exposure was not recovered following the removal of CNT-30 from the

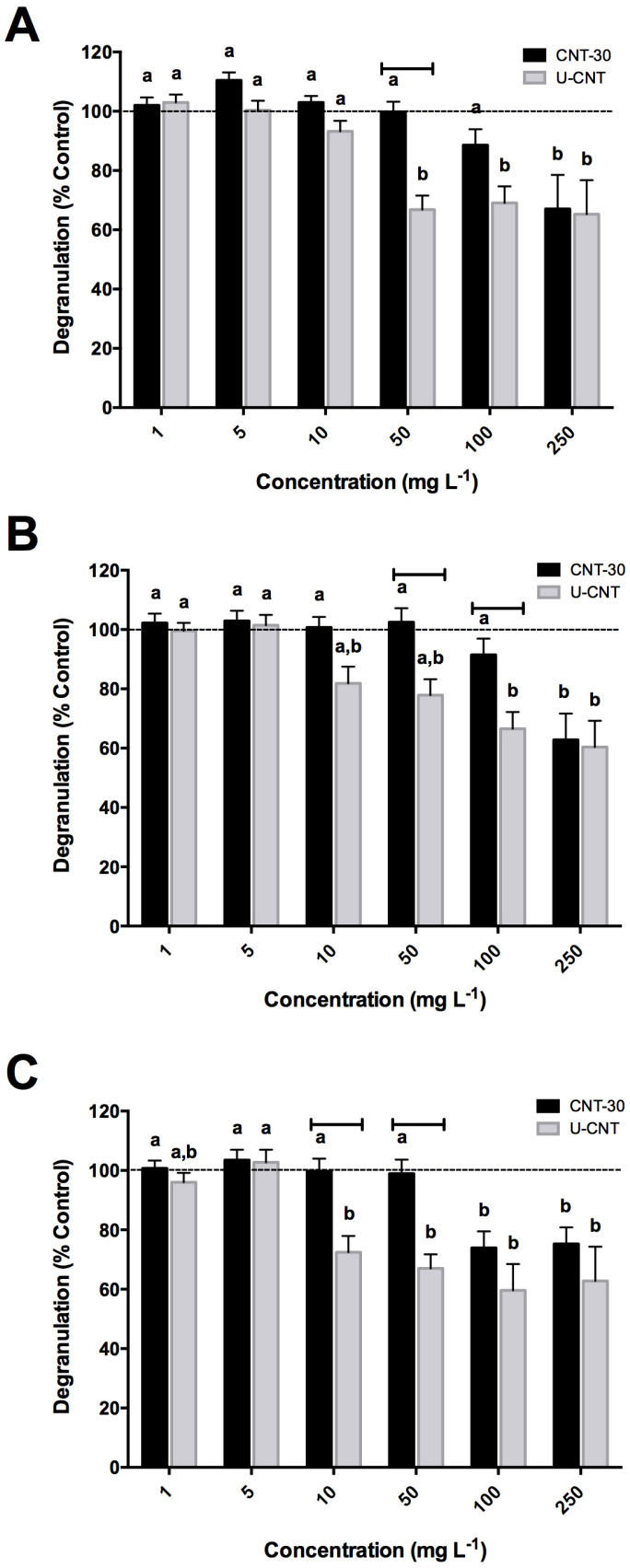
A
B
C
CNT-30
U-CNT
Degranulation (% Control)
Concentration (mg L-1)
0
20
40
60
80
100
120
1
5
10
50
100
250
a
a,b
b

Figure 5-2. RBL-2H3 cells had a diminished degranulatory response following exposure to CNTs. RBL-2H3 cells were seeded at a density of 4 x 10^4 cells per well and exposed to 1, 5, 10, 50, 100 or 250 mg L^{-1} of CNT-30 or U-CNT for 2 (A) 4 (B) or 6 (C) h. Cells were subsequently sensitized with 100 ng mL^{-1} IgE and stimulated to degranulate with 0.05 µg mL^{-1} DNP-HSA. Supernatant was collected and assayed for β-hexosaminidase activity. Activity of β-hexosaminidase released from CNT treated cells were standardized to control and expressed as percent control. Values are mean ± SE (n=4). Letters indicate significant differences in elicited degranulatory response ($p<0.05$, two-way ANOVA followed by Tukey's post hoc comparison). Horizontal lines indicate significant differences in degranulatory response between CNT-30 and U-CNT functionalizations ($p<0.05$, two-way ANOVA followed by Sidak's post-hoc comparison).

exposure solution. Removal of CNT-30 from the exposure media still resulted in significantly lowered degranulation after exposure to 250 mg L^{-1} for 2, 4 or 6 h (2 h: 70.5±7%, 4 h: 67.2±8% and 6 h: 70.5±7% of control). There was no significant difference in the degranulatory response of cells exposed to CNT-30 versus those that were exposed to CNT-30 and subsequently washed to remove the NM from the exposure media.

RBL-2H3 cells exposed to 100 and 250 mg L^{-1} U-CNT for 2, 4 or 6 h had a significant decrease in IgE-FcεRI-mediated degranulation compared to controls **(Figure 5-3D, E, F)**. When the cells were washed post exposure, a recovery of the diminished degranulation was observed. For example, after 6 h exposure to 10, 50, 100 or 250 mg L^{-1} U-CNT, RBL-2H3 IgE-FcεRI-mediated degranulation was reduced to 72.4±5%, 67.0±5%, 59.6±9%, 62.8±11% control, respectively **(Figure 5-3F)**. Removing U-CNT following the 6 h exposure to 10, 50, 100 or 250 mg L^{-1}, RBL-2H3 degranulation recovered to 99.1±5%, 98.2±5%, 94.2±5%, 87.2±6% control, respectively and were significantly different compared to the unwashed treatment **(Figure 5-3F)**.

5.3.5 Examination of MAPK ERK1(p44)/ERK2(p42) signaling following CNT exposure in stimulated RBL-2H3 cells

RBL-2H3 cells exposed to U-CNT and subsequently stimulated to degranulate through IgE-FcεRI had significantly reduced activation of the MAPK/ERK signaling pathway compared to vehicle control (**Figure 5-4A**). In RBL-2H3 cells stimulated to degranulate, a significant reduction of

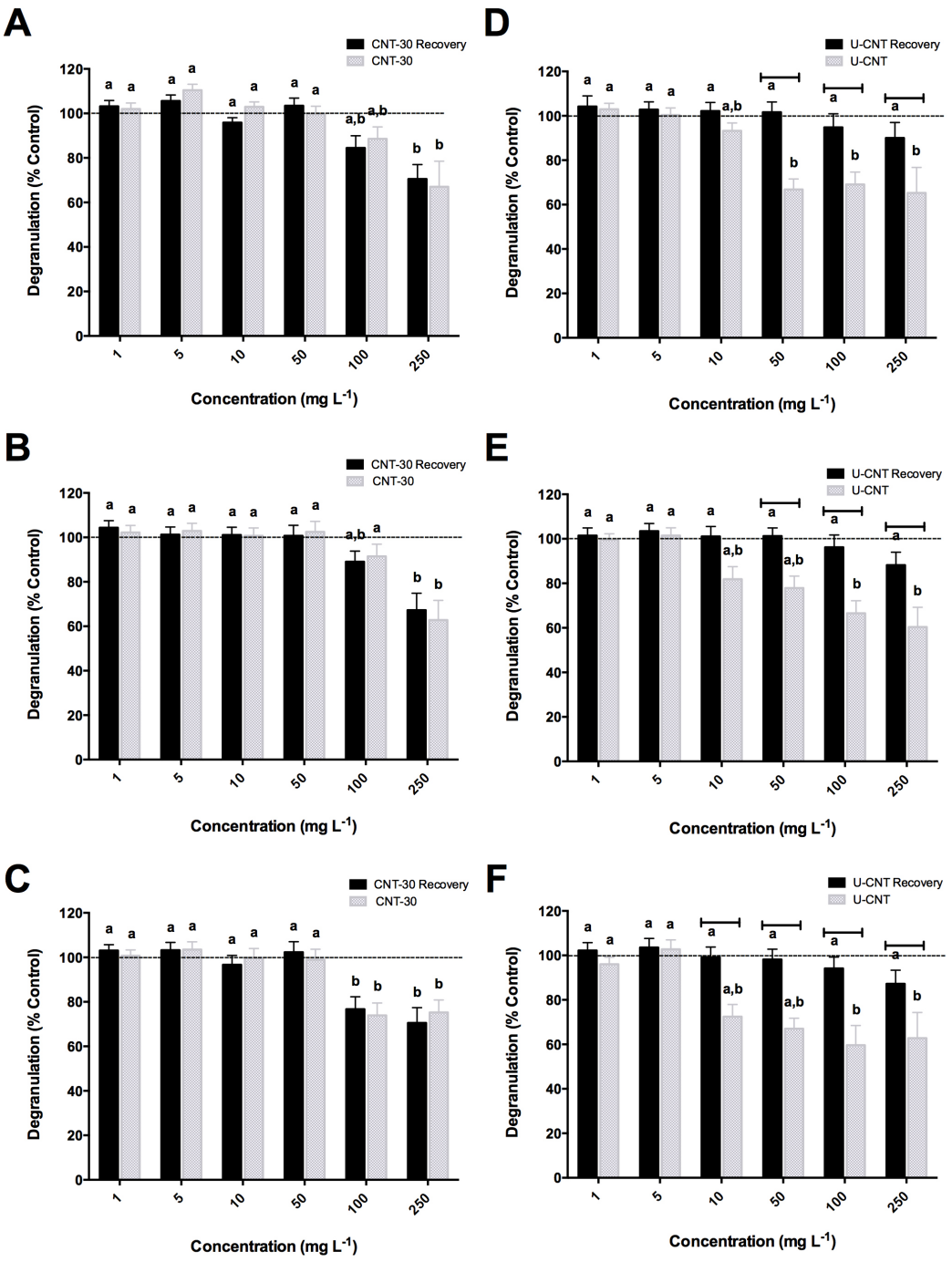
A
CNT-30 Recovery
CNT-30
Degranulation (% Control)
Concentration (mg L-1)
B
CNT-30 Recovery
CNT-30
Degranulation (% Control)
Concentration (mg L-1)
C
CNT-30 Recovery
CNT-30
Degranulation (% Control)
Concentration (mg L-1)
D
U-CNT Recovery
U-CNT
Degranulation (% Control)
Concentration (mg L-1)
E
U-CNT Recovery
U-CNT
Degranulation (% Control)
Concentration (mg L-1)
F
U-CNT Recovery
U-CNT
Degranulation (% Control)
Concentration (mg L-1)

Figure 5-3. RBL-2H3 diminished degranulation following U-CNT exposure recovers by removing U-CNT from the exposure solution. RBL-2H3 cells were seeded at a density of 4 x 10^4 cells per well and exposed to 1, 5, 10, 50, 100 or 250 mg L^{-1} of CNT-30 for 2 (A) 4 (B) or 6 (C) h or U-CNT for 2 (D) 4 (E) or 6 (F) h. Two protocols were devised, in the first cells were subsequently sensitized with 100 ng mL^{-1} IgE and stimulated to degranulate with 0.05 μg mL^{-1} DNP-HSA following CNT exposure (CNT-30, U-CNT; white bars). In the second protocol, a wash step was introduced to remove CNTs before sensitization and stimulation of RBL-2H3 cells (CNT-30 Recovery, U-CNT Recovery; black bars). Activity of β-hexosaminidase released from treated cells was assayed and expressed as percent control. Values are mean ± SE (n=4). Letters indicate significant differences in elicited degranulatory response ($p<0.05$, two-way ANOVA followed by Tukey's post hoc comparison). Horizontal lines indicate significant differences in degranulatory response between CNT (U-, -30) treatments and CNT Recovery (U-, -30) treatments ($p<0.05$, two-way ANOVA followed by Sidak's post-hoc comparison).

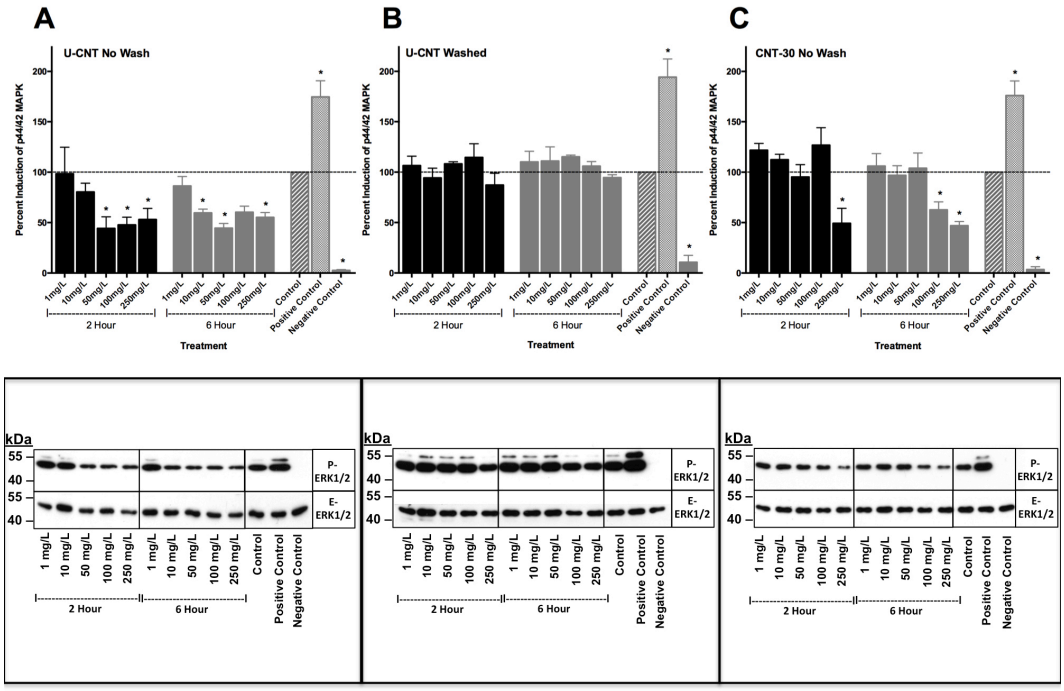

Figure 5-4. Reduced activation of MAPK/ERK signaling pathway in stimulated RBL-2H3 cells previously exposed to CNTs. RBL-2H3 cells were exposed to 1, 10, 50, 100 or 250 mg L^{-1} (A) U-CNT for 2 or 6 h (B) U-CNT for 2 or 6 h then washed or (C) CNT-30 for 2 or 6 h. Cells were subsequently sensitized (100 ng mL^{-1} IgE) and stimulated (0.05 µg mL^{-1} DNP-HSA) to degranulate. Positive control treatments were stimulated with 0.625 µM calcium ionophore, negative controls were left undisturbed. Densitometry of western blot bands was used to quantify changes in p44/42 MAPK phosphorylation, corrected with endo-p44/42 and is expressed as a percent induction relative to vehicle control exposed RBL-2H3 cells, which was normalized to a value of 100. Differences between CNT exposure and vehicle control was analyzed by one-way ANOVA followed by Dunnetts *post hoc* test. Asterisks denote significant difference from control.

MAPK/ERK phosphorylation occurred with prior exposure to 50, 100 and 250 mg L^{-1} U-CNT for 2 h, declining to 44.2±12%, 47.7±8% and 53.0±11% of control, respectively. Significant reduction of ERK phosphorylation was also found in stimulated cells after prior exposure to 10, 50, and 250 mg L^{-1} U-CNT for 6 h. In contrast, when a wash step was introduced following U-CNT exposure, a recovery of MAPK/ERK signaling activity in stimulated RBL-2H3 cells was observed after both 2 and 6 h prior U-CNT exposure (**Figure 5-4B**).

RBL-2H3 cells exposed to CNT-30 for 2 or 6 h and subsequently stimulated to degranulate had significantly reduced activation of the MAPK/ERK signaling pathway at the highest doses examined (**Figure 5-4C**). Exposure of RBL-2H3 cells to CNT-30 for 2 h at 250 mg L^{-1} or 6 h at 100 and 250 mg L^{-1} significantly reduced MAPK/ERK phosphorylation when stimulated to degranulate.

5.3.6 Examination of CNTs interaction with RBL-2H3 cells by confocal microscopy

Confocal microscopy was used to assess if CNTs might be interacting with RBL-2H3 cells and the nature of any potential interaction. Exposure to CNT-30 for 6 h resulted in deposits of CNT-30. The overlap of some of these CNT-30 deposits with FcεRI fluorescence suggests that CNT-30 are associated with RBL-2H3 cell membrane in general. In several collected micrographs, the presence of large vacuoles of CNT-30 suggests the internalization of CNT-30 in RBL-2H3 cells **(Figure 5-5, middle row).**

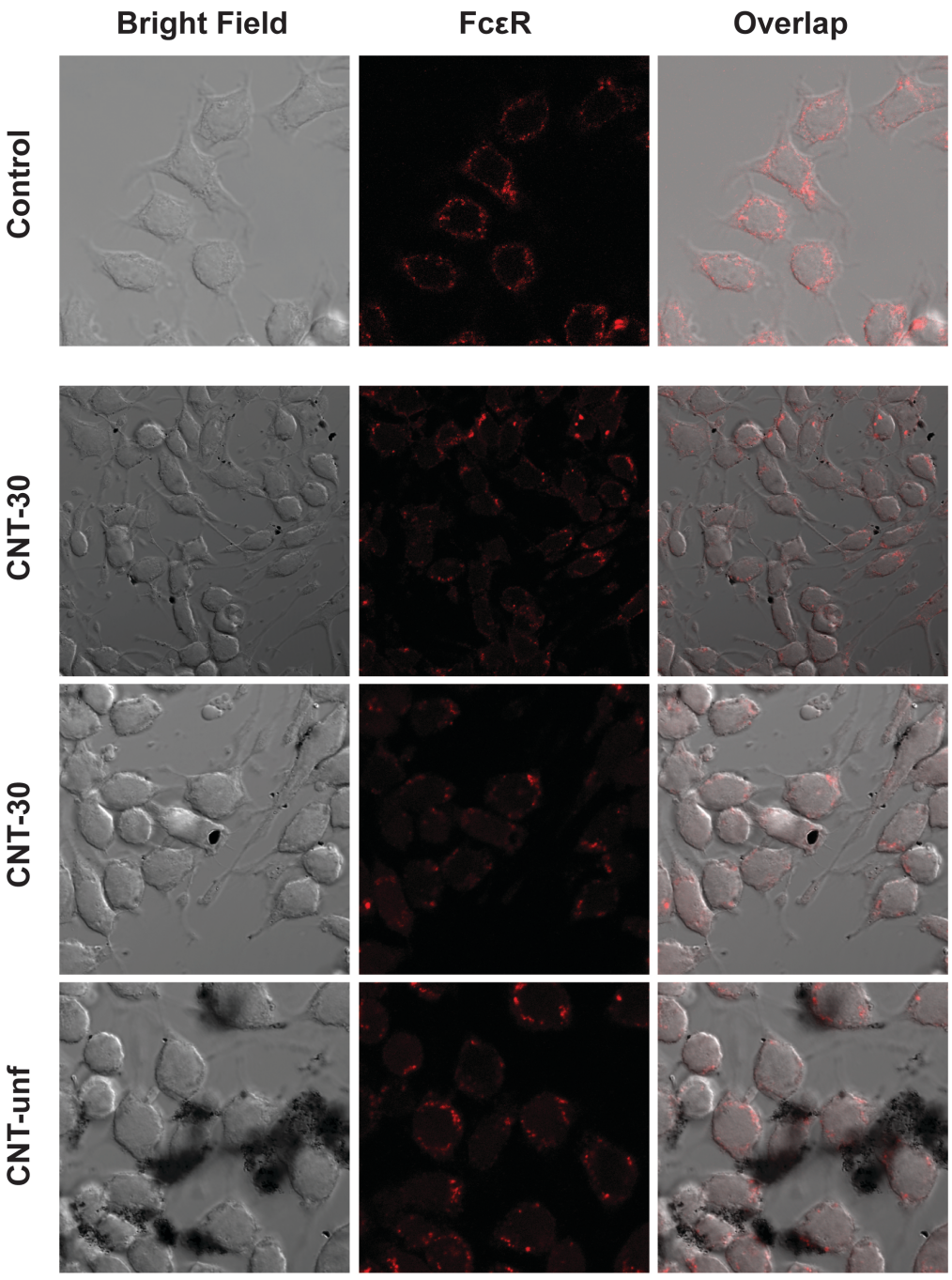
Bright Field
FcεR
Overlap
Control
CNT-30
CNT-30
CNT-unf

Figure 5-5. Confocal micrographs showing association of CNTs with RBL-2H3 cells. RBL-2H3 cells were dosed with 250 mg L^{-1} of either CNT-30 or U-CNT for 6 h. Cells were stained for FCεRI using IgE primary antibody and goat anti-mouse IgG PE-conjugated secondary antibody before being fixed. Laser scanning confocal micrographs with bright-field, FcεRI fluorescence and overlay were collected.

However, because we were unable to fluorescently label CNTs direct localization of these materials is not possible.

Confocal micrographs of RBL-2H3 cells exposed to U-CNT for 6 h suggest a more diffuse association of CNTs with the cell membrane. In contrast to CNT-30, U-CNT appeared as large and dispersed aggregate associating with a larger area of RBL-2H3 membranes. Similar to CNT-30, the overlap of U-CNT with FcεRI fluorescence suggests that U-CNT are associated with RBL-2H3 cell membranes in general **(Figure 5-5).**

5.4 DISCUSSION

5.4.1 Effect of CNT exposure on RBL-2H3 cell viability

The present study has demonstrated that exposure to CNTs caused a significant decline in RBL-2H3 viability that was functionalization-, dose- and time-dependent. Unfunctionalized CNTs (U-CNTs), the direct product of the induction thermal plasma process, exhibited the lowest cytotoxicity of all CNTs examined. Purified and differentially acid-functionalized CNTs (CNT-30, CNT-40 and CNT-50) were more cytotoxic to RBL-2H3 cells, inducing significant declines in viability at lower exposure concentrations and resulting in larger overall declines in viability at each exposure concentration.

Reports on the cytotoxicity of CNTs to innate immune cells varies depending on the type and architecture of the nanotube investigated, the

surface chemistry of the nanotube, as well as the experimental model and exposure conditions. Initial reports on the toxicity of pristine, unfunctionalized CNTs caused alarm when exposure resulted in asbestos-like toxicity and granuloma formation (Poland et al., 2008). Additional reports of mesothelial cells exposed to pristine CNTs (P-CNTs) had significant reductions in cell viability, elevated DNA damage and activated molecular signaling associated with oxidative stress; however the presence of significant metal contamination was a major determinant of P-CNT toxicity (Pacurari et al., 2008). Toxicity associated with P-CNTs has also been demonstrated to vary with CNT architecture. Human primary macrophage exposure to P-MWCNTs with longer lengths (>10nm) caused activation of molecular signaling associated with oxidative stress and inflammasome activation while short P-MWCNTs (<10nm) were relatively benign and did not induce secretion of proinflammatory cytokines IL-1α or IL-1β (Palomäki et al., 2011). P-CNT toxicity has also varied with the state and type of agglomeration. Well-suspended and dispersed P-CNTs have been demonstrated to be less cytotoxic than large agglomerates of P-CNTs (Wick et al., 2007) and long, parallel, bundled agglomerates have been shown to be more toxic than tangled, spherical agglomerates of P-CNTs (Palomäki et al., 2011; Poland et al., 2008). Together, these studies suggest that P-CNT toxicity is largely dependent upon the presence of metal impurities, CNT length and it's agglomeration characteristics in aqueous media. The present study adds to reports of limited cytotoxicity of P-CNTs in immune cells with

only small declines in RBL-2H3 viability at the highest doses examined. Physico-chemical analysis of U-CNT revealed a tangled, spherical state of agglomeration of SWCNTs and amorphous carbon with low levels of metal contamination. Together, these characteristics likely contribute to the low toxicity of U-CNTs we observe in RBL-2H3 cells.

There have been reports of enhanced *in vivo* and *in vitro* cytotoxicity from acid functionalizing CNTs. Saxena et al., (2009) found enhanced toxicity of AF-CNTs in LA4 mouse lung epithelial cells compared to P-CNTs, with significant cytotoxic effects of AF-CNTs at exposures as low as 5 mg L^{-1}. However, in general, acid functionalization has been associated with reduced toxicity of SWCNTs in immune cells (Fadel and Fahmy, 2014). AF-CNTS were readily taken up in human monocyte macrophage cells but showed no toxicity at concentrations up to 10 mg L^{-1} in one study (Porter et al., 2009) or up to 100 mg L^{-1} in another (Witasp et al., 2009). Isolated peripheral blood mononuclear cells exposed to 100 mg L^{-1} of AF-CNTs for 24 h had no significant change in cell viability or the number of apoptotic cells in culture (Delogu et al., 2012). This study indicates that AF-CNTs are generally very biocompatible, with no observed toxicity in RBL-2H3 cells exposed to CNT-30, CNT-40 or CNT-50 at concentrations as high as 250 mg L^{-1} for 2 or 6 h of exposure. Characterization of CNT-30, -40 and -50 revealed these materials are highly soluble and dispersed in solution due to the introduced carboxy functionalization. DLS measurements also show that increasing oxidation temperature yielded significantly and progressively shorter AF-CNTs.

Together, the increased solubility and shorter nanotube length likely contributed to the limited cytotoxicity we observe in in RBL-2H3 cells. However, we did find significant declines in viability after exposure to high concentrations of AF-CNT for 24 h.

5.4.2 Effects of CNT exposure on IgE-FcεRI-mediated degranulation in RBL-2H3 cells

The present study has demonstrated that CNT exposure significantly reduced IgE-FcεRI-mediated degranulation of RBL-2H3 cells and was functionalization-, dose- and time-dependent. In contrast to RBL-2H3 viability, U-CNT exposure caused the greatest declines in RBL-2H3 function, decreasing IgE-FcεRI-mediated degranulation to a greater extent and at lower exposure concentrations, compared to purified and acid functionalized CNT-30. However, the diminished degranulatory response of RBL-2H3 cells exposed to U-CNTs could be recovered following removal of U-CNTs from the exposure condition while no recovery was found in cells exposed to purified and acid functionalized CNTs. An examination of the underlying intracellular signaling mechanisms for IgE-FcεRI-mediated degranulation found a concomitant reduction in the activation of MAPK/ERK signaling following CNT exposure and, similar to our results from the degranulation assay, MAPK/ERK activity could be rescued in RBL-2H3 cells exposed to U-CNTs. Examination of CNT interaction with RBL-2H3 cells by confocal microscopy suggests an affiliation with the cellular membrane. Together, the reduced

downstream activation of signaling kinases and high level of association with the cellular membrane suggests that the diminished degranulatory response observed after CNT exposure may result from a reduction in IgE-FcεRI aggregation.

Previous studies have suggested that CNT exposure can cause immunomodulatory effects in various immune cells. U-CNT and AF-CNT exposure has been associated with both immunoactivation and immunosuppression. U-CNT exposure to monocytes resulted in the release of proinflammatory mediators such as TNF-α and ROS production (Brown et al., 2007). AF-CNT exposure to monocytes and NK-cells resulted in cellular activation *ex vivo* (Delogu et al., 2012). Others have reported that U-CNT and AF-CNT exposure causes immunosuppression. In studies of U-CNT exposure, Mitchel et al., (2009) reported that U-MWCNT exposure resulted in a decreased T-cell-dependent antibody response in mice. AF-CNT immunosuppression was documented by Alam et al., (2013) when exposure to AF-CNTs significantly suppressed the cytotoxic T-cell response in a mixed lymphocyte reaction. The present study adds to reports of immunosuppression caused by CNT exposure *in vitro*. The decline in β-hexosaminidase activity following CNT exposure indicates a suppressed IgE-FcεRI-mediated degranulatory response of sensitized and stimulated RBL-2H3 cells. There was also evidence of reduced activation of the intracellular signaling required to elicit IgE-FcεRI-mediated degranulation.

Several mechanisms have been proposed to account for immunosuppression of mast cell following NM exposure. Exposure of murine peritoneal mast cells to non-porous silica nanoparticles diminished exocytotic function and the authors hypothesized that based on secretion frequencies, this was likely due to NMs interfering with cytoskeletal or fusion machinery (Maurer-Jones et al., 2010). Tahara et al., (2012) reported the suppression of IgE-mediated histamine release from RBL-2H3 cells *in vitro* following exposure to polymeric nanoparticles. In their study, confocal microscopy confirmed polymeric nanoparticles were actively taken up by these cells and subsequently excluded through exocytosis. They concluded that the exocytosis of NMs reduced IgE-mediated exocytosis of histamine by competitively utilizing the exocytic machinery (Tahara et al., 2012). AF-CNTs have been shown to be actively internalized in human macrophage cells (Porter et al., 2009) and our confocal microscopy results suggest the internalization of CNT-30. However, this mechanism likely doesn't fully explain the reduced IgE-FcεRI-mediated degranulatory response we observe. Analyses of IgE-FcεRI-mediated intracellular signal transduction following CNT exposure found reduced phosphorylation of MAPK/ERK. This signaling kinase, responsible for regulating a diverse array of cellular processes in mast cells including degranulation, is far upstream of the engagement of exocytosis machinery involved in eliciting degranulation (Gilfillan and Tkaczyk, 2006). Further, we found an almost immediate recovery of IgE-FcεRI-mediated degranulation when U-CNTs were removed from the

exposure solution; if the exocytosis of U-CNTs was competing with the exocytic machinery and resulting in diminished IgE-FcεRI-mediated degranulation, we would expect a gradual recovery of degranulation as the competitive inhibition was reduced with increasing exocytotic clearance of CNTs from the intracellular compartment.

Alternatively, diminished degranulation from NM exposed mast cells has been proposed to occur through NM interference with antibody-receptor (IgE-FcεRI) binding and/or antigen cross-linking (Huang et al., 2009). CNTs have been shown to bind and alter the function of soluble proteins (Casey et al., 2008; Rybak-Smith and Sim, 2011; Salvador-Morales et al., 2006) and affiliate directly with cellular membranes (Lelimousin and Sansom, 2013). Our confocal results found overlap between CNTs with FcεRI fluorescence and it is possible CNTs diminish the IgE-FcεRI-mediated degranulatory response of RBL-2H3 cells by interfering with sensitization (IgE-FcεRI binding) or stimulation (IgE-FcεRI crosslinking by antigen). In support of this, phosphorylation of the underlying FcεRI signaling intermediate MAPK/ERK was reduced and suggests alterations in IgE-FcεRI crosslinking occurred. Further, removal of U-CNTs caused an almost immediate recovery of IgE-FcεRI-mediated degranulation. Together, this suggests that the significant inhibition of IgE-FcεRI-mediated degranulation by U-CNT exposure likely results from U-CNT preventing FcεRI activation. This may occur either by preventing IgE from binding its congnate receptor FcεRI during sensitization or preventing the subsequent cross-linking of the FcεRI

complex by its antigen during stimulation. Interestingly, although CNT-30 exposure inhibited IgE-FcεRI-mediated degranulation to a much lesser extent than U-CNT, there was no recovery of function when this nanomaterial was removed. This suggests CNT-30 may be binding RBL-2H3 membranes to a greater extent and cannot be removed by washing or the inhibition of degranulation observed at high doses occurs by another mechanism.

5.5 CONCLUSIONS

CNT exposure significantly reduced IgE-FcεRI-mediated degranulation of RBL-2H3 cells at sub-lethal levels of exposure. U-CNT exposure caused a greater decline in IgE-FcεRI-mediated degranulation at lower concentrations compared to purified and acid functionalized CNT-30. However, removal of U-CNTs recovered IgE-FcεRI-mediated degranulation while no recovery was found in cells exposed to CNT-30. An examination of MAPK/ERK signaling in stimulated RBL-2H3 cells following CNT exposure found a concomitant reduction in activation and, similar to our results from the degranulation assay, MAPK/ERK activity could be rescued in RBL-2H3 cells exposed to U-CNTs. Imaging of CNTs using confocal microscopy revealed these materials affiliate with the cellular membrane in RBL-2H3 cells. Together, the reduced downstream activation of signaling kinases and high level of association with the cellular membrane suggests that the diminished degranulatory response observed after CNT exposure may result from a reduction in IgE-FcεRI aggregation.

CHAPTER 6

Cellulose nanocrystals have minimal effects on teleost and mammalian leukocyte viability and function

6.1 INTRODUCTION

Produced from cellulose, an abundant and renewable material, cellulose nanocrystals (CNC) are a low cost nanomaterial that is biodegradable and exhibits high mechanical strength and low density (Lam et al., 2012). In addition, CNCs are easily functionalized with a variety of chemical groups. These properties have facilitated the incorporation and use of CNCs in commercial and biomedical applications. The largest projected commercial markets for nanocellulose includes packaging, paper and plastic applications, with an estimated global market of 33 million metric tons (Cowie et al., 2014; Shatkin et al., 2014). In addition, several biomedical applications of CNCs have been proposed including cellular imaging (Dong and Roman, 2007), tissue engineering (Schumann et al., 2009) and drug delivery (Akhlaghi et al., 2013; Lam et al., 2012).

The starting material utilized to produce CNCs can come from several sources including tuncin, bacterial cellulose, algal cellulose, wood pulp and cotton linters (Roman, 2015) with wood and plant fibers being the most abundant sources (Leung et al., 2011). Extraction of cellulose fibers from these sources requires removal of several non-cellulose constituents including lignin, pectin, hemicellulose and wax (Leung et al., 2011). Isolated cellulose fibers contain both crystalline and amorphous cellulose; cellulose nanocrystals (CNCs) are obtained by isolating crystalline regions from cellulose fibers, producing rod-like nanocrystals usually accomplished by acid hydrolysis (Habibi et al., 2010).

Many nanomaterials have been demonstrated to have adverse biological effects (Poland et al., 2008). Given the utility and projected market production of CNCs, safe development of this material must include an evaluation of their toxicity. Exposure to CNCs could occur by inhalation, ingestion or transdermal absorption. In addition, the potential biomedical applications of CNCs suggests direct *in vivo* exposure of CNCs to cells and tissues is possible. One important factor in assessing the biocompatibility of nanomaterials is their interaction with immune cells and immune function, including both myeloid cells and lymphoid cells. Myeloid cells, including macrophages and granulocytes, are leukocytes that are important contributors to innate immunity and one of the first activators of the inflammatory response (Passante and Frankish, 2009). In particular, granulocytes (*i.e.* neutrophils and mast cells) release various mediators of immunity from granules in their cytoplasm in a process called degranulation. Lymphoid cells, including B-cells and T-cells, are important in the humoral and cell-mediated aspects of acquired immunity (Hussain et al., 2012).

Here we investigated the cytotoxicity of CNC by examining fish and mammalian leukocyte viability following CNC exposure. Several cell lines were tested, including both lymphoid and myeloid cells. Channel catfish are the only fish species with several characterized lymphoid cell lines, including two cell lines characterized as B-cell-like termed 3B11 and 1G8, and one characterized as T-cell-like called 28S.3, utilized in this study. We also examined if CNC exposure affected the ability of immune cells to elicit

appropriate effector responses *in vitro.* Rat basophilic leukocyte (RBL)-2H3 is a granulocyte cell line that has been used in studies of allergies and inflammation. These cells express an endogenous, high affinity Fcε receptor (FcεRI) on their cell membrane, making them useful model for studies on receptor-mediated degranulation. When FcεRI is sensitized, by binding immunoglobulin E (IgE), and subsequently stimulated, by antigen induced receptor cross-linking, it induces degranulation (Gilfillan and Tkaczyk, 2006). Using FcεR1-mediated degranulation, we examined if sub-lethal CNC exposure affected the ability of RBL-2H3 cells to degranulate following sensitization and stimulation. We hypothesize that CNCs will affiliate with teleost and mammalian cells *in vitro*, reducing their viability and interfereing with their ability to elicit appropriate effector responses.

6.2 MATERIALS AND METHODS

6.2.1 Synthesis and physico-chemical characterization of CNCs

Carboxylated CNC was produced from microcrystalline cellulose (MCC; Avicel PH 101) using the ammonium persulfate method described in Leung et al., (2011). MCC (10 g) was mixed with 1 M APS solution and heated to 60 °C for 16 h. CNCs were isolated by centrifugation (12 000 rpm for 10 min). The collected CNC pellet was washed with deionized water a total of 5 times, neutralized to pH 7 with sodium hydroxide and subsequently washed with deionized water, converting the carboxylic acid groups to carboxylate

form (Leung et al., 2011). CNCs were lyophilized to yield a white powder used in these studies.

A complete characterization of the CNCs used in this study was completed by Leung et al., (2011). Low voltage transmission electron microscopy (LVTEM) micrographs and height mode atomic force microscopy (AFM) micrographs (**Supplemental Figure S6-1**) confirmed the produced CNCs were uniform in size, with an average length (mean ± SD, n=100) of 128 ± 4 nm and an average diameter of (mean ± SD, n=2291) 5.5 ± 0.1 nm (Leung et al., 2011).

Hydrodynamic diameter and zeta potential of CNC suspensions in ddH_2O at a concentration of 50 mg L^{-1} and 200 mg L^{-1} were measured using dynamic light scattering (DLS; Zetasizerr, Malvern) in 173 ° backscatter mode. An average hydrodynamic diameter of (mean ± SEM, n=4) 1194 ± 782 nm and 998 ± 624 nm was measured for 50 mg L^{-1} and 200 mg L^{-1} CNC suspensions, respectively. The measured zeta potential (mean ± SEM, n=4) for 50 mg L^{-1} and 200 mg L^{-1} CNC suspensions was -12.3 ± 2 mV and -11.9 ± 1 mV, respectively. DLS measurements in cell culture media were not possible.

6.2.2 Cell culture and CNC exposures

The three channel catfish cell lines utilized in this study, 3B11, 1G8 and 28S.3, were grown at 27 °C and 5 % CO_2 in filter sterilized (0.22 µm filter; Corning) culture media (1:1 AIM-V:L-15 media (Gibco) supplemented with sodium bicarbonate (0.5 g; Sigma), penicillin (100 units mL^{-1}; Gibco),

streptomycin (100 μg mL^{-1}; Gibco) and 3% catfish serum). Cells were grown until confluence was reached before being passed (~ every 3-5 days).

RBL-2H3 cells were grown at 37 °C and 5 % CO_2 in filter sterilized (0.22 μm filter; Corning) culture media (Minimum essential media (MEM/EBSS; Hyclone) supplemented with L-glutamine (2mM; Gibco), penicillin (100 units mL^{-1}; Gibco), streptomycin (100 μg mL^{-1}; Gibco) and 10% heat inactivated fetal bovine serum (FBS; Hyclone). Cells were grown until confluence was reached (~ every 3-4 days) before being harvested using RBL harvest buffer (1.5 mM EDTA, 135 mM NaCl, 20 mM HEPES, 5 mM KCl, pH 7.4) to remove RBL-2H3 cells from the substrate. Cells were passed by seeding into fresh culture media and thereafter grown to confluence (37 °C and 5 % CO_2).

A stock solution of 1000 mg L^{-1} CNC was prepared by suspending 0.05 g of CNC in 50 mL of ddH_2O. CNC stock solution was vortexed for 30 seconds and subsequently sonicated for 30 seconds (Sonifer Cell Disruptor; Branson Ultrasonics) before completing serial dilutions in culture media to create CNC exposure solutions at final concentrations of 1, 10, 50, 100 and 200 mg L^{-1}.

6.2.3 Determining leukocyte viability following CNC exposure

To examine leukocyte viability following CNC exposure we utilized flow cytometric analysis of propidium iodide (PI) fluorescence, a marker for cell death. Dead, necrotic and apoptotic cells have compromised cellular

membranes, allowing cellular penetration of PI which exhibits enhanced fluorescence upon intercalation with nucleic acids (Brana et al., 2002).

To examine the effect of CNC exposure on leukocyte viability, channel catfish 3B11, 1G8 and 28S.3 cells were enumerated and seeded into round-bottom 96 well plates (Becton Dickinson) at a density of 20,000 cells per well before being exposed to 1, 10, 50, 100 or 200 mg L^{-1} CNC for 6, 12, 24 or 48 h at 27 °C and 5 % CO_2. Control treatments received ddH_2O (vehicle) or culture media (negative control). Following exposures, cells were stained with PI (100 µg mL^{-1}) and then underwent flow cytometric analysis (Quanta SC, Beckman Coulter). Using negative controls to establish all gates, whole cell populations for 3B11, 1G8, 28S.3 and RBL-2H3 were gated using forward scatter and side scatter metrics. To separate viable from non-viable cells, whole cell populations were analyzed for PI fluorescence using the FL2 filter. The percentage of viable cells in culture was determined by calculating the percentage of cells within the whole cell population gate that concurrently exhibited low levels of PI fluorescence.

To examine the effect of CNC exposure on RBL-2H3 viability, cells were enumerated and seeded into flat-bottom 96 well plates (Costar) at a density of 40,000 cells per well. Cells were incubated at 37 °C and 5 % CO_2 for 1 h to allow attachment to the substrate. Media was removed and cells were exposed to 1, 10, 50, 100 or 200 mg L^{-1} CNC for 6, 12, 24 or 48 h at 37 °C and 5 % CO_2. Control treatments were exposed to ddH_2O (vehicle) or culture media alone (negative control). Following exposure, cells were washed with

1x PBS and harvested using RBL harvest buffer. Harvested RBL-2H3 suspensions were stained with PI and analyzed by flow cytometric analysis as outlined above.

6.2.4 Examination of IgE-FcεRI-mediated degranulation in RBL-2H3 cells following CNC exposure

To asses degranulation following CNC exposure, we assayed the activity of β-hexosaminidase, one of several mediators released by RBL-2H3 cells through FcεRI-mediated degranulation (Huang et al., 2009). RBL-2H3 cells were enumerated and seeded into a flat-bottomed 96 well plate (Costar) at a density of 40,000 cells per well in cell culture media. Cells were incubated at 37 °C and 5 % CO_2 for 2 h to allow attachment to the substrate. The cell culture media was removed and cells were exposed to 1, 10, 50, 100 or 200 mg L^{-1} CNC for 6, 12, 24 or 48 h at 37 °C and 5 % CO_2. Vehicle control exposures were ddH_2O; negative and positive controls treatments were incubated with culture media alone. Following exposure, RBL-2H3 cells were activated to degranulate in a two-step process. The first step, termed sensitization, is accomplished when FcεRI binds IgE. IgE-FcεRI can then detect foreign antigens, and when IgE-FcεRI are crosslinked by antigen, it induces degranulation in a step termed stimulation. Incubation with 100 ng mL^{-1} of mouse anti-DNP IgE mAb (Sigma-Aldrich) in incomplete Tyrodes buffer (25 mM HEPES, 140 mM NaCl, 1.8 mM $CaCl_2$, 5.6 mM D-glucose, 12 mM $NaHCO_3$, 0.37 mM NaH_2PO_4 and $MgCl_2$, pH 7.4) for 1 h at 37 °C and 5 % CO_2

sensitized RBL-2H3 cells. Following sensitization, cells were washed with Tyrodes buffer supplemented with 0.1% bovine serum albumin (BSA; Sigma-Aldrich). Negative and positive controls received no wash step. Cells were stimulated to degranulate with the addition of DNP-HSA (0.05 μg mL^{-1} in 0.1% BSA/Tyrodes buffer) for 1 h at 37 °C and 5 % CO_2. Negative controls were exposed to 0.1% BSA/Tyrodes buffer alone for 1 h at 37 °C and 5 % CO_2; positive controls were exposed to calcium ionophore A23187 (0.625 μM in 0.1% BSA/Tyrodes buffer; Sigma-Aldrich) for 1 h at 37 °C and 5 % CO_2. Following stimulation, degranulation was assessed through the activity of released β-hexosaminidase using the β-hexosaminidase release assay as described previously (Cortes et al., 2012; Naal et al., 2004). Supernatant from each exposure was combined with β-hexosaminidase substrate buffer (2 mM 4-methylumbelliferyl N-acetyl-b-D-glucosaminide (Sigma-Aldrich), 100mM citrate, pH 4.5) for 30 min at 37 °C and 5 % CO_2. The addition of quench buffer (200 mM L-glycine, pH 10.7) halted β-hexosaminidase activity and sample fluorescence was measured with a microplate reader (360 nm excitation filter, 450 nm emission filter; WALLAC 1420, Perkin Elmer). Fluorescence, resulting from the cleavage of 4-methylumbelliferyl N-acetyl-b-D-glucosaminide by β-hexosaminidase, is indicative of the amount of β-hexosaminidase in solution and is used as a measure of the extent of RBL-2H3 degranulation. The relative fluorescent units for each CNC exposure was standardized to control treated cells and expressed as % control.

6.2.5 Statistical analysis

All statistical analysis were completed using GraphPad 6.0 statistical software with significance set at $p<0.05$. To examine the effect of CNC exposure on cell viability, a one-way Analysis of Variance (ANOVA) followed by a post-hoc Dunnett's test was performed. To examine the effect of CNC exposure on RBL-2H3 degranulation, a one-way ANOVA followed by post-hoc Dunnett's test was performed.

6.3 RESULTS

6.3.1 Effect of CNC exposure on catfish lymphocyte viability

3B11 cells exposed to 1, 10, 50, 100 or 200 mg L^{-1} CNCs did not have a significant reduction in cell viability (**Figure 6-1**). Flow cytometric analysis revealed that the number of viable cells in culture after CNC exposure for 6 h (**Figure 6-1A**), 12 h (**Figure 6-1B**), 24 h (**Figure 6-1C**) or 48 h (**Figure 6-1D**) remained unchanged compared to control treatments. Even after exposure to the highest concentration of CNC (200 mg L^{-1}) for the longest exposure period (48 h), (mean ± SEM, n=4) 79.9 ± 3% of cells remained viable in culture and this was not significantly different from control (88.8 ± 2.8%).

Channel catfish 1G8 cells did not have a significant reduction in viability at any concentration tested after 6 h exposure to CNC (**Figure 6-2A**). Following 12 h exposure, there was no significant change in the number of

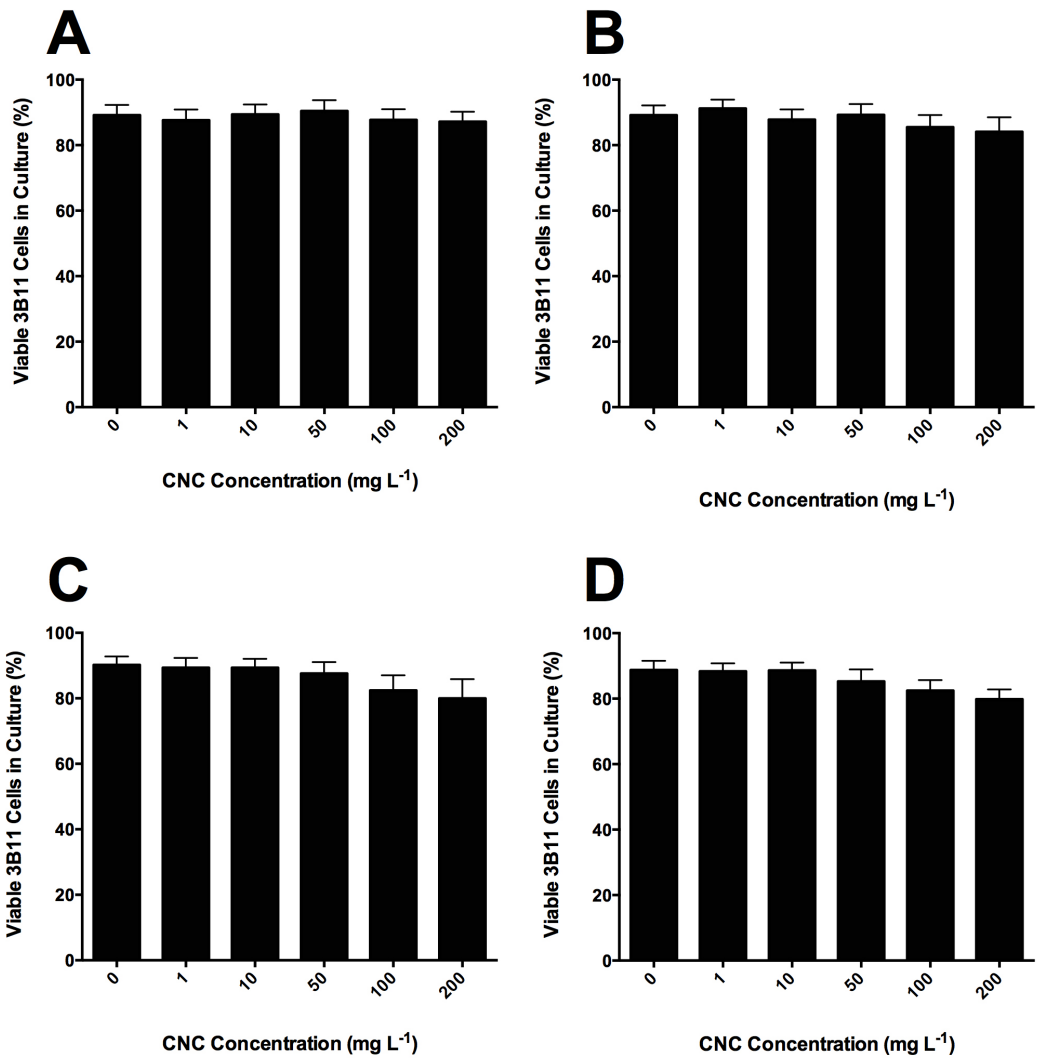

Figure 6-1. CNC exposure did not affect channel catfish 3B11 cell viability. 3B11 cells at a density of 20,000 cells per well were exposed to 1, 10, 50, 100 or 200 mg L^{-1} CNC for 6 (A), 12 (B), 24 (C) or 48 h (D). Cells were stained with propidium iodide (100 µg mL^{-1}) and analyzed using flow cytometric analysis. Data were analyzed by one-way ANOVA with a Dunnett's post hoc test ($p<0.05$). Mean ± SEM shown, n=4.

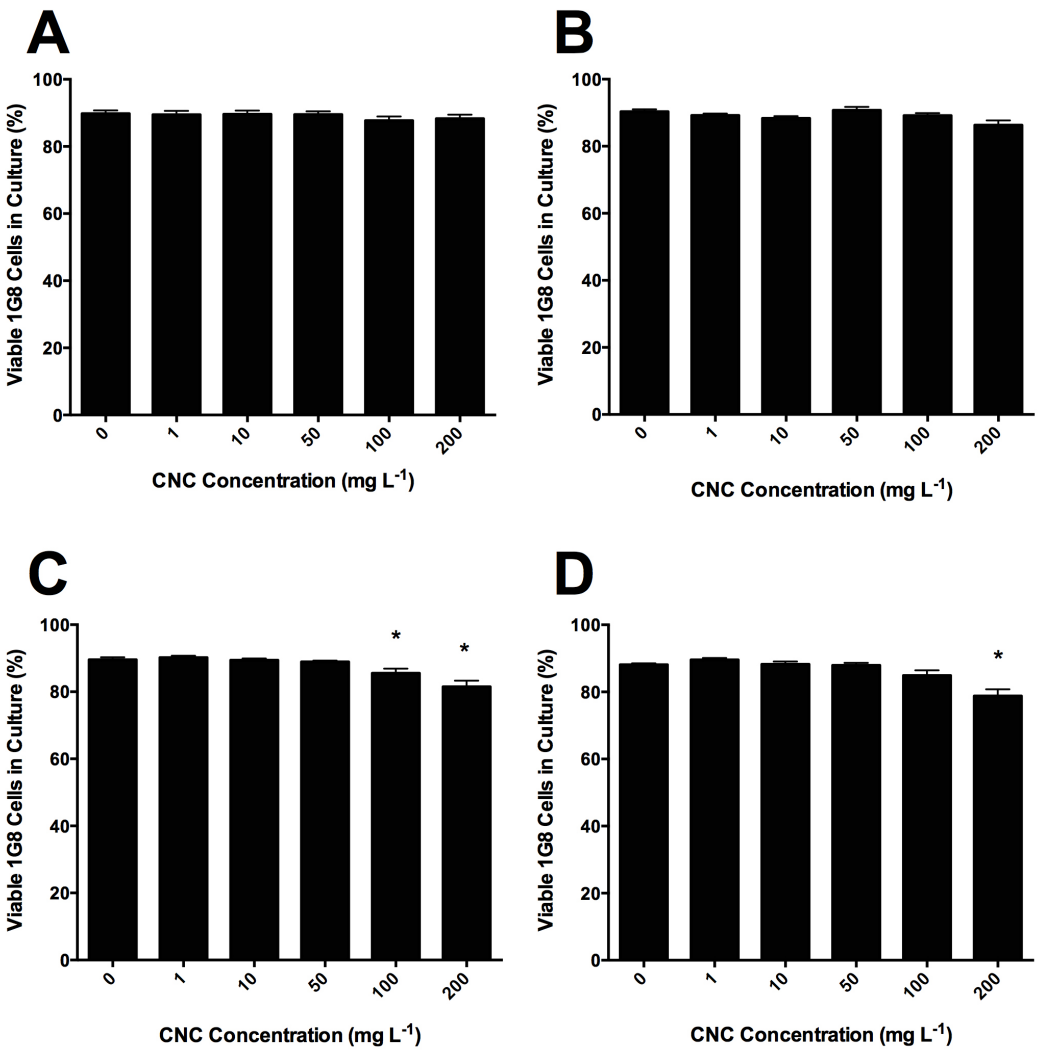

Figure 6-2. CNC exposure affected channel catfish 1G8 cell viability at the highest doses examined. 1G8 cells at a density of 20,000 cells per well were exposed to 1, 10, 50, 100 or 200 mg L^{-1} CNC for 6 (A), 12 (B), 24 (C) or 48 h (D). Cell viability was determined using propidium iodide (100 µg mL^{-1}) staining and flow cytometric analysis. Data were analyzed by one-way ANOVA with a Dunnett's post hoc test ($p<0.05$). Asterisk denotes significant difference between CNC exposure and control treatment. Mean ± SEM shown, n=4.

viable cells in culture following exposure to 1, 10, 50 or 100 mg L^{-1}; however, exposure to 200 mg L^{-1} CNC caused the percentage of viable 1G8 cells in culture to fall to 86.3 ± 2%, a value significantly different from control treated cells (90.4 ± 1%) (**Figure 6-2B**). After 24 h of CNC exposure, significant declines in 1G8 viability was found at concentrations of 100 and 200 mg L^{-1} (**Figure 6-2C**); while 48 h of CNC exposure significantly reduced 1G8 viability following 200 mg L^{-1} exposure (**Figure 6-2D**).

The last channel catfish leukocyte examined, 28S.3, had small changes in viability at the highest dose and longest exposure of CNC (**Figure 6-3**). Flow cytometric analysis found no significant change in the number of viable 28S.3 cells in culture following 6 h (**Figure 6-3A**), 12 h (**Figure 6-3B**) or 24 h (**Figure 6-3C**) exposure to 1, 10, 50, 100 or 200 mg L^{-1} CNC. There was a significant decline in the percentage of viable 28S.3 cells in culture following 48 h exposure to 200 mg L^{-1} CNC (**Figure 6-3D**).

6.3.2 Effect of CNC exposure on RBL-2H3 viability and function

RBL-2H3 cells did not have a significant change in viability following CNC exposure. Following 6 (**Figure 6-4A**), 12 (**Figure 6-4B**), 24 (**Figure 6-4C**) or 48 h (**Figure 6-4D**) exposure to 1, 10, 50, 100 or 200 mg L^{-1} CNC there was no significant change in the number of viable RBL-2H3 cells in culture.

With no significant change in RBL-2H3 viability following CNC exposure, we examined the ability of these cells to degranulate following sub lethal CNC exposure for 6, 12, 24 or 48 h. Our positive control, exposure to

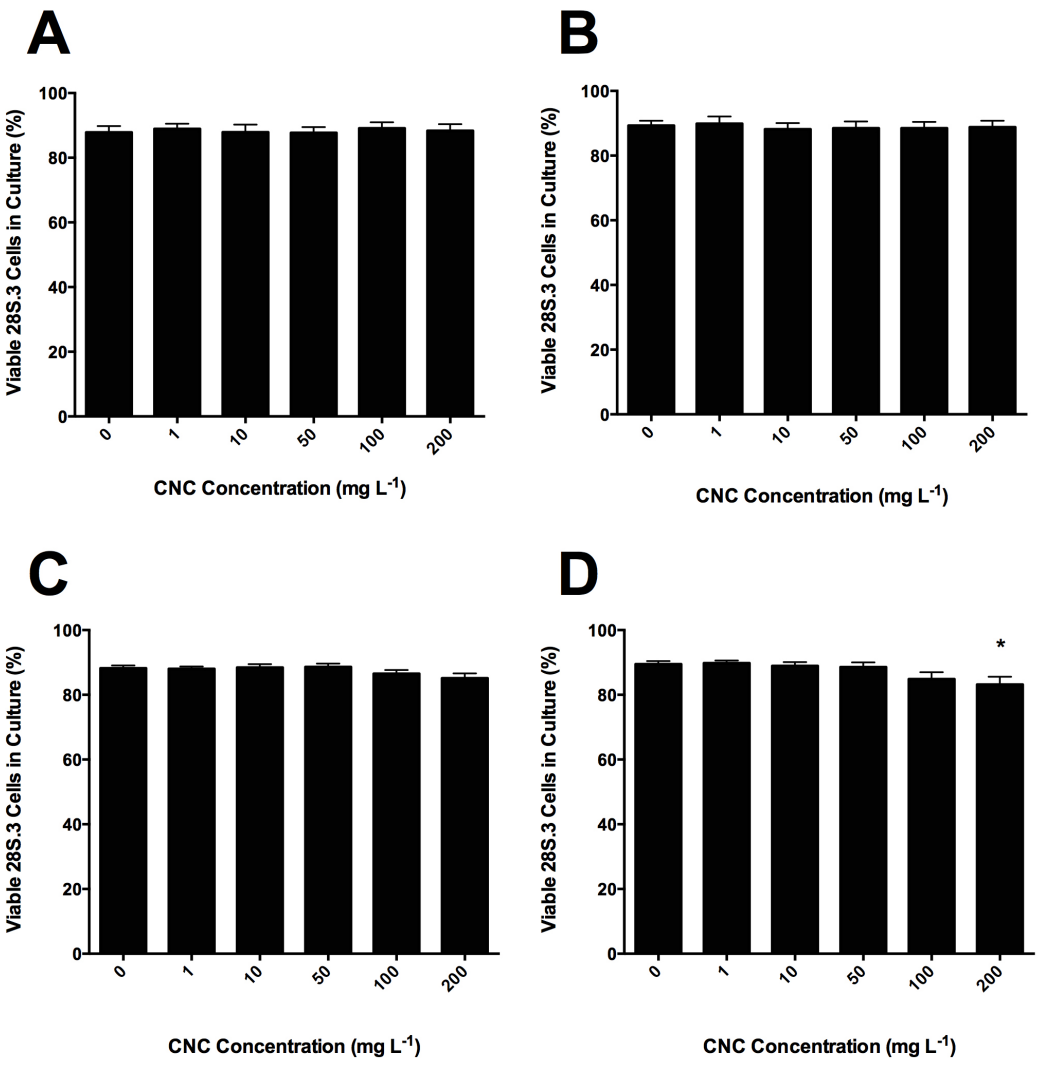

Figure 6-3. CNC exposure affected channel catfish 28S.3 cell viability at the highest dose examined. 28S.3 cells at a density of 20,000 cells per well were exposed to 1, 10, 50,100 or 200 mg L^{-1} CNC for 6 (A), 12 (B), 24 (C) or 48 h (D). Flow cytometric analysis was used to measure propidium iodide (100 µg mL^{-1}) staining to determine cell viability. Data were analyzed by one-way ANOVA with a Dunnett's post hoc test ($p<0.05$). Asterisk denotes significant difference between CNC exposure and control treatment. Mean ± SEM shown, n=4.

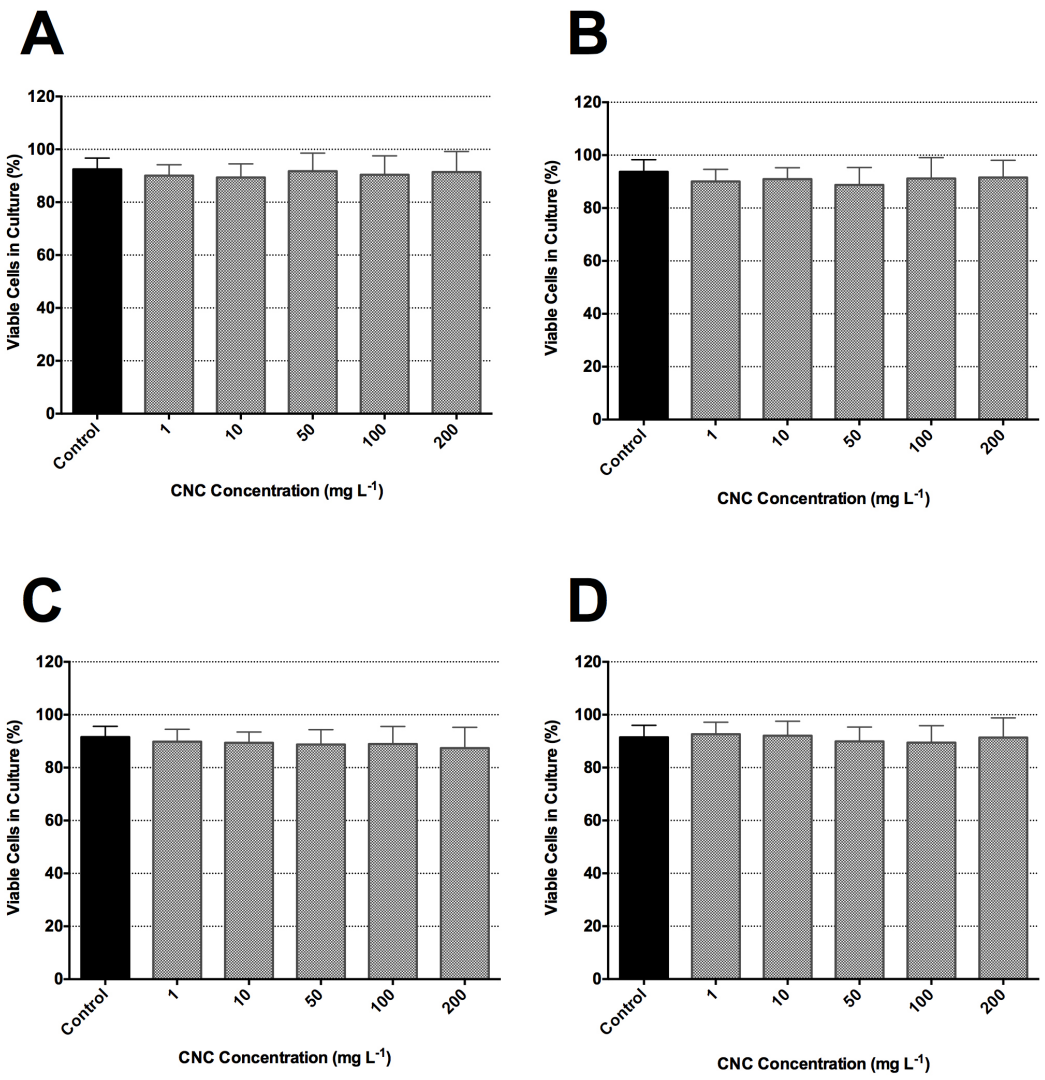

Figure 6-4. There was no change in RBL-2H3 viability following CNC exposure. RBL-2H3 cells at a density of 40,000 cells per well were exposed to 1, 10, 50, 100 or 200 mg L^{-1} CNC for 6 (A), 12 (B), 24 (C) or 48 h. Cells stained with propidium iodide (100 µg mL^{-1}) and analyzed by flow cytometry revealed no significant change in viability. Data were analyzed by one-way ANOVA with a Dunnett's post hoc test ($p<0.05$). Mean ± SEM shown, n=4.

calcium ionophore, caused a significantly increased degranulatory response compared to control, ranging from 422.2 ± 83 to 481.3 ± 89 % control. RBL-2H3 cells that were not sensitized or stimulated, the negative control treatment, had a significantly reduced degranulatory response compared to control, ranging from 22.5 ± 3 to 27.5 ± 4 % control. When RBL-2H3 cells were exposed to CNC for 6 (**Figure 6-5A**), 12 (**Figure 6-5B**), 24 (**Figure 6-5C**) or 48 h (**Figure 6-5D**) and subsequently sensitized and stimulated, there was no significant change in IgE-FcεRI-mediated degranulation compared to control. The largest reduction in FcεRI-mediated degranulation occurred after 48 h exposure to 200 mg L^{-1} CNC, declining to 91.4 ± 18 % compared to control.

6.4 DISCUSSION

This study is the first to examine the effect of CNC exposure on fish lymphocytes. CNC exposures as high as 50 mg L^{-1} did not caused any significant declines in 3B11, 1G8 (B-cell-like) or 28S.3 (T-cell-like) lymphocyte viability at any time points examined; however, declines in viability were noted at 200 mg L^{-1} CNC exposures in both 1G8 and 28S.3 cell lines. Examination of CNC exposure on a mammalian granulocyte, RBL-2H3, revealed no change in viability at exposure concentrations up to 200 mg L^{-1}. In addition, FcεRI-mediated degranulation in RBL-2H3 was unaffected by CNC exposure.

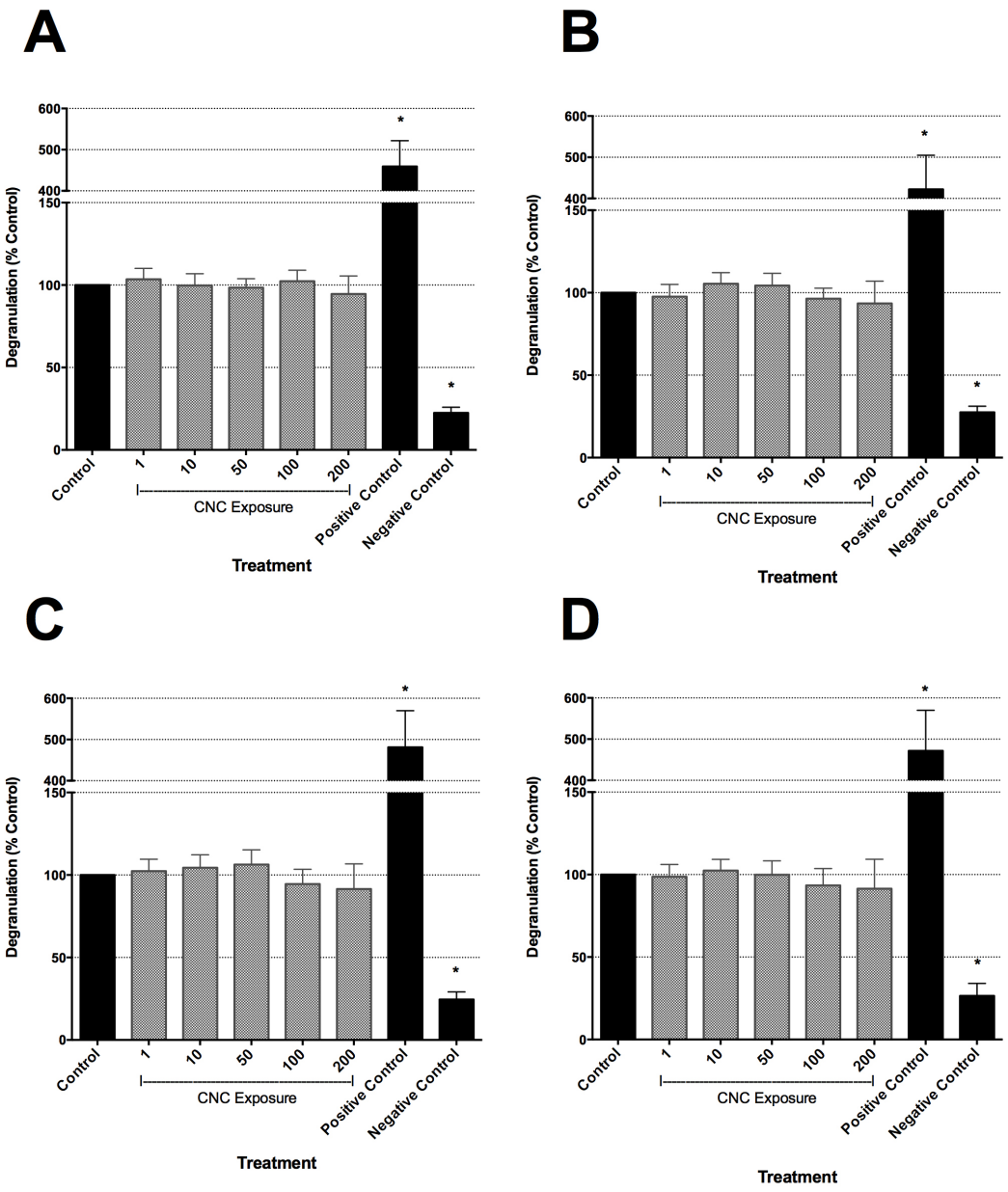
A
B
C
D
Degranulation (% Control)
600
500
400
150
100
50
0
*
Control
1
10
50
100
200
CNC Exposure
Positive Control
Negative Control
Treatment

Figure 6-5. Sub-lethal CNC exposure did not affect IgE-FcεRI-mediated degranulation in RBL-2H3 cells. RBL-2H3 cells were seeded at a density of 40,000 cells per well and exposed to 1, 10, 50, 100 or 200 mg L^{-1} CNC for 6 (A), 12 (B), 24 (C) or 48 h. Cells were sensitized with IgE (100 ng mL^{-1}) and stimulated to degranulate with DNP-HSA (0.05 µg mL^{-1}). Positive controls were exposed to calcium ionophore A23187 (0.625 µM); negative control treatments were not sensitized or stimulated to degranulate. Supernatant was collected and assayed for β-hexosaminidase activity. The relative fluorescent units for each CNC exposure was standardized to control treated cells and expressed as the change in degranulation compared to control (% control). Data were analyzed by one-way ANOVA with a Dunnett's post hoc test ($p<0.05$). Asterisk denotes significant difference between treatment and control. Mean ± SEM shown, n=4.

One of the few studies to examine the cytotoxicity of CNCs in fish also reported one of largest declines in cellular viability following exposure (Roman, 2015). Rainbow trout hepatocytes exposed to CNC had a 20% decline in viability at estimated CNC exposure concentrations of 34 mg L^{-1} (Kovacs et al., 2010). In contrast, we noted only small declines catfish lymphocyte viability following CNC exposure. For example, after 48 h exposure to 200 mg L^{-1} CNC, 1G8 viability declined by 10.5%. Thus, this study adds to several reports suggesting minimal cytotoxicity of CNCs *in vitro.* While no other studies have examined CNC cytotoxicity in fish, several other cell models have been utilized. No significant cytotoxicity was found in human brain microvascular endothelial cells exposed to CNCs for 24 to 72 h (Roman, 2015). In agreement, Zoppe et al., (2014) found that over 90% of human corneal epithelial cells remained viable following exposure to 1000 mg L^{-1} CNC and Villanova et al., (2011) found no significant effect of 10 000 mg L^{-1} CNC exposure on human gingival fibroblasts (Villanova et al., 2011; Zoppe et al., 2014). Interestingly, Mahmoud et al., (2010) demonstrated that CNC functionalization affects cytotoxicity. CNCs were functionalized with once of two fluorophores, rhodamine B isothicyanate (RBITC) resulting in a positively charged CNC (RBTIC-CNC; zeta potential: +8.7 mV) or fluorescein isothiocyanate (FITC) resulting in a negatively charged CNC (FITC-CNC; zeta potential: -46.4 mV). Using the trypan blue assay, they documented a significant decline in *Spodoptera frugiperda* (Sf)-9 and human embryonic kidney (HEK)-293 cells following a 12 h exposure to negatively charged FITC-

CNC, while no significant decline was found for positively charged RBTIC-CNC (Mahmoud et al., 2010). The CNCs utilized in this study were carboxy-functionalized and had an overall negative charge (-11.9 mV), if surface charge is a major determinate of CNC toxicity, this suggests that the limited cytotoxicity we observed in fish lymphocytes following CNC exposure could be ameliorated with the introduction of a positively charged functionalization.

In addition to a paucity of data examining the cytotoxicity of CNCs in immune cells, few studies have examined the effect of CNC exposure on immune function. One of the few studies conducted by Clift et al., (2011) examined the effect of CNC exposure to a human lung cell co-culture of human monocyte derived macrophages (MDM), human monocyte derived dendritic cells (MDDC) and a human bronchial epithelial cell line (16HBE14o). They report significant cytotoxicity at CNC exposure concentrations of 15 mg L^{-1} and the release of the proinflammatory chemokine interleukin (IL)-8 at CNC exposure concentrations of 30 mg L^{-1} (Clift et al., 2011). In contrast, we found no significant declines in the viability of the granulocyte RBL-2H3 at exposure concentrations up to 200 mg L^{-1}. We also did not observe any significant change in the effector function of this granulocyte following CNC exposure. RBL-2H3 FcεRI-mediated degranulation remained unchanged compared to control following CNC exposure.

While most studies suggest limited cytotoxicity of CNCs, more data is needed as only a handful of studies have been completed (Roman, 2015). To facilitate cross study comparisons of CNC cytotoxicity, details on how cellulose source material, CNCs production procedures and post-production modifications change CNC physicochemical properties such as particle dimension and surface functionality need to be reported (Roman, 2015). In addition, special consideration of CNC cytotoxicity has been highlighted due to their acidic nature owing to acid hydrolysis during production; significant declines in culture media pH upon CNC addition could significantly affect cell viability (Roman, 2015). The CNCs used in this study were treated with sodium hydroxide post-production to yield a sodium salt form with minimal effects on pH upon introduction in aqueous suspensions.

6.5 CONCLUSIONS

CNC exposure to catfish lymphocytes did not cause any significant reductions in viability at exposure concentrations as high as 50 mg L^{-1} for any time point examined; however reductions in viability were noted for some cell lines at higher exposure concentrations. Examination of CNC exposure on a mammalian granulocyte, RBL-2H3, revealed no change in viability at exposure concentrations up to 200 mg L^{-1} for any time point examined. An evaluation of IgE- FcεRI-mediated degranulation in RBL-2H3 cells revealed no change in the degranulatory response following CNC exposure. Together,

this data suggests CNC exposure has minimal effects on teleost and mammalian leukocyte viability and function.

CHAPTER 7

Conclusions and Future Directions

7.1 GENERAL CONCLUSIONS

My doctoral thesis examined the immunomodulatory potential of high aspect ratio nanomaterials (HARNs) utilizing *in vitro* mammalian and teleost models. Immunological endpoints have been highlighted in nanotoxicology for their applicability to both accidental exposure to NMs (e.g. environmental) since many cells of the immune system exist at the interface between the body and environment, and therapeutic exposure to NMs (e.g. targeted drug delivery, vaccinations) since the immunomodulatory potential of these materials has significant impacts on their biocompatibility and use as therapeutics (Remes and Williams, 1992). The experiments presented here focused on addressing the four main goals of my thesis set out in the introduction: (1) to develop and optimize a suite of techniques to assess the immunotoxicity of HARNs; (2) to determine the toxicity of carbon nanotube (CNT), helical rosette nanotube (RNT) and cellulose nanocrystal (CNC) exposure on several immune cell lines and elucidate the mechanism of any observed toxicity; (3) to determine if exposure to these HARNs can affect the ability of immune cells to elicit effector responses and elucidate the mechanisms of interference; and (4) to examine if differential functionalization of HARNs impacts their immunotoxicity *in vitro*.

The architecture of HARNs was highlighted for their potential toxicity based on the fiber toxicology paradigm (Donaldson et al., 2006) and several initial reports of asbestos-like toxicity of CNTs emphasized these concerns (Poland et al., 2008). However, the data presented in this thesis contributes

to a growing body of evidence that HARNs are not necessarily associated with high levels of toxicity. Nevertheless, I did observe differential toxicity of all three HARNs investigated and differential toxicity of each material based on surface functionalization. While a high aspect ratio may contribute to the toxicity of some NMs, it is not an essential determinate and several other physico-chemical characteristics contribute to modifying toxicity. To synthesize the data from each Chapter and to facilitate comparisons, I have highlighted my results in three comparative Tables (**Table 7-1, 7-2 and 7-3**).

In Chapters 4, 5 and 6 I investigated the effects of RNT, CNT and CNC exposure on rat basophilic leukemia (RBL)-2H3 cells. While all of these materials exhibit a high aspect ratio (length:diameter greater than 20:1; **Table 7-1**) my investigation of RBL-2H3 cytotoxicity in Chapter 6 found that CNC exposure had the lowest levels of measured toxicity while Chapters 4 and 5 found relatively higher levels of toxicity in RBL-2H3 cells exposed to RNTs and CNTs (**Table 7-2**). However, the declines in RBL-2H3 viability occurred at concentrations of NMs that are above those anticipated for either environmental (Gottschalk et al., 2009) or therapeutic applications (Fadel and Fahmy, 2014) and suggests these materials are relatively biocompatible. In addition, in my investigation of differentially functionalized RNTs in Chapter 2 (**Table 7-3**) and differentially functionalized CNTs in Chapter 5, I observed significant differences in the toxicity of the each material based on surface functionalization. Together, this suggests HARNs do not always exhibit high levels of cytotoxicity and that differences in other physico-

Table 7-1. Physico-chemical characteristics of high aspect ratio nanomaterials showing diameter, hydrodynamic radius, zeta potential and dispersion.

	Rosette Nanotube				Carbon Nanotube				Cellulose Nanocrystal
Functionalization	K	TBL	RGDSK	FITC	U	Carboxy			Carboxy
						30	40	50	
NM Physico-chemical Characterization									
Diameter[1]	3.5 nm				1.5 nm				5.5 nm
Hydrodynamic Radius[2]	300 nm	358 nm	384 nm	312 nm	ND	6719 nm	4382 nm	3248 nm	1194 nm
ζ-potential[3]	+72 mV	+55 mV	+54 mV	+17 mV	ND	-15 mV	-15 mV	-15 mV	-12 mV
Dispersed	Yes	Yes	Yes	Yes	No	Yes	Yes	Yes	Yes

Footnotes: [1]Reported diameter as determined by transmission electron micrographs [2] Hydrodynamic radius measured with dynamic light scattering at a concentration of 5 mg L^{-1}(RNTs) 10 mg L^{-1} (CNTs) or 50 mg L^{-1} (CNC) [3]Reported zeta-potential at concentrations of 5 mg L^{-1}(RNTs) 10 mg L^{-1} (CNTs) or 50 mg L^{-1} (CNC)

Abbreviations: (K) lysine, (TBL) butylamine, (RGDSK) Arg-Gly-Asp-Ser-Lys peptide, (FITC) fluorescein isothiocyanante, (U) unfunctionalized, (Carboxy) carboxylic acid functionalized, (30) oxidized at 30 °C, (40) oxidized at 40 °C, (50) oxidized at 50 °C

Table 7-2. Comparison of rosette nanotube, carbon nanotube and cellulose nanocrystal exposure on rat basophilic leukemia (RBL)-2H3 viability and IgE-FcεRI-mediated degranulation.

	Rosette Nanotube	Carbon Nanotube				Cellulose Nanocrystal
Functionalization	K	U	Carboxy			Carboxy
			30	40	50	
Rat Basophilic Leukemia (RBL)-2H3 Viability						
Decreased Viability[1]	Yes	Yes				No
Lowest Dose for Observed Effect[2]	100 mg L^{-1}	250 mg L^{-1}	50 mg L^{-1}	50 mg L^{-1}	50 mg L^{-1}	NE
Functionalization-dependent[3]	ND	Yes				ND
IgE-FcεRI-mediated Degranulation						
Decreased Viability[4]	200 mg L^{-1}	No	No	No	No	No
IgE-FcεRI-mediated Degranulation[5]	↑	↓				NE
Lowest Dose for Observed Effect[6]	50 mg L^{-1}	50 mg L^{-1}	250 mg L^{-1}	250 mg L^{-1}	250 mg L^{-1}	NE
Functionalization-dependent[7]	ND	Yes				ND

Footnotes: [1]Significant changes in viability following 24 h of NM exposure [2]Lowest tested concentration of NM that significantly reduced viability [3]Significantly different changes in viability between different functionalizations [4]Significant changes in RBL-2H3 viability during degranulation assay [5]Increased or decreased IgE-FcεRI-mediated degranulatory response following NM exposure [6]Lowest tested concentration of NM that significantly altered IgE-FcεRI-mediated degranulation [7]Significantly different changes in IgE-FcεRI-mediated degranulation between different functionalizations

Abbreviations: (K) lysine, (U) unfunctionalized, (Carboxy) carboxylic acid functionalized, (30) oxidized at 30 °C, (40) oxidized at 40 °C, (50) oxidized at 50 °C, (↑) increased IgE-FcεRI-mediated degranulation, (↓) decreased IgE-FcεRI-mediated degranulation, (NE) no effect, (ND) not determined

Table 7-3. Comparison of rosette nanotube, carbon nanotube and cellulose nanocrystal exposure on channel catfish leukocyte viability and IpLITR-mediated phagocytosis.

	Rosette Nanotube				Carbon Nanotube				Cellulose Nanocrystal
Functionalization	K	TBL	RGDSK	FITC	U	Carboxy			Carboxy
						30	40	50	
Channel Catfish Leukocyte Viability									
3B11 Cell Line									
Decreased Viability[1]	Yes	Yes	Yes	ND	Yes	Yes	Yes	Yes	No
Lowest Dose for Observed Effect[2]	1 mg L^{-1}	5 mg L^{-1}	1 mg L^{-1}	ND	10 mg L^{-1}	10 mg L^{-1}	10 mg L^{-1}	10 mg L^{-1}	NE
Functionalization-dependent[3]	Yes				No				ND
1G8 Cell Line									
Decreased Viability[1]	Yes	Yes	Yes	ND	Yes	Yes	Yes	Yes	Yes
Lowest Dose for Observed Effect[2]	1 mg L^{-1}	5 mg L^{-1}	1 mg L^{-1}	ND	10 mg L^{-1}	10 mg L^{-1}	10 mg L^{-1}	10 mg L^{-1}	100 mg L^{-1}
Functionalization-dependent[3]	Yes				No				ND
28S.3 Cell Line									
Decreased Viability[1]	Yes	Yes	Yes	ND	Yes	Yes	Yes	Yes	No
Lowest Dose for Observed Effect[2]	1 mg L^{-1}	5 mg L^{-1}	1 mg L^{-1}	ND	25 mg L^{-1}	10 mg L^{-1}	25 mg L^{-1}	25 mg L^{-1}	NE
Functionalization-dependent[3]	Yes				No				ND
IpLITR-mediated Phagocytosis									
Decreased Viability[4]	15 mg L^{-1}	25 mg L^{-1}	25mg L^{-1}	ND	No	No	No	No	ND
IpLITR-mediated phagocytosis[5]		↓				↓			ND
Lowest Dose for Observed Effect[6]	10 mg L^{-1}	20 mg L^{-1}	20 mg L^{-1}	ND	25 mg L^{-1}	25 mg L^{-1}	25 mg L^{-1}	25 mg L^{-1}	ND

Footnotes: [1]Significant changes in viability following 24 h of NM exposure [2]Lowest tested concentration of NM that significantly reduced viability [3]Significantly different changes in viability between different functionalizations [4]Significant changes in viability during phagocytosis assay [5]Increased or decreased IpLITR-mediated phagocytic response following NM exposure [6]Lowest tested concentration of NM that significantly altered IpLITR-mediated phagocytosis
Abbreviations: (K) lysine, (TBL) butylamine, (RGDSK) Arg-Gly-Asp-Ser-Lys peptide, (FITC) fluorescein isothiocyanante, (U) unfunctionalized, (Carboxy) carboxylic acid functionalized, (30) oxidized at 30 °C, (40) oxidized at 40 °C, (50) oxidized at 50 °C, (↑) increased IpLITR-mediated phagocytosis (↓) decreased IpLITR-mediated phagocytosis (NE) no effect (ND) not determined

chemical characteristics between these materials including charge, core composition, dispersability and functionalization (**Table 7-1**) alter their toxicity *in vitro*.

The modification of immune cell effector responses by HARNs has been highlighted as an important endpoint to consider for both inadvertent environmental exposures (Fadeel, 2012) and therapeutic applications (Fadel and Fahmy, 2014). The work presented in this thesis has demonstrated that several HARNs interfere with receptor-mediated immune effector responses *in vitro* at sub-lethal levels of exposure and these effects differ between the types of HARNs and their functionalization. In Chapter 2 and Chapter 3 I demonstrated that RNT and CNT exposure significantly reduced IpLITR-mediated phagocytosis (**Table 7-3**) and this adds to a growing body of literature suggesting that phagocytosis is altered by exposure to certain NMs (Witasp et al., 2009). I also found significant differential modification of IgE-FcεRI-mediated degranulation following HARN exposure. Sub-lethal exposure to RNTs enhanced (Chapter 4) while CNT exposure reduced (Chapter 5) IgE-FcεRI-mediated degranulation. Exposure to CNCs did not alter IgE-FcεRI-mediated degranulation in RBL-2H3 cells (Chapter 6) (**Table 7-2**). In addition, the inhibition of IgE-FcεRI-mediated degranulation by CNTs was functionalization-dependent. Such differential responses of HARNs highlights that physico-chemical parameters other than aspect ratio are important in determining immunomodulatory effects *in vitro* and include differences in dispersion, surface charge, core composition, and

functionalization (**Table 7-1**). In addition, I propose one mechanism for the modification of receptor-mediated immune effector responses by HARN exposure, suggesting that the presence of NMs can interfere with receptor binding and activation. For example, in Chapter 5 I show that the decrease in IgE-FcεRI-mediated degranulation following CNT exposure likely results from preventing FcεRI activation, either by preventing IgE binding its cognate receptor FcεRI or preventing subsequent cross-linking of IgE-FcεRI complex by it's antigen. This mechanism of HARN interference is supported by confocal data showing a high degree of CNT affiliation with the cellular membrane, a concomitant reduction in the activation of p44/p42 MAPK pathway, a known downstream signaling intermediate of IgE-FcεRI activation, and an immediate recovery of both degranulation and activation of p44/p42 MAPK pathway following removal of CNT during sensitization and stimulation (Chapter 5).

The work presented here was one of the first to examine the effect of NM exposure on fish lymphoid cells (i.e. B-cells and T-cells), an area highlighted as lacking in current evaluations of NM toxicity in fish (Jovanović and Palić, 2012). Exposure of channel catfish lymphocytes to RNTs (Chapter 2) and CNTs (Chapter 3) resulted in significant declines in viability at concentrations that were an order of magnitude lower than mammalian models (**Table 7-3**). In addition, the channel catfish lymphocytes examined were differentially susceptible to both RNT and CNT exposure, with B-cell-like lines (3B11 and 1G8) exhibiting higher cytotoxicity compared to the T-

cell-like line (28S.3)(**Table 7-3**) following RNT and CNT exposure. This suggests that channel catfish may be a particularly sensitive model for examining NM toxicity. This differential toxicity could be due to a variety of variables including differences in media composition, temperature, metabolic rate, membrane lipid composition and state of adherence. It should be noted that the teleost leukocytes examined in these studies are non-adherent cell lines and remain suspended in culture throughout the exposure protocols utilized here. In contrast, the mammalian cell lines tested are adherent and remain attached to a substrate through the NM exposures. These differences in state of adherence results in the teleost leukocytes having a much higher suface area for exposure compared to the mammalian cell lines and may partially account for the differences in toxicity we observed.

Molecular and biochemical characterization of *Ictalurus punctatus* Immune Type Receptors (IpLITRs), provides a model to examine the effect of NM exposure on teleost receptor-mediated effector responses such as degranulation and phagocytosis (Cortes et al., 2014; 2012) I present data in Chapter 2 and 3 showing the inhibition if IpLITR-mediated phagocytosis following sublethal exposure to both RNTs and CNTs. Together, the availability of several *in vitro* leukocyte cell lines and the use of IpLITR as a model to examine sub-lethal effects of NM exposure on immune cell effector function, makes channel catfish an excellent model for future aquatic nanotoxicty testing investigating the immunomodulatory potential of NMs.

7.2 FUTURE DIRECTIONS

While my thesis provided novel information on the interaction of HARNs with immune cells resulting in differential modulation of effector responses, there is still substantial research that needs to be completed to contribute to our understanding of the immunomodulatory potential of HARNs. Below I list a number of key future directions that need to be addressed.

What is the mechanism(s) of toxicity for CNTs, RNTs and CNCs?

The work presented here has shown that three HARNs have differential toxicity *in vitro*. Furthermore, altering the functionalization of each material can change its toxicity. An initial survey of 10 broad toxicity-related signaling pathways in Chapter 4 did not reveal any potential candidates for RNT toxicity; however it is possible that the incorrect time periods or concentrations were examined. Several mechanisms have been proposed for HARN toxicity, and based on the observed differential declines in viability, may be unique for different materials and functionalizations. Frustrated phagocytosis (Murphy et al., 2012), lysosomal membrane destabilization (Tahara et al., 2012) and release of contaminants (Pulskamp et al., 2007), all associated with oxidative stress (Pacurari et al., 2008) have been proposed as mechanisms for CNT cytotoxicity. In addition, indirect mechanisms of toxicity of CNTs have also been proposed, such as nutrient depletion (Guo et al., 2008). Exploration of these mechanisms would

contribute to our understanding of the immunomodulatory potential of HARNs, allowing for the design of tailored NMs with minimal cellular interactions (in the case of environmental exposure) or for therapeutic applications.

Complete characterization of materials is still a major limitation in nanotoxicological assessments, and we were unable to fully characterize RNTs, CNTs and NCCs in the complex media used for cell viability studies based on limitations of the available techniques (Balog et al., 2015; Boluk and Danumah, 2014). As techniques become available, complete characterization over time and in complex media will help to further correlate physico-chemical characteristics with biological interactions. For example, a recent study has shown that one of the limitations in characterizing HARNs in complex media can be overcome with depolarized dynamic light scattering (DDLS), allowing suppression of background signals in multicomponent and optically complex media (Balog et al., 2015).

What is the pathway(s) for cellular internalization of these materials?

Confocal imaging of RNTs in Chapter 4 confirmed their cellular internalization; however future work also needs to examine if the CNTs and CNCs used in these studies are also internalized. In addition, an evaluation of the mechanism of internalization would contribute to our understanding of the interaction of HARNs with cells. The cellular uptake of NMs can occur through phagocytosis or one of the three main endocytic pathways, namely

clathrin-mediated endocytosis, caveolae-mediated endocytosis and macropinocytosis (Kafshgari et al., 2015). An improved understanding of the mechanism of uptake of these materials would help in optimizing them for several of their therapeutic applications or in designing them for minimal interactions with cells. Different classes of NMs and differential surface functionalizations have also been shown to affect the rate and/or mechanism of cellular uptake (Gratton et al., 2008; Rejman et al., 2004) and RNTs may be particularity well suited to investigate the effect of changing NM physico-chemical properties on the mechanism of internalization given that they are easily tailored with a variety of covalently bound functional groups. It also remains to be determined if internalization of these materials may be contributing to the modulation of immune cell effector function we observe *in vitro*.

What is the nature of the interaction of HARNs with membrane bound receptors?

We have shown that HARNs can impact receptor-mediated effector functions such as degranulation and phagocytosis and confocal microscopy experiments confirmed the interaction of these materials with the cellular membrane. However, the exact nature of this interaction and its effects on receptor mediated effector responses remains to be determined. For example, in Chapter 5 we propose that the reduced degranulatory response in RBL-2H3 cells following CNT exposure results from reduced activation of FcεRI. However, the exact nature of this interference remains to be

determined. CNT exposure could prevent FcεRI-mediated degranulation by preventing IgE from binding FcεRI during sensitization. CNTs have been shown to associate with a variety of soluble proteins in solution, including immunoglobulins (Lundqvist et al., 2008). Alternatively, CNT exposure could reduce IgE-FcεRI-mediated degranulation by preventing the cross-linking of IgE-FcεRI complex by its antigen during stimulation. Of course, CNT exposure could also be reducing IgE-FcεRI-mediated degranulation through a combination of both mechanisms and a more thorough understanding would contribute to our knowledge on the immunomodulatory potential of NMs, especially for receptor mediated effector responses.

7.3 SUMMARY

The field of nanotoxicology has progressed rapidly over the course of my PhD. When I started, reports of asbestos-like toxicity of CNTs suggested HARNs may be particularly toxic based on their architecture. The work presented here adds to reports that HARN toxicity is not as straight forward as knowing the architecture of the material. A high aspect ratio is not necessarily associated with high levels of toxicity in NMs. The unique properties of NMs made early nanotoxicological assessment difficult and over time, scientists have recognized the importance of NM characterization in the evaluation of their toxicity. Given the array of new NMs being produced and the diversity of their intended applications, classical endpoints in toxicity may not be possible or applicable for every new NM. Current toxicological evaluations of NMs has moved towards linking physico-chemical traits of

NMs to their toxicity. However, even this has proven a challenge. Many of these parameters are interdependent and characterization of NMs in complex media has proven difficult with current methods. Despite these challenges, significant advances have been made in understanding the toxicity of NMs. Given the continued use of NMs for a variety of applications, nanotoxicologists must continue to understand how these materials interact with biological matrices to support the continued development of novel nanomaterials.

LITERATURE CITED

Aam, B.B., Fonnum, F., 2007. Carbon black particles increase reactive oxygen species formation in rat alveolar macrophages in vitro. Arch Toxicol 81, 441–446.

Abraham, S.N., John, A.L., 2010. Mast cell-orchestrated immunity to pathogens. Nat. Rev. Immunol. 10.

Akhlaghi, S.P., Berry, R.C., Tam, K.C., 2013. Surface modification of cellulose nanocrystal with chitosan oligosaccharide for drug delivery applications. Cellulose 20, 1747–1764.

Alam, A., Sachar, S., Puri, N., Saxena, R.K., 2013. Interactions of polydispersed single-walled carbon nanotubes with T cells resulting in downregulation of allogeneic CTL responses in vitro and in vivo. Nanotoxicology 7, 1351–1360.

Alsbaiee, A., St Jules, M., Beingessner, R.L., Fenniri, H., 2011. Towards radiolabeled GΛC module for cellular imaging of bioactive rosette nanotubes. Mater. Res. Soc. Symp. Proc. 1316, 1–5.

Anderson, W., Kozak, D., Coleman, V.A., Jämting, Å.K., Trau, M., 2013. A comparative study of submicron particle sizing platforms: accuracy, precision and resolution analysis of polydisperse particle size distributions. J. Colloid Interface Sci. 405, 322–330.

Arvizo, R.R., Miranda, O.R., Thompson, M.A., Pabelick, C.M., Bhattacharya, R., Robertson, J.D., Rotello, V.M., Prakash, Y.S., Mukherjee, P., 2010. Effect of nanoparticle surface charge at the plasma membrane and beyond. Nano Lett. 10, 2543–2548.

Balog, S., Rodriguez-Lorenzo, L., Monnier, C.A., Obiols-Rabasa, M., Rothen-Rutishauser, B., Schurtenberger, P., Petri-Fink, A., 2015. Characterizing nanoparticles in complex biological media and physiological fluids with depolarized dynamic light scattering. Nanoscale 7, 5991–5997.

Beingessner, R.L., Deng, B.L., Fanwick, P.E., Fenniri, H., 2008. A regioselective approach to trisubstituted 2 (or 6)-arylaminopyrimidine-5-carbaldehydes and their application in the synthesis of structurally and electronically unique G^C base precursors. J. Org. Chem. 73, 931–939.

Beingessner, R.L., Diaz, J.A., Hemraz, U.D., Fenniri, H., 2011. Synthesis of a β-glycoside functionalized GΛC motif for self-assembly into rosette nanotubes with predefined length. Tetrahedron Lett. 52, 661–664.

Bengtén, E., Clem, L.W., Miller, N.W., Warr, G.W., Wilson, M., 2006. Channel catfish immunoglobulins: repertoire and expression. Dev. Comp. Immunol. 30, 77–92.

Bian, S.-W., Mudunkotuwa, I.A., Rupasinghe, T., Grassian, V.H., 2011. Aggregation and Dissolution of 4 nm ZnO Nanoparticles in Aqueous Environments: Influence of pH, Ionic Strength, Size, and Adsorption of Humic Acid. Langmuir 27, 6059–6068.

Boluk, Y., Danumah, C., 2014. Analysis of cellulose nanocrystal rod lengths by dynamic light scattering and electron microscopy. J Nanopart. Res. 16, 1–

7.
Borzsonyi, G., Beingessner, R.L., Yamazaki, T., Cho, J.Y., Myles, A.J., Malac, M., Egerton, R., Kawasaki, M., Ishizuka, K., Kovalenko, A., Fenniri, H., 2010. Water-soluble J-type rosette nanotubes with giant molar ellipticity. J. Am. Chem. Soc. 132, 15136–15139.
Braden, B.C., Goldbaum, F.A., Chen, B.X., Kirschner, A.N., Wilson, S.R., Erlanger, B.F., 2000. X-ray crystal structure of an anti-Buckminsterfullerene antibody Fab fragment: biomolecular recognition of C60. Proc. Natl. Acad. Sci. U.S.A. 97, 12193–12197.
Brana, C., Benham, C., Sundstrom, L., 2002. A method for characterising cell death in vitro by combining propidium iodide staining with immunohistochemistry. Brain Research Protocols 10, 109–114.
Brown, D.M., Kinloch, I.A., Bangert, U., Windle, A.H., Walter, D.M., Walker, G.S., Scotchford, C.A., Donaldson, K., Stone, V., 2007. An in vitro study of the potential of carbon nanotubes and nanofibres to induce inflammatory mediators and frustrated phagocytosis. Carbon 45, 1743–1756.
Burleson, D.J., Driessen, M.D., Penn, R.L., 2012. On the Characterization of Environmental Nanoparticles. J. Env. Sci. Health 39, 2707–2753.
Casey, A., Herzog, E., Lyng, F.M., Byrne, H.J., Chambers, G., Davoren, M., 2008. Single walled carbon nanotubes induce indirect cytotoxicity by medium depletion in A549 lung cells. Toxicol. Lett. 179, 78–84.
Cedervall, T., Lynch, I., Lindman, S., Berggård, T., Thulin, E., Nilsson, H., Dawson, K.A., Linse, S., 2007. Understanding the nanoparticle-protein corona using methods to quantify exchange rates and affinities of proteins for nanoparticles. Proc. Natl. Acad. Sci. U.S.A. 104, 2050–2055.
Chang, E., Yu, W.W., Colvin, V.L., Drezek, R., 2005. Quantifying the Influence of Surface Coatings on Quantum Dot Uptake in Cells. J. Biomed. Res. 1, 397–401.
Chang, J.S., Chang, K.L.B., Hwang, D.F., Kong, Z.L., 2007. In vitro cytotoxicitiy of silica nanoparticles at high concentrations strongly depends on the metabolic activity type of the cell line. Environ. Sci. Technol. 41, 2064–2068.
Chen, B.A., Jin, N., Wang, J., Ding, J., Gao, C., Cheng, J., Xia, G., Gao, F., Zhou, Y., Chen, Y., Zhou, G., Li, X., Zhang, Y., Tang, M., Wang, X., 2010. The effect of magnetic nanoparticles of Fe_3O_4 on immune function in normal ICR mice. Int. J. Nanomed. 5, 593–599.
Chen, B.X., Wilson, S.R., Das, M., Coughlin, D.J., Erlanger, B.F., 1998. Antigenicity of fullerenes: antibodies specific for fullerenes and their characteristics. Proc. Natl. Acad. Sci. U.S.A. 95, 10809–10813.
Cheng, J., Cheng, S., 2012. Influence of carbon nanotube length on toxicity to zebrafish embryos. Int. J. Nanomed. 7, 3731–3739.
Chhabra, R., Moralez, J.G., Raez, J., Yamazaki, T., Cho, J.Y., Myles, A.J., Kovalenko, A., Fenniri, H., 2009. One-pot nucleation, growth, morphogenesis, and passivation of 1.4 nm Au nanoparticles on self-assembled rosette nanotubes. J. Am. Chem. Soc. 132, 32–33.

Cho, E.C., Xie, J., Wurm, P.A., Xia, Y., 2009. Understanding the Role of Surface Charges in Cellular Adsorption versus Internalization by Selectively Removing Gold Nanoparticles on the Cell Surface with a I2/KI Etchant. Nano Lett. 9, 1080–1084.

Chun, A.L., Moralez, J.G., Webster, T.J., Fenniri, H., 2005. Helical rosette nanotubes: a biomimetic coating for orthopedics? Biomaterials 26, 7304–7309.

Clift, M.J.D., Foster, E.J., Vanhecke, D., Studer, D., Wick, P., Gehr, P., Rothen-Rutishauser, B., Weder, C., 2011. Investigating the interaction of cellulose nanofibers derived from cotton with a sophisticated 3D human lung cell coculture. Biomacromolecules 12, 3666–3673.

Cormode, D.P., Skajaa, T., Fayad, Z.A., Mulder, W.J.M., 2009. Nanotechnology in medical imaging: probe design and applications. Arterioscler. Thromb. Vasc. Biol. 29, 992–1000.

Cortes, H.D., Lillico, D.M.E., Zwozdesky, M.A., Pemberton, J.G., O'Brien, A., Montgomery, B.C.S., Wiersma, L., Chang, J.P., Stafford, J.L., 2014. Induction of phagocytosis and intracellular signaling by an inhibitory channel catfish leukocyte immune-type receptor: evidence for immunoregulatory receptor functional plasticity in teleosts. J. Innate Immun. 6, 435–455.

Cortes, H.D., Montgomery, B.C., Verheijen, K., García-García, E., Stafford, J.L., 2012. Examination of the stimulatory signaling potential of a channel catfish leukocyte immune-type receptor and associated adaptor. Dev. Comp. Immunol. 36, 62–73.

Cowie, J., Bilek, E.M., Wegner, T.H., Shatkin, J.A., 2014. Market projections of cellulose nanomaterial-enabled products—Part 2: Volume estimates. Tappi Journal.

Cross, S.E., Innes, B., Roberts, M.S., Tsuzuki, T., Robertson, T.A., McCormick, P., 2007. Human skin penetration of sunscreen nanoparticles: in-vitro assessment of a novel micronized zinc oxide formulation. Skin Pharmacol. Physiol. 20, 148–154.

Daniel, M.C., Astruc, D., 2004. Gold nanoparticles: assembly, supramolecular chemistry, quantum-size-related properties, and applications toward biology, catalysis, and nanotechnology. Chem. Rev. 104, 293–346.

Davis, R.R., Lockwood, P.E., Hobbs, D.T., Messer, R.L.W., Price, R.J., Lewis, J.B., Wataha, J.C., 2007. In vitro biological effects of sodium titanate materials. J. Biomed. Mater. Res. Part B Appl. Biomater. 83, 505–511.

De Volder, M.F.L., Tawfick, S.H., Baughman, R.H., Hart, A.J., 2013. Carbon nanotubes: present and future commercial applications. Science 339, 535–539.

Delogu, L.G., Venturelli, E., Manetti, R., Pinna, G.A., Carru, C., Madeddu, R., Murgia, L., Sgarrella, F., Dumortier, H., Bianco, A., 2012. Ex vivo impact of functionalized carbon nanotubes on human immune cells. Nanomedicine 7, 231–243.

Dhawan, A., Sharma, V., 2010. Toxicity assessment of nanomaterials: methods and challenges. Bioanal. Chem. 398, 589–605.

Donaldson, K., Aitken, R., Tran, L., Stone, V., Duffin, R., Forrest, G., Alexander,

A., 2006. Carbon Nanotubes: A Review of Their Properties in Relation to Pulmonary Toxicology and Workplace Safety. Tox. Sci. 92, 5–22.
Dong, S., Roman, M., 2007. Fluorescently labeled cellulose nanocrystals for bioimaging applications. J. Am. Chem. Soc. 129, 13810–13811.
Dwivedi, P.D., Tripathi, A., Ansari, K.M., Shanker, R., Das, M., 2011. Impact of Nanoparticles on the Immune System 7, 193–194.
Fadeel, B., 2012. Clear and present danger? Engineered nanoparticles and the immune system. Swiss Med. Wkly 142, 13609.
Fadel, T.R., Fahmy, T.M., 2014. Immunotherapy applications of carbon nanotubes: from design to safe applications. Trends Biotechnol. 32, 198–209.
Fenniri, H., Deng, B.L., Ribbe, A.E., 2002a. Helical rosette nanotubes with tunable chiroptical properties. J. Am. Chem. Soc. 124, 11064–11072.
Fenniri, H., Deng, B.L., Ribbe, A.E., Hallenga, K., Jacob, J., Thiyagarajan, P., 2002b. Entropically driven self-assembly of multichannel rosette nanotubes. Proc. Natl. Acad. Sci. U.S.A. 99, 6487–6492.
Fenniri, H., Mathivanan, P., Vidale, K.L., Sherman, D.M., Hallenga, K., Wood, K.V., Stowell, J.G., 2001. Helical rosette nanotubes: design, self-assembly, and characterization. J. Am. Chem. Soc. 123, 3854–3855.
Feynman, R.P., 1960. There's plenty of room at the bottom. Engineering and science.
Fine, E., Zhang, L., Fenniri, H., Webster, T.J., 2009. Enhanced endothelial cell functions on rosette nanotube-coated titanium vascular stents. Int. J. Nanomed. 4, 91–97.
Fowlkes, V., Wilson, C.G., Carver, W., Goldsmith, E.C., 2013. Mechanical loading promotes mast cell degranulation via RGD-integrin dependent pathways. J. Biomech. 46, 788–795.
Fubini, B., Ghiazza, M., Fenoglio, I., 2010. Physico-chemical features of engineered nanoparticles relevant to their toxicity. Nanotoxicology 4, 347–363.
Gibbs, B.F., Amon, U., Pearce, F.L., 1997. Spontaneous histamine release from mast cells and basophils is controlled by the cellular environment. Inflamm. Res. 46 Suppl 1, S25–6.
Gilfillan, A.M., Tkaczyk, C., 2006. Integrated signalling pathways for mast-cell activation. Nat. Rev. Immunol. 6, 218–230.
Goodman, C.M., McCusker, C.D., Yilmaz, T., Rotello, V.M., 2004. Toxicity of gold nanoparticles functionalized with cationic and anionic side chains. Bioconjugate Chem. 15, 897–900.
Gottschalk, F., Nowack, B., 2011. The release of engineered nanomaterials to the environment. J. Environ. Monit. 13, 1145–1155.
Gottschalk, F., Sonderer, T., Scholz, R.W., Nowack, B., 2009. Modeled Environmental Concentrations of Engineered Nanomaterials (TiO 2, ZnO, Ag, CNT, Fullerenes) for Different Regions. Environ. Sci. Technol. 43, 9216–9222.
Granberg, M., Fowler, C.J., Jacobsson, S.O., 2001. Effects of the cannabimimetic fatty acid derivatives 2-arachidonoylglycerol, anandamide,

palmitoylethanolamide and methanandamide upon IgE-dependent antigen-induced beta-hexosaminidase, serotonin and TNF alpha release from rat RBL-2H3 basophilic leukaemic cells. Arch. Pharmacol. 364, 66–73.

Gratton, S.E.A., Ropp, P.A., Pohlhaus, P.D., Luft, J.C., Madden, V.J., Napier, M.E., DeSimone, J.M., 2008. The effect of particle design on cellular internalization pathways. Proc. Natl. Acad. Sci. U. S. A. 105, 11613–11618.

Guo, L., Bussche, von dem, A., Buechner, M., Yan, A., Kane, A.B., Hurt, R.H., 2008. Adsorption of essential micronutrients by carbon nanotubes and the implications for nanotoxicity testing. Small 4, 721–727.

Gustafsson, Å., Lindstedt, E., Elfsmark, L.S., Bucht, A., 2011. Lung exposure of titanium dioxide nanoparticles induces innate immune activation and long-lasting lymphocyte response in the Dark Agouti rat. J. Immunotoxicol. 8, 111–121.

Habibi, Y., Lucia, L.A., Rojas, O.J., 2010. Cellulose nanocrystals: chemistry, self-assembly, and applications. Chem. Rev. 110, 3479–3500.

Hamad, I., Al-Hanbali, O., Hunter, A.C., Rutt, K.J., Andresen, T.L., Moghimi, S.M., 2010. Distinct polymer architecture mediates switching of complement activation pathways at the nanosphere–serum interface: implications for stealth nanoparticle engineering. ACS Nano 4, 6629–6638.

Handy, R.D., Bairuty, Al, G., Jubory, Al, A., Ramsden, C.S., Boyle, D., Shaw, B.J., Henry, T.B., 2011. Effects of manufactured nanomaterials on fishes: a target organ and body systems physiology approach. Journal of Fish Biology 79, 821–853.

Harush-Frenkel, O., Rozentur, E., Benita, S., Altschuler, Y., 2008. Surface Charge of Nanoparticles Determines Their Endocytic and Transcytotic Pathway in Polarized MDCK Cells. Biomacromolecules 9, 435–443.

Hendren, C.O., Mesnard, X., Dröge, J., Wiesner, M.R., 2011. Estimating Production Data for Five Engineered Nanomaterials As a Basis for Exposure Assessment. Environ. Sci. Technol. 45, 2562–2569.

Henry, T.B., Petersen, E.J., Compton, R.N., 2011. Aqueous fullerene aggregates (nC60) generate minimal reactive oxygen species and are of low toxicity in fish: a revision of previous reports. Current Opinion in Biotechnology 22, 533–537.

Holsapple, M.P., Farland, W.H., Landry, T.D., Monteiro-Riviere, N.A., Carter, J.M., Walker, N.J., Thomas, K.V., 2005. Research strategies for safety evaluation of nanomaterials, part II: toxicological and safety evaluation of nanomaterials, current challenges and data needs. Tox. Sci. 88, 12–17.

Horev-Azaria, L., Baldi, G., Beno, D., Bonacchi, D., 2013. Predictive toxicology of cobalt ferrite nanoparticles: comparative in-vitro study of different cellular models using methods of knowledge discovery from data. Part. Fibre Toxicol. 10, 32–49.

Huang, Y.F., Liu, H., Xiong, X., Chen, Y., Tan, W., 2009. Nanoparticle-mediated IgE-receptor aggregation and signaling in RBL mast cells. J. Am. Chem. Soc. 131, 17328–17334.

Hussain, S., Vanoirbeek, J.A.J., Hoet, P.H.M., 2012. Interactions of

nanomaterials with the immune system. Nanomed. Nanobiotech. 4, 169–183.
Johnston, H.J., Hutchison, G.R., Christensen, F.M., Peters, S., Hankin, S., Aschberger, K., Stone, V., 2010. A critical review of the biological mechanisms underlying the in vivo and in vitro toxicity of carbon nanotubes: The contribution of physico-chemical characteristics. Nanotoxicology 4, 207–246.
Journeay, W.S., Suri, S.S., Moralez, J.G., Fenniri, H., Singh, B., 2008. Low inflammatory activation by self-assembling rosette nanotubes in human Calu-3 pulmonary epithelial cells. Small 4, 817–823.
Journeay, W.S., Suri, S.S., Moralez, J.G., Fenniri, H., Singh, B., 2009. Macrophage inflammatory response to self-assembling rosette nanotubes. Small 5, 1446–1452.
Jovanović, B., Anastasova, L., Rowe, E.W., Palić, D., 2011a. Hydroxylated fullerenes inhibit neutrophil function in fathead minnow (Pimephales promelas Rafinesque, 1820). Aquat. Toxicol. 101, 474–482.
Jovanović, B., Anastasova, L., Rowe, E.W., Zhang, Y., Clapp, A.R., Palić, D., 2011b. Effects of nanosized titanium dioxide on innate immune system of fathead minnow. Ecotoxicol. Environ. Saf. 74, 675–683.
Jovanović, B., Palić, D., 2012. Immunotoxicology of non-functionalized engineered nanoparticles in aquatic organisms with special emphasis on fish: review of current knowledge, gap identification, and call for further research. Aquat. Toxicol. 118-119, 141–151.
Kafshgari, M.H., Harding, F.J., Voelcker, N.H., 2015. Insights into cellular uptake of nanoparticles. Curr. Drug Deliv. 12, 63–77.
Kammer, von der, F., Ferguson, P.L., Holden, P.A., Masion, A., Rogers, K.R., Klaine, S.J., Koelmans, A.A., Horne, N., Unrine, J.M., 2012. Analysis of engineered nanomaterials in complex matrices (environment and biota): general considerations and conceptual case studies. Envir. Tox. and Chem. 31, 32–49.
Katwa, P., Wang, X., Urankar, R.N., Podila, R., Hilderbrand, S.C., Fick, R.B., Rao, A.M., Ke, P.C., Wingard, C.J., Brown, J.M., 2012. A carbon nanotube toxicity paradigm driven by mast cells and the IL-$_{33}$/ST$_2$ axis. Small 8, 2904–2912.
Kim, K.S., Cota-Sanchez, G., Kingston, C.T., Imris, M., Simard, B., Soucy, G., 2007. Large-scale production of single-walled carbon nanotubes by induction thermal plasma. J. Phys. D: Appl. Phys. 40, 2375–2387.
Kim, K.S., Moradian, A., Mostaghimi, J., 2009. Synthesis of single-walled carbon nanotubes by induction thermal plasma. NRC Publication Archives.
Kim, S.T., Saha, K., Kim, C., Rotello, V.M., 2013. The Role of Surface Functionality in Determining Nanoparticle Cytotoxicity. Acc. Chem. Res. 46, 681–691.
Klaine, S.J., Alvarez, P.J.J., Batley, G.E., Fernandes, T.F., Handy, R.D., Lyon, D.Y., Mahendra, S., McLaughlin, M.J., Lead, J.R., 2008. Nanomaterials in the environment: behavior, fate, bioavailability, and effects. Environ. Toxicol.

Chem. 27, 1825–1851.
Klaper, R., Arndt, D., Setyowati, K., Chen, J., Goetz, F., 2010. Functionalization impacts the effects of carbon nanotubes on the immune system of rainbow trout, Oncorhynchus mykiss. Aquat. Toxicol. 100, 211–217.
Kolosnjaj-Tabi, J., Hartman, K.B., Boudjemaa, S., Ananta, J.S., Morgant, G., Szwarc, H., Wilson, L.J., Moussa, F., 2010. In vivo behavior of large doses of ultrashort and full-length single-walled carbon nanotubes after oral and intraperitoneal administration to swiss mice. ACS Nano 4, 1481–1492.
Kovacs, T., Naish, V., O'Connor, B., Blaise, C., Gagné, F., Hall, L., Trudeau, V., Martel, P., 2010. An ecotoxicological characterization of nanocrystalline cellulose (NCC). Nanotoxicology 4, 255–270.
Kroll, A., Dierker, C., Rommel, C., Hahn, D., Wohlleben, W., Schulze-Isfort, C., Göbbert, C., Voetz, M., Hardinghaus, F., Schnekenburger, J., 2011. Cytotoxicity screening of 23 engineered nanomaterials using a test matrix of ten cell lines and three different assays. Part. Fibre Toxicol. 8, 9.
Kroll, A., Pillukat, M.H., Hahn, D., Schnekenburger, J., 2009. Current in vitro methods in nanoparticle risk assessment: limitations and challenges. Eur J Pharm Biopharm 72, 370–377.
Lam, E., Male, K.B., Chong, J.H., Leung, A.C.W., Luong, J.H.T., 2012. Applications of functionalized and nanoparticle-modified nanocrystalline cellulose. Trends Biotechnol. 30, 283–290.
Lanone, S., Andujar, P., Kermanizadeh, A., Boczkowski, J., 2013. Determinants of carbon nanotube toxicity. Adv. Drug Delivery Rev. 65, 2063–2069.
Lanone, S., Rogerieux, F., Geys, J., Dupont, A., Maillot-Marechal, E., Boczkowski, J., Lacroix, G., Hoet, P., 2009. Comparative toxicity of 24 manufactured nanoparticles in human alveolar epithelial and macrophage cell lines. Part. Fibre Toxicol. 6, 14.
Laurent, S., Burtea, C., Thirifays, C., Häfeli, U.O., Mahmoudi, M., 2012. Crucial Ignored Parameters on Nanotoxicology: The Importance of Toxicity Assay Modifications and cell vision. PLoS ONE 7, 29997.
Lelimousin, M., Sansom, M.S.P., 2013. Membrane perturbation by carbon nanotube insertion: pathways to internalization. Small 9, 3639–3646.
Leung, A.C.W., Hrapovic, S., Lam, E., Liu, Y., Male, K.B., Mahmoud, K.A., Luong, J.H.T., 2011. Characteristics and Properties of Carboxylated Cellulose Nanocrystals Prepared from a Novel One-Step Procedure. Small 7, 302–305.
Lin, J., Zhang, H., Chen, Z., Zheng, Y., 2010. Penetration of lipid membranes by gold nanoparticles: insights into cellular uptake, cytotoxicity, and their relationship. ACS Nano 4, 5421–5429.
Linse, S., Cabaleiro-Lago, C., Xue, W.-F., Lynch, I., Lindman, S., Thulin, E., Radford, S.E., Dawson, K.A., 2007. Nucleation of protein fibrillation by nanoparticles. Proc. Natl. Acad. Sci. U.S.A. 104, 8691–8696.
Liu, D., Wang, L., Wang, Z., Cuschieri, A., 2012. Different cellular response mechanisms contribute to the length-dependent cytotoxicity of multi-walled carbon nanotubes. Nanoscale Res Lett 7, 361.

Liu, Y., Zhao, Y., Sun, B., Chen, C., 2012. Understanding the toxicity of carbon nanotubes. Acc. Chem. Res. 46, 702–713.

Love, S.A., Maurer-Jones, M.A., Thompson, J.W., Lin, Y.-S., Haynes, C.L., 2012. Assessing nanoparticle toxicity. Annu Rev Anal Chem 5, 181–205.

Lucarelli, M., Gatti, A.M., Savarino, G., Quattroni, P., Martinelli, L., Monari, E., Boraschi, D., 2004. Innate defence functions of macrophages can be biased by nano-sized ceramic and metallic particles. Eur. Cytokine Netw. 15, 339–346.

Lundqvist, M., Stigler, J., Elia, G., Lynch, I., Cedervall, T., Dawson, K.A., 2008. Nanoparticle size and surface properties determine the protein corona with possible implications for biological impacts. Proc. Natl. Acad. Sci. U.S.A. 105, 14265–14270.

Maccormack, T.J., Clark, R.J., Dang, M.K.M., Ma, G., Kelly, J.A., Veinot, J.G.C., Goss, G.G., 2012. Inhibition of enzyme activity by nanomaterials: potential mechanisms and implications for nanotoxicity testing. Nanotoxicology 6, 514–525.

Maccormack, T.J., Goss, G.G., 2008. Identifying and predicting biological risks associated with manufactured nanoparticles in aquatic ecosystems. J. Ind. Ecol. 12, 286–296.

Mahmoud, K.A., Mena, J.A., Male, K.B., Hrapovic, S., Kamen, A., Luong, J.H.T., 2010. Effect of Surface Charge on the Cellular Uptake and Cytotoxicity of Fluorescent Labeled Cellulose Nanocrystals. ACS Appl. Mater. Interfaces 2, 2924–2932.

Majji, S., Thodima, V., Arnizaut, A., Deng, Y., May, W., Sittman, D., Waldbieser, G.C., Hanson, L., Cuchens, M.A., Bengten, E., Chinchar, V.G., 2009. Expression profiles of cloned channel catfish (Ictalurus punctatus) lymphoid cell lines and mixed lymphocyte cultures. Dev. Comp. Immunol. 33, 224–234.

Maurer-Jones, M.A., Lin, Y.-S., Haynes, C.L., 2010. Functional assessment of metal oxide nanoparticle toxicity in immune cells. ACS Nano 4, 3363–3373.

Maynard, A.D., 2006. Nanotechnology: assessing the risks. Nano Today 1, 22–33.

Maynard, A.D., Aitken, R.J., Butz, T., Colvin, V., Donaldson, K., 2006. Safe handling of nanotechnology. Nature 444, 267-269.

Meng, J., Yang, M., Jia, F., Xu, Z., Kong, H., Xu, H., 2011. Immune responses of BALB/c mice to subcutaneously injected multi-walled carbon nanotubes. Nanotoxicology 5, 583–591.

Mewes, J., Verheijen, K., Montgomery, B.C.S., Stafford, J.L., 2009. Stimulatory catfish leukocyte immune-type receptors (IpLITRs) demonstrate a unique ability to associate with adaptor signaling proteins and participate in the formation of homo- and heterodimers. Mol. Immunol. 47, 318–331.

Miller, N.W., Chinchar, V.G., Clem, L.W., 1994. Development of leukocyte cell lines from the channel catfish (Ictalurus punctatus). J. Tissue Cult. Methods 16, 117–123.

Mitchell, L.A., Lauer, F.T., Burchiel, S.W., McDonald, J.D., 2009. Mechanisms for how inhaled multiwalled carbon nanotubes suppress systemic immune function in mice. Nat. Nanotechnol. 4, 451–456.

Monteiro-Riviere, N.A., Inman, A.O., Zhang, L.W., 2009. Limitations and relative utility of screening assays to assess engineered nanoparticle toxicity in a human cell line. Toxicol. Appl. Pharmacol. 234, 222–235.

Montgomery, B.C., Cortes, H.D., Burshtyn, D.N., Stafford, J.L., 2012. Channel catfish leukocyte immune-type receptor mediated inhibition of cellular cytotoxicity is facilitated by SHP-1-dependent and -independent mechanisms. Dev. Comp. Immunol. 37, 151–163.

Montgomery, B.C., Cortes, H.D., Mewes-Ares, J., Verheijen, K., Stafford, J.L., 2011. Teleost IgSF immunoregulatory receptors. Dev. Comp. Immunol. 35, 1223–1237.

Montgomery, B.C.S., Mewes, J., Davidson, C., Burshtyn, D.N., Stafford, J.L., 2009. Cell surface expression of channel catfish leukocyte immune-type receptors (IpLITRs) and recruitment of both Src homology 2 domain-containing protein tyrosine phosphatase (SHP)-1 and SHP-2. Dev. Comp. Immunol. 33, 570–582.

Moralez, J.G., Raez, J., Yamazaki, T., Motkuri, R.K., Kovalenko, A., Fenniri, H., 2005. Helical rosette nanotubes with tunable stability and hierarchy. J. Am. Chem. Soc. 127, 8307–8309.

Murphy, F.A., Schinwald, A., Poland, C.A., 2012. The mechanism of pleural inflammation by long carbon nanotubes: interaction of long fibres with macrophages stimulates them to amplify pro-inflammatory responses in mesothelial cells. Part. Fibre Toxicol. 9, 1-15.

Naal, R.M.Z.G., Tabb, J., Holowka, D., Baird, B., 2004. In situ measurement of degranulation as a biosensor based on RBL-2H3 mast cells. 20, 791–796.

Nel, A., Xia, T., Mädler, L., Li, N., 2006. Toxic potential of materials at the nanolevel. Science 311, 622–627.

Nel, A., Xia, T., Meng, H., Wang, X., Lin, S., Ji, Z., Zhang, H., 2013. Nanomaterial toxicity testing in the 21st century: use of a predictive toxicological approach and high-throughput screening. Acc. Chem. Res. 46, 607–621.

Nel, A.E., Madler, L., Velegol, D., Xia, T., Hoek, E.M.V., Somasundaran, P., Klaessig, F., Castranova, V., Thompson, M., 2009. Understanding biophysicochemical interactions at the nano-bio interface. Nat. Mater. 8, 543–557.

Oberdörster, G., Oberdörster, E., Oberdörster, J., 2005. Nanotoxicology: an emerging discipline evolving from studies of ultrafine particles. Environ. Health Perspect. 113, 823–839.

Oberdörster, G., Oberdörster, E., Oberdörster, J., 2007. Concepts of nanoparticle dose metric and response metric. Environ. Health Perspect. 115, A290.

Ogunwale, B., Schmidt-Ott, A., Meek, R.M.D., Brewer, J.M., 2009. Investigating the immunologic effects of CoCr nanoparticles. Clin. Orthop. Relat. Res. 467, 3010–3016.

Ong, K.J., Maccormack, T.J., Clark, R.J., Ede, J.D., Ortega, V.A., Felix, L.C., Dang,

M.K.M., Ma, G., Fenniri, H., Veinot, J.G.C., Goss, G.G., 2014. Widespread nanoparticle-assay interference: implications for nanotoxicity testing. PLoS ONE 9, 90650.

Ortega, V.A., Katzenback, B.A., Stafford, J.L., Belosevic, M., Goss, G.G., 2013. Effects of polymer-coated metal oxide nanoparticles on goldfish (Carassius auratus) neutrophil viability and function. Nanotoxicology EO, 1–11.

Owens, D., Peppas, N., 2006. Opsonization, biodistribution, and pharmacokinetics of polymeric nanoparticles. International Journal of Pharmaceutics 307, 93–102.

Pacurari, M., Yin, X.J., Zhao, J., Ding, M., Leonard, S.S., Schwegler-Berry, D., Ducatman, B.S., Sbarra, D., Hoover, M.D., Castranova, V., Vallyathan, V., 2008. Raw Single-Wall Carbon Nanotubes Induce Oxidative Stress and Activate MAPKs, AP-1, NF-κB, and Akt in Normal and Malignant Human Mesothelial Cells. Environ. Health Perspect. 116, 1211–1217.

Pal, A.K., Aalaei, I., Gadde, S., Gaines, P., Schmidt, D., Demokritou, P., Bello, D., 2014. High resolution characterization of engineered nanomaterial dispersions in complex media using tunable resistive pulse sensing technology. ACS Nano 8, 9003–9015.

Palomäki, J., Välimäki, E., Sund, J., Vippola, M., Clausen, P.A., Jensen, K.A., Savolainen, K., Matikainen, S., Alenius, H., 2011. Long, needle-like carbon nanotubes and asbestos activate the NLRP3 inflammasome through a similar mechanism. ACS Nano 5, 6861–6870.

Park, H., Grassian, V.H., 2010. Commercially manufactured engineered nanomaterials for environmental and health studies: Important insights provided by independent characterization. Environ. Tox. and Chem. 29, 715–721.

Park, J., Nam, J., Won, N., Jin, H., Jung, S., Jung, S., Cho, S.H., Kim, S., 2011. Compact and Stable Quantum Dots with Positive, Negative, or Zwitterionic Surface: Specific Cell Interactions and Non-Specific Adsorptions by the Surface Charges. Adv. Func. Mat. 21, 1558–1566.

Passante, E., Ehrhardt, C., Sheridan, H., Frankish, N., 2009. RBL-2H3 cells are an imprecise model for mast cell mediator release. Inflamm. Res. 58, 611–618.

Passante, E., Frankish, N., 2009. The RBL-2H3 cell line: its provenance and suitability as a model for the mast cell. Inflamm. Res. 58, 737–745.

Petersen, E.J., Zhang, L., Mattison, N.T., O'Carroll, D.M., Whelton, A.J., Uddin, N., Nguyen, T., Huang, Q., Henry, T.B., Holbrook, R.D., Chen, K.L., 2011. Potential release pathways, environmental fate, and ecological risks of carbon nanotubes. Environ. Sci. Technol. 45, 9837–9856.

Pfaller, T., Puntes, V., Casals, E., Duschl, A., Oostingh, G.J., 2009. In vitro investigation of immunomodulatory effects caused by engineered inorganic nanoparticles – the impact of experimental design and cell choice. Nanotoxicology 3, 46–59.

Poland, C.A., Duffin, R., Kinloch, I., Maynard, A., Wallace, W.A.H., Seaton, A., Stone, V., Brown, S., MacNee, W., Donaldson, K., 2008. Carbon nanotubes

introduced into the abdominal cavity of mice show asbestos-like pathogenicity in a pilot study. Nature Nanotech. 3, 423–428.
Porter, A.E., Gass, M., Bendall, J.S., Muller, K., Goode, A., Skepper, J.N., Midgley, P.A., Welland, M., 2009. Uptake of noncytotoxic acid-treated single-walled carbon nanotubes into the cytoplasm of human macrophage cells. ACS Nano 3, 1485–1492.
Price, K., Lomeda, J.R., Tour, J.M., 2009. Aggressively Oxidized Ultra-Short Single-Walled Carbon Nanotubes Having Oxidized Sidewalls. Chem. Mater. 21, 3917–3923.
Pulskamp, K., Diabaté, S., Krug, H.F., 2007. Carbon nanotubes show no sign of acute toxicity but induce intracellular reactive oxygen species in dependence on contaminants. Toxicol. Lett. 168, 58–74.
Rabinovitch, M., 1995. Professional and non-professional phagocytes: an introduction. Trends in Cell Biology 5, 85–87.
Rai, P.K., Parra-Vasquez, A.N.G., Chattopadhyay, J., Pinnick, R.A., Liang, F., Sadana, A.K., Hauge, R.H., Billups, W.E., Pasquali, M., 2007. Dispersions of Functionalized Single-Walled Carbon Nanotubes in Strong Acids: Solubility and Rheology. J. Nanosci. Nanotech. 7, 3378–3385.
Rallo, R., France, B., Liu, R., Nair, S., George, S., Damoiseaux, R., Giralt, F., Nel, A., Bradley, K., Cohen, Y., 2011. Self-organizing map analysis of toxicity-related cell signaling pathways for metal and metal oxide nanoparticles. Environ. Sci. Technol. 45, 1695–1702.
Ravi Shukla, Vipul Bansal, Minakshi Chaudhary, Atanu Basu, Ramesh R Bhonde, A., Murali Sastry, 2005. Biocompatibility of Gold Nanoparticles and Their Endocytotic Fate Inside the Cellular Compartment: A Microscopic Overview. Langmuir 21, 10644-10654.
Rejman, J., Oberle, V., Zuhorn, I., Hoekstra, D., 2004. Size-dependent internalization of particles via the pathways of clathrin- and caveolae-mediated endocytosis. Biochem. J. 377, 159.
Remes, A., Williams, D.F., 1992. Immune response in biocompatibility. Biomaterials 13, 731–743.
Riley, M.R., Boesewetter, D.E., Turner, R.A., Kim, A.M., Collier, J.M., Hamilton, A., 2005. Comparison of the sensitivity of three lung derived cell lines to metals from combustion derived particulate matter. Toxicol. In Vitro 19, 411–419.
Rivera-Gil, P., Jimenez de Aberasturi, D., Wulf, V., Pelaz, B., del Pino, P., Zhao, Y., la Fuente, de, J.M., Ruiz de Larramendi, I., Rojo, T., Liang, X.-J., Parak, W.J., 2013. The challenge to relate the physicochemical properties of colloidal nanoparticles to their cytotoxicity. Acc. Chem. Res. 46, 743–749.
Roman, M., 2015. Toxicity of Cellulose Nanocrystals: A Review. Industrial Biotech 11, 25–33.
Ryan, J.J., Bateman, H.R., Stover, A., Gomez, G., Norton, S.K., Zhao, W., Schwartz, L.B., Lenk, R., Kepley, C.L., 2007. Fullerene nanomaterials inhibit the allergic response. J. Immunol. 179, 665–672.
Rybak-Smith, M.J., Sim, R.B., 2011. Complement activation by carbon nanotubes. Adv. Drug Delivery Rev. 63, 1031–1041.

Salvador-Morales, C., Flahaut, E., Sim, E., Sloan, J., Green, M.L.H., Sim, R.B., 2006. Complement activation and protein adsorption by carbon nanotubes. Mol. Immunol. 43, 193–201.

Sato, Y., Yokoyama, A., Shibata, K.-I., Akimoto, Y., Ogino, S.-I., Nodasaka, Y., Kohgo, T., Tamura, K., Akasaka, T., U, M., Motomiya, K., Jeyadevan, B., Ishiguro, M., Hatakeyama, R., Watari, F., Tohji, K., 2005. Influence of length on cytotoxicity of multi-walled carbon nanotubes against human acute monocytic leukemia cell line THP-1 in vitro and subcutaneous tissue of rats in vivo. Mol. Biosyst. 1, 176–182.

Saxena, R.K., Williams, W., Mcgee, J.K., Daniels, M.J., Boykin, E., Gilmour, D.M.I., 2009. Enhanced in vitro and in vivo toxicity of poly-dispersed acid-functionalized single-wall carbon nanotubes. Nanotoxicology 1, 291-300.

Schultz, A.C., 2007. Nanotechnology: Industrial Revolution or Emerging Hazard? Env. Claims J. 19, 199–205.

Schumann, D.A., Wippermann, J., Klemm, D.O., Kramer, F., Koth, D., Kosmehl, H., Wahlers, T., Salehi-Gelani, S., 2009. Artificial vascular implants from bacterial cellulose: preliminary results of small arterial substitutes. Cellulose 16, 877–885.

Scown, T.M., van Aerle, R., Tyler, C.R., 2010. Review: do engineered nanoparticles pose a significant threat to the aquatic environment? Crit. Rev. Toxicol. 40, 653–670.

Shatkin, J.A., Wegner, T.H., Bilek, E.M., Cowie, J., 2014. Market projections of cellulose nanomaterial-enabled products-Part 1: Applications. Tappi Journal 10, 57-69.

Shaw, B.J., Handy, R.D., 2011. Physiological effects of nanoparticles on fish: a comparison of nanometals versus metal ions. Envir. Intern. 37, 1083–1097.

Shemetov, A.A., Nabiev, I., Sukhanova, A., 2012. Molecular interaction of proteins and peptides with nanoparticles. ACS Nano 6, 4585–4602.

Shew, A., 2008. Nanotech's History An Interesting, Interdisciplinary, Ideological Split. Bulletin of Science Technology & Society 28, 390–399.

Sim, R.B., Wallis, R., 2011. Surface properties: immune attack on nanoparticles. Nat. Nanotechnol. 6, 80–81.

Smith, C.J., Shaw, B.J., Handy, R.D., 2007. Toxicity of single walled carbon nanotubes to rainbow trout, (Oncorhynchus mykiss): respiratory toxicity, organ pathologies, and other physiological effects. Aquat. Toxicol. 82, 94–109.

Song, S., Chen, Y., Yan, Z., Webster, T.J., Fenniri, H., 2011. Self-assembled rosette nanotubes for incorporating hydrophobic drugs in physiological environments. Int. J. Nanomed. 6, 101–107.

Song, Y., Li, X., Du, X., 2009. Exposure to nanoparticles is related to pleural effusion, pulmonary fibrosis and granuloma. Eur. Respir. J. 34, 559–567.

Stafford, J.L., Bengten, E., Pasquier, L.D., Chandler, R., Quiniou, S.M., Clem, L.W., Miller, N.W., Wilson, M., 2006. A novel family of diversified immunoregulatory receptors in teleosts is homologous to both mammalian Fc receptors and molecules encoded within the leukocyte

receptor complex. Immunogenet. 58, 758-773.
Stafford, J.L., Nayak, D., Wilson, M., Quiniou, S.M., Clem, L.W., Miller, N.W., Bengten, E., 2007. Channel catfish leukocyte immune-type receptors contain a putative MHC class I binding site. Immunogenet. 59, 77-91.
Stueker, O., Ortega, V.A., Goss, G.G., Stepanova, M., 2014. Understanding Interactions of Functionalized Nanoparticles with Proteins: A Case Study on Lactate Dehydrogenase. Small 10, 2006–2021.
Sun, L., Wang, X., 2014. A new kind of cell suicide: mechanisms and functions of programmed necrosis. Trends Biochem. Sci. 39, 587–593.
Sun, L., Zhang, L., Hemraz, U.D., Fenniri, H., Webster, T.J., 2012. Bioactive rosette nanotube-hydroxyapatite nanocomposites improve osteoblast functions. Tissue Eng., Part A 18, 1741–1750.
Sun, T.Y., Gottschalk, F., Hungerbühler, K., Nowack, B., 2014. Comprehensive probabilistic modelling of environmental emissions of engineered nanomaterials. Environ. Pollut. 185, 69–76.
Suri, S., Fenniri, H., Singh, B., 2007. Nanotechnology-based drug delivery systems. J. Occup. Med. Toxicol. 2, 16–22.
Suri, S.S., Rakotondradany, F., Myles, A.J., Fenniri, H., Singh, B., 2009. The role of RGD-tagged helical rosette nanotubes in the induction of inflammation and apoptosis in human lung adenocarcinoma cells through the P38 MAPK pathway. Biomaterials 30, 3084–3090.
Tahara, K., Tadokoro, S., Yamamoto, H., Kawashima, Y., Hirashima, N., 2012. The suppression of IgE-mediated histamine release from mast cells following exocytic exclusion of biodegradable polymeric nanoparticles. Biomaterials 33, 343–351.
Tahara, Y., Nakamura, M., Yang, M., Zhang, M., Iijima, S., Yudasaka, M., 2012. Lysosomal membrane destabilization induced by high accumulation of single-walled carbon nanohorns in murine macrophage RAW 264.7. Biomaterials 33, 2762–2769.
Tan, F., Wang, M., Wang, W., Lu, Y., 2008. Comparative evaluation of the cytotoxicity sensitivity of six fish cell lines to four heavy metals in vitro. Toxicol. In Vitro 22, 164–170.
Teeguarden, J.G., Hinderliter, P.M., Orr, G., Thrall, B.D., Pounds, J.G., 2007. Particokinetics in vitro: dosimetry considerations for in vitro nanoparticle toxicity assessments. Toxicological Sciences 95, 300–312.
Tikhomirov, G., Oderinde, M., Makeiff, D., Mansouri, A., Lu, W., Heirtzler, F., Kingsley, S., Kwok, D.Y., Fenniri, H., 2008. Synthesis of hydrophobic derivatives of the G/\C base for rosette nanotube self-assembly in apolar media. J. Org. Chem. 73, 4248–4251.
Vardharajula, S., Ali, S.Z., Tiwari, P.M., Eroğlu, E., Vig, K., Dennis, V.A., Singh, S.R., 2012. Functionalized carbon nanotubes: biomedical applications. Int. J. Nanomed. 7, 5361–5374.
Verma, A., Stellacci, F., 2010. Effect of Surface Properties on Nanoparticle–Cell Interactions. Small 6, 12–21.
Villanova, J.C.O., Ayres, E., Carvalho, S.M., Patrício, P.S., Pereira, F.V., Oréfice, R.L., 2011. Pharmaceutical acrylic beads obtained by suspension

polymerization containing cellulose nanowhiskers as excipient for drug delivery. Eur. J. Pharm. Sci. 42, 406–415.
Westerhoff, P., Nowack, B., 2013. Searching for global descriptors of engineered nanomaterial fate and transport in the environment. Acc. Chem. Res. 46, 844–853.
Wick, P., Manser, P., Limbach, L.K., Dettlaff-Weglikowska, U., Krumeich, F., Roth, S., Stark, W.J., Bruinink, A., 2007. The degree and kind of agglomeration affect carbon nanotube cytotoxicity. Toxicol. Lett. 168, 121–131.
Wingard, C.J., Walters, D.M., Cathey, B.L., Hilderbrand, S.C., Katwa, P., Lin, S., Ke, P.C., Podila, R., Rao, A., Lust, R.M., Brown, J.M., 2011. Mast cells contribute to altered vascular reactivity and ischemia-reperfusion injury following cerium oxide nanoparticle instillation. Nanotoxicology 5, 531–545.
Witasp, E., Shvedova, A.A., Kagan, V.E., Fadeel, B., 2009. Single-walled carbon nanotubes impair human macrophage engulfment of apoptotic cell corpses. Inhal. Toxicol. 1, 131–136.
Wittmaack, K., 2007. In search of the most relevant parameter for quantifying lung inflammatory response to nanoparticle exposure: particle number, surface area, or what? Environ. Health Perspect. 115, 187–194.
Wörle-Knirsch, J.M., Pulskamp, K., Krug, H.F., 2006. Oops they did it again! Carbon nanotubes hoax scientists in viability assays. Nano Lett. 6, 1261–1268.
Xie, J., Xu, C., Kohler, N., Hou, Y., Sun, S., 2007. Controlled PEGylation of Monodisperse Fe3O4 Nanoparticles for Reduced Non-Specific Uptake by Macrophage Cells. Advanced Materials 19, 3163–3166.
Yamashita, K., Yoshioka, Y., Higashisaka, K., Morishita, Y., Yoshida, T., Fujimura, M., Kayamuro, H., Nabeshi, H., Yamashita, T., Nagano, K., Abe, Y., Kamada, H., Kawai, Y., Mayumi, T., Yoshikawa, T., Itoh, N., Tsunoda, S.-I., Tsutsumi, Y., 2010. Carbon nanotubes elicit DNA damage and inflammatory response relative to their size and shape. Inflammation 33, 276–280.
Yang, S.-T., Wang, X., Jia, G., Gu, Y., Wang, T., Nie, H., Ge, C., Wang, H., Liu, Y., 2008. Long-term accumulation and low toxicity of single-walled carbon nanotubes in intravenously exposed mice. Toxicol. Lett. 181, 182–189.
Zapata, A., Diez, B., Cejalvo, T., Gutiérrez-de Frías, C., Cortés, A., 2006. Ontogeny of the immune system of fish. Fish Shellfish Immunol. 20, 126–136.
Zhang, L., Chen, Y., Rodriguez, J., Fenniri, H., 2008. Biomimetic helical rosette nanotubes and nanocrystalline hydroxyapatite coatings on titanium for improving orthopedic implants. Int. J. Nanomed. 3, 323–333.
Zhang, L., Rodriguez, J., Raez, J., Myles, A.J., Fenniri, H., Webster, T.J., 2009. Biologically inspired rosette nanotubes and nanocrystalline hydroxyapatite hydrogel nanocomposites as improved bone substitutes. Nanotechnology 20, 175101.
Zhang, L.W., Monteiro-Riviere, N.A., 2009. Mechanisms of quantum dot

nanoparticle cellular uptake. Toxicol. Sci. 110, 138–155.
Zhao, X., Ong, K.J., Ede, J.D., Stafford, J.L., Ng, K.W., Goss, G.G., Loo, S.C.J., 2013. Evaluating the toxicity of hydroxyapatite nanoparticles in catfish cells and zebrafish embryos. Small 9, 1734–1741.
Zoppe, J.O., Ruottinen, V., Ruotsalainen, J., Rönkkö, S., Johansson, L.-S., Hinkkanen, A., Järvinen, K., Seppälä, J., 2014. Synthesis of cellulose nanocrystals carrying tyrosine sulfate mimetic ligands and inhibition of alphavirus infection. Biomacromolecules 15, 1534–1542.

APPENDICES

Supplemental Tables

Table S2-1. Review of characterization data for rosette nanotubes from select publications.

Source	Functionalization	Media	Characterization Technique	Measurement
1	crown ether	water	DLS (20, 30, 40 °C)	25.3, 52.7, 81.3 nm
			SAXS	3.6 nm diameter
			TEM	3.9 nm diameter
2	lysine	MES buffer	DLS	30.4 nm
			TEM	4.0 nm diameter 60 nm length (average)
3	lysine	water	TEM	3.5 nm diameter
4	lysine	titanium substrate	TEM	3.4 nm diameter
			AFM	3.1 nm diameter
5	lysine	water	DLS	36 nm
			TEM	3.4 nm diameter
			AFM	3.2 nm diameter

References: [1]Fenniri et al. (2002) [2]Fenniri et al. (2001) [3]Fine et al. (2009) [4]Chun et al. (2005) [5]Moralez et al. (2005)
Abbreviations: (DLS) – dynamic light scattering, reported as hydrodynamic radius (R_H); (SAXS) – small angle x-ray scattering; (TEM) – transmission electron microscopy ; (AFM) – atomic force microscopy

Table S2-2. Alternate dosing metric conversions for lysine functionalized and FITC-functionalized rosette nanotubes.

Functionalization	Molar Mass ($g\ mol^{-1}$)	Equivalent Nanomaterial Dosing Metrics		
		Mass Per Volume ($mg\ L^{-1}$)	Particle Number per Volume ($mol\ L^{-1}$)	Surface Area ($m^2\ g^{-1}$)
K-RNT	564.89	10	1.77×10^{-5}	2.5×10^{3}
		50	8.85×10^{-5}	2.5×10^{3}
		100	1.77×10^{-4}	2.5×10^{3}
$FITC^{1}/TBL^{19}$-RNTs	748.60	10	1.34×10^{-5}	2.5×10^{3}

Table S3-1. Physico-chemical characterization using dynamic light scattering showing hydrodynamic diameter (nm), polydispersity and zeta potential (mV) of CNT-30, CNT-40 and CNT-50 diluted to 10, 50, 100 or 250 mg L^{-1}.

Material	Concentration (mg L^{-1})	Hydrodynamic Diameter (nm)	Polydispersity	Zeta Potential (mV)
CNT-30	10	6719±572	0.74±0.11	-14.61±0.54
	50	6945±408	0.51±0.04	-14.29±0.42
	100	7018±462	0.47±0.07	-13.76±0.61
	250	6984±514	0.41±0.05	-14.09±0.39
CNT-40	10	4382±349	0.71±0.14	-14.99±0.67
	50	4435±462	0.49±0.03	-14.72±0.29
	100	4197±332	0.51±0.09	-14.63±0.38
	250	4463±429	0.46±0.05	-14.84±0.53
CNT-50	10	3248±512	0.81±0.15	-14.81±0.38
	50	3044±349	0.44±0.04	-15.94±0.27
	100	3107±444	0.41±0.05	-15.43±0.65
	250	3057±374	0.43±0.02	-14.57±0.91

Table S3-2. Analysis of potassium content using ICP-AES following production of U-CNT and AF-CNT potassium salts and subsequent calculation of corresponding carboxylic acid group weight and degree of carboxylic acid group functionalization.

	K Concentration (mg g^{-1})	Carboxylic Acid Group Weight (%)	Functionalization Degree (Mole %)[1]
U-CNT	1.2±0.1	0.25	0.04
CNT-30	105.8±1.3	22.46	4.0
CNT-40	116.8±1.1	28.86	5.5
CNT-50	173.4±2.4	36.9	7.8

Footnotes: [1]carbon atoms per 100 in the carbon nanotube backbone with carboxylic acid group functionalization

Supplemental Figures

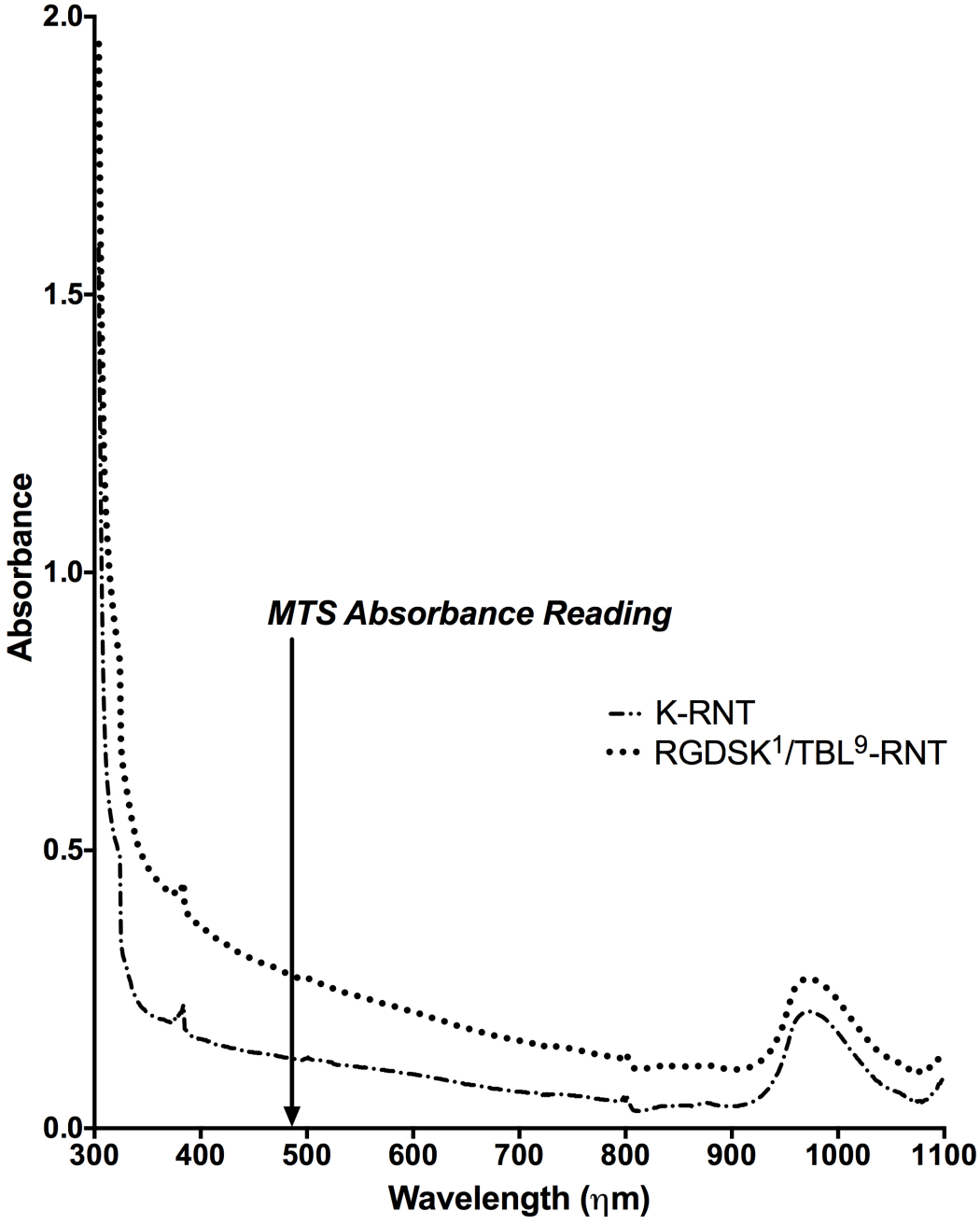

Figure S2-1. RNTs absorb light at wavelengths important for toxicological assays. A 300-1100 nm absorbance spectrum for 100 mg L^{-1} suspensions of K- and $RGDSK^{1}/TBL^{9}$-RNTs demonstrates the intrinsic optical properties of these materials. Significant absorbance at 490 nm suggests potential interference with MTS assay outputs.

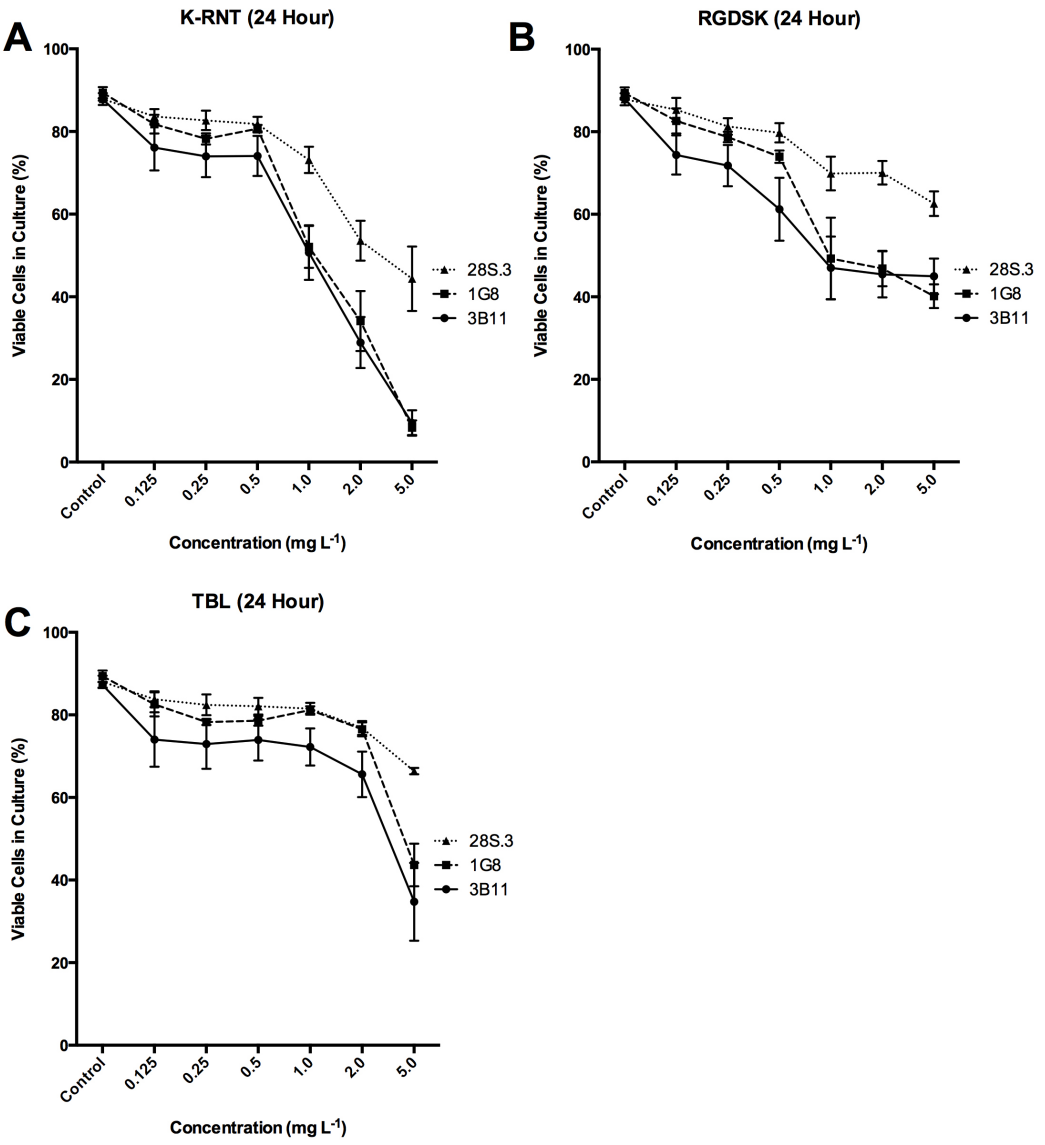

Figure S2-2. 3B11, 1G8 and 28S.3 response to RNT exposure was cell-line dependent. Flow cytometric data grouped by functionalization allowed a more direct comparison between cell-lines. $2.0x10^4$ 3B11, 1G8 or 28S.3 cells were incubated with 0.125, 0.25, 0.5, 1.0, 2.0 or 5.0 mg L^{-1} (A) K-RNT, (B) TBL-RNT or (C) RGDSK[1]/TBL[9]-RNT for 24 h. At high concentrations (1, 2 and 5 mg L^{-1} RNT), the response of 3B11 and 1G8 cell lines was similar, and significantly different, from 28S.3 cells. Data were analyzed by three-way ANOVA with a Holm-Sidak *post hoc* test ($p<0.05$). Means ± SEM are shown, n=5.

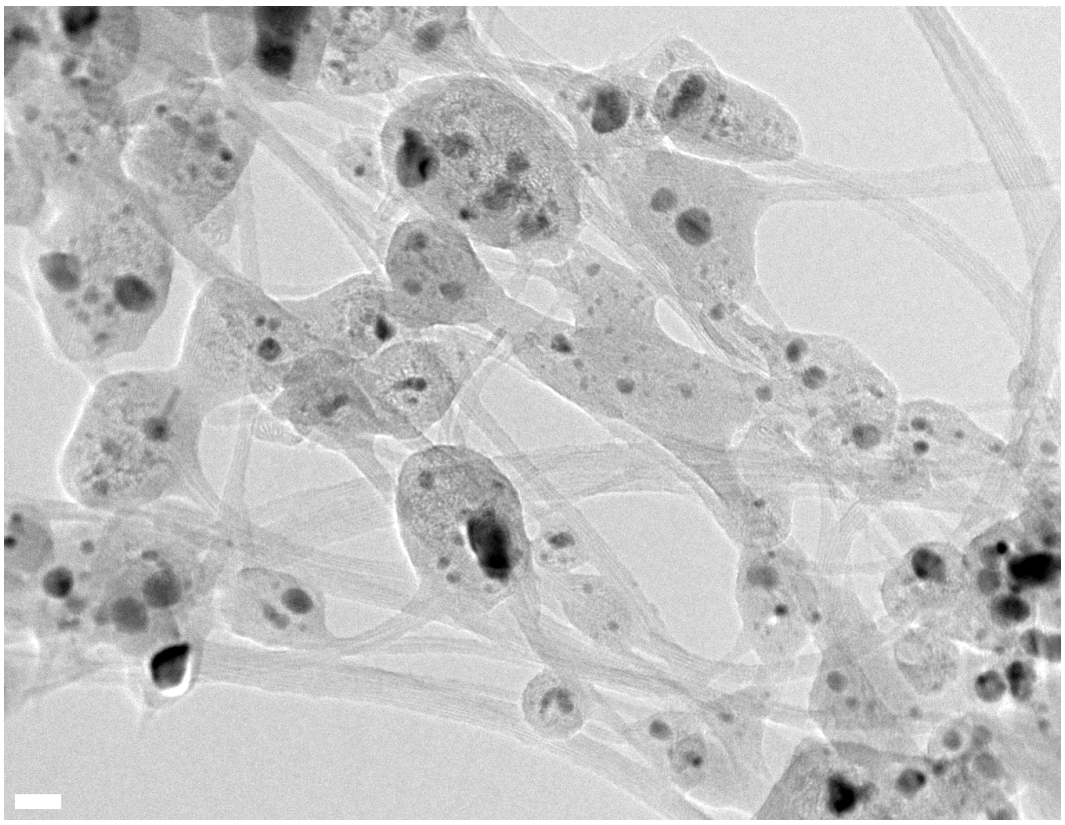

Figure S3-1. Unfunctionalized CNTs (U-CNTs) have a diameter of ~1.5-1.6 nm and extend in parallel bundles up to several micrometers in length. High resolution transmission electron microscopy micrographs of U-CNTs produced by induction thermal plasma technique before purification and oxidation. Scale bar = 20nm.

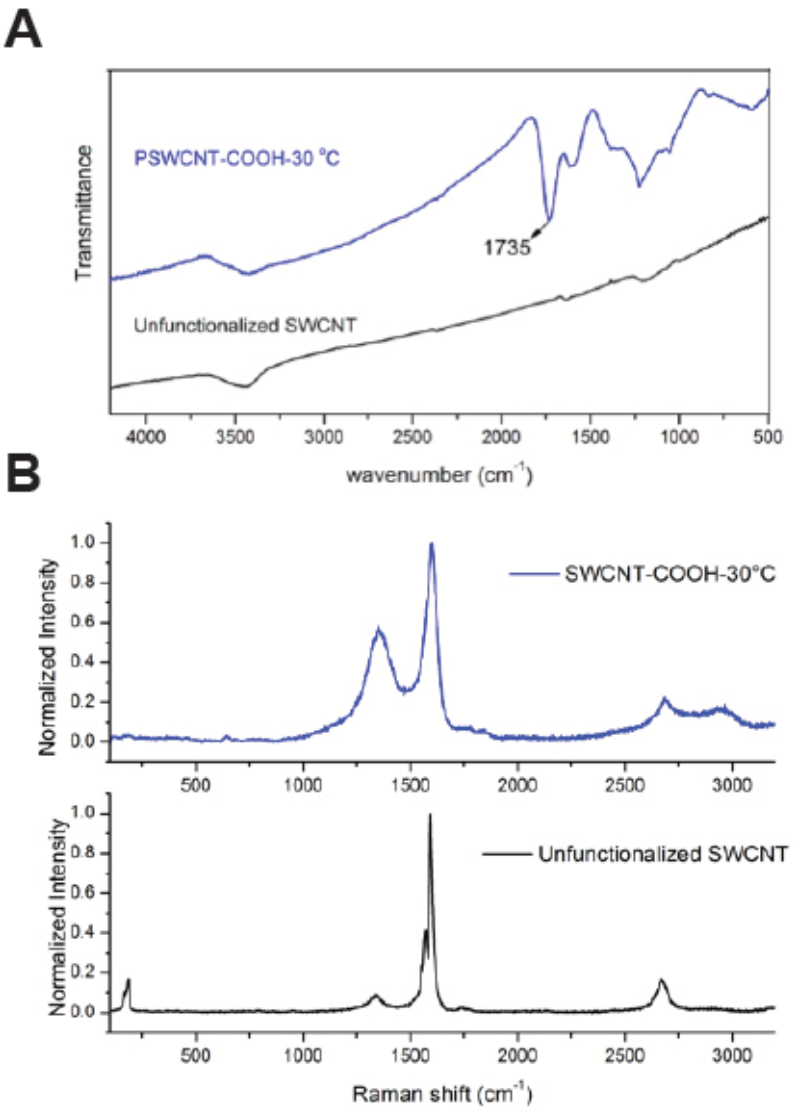

Figure S3-2. Infrared and Raman spectroscopy verified the introduction of carboxylic acid group functionalization to CNT-30. (A) Fourier transformed infrared spectra of U-CNT (black) and CNT-30 (blue) shows introduction of display peak at 1735 cm^{-1} for CNT-30 corresponding to carbonyl stretching of carboxylic acid moiety. (B) Raman spectra of U-CNT (black) and CNT-30 (blue) show U-CNT having a disorder mode (D-band) with a low intensity at 1340 cm^{-1}. CNT-30 have an increased intensity in the D-band, indicating sidewall functionalization.

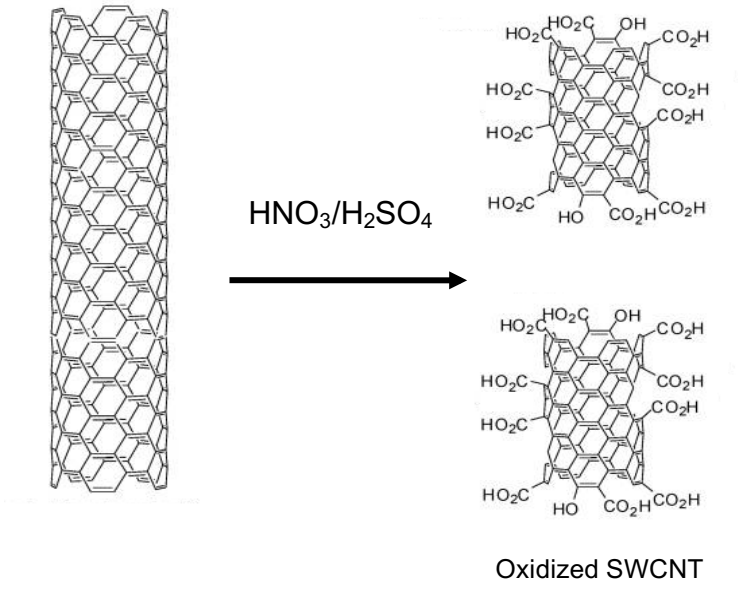

Figure S5-1. Schematic of oxidation process used to purify and functionalize CNT-30, CNT-40 and CNT-50 from U-CNTs. U-CNTs were produced by the induction thermal plasma process (Kim et al., 2007). U-CNTs were oxidized in a HNO_3/H_2SO_4 mixture for 2 h at 30, 40, and 50 °C to yield mostly carboxylic acid groups on the ends and sidewalls, termed CNT-30, CNT-40 and CNT-50 respectively.

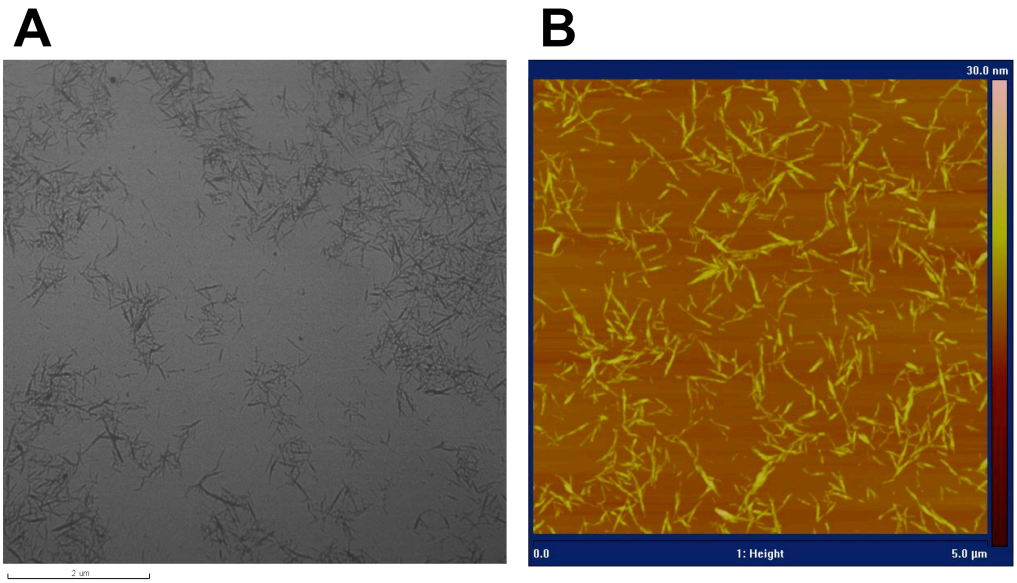

Figure S6-1. Low voltage transmission electron microscopy (LVTEM) micrographs (A) and height mode atomic force microscopy (AFM) micrographs (B) of crystalline nanocellulose (CNC) produced using the APS method. CNCs were uniform in size, with an average length of 128 ± 4 nm and diameter of 5.5 ± 0.1 nm.